

AD 657326



GEOPHYSICAL STUDY OF BASIN-RANGE STRUCTURE
DIXIE VALLEY REGION, NEVADA

BY

GEORGE A. THOMPSON, LAURENT J. MEISTER, ALAN T. HERRING,
THOMAS E. SMITH, DENNIS B. BURKE, ROBERT L. KOVACH,
ROBERT O. BURFORD, IRAJ A. SALEHI, AND M. DARROLL WOOD

GEOPHYSICS DEPARTMENT
STANFORD UNIVERSITY, STANFORD, CALIFORNIA

CONTRACT NO. AF 19(628)-3887

Project No. 8623, 5710

Task No. 862303

Work Unit No. 86230301

FINAL SCIENTIFIC REPORT
PARTS I-VIII

Period covered: January, 1964-December, 1966

JULY, 1967

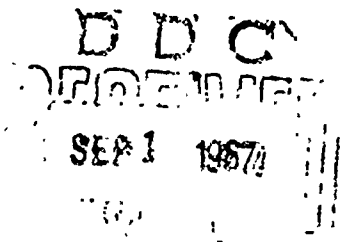
DISTRIBUTION OF THIS REPORT IS UNLIMITED

Contract Monitor: Gerry H. Cabaniss
Terrestrial Sciences Laboratory

PREPARED FOR

AIR FORCE CAMBRIDGE RESEARCH LABORATORIES
OFFICE OF AEROSPACE RESEARCH
UNITED STATES AIR FORCE
BEDFORD, MASSACHUSETTS

This research was supported in part by the Defense Atomic
Support Agency through the Air Force Weapons Laboratory



322

GEOPHYSICAL STUDY OF BASIN-RANGE STRUCTURE
DIXIE VALLEY REGION, NEVADA

BY

GEORGE A. THOMPSON, LAURENT J. MEISTER, ALAN T. HERRING,
THOMAS E. SMITH, DENNIS B. BURKE, ROBERT L. KOVACH,
ROBERT O. BURFORD, IRAJ A. SALEHI, AND M. DARROLL WOOD

GEOPHYSICS DEPARTMENT
STANFORD UNIVERSITY, STANFORD, CALIFORNIA

CONTRACT NO. AF 19(628)-3867

Project No. 8623, 5710
Task No. 862303
Work Unit No. 86230301

FINAL SCIENTIFIC REPORT
PARTS I-VIII

Period covered: January, 1964-December, 1966

JULY, 1967

DISTRIBUTION OF THIS REPORT IS UNLIMITED

Contract Monitor: Gerry H. Cabaniss
Terrestrial Sciences Laboratory

PREPARED FOR

AIR FORCE CAMBRIDGE RESEARCH LABORATORIES
OFFICE OF AEROSPACE RESEARCH
UNITED STATES AIR FORCE
BEDFORD, MASSACHUSETTS

This research was supported in part by the Defense Atomic
Support Agency through the Air Force Weapons Laboratory

ABSTRACT

The study aims to determine the subsurface structure and origin of a tectonically active part of the Basin and Range province, which has structural similarities to the ocean ridge system and to continental block-fault structure such as the Rift Valleys of East Africa. A variety of techniques was utilized, including seismic refraction, gravity measurements, magnetic measurements, photogeologic mapping, strain analysis of existing geodetic data, and elevation measurements on shorelines of ancient lakes.

Dixie Valley contains more than 10,000 feet of Cenozoic deposits and is underlain by a complex fault trough concealed within the main graben. The bounding faults, studied by side refractions, are markedly crooked in strike and comparatively constant in dip. Dip-slip motion predominates. The computed strain energy is comparable to the energy derived from the magnitudes of the 1954 earthquakes. Ancient beach ridges record a maximum 14 feet of westward tilting in approximately the last 10,000 years; the valley has been subsiding with little net tilting.

COMPOSITE TABLE OF CONTENTS

BACKGROUND AND RESULTS

George A. Thompson (Principal Investigator)

PART

SEISMIC REFRACTION STUDY OF DIXIE VALLEY, NEVADA

Laurent J. Meister I

SEISMIC REFRACTION STUDY OF A FAULT ZONE IN DIXIE VALLEY, NEVADA

Alan T. Herring II

AEROMAGNETIC MEASUREMENTS IN DIXIE VALLEY, NEVADA: IMPLICATIONS REGARDING BASIN-RANGE STRUCTURE

Thomas E. Smith III

AERIAL PHOTOGRAPH SURVEY OF DIXIE VALLEY, NEVADA

Dennis B. Burke IV

SURFACE STRAIN CHANGES AND STRAIN ENERGY RELEASE IN THE DIXIE VALLEY-FAIRVIEW PEAK AREA, NEVADA

L. J. Meister, R. O. Burford, G. A. Thompson
and R. L. Kovach V

SEISMIC REFRACTION STUDY OF SMITH CREEK VALLEY, NEVADA

Alan T. Herring VI

AEROMAGNETIC SURVEY OF SMITH CREEK VALLEY, NEVADA

Iraj A. Salehi VII

SEISMIC REFRACTION STUDY OF FOURMILE FLAT, NEVADA

M. Darroll Wood VIII

BACKGROUND AND RESULTS

by

George A. Thompson
Principal Investigator

I. INTRODUCTION

We chose to study this tectonically active part of the Basin and Range province for two reasons. First, the origin and significance of block-fault depressions in the earth's crust is not fully understood. These depressions include the Rift Valleys of East Africa, the Central Rift of the mid-Atlantic Ridge and many others, all of which have fundamental similarities with each other and with the grabens of the Basin and Range province. All were formed in response to spreading, or pulling apart, of the shallow outer layers of the earth, a process that contrasts with, and may be complementary to, compressional deformation in folded and thrust faulted mountain belts. Second, one of the spreading oceanic ridges, the East Pacific Rise, projects into the North American continent, where characteristic features of the Rise are well represented in the Basin-Range structures. On land the opportunity is superb for exploring the detailed workings of this great structural system.

The Basin and Range province, characterized structurally by horsts, grabens and tilted blocks bounded by a pervasive system of Cenozoic normal faults, lies mainly between the Sierra Nevada on the west and the Wasatch Mountains on the east. The characteristic block faulting has a broader extent, however. Similar but more widely spaced faults cut the Colorado Plateau, Western Montana, eastern Oregon, westernmost Texas and a broad region of Mexico extending from the Gulf of California eastward roughly 500 miles are structurally similar. The active crest of the East Pacific Rise is generally thought to coincide with the Gulf of California. Not all of the region of Cenozoic block faulting is seismically active; a zone in Utah and the zone including Dixie Valley in western Nevada and eastern California are highly active.

Dixie Valley is unique in several ways. It had large earthquakes with surface faulting in 1903 and 1954 (see Fig 1 on p 2 Part I). It contains an enormous thickness of fill for so narrow a valley. Its topographic floor lies hundreds of feet below adjacent Carson Sink, dammed off by the narrow Stillwater Range. Moreover, the evidence is clear that the 1954 faulting was only the last in a long series of similar events that produced not only the relief of the present mountains and valley but a series of relief of even greater magnitude.

II. SCOPE AND METHODS

The Dixie Valley region is one of the most active parts of the Basin and Range province, and the geometrical and temporal relations here are critical in the larger picture of ridges and rifts; therefore we have tried to explore these relations by every available means, including seismic, gravity, magnetic, geomorphic and geodetic studies. The gravity work, sponsored by the U. S. Geological Survey, was not completed in time to include here. Gravity measurements first called attention to the great depth of fill in Dixie Valley (Thompson, 1959), and the later gravity work guided and verified the other geophysical investigations. No measurements of heat flow were included in our study, but we hope that the new knowledge of subsurface structure and geometry may make possible meaningful studies of local variations in heat flow. Our studies must be regarded as reconnaissance in nature, because the Dixie Valley region is very large.

III. RELATION TO MAJOR STRUCTURES

A. East Pacific Rise

Vine (1966) presented dramatic new evidence of rifting of oceanic ridges and spreading of ocean floors at rates of 1 to 5 cm/yr. One of these ridges, the East Pacific Rise (Fig.1), intersects the North American continent and may extend into the Basin and Range province (Heezen, 1960; Menard, 1960; Cook, 1966; Thompson, 1966), although Wilson (1965) and Hamilton and Myers (1966) prefer different interpretations. The principal structural similarities of the Basin and Range province with the Rise include (1) thin crust, (2) anomalous upper mantle, (3) volcanism and high heat flow, (4) shallow seismic activity, and (5) block faulting. Most of these extend over a broader region of western North America but the rift zone may be defined simply as the region of Cenozoic normal faults (Thompson, 1966); see Fig.2. According to Menard (1964), ridges and troughs, presumably resulting from normal faulting, are typical of the crest of the Mid-Atlantic Ridge and the flanks of the East Pacific Rise. Regardless of the exact course of the Rise in relation to the

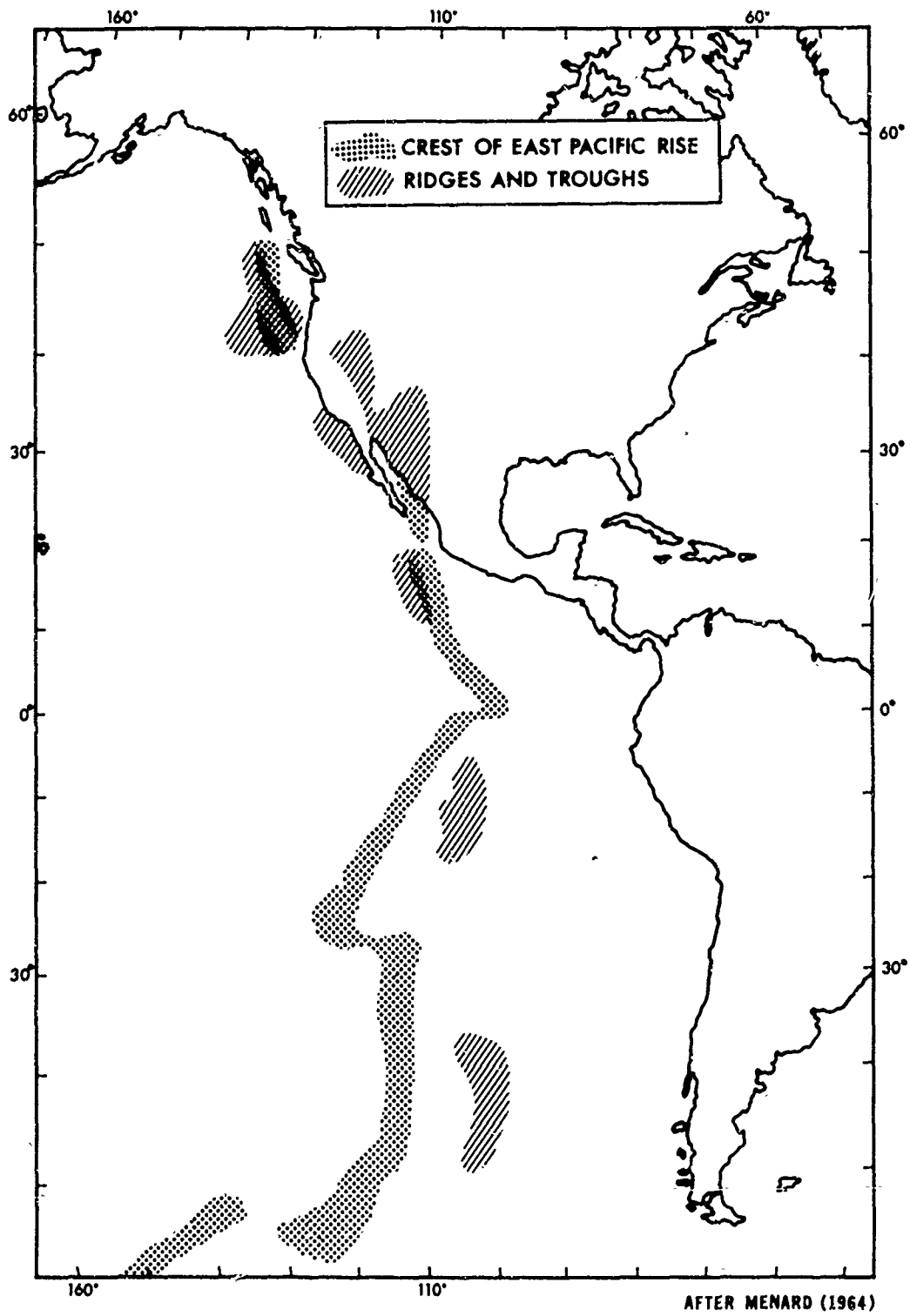
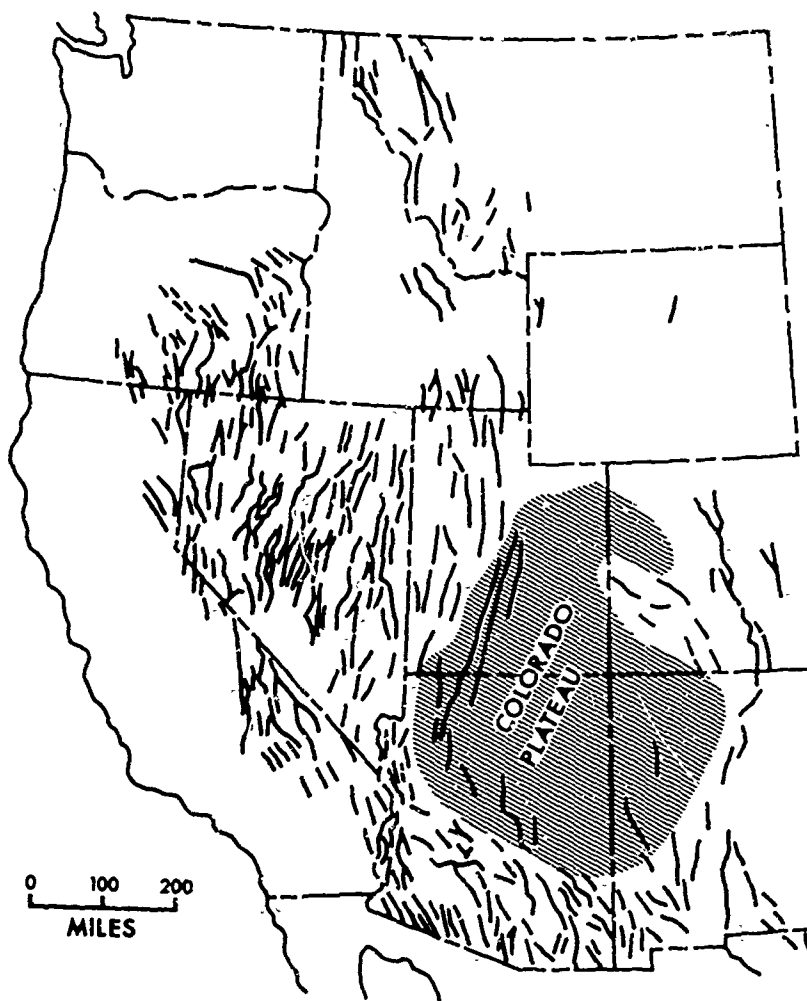


Fig.1 The East Pacific Rise, after Menard (1964).



FROM GILLULY (1963)

Fig.2 Cenozoic normal faults of western United States, from Gilluly (1963). The extent of normal faulting best defines the rift system.

continent and regardless of the complex shifting of the locus of activity during Cenozoic time, a common mechanism of lateral spreading focuses attention on the comparison of Basin and Range structure with the structure of the Rise.

B. San Andreas System

Various relationships of the Basin and Range system with the San Andreas fault system of California have been postulated. The most important similarity is a component of right lateral slip on several large faults in the Basin and Range province. These faults, such as the Las Vegas shear zone and the Walker Lane, trend northwestward subparallel with the San Andreas system and the Sierran front. Farther to the north and east, most of the Basin-Range faults trend more northerly, though the trends are quite variable, and large strike-slip offsets have not been demonstrated; dip slip is evident on many faults. In the 1954 faulting of the Dixie Valley area a component of right lateral slip was clearly evident to the south near Fairview Peak, and geodetic data indicate right lateral displacement in addition to dip slip in southern Dixie Valley. One of our major objectives was to assess the long term strike slip, if any, by geophysical measurements.

To the writer it appears that average directions of principal strains across the whole region including the San Andreas system and the Basin Ranges may be nearly constant, with the maximum principal extension oriented in the northwest quadrant and the other principal strain in the northeast quadrant. Near the San Andreas system, however, the principal compression is greater than the principal extension (demonstrated by folding and thrust faulting), whereas in the Basin Ranges the extension greatly exceeds the compression. In any such system all faults will have a component of strike-slip movement except those that are exactly parallel to a principal strain direction. In this view it is the average strains that are fundamental; secondarily the orientation of individual faults with respect to the strains determines slip directions on the faults. There can be little question that the strain in the vicinity of the San Andreas system is basically different from that in the Basin Ranges; one involves contraction of surface area, the other expansion of surface area.

IV. PRINCIPAL FINDINGS

A. Gravity

Although the gravity measurements are not included in the present report a brief statement may be useful. First, the gravity data accord well with the seismic refraction data, outlining the deep concealed trough beneath Dixie Valley and giving approximate depths to bedrock. Second, unexpectedly the gravity data indicate large structural basins extending into the mountain blocks. The best example is in the Clan Alpine Range at Horse Creek (Fig. 2 on p. 6, Part I). These basins, now completely filled with Cenozoic volcanic and sedimentary rocks, are, unlike the main valley, not reflected in topography. Hence they record a phase of Cenozoic structural deformation earlier than the present topography and the younger valley fill. The rocks that fill these basins probably are correlative with the deeper, higher velocity fill in Dixie Valley. Thus a picture emerges of shifting structural deformation over a considerable period of Cenozoic time but persistent sinking of the bedrock floor of Dixie Valley.

B. Inner Graben

A complex concealed inner graben was discovered and outlined in considerable detail by Meister's refraction seismic experiments. (See, for example, Fig. 10 on p. 35, Part I, and generalized section Fig. 5 on p. 22, Part IV). In the deepest part the graben contains more than 10,000 ft of Cenozoic deposits although it is only 5 mi wide. The asymmetrical topographic form of Dixie Valley is explained partly by the location of the inner trough near the west side of the valley (see Smith's interpretation of magnetic measurements, Fig. 4 on p. 16, Part III) rather than by block tilting alone. The nested "graben in graben" structure is lucidly represented in Fig. 6 of Burke (p. 23, part IV), who demonstrated that the bedrock faults usually remain intermittently active and can be detected as faint traces on the alluvial surface (Plate I, in pocket, Part IV).

C. Strike Slip

The question of large scale strike-slip faulting in Dixie Valley was raised by the 1954 faulting and by geodetic indications of a component of strike slip (Whitten, 1957). Smith (Part III) found that the magnetic gradients along the boundaries of a gabbro body could be traced across the valley. Their offset, if any, is in a right lateral sense and amounts to less than 2 mi (3 km) (Fig.1 on p.6 and Fig.3 on p.13, Part III).

Both Herring and Meister succeeded in obtaining side refractions from fault surfaces to depths of over 3000 ft (Fig.16 on p.46 and Fig.21 on p.66, Part I; Fig.10 on p.26, Part II). They thus determined the subsurface strike and dip of faults. Sharp bends in the strike of as much as 90° persist at depth and preclude large scale strike slip on these faults. Dip slip is predominant.

D. Transform Faults

The sharp bends in strike of faults noted in the preceding section may be compared with what Wilson (1965) on a large scale called transform faults. Sykes (1967) showed from seismic first-motion solutions that the displacements are consistent with Wilson's theory: dip-slip faulting along the crests of oceanic ridges and strike-slip faulting on the transverse zones (Fig.3). In a few places on the west side of Dixie Valley a strike-slip component of displacement is shown by inclined grooves on fault surfaces in hard rock. Both left-lateral and right-lateral components are evident on the appropriate segments of crooked faults. The writer has observed similar evidence on Basin-Range faults in west Texas (Yates and Thompson, 1959) and on the bounding faults of the Oslo graben in Norway (unpublished). Crooked faults with local strike-slip components of movement in both senses are probably very common or even characteristic of normal fault structures.

E. Dip and Depth of Intersection of Faults

Herring found from side refractions that the step faults on the west side of Dixie Valley dip 55° to 70° near Mud Springs (Fig.10 on p.26, Part II). Farther north Meister found dips of 35° and 45° based on a single-fault interpretation (Fig.16 on p.46, Part I); if step faults are assumed they would be steeper. The geophysical measurements are therefore consistent with

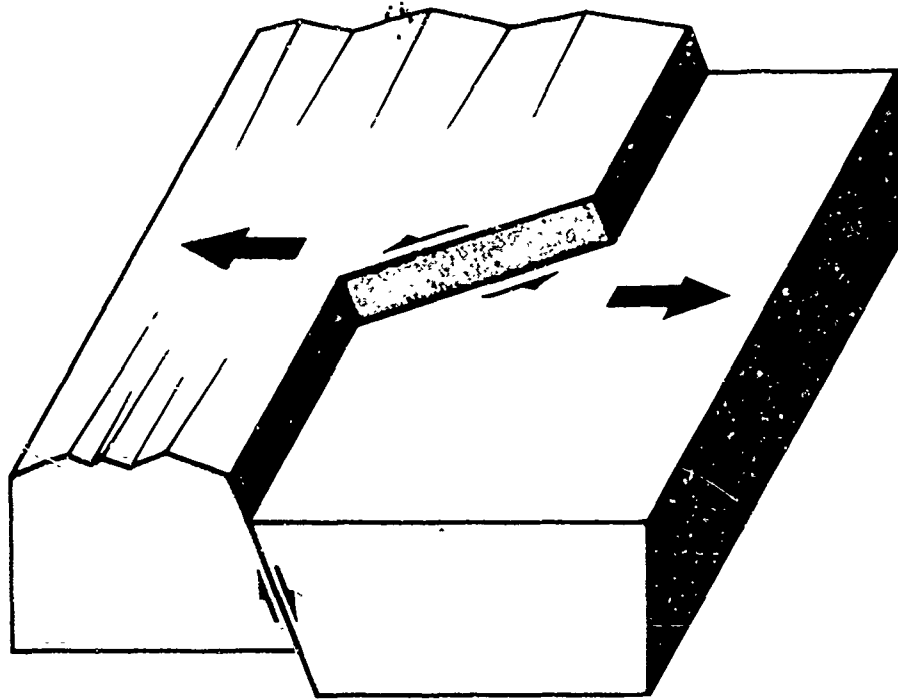


Fig.3 Diagrammatic representation of transform fault, showing identity with crooked normal fault.

outcrop evidence that the faults in bedrock dip about 60° . No evidence of flattening with depth can be discerned within the attainable precision of the seismic work.

The outer bounding faults of Dixie Valley intersect at a depth of about 11 mi (17 km) if a dip of 60° is maintained, and the inner graben faults intersect at 7 mi (11 km) or less (Fig.5 on p.22, Part IV). According to various alternative hypotheses the rocks deeper than 11 mi (less if the faults flatten) may be yielding more by ductile creep, or they may be spread apart by dike swarms, or the shallower rocks may be sliding on sub-horizontal surfaces. Either ductile spreading or dike spreading involve deep seated deformation, whereas horizontal sliding is superficial. Evison (1960), Moore (1960) and Hamilton and Myers (1966) are among those who have postulated superficial deformation. The present writer (Thompson, 1966) favors deeper seated deformation comparable to that envisioned for ocean ridges (Hess, 1965). Critical geophysical tests for possible dike intrusions, particularly by heat flow and magnetic measurements, need to be carried out.

F. Strain and Strain Energy

Geodetic observations before and after the 1954 faulting, converted to surface strain patterns (Fig.3 on p.9, Part V), show a predominant NW-SE extension across the faults and parallel contraction in adjacent areas. The strain changes thus indicate slow elastic stretching of the area in a NW-SE direction prior to the earthquakes and elastic rebound at the time of the earthquakes. The strain pattern also shows that the horizontal component of displacement perpendicular to the strike (the fault heave) on the average exceeds the strike-slip component; hence the dip-slip component on the 1954 faults, which dip about 60° , must be more than twice the strike-slip component.

If the thickness of strained crust is assumed, the changes in elevation can also be utilized and the volumetric dilatation computed (Fig.4 on p.10, Part V). With additional assumptions of elastic constants the strain energy is computed and found to be comparable to the energy derived from earthquake magnitudes. The gravitational potential energy of subsidence is greater than the total elastic energy, however; possibly it was not efficiently converted into seismic energy and was partly dissipated as a minor uplift (Poisson

bulge) in a broad region.

Although it is not possible to determine accurately the strains prior to the first geodetic surveys, Burke's mapping of the beach ridges of ancient Dixie Lake supplies a measure of tilting and offset in approximately the last 10,000 years. (Plate 2, in pocket, and Fig 2 on p.16, Part IV). A maximum of 14 ft of westward tilt was observed near the southern end of the former lake and 8 ft near the northern end. These values are no greater than longitudinal variations in elevation. It is suggested that the basin has been subsiding with little net tilting.

G. General

To extend the findings in Dixie Valley, Herring carried out seismic refraction work and Salehi made an aeromagnetic study of Smith Creek Valley, and Wood made seismic refraction studies of Fourmile Flat. (For location map see Fig.1 on p.2, Part I). Maximum depths to basement measured in Smith Creek Valley range from 6500 to 8000 ft, and concealed faults like those in Dixie Valley were discovered (see for example Fig.3 on p.7, Part VI). Salehi discovered strong magnetic anomalies in the western part of Smith Creek Valley, one of which evidently results from a reversely magnetized body (Fig.2 on p.7, Part VII). Whether some of the anomalies are caused by Cenozoic igneous rocks rather than pre-Cenozoic basement remains a problem.

At Fourmile Flat, Wood found units within the fill comparable to those in Dixie Valley. Basement, found at a maximum depth of 3500 ft, is overlain by a wedging unit of volcanic rocks or consolidated sediments (Fig.2 on p.3, Part VIII).

ACKNOWLEDGMENTS

The writer delegated a major share of responsibility for the Dixie Valley project to Laurent Meister, who energetically planned and coordinated the separate investigations. Mrs. Mary Dowden, with characteristic good-natured vigor, assisted in all phases of administration. Gerry Cabaniss of the Air Force Cambridge Research Laboratories expedited the study and participated in field work. Finally, Darroll and Deanna Wood generously took on the task of editing and reproducing the manuscript.

My warm thanks go to all of these people and to the many others acknowledged in each part of the report.

BIBLIOGRAPHY

- Cook, K.L., 1966, Rift system in the Basin and Range province, in The World Rift System; Geol.Surv.of Canada paper 66-14, pp. 246-279.
- Evison, F.F., 1960, On the growth of continents by plastic flow under gravity; Geoph.Jour.Royal Astron.Soc., Vol.3, pp.155-190.
- Gilluly, J., 1963, The tectonic evolution of the western United States; Quar.Jour.Geol.Soc.London, Vol.119, pp.133-174.
- Hamilton, W. and W.B.Myers, 1966, Cenozoic tectonics of the western United States; Reviews of Geophysics, Vol.4, pp.509-549.
- Hess, H.H., 1965, Mid-ocean ridges and tectonics of the sea-floor, in Submarine Geology and Geophysics, pp.317-332; Whittard, W.F. and R.Bradshaw, eds., Butterworth, London.
- Heezen, B.C., 1960, The rift in the ocean floor; Sci.American, Vol.203, pp.98-110.
- Menard, H.W., 1960, The East Pacific Rise; Science, Vol.132, pp.1737-1746.
- Menard, H.W., 1964, Marine Geology of the Pacific, McGraw-Hill, New York, 271 pp.
- Moore, J.G., 1960, Curvature of normal faults in the Basin and Range province of the western United States; U.S.Geol.Surv.Prof.Paper 400-B, pp.409-411.
- Sykes, L.R., 1967, Mechanism of earthquakes and nature of faulting on mid-ocean ridges; Jour.Geophys Res, Vol.72, pp.2131-2153.
- Thompson, G.A., 1959, Gravity measurements between Hazen and Austin, Nevada; a study of Basin-Range structure; Jour.Geophys.Res., Vol.64, pp.217-229.
- Thompson, G.A., 1966, The rift system of the western United States, in The World Rift System; Geol.Surv.of Canada paper 66-14, pp.280-290.
- Whitten, C.A., 1957, The Dixie Valley-Fairview Peak, Nevada, earthquake of December 16, 1954 - geodetic measurements; Bull.Seismol.Soc. Am., Vol.47, pp.321-325.

- Wilson, J.T., 1965. Transform faults, oceanic ridges and magnetic anomalies southwest of Vancouver Island; Science, Vol.150, pp.482-485.
- Vine, F.J., Spreading of the ocean floor: new evidence, 1966; Science, Vol.154, pp.1405-1415.
- Yates, R.G. and G.A.Thompson, 1959, Geology and quicksilver deposits of the Terlingua district, Texas; U.S.Geol.Surv.Prof.Paper 312, 114 pp.

PART I.

SEISMIC REFRACTION STUDY OF DIXIE VALLEY, NEVADA

by

Laurent J. Meister

ABSTRACT

Seismic refraction studies of Dixie Valley, Nevada, have revealed a buried complex of normal faults which form a long subsurface trough with a "graben in graben" structure. The inner graben, situated beneath the west side of the valley floor, narrows to five miles and contains an accumulation of sedimentary and volcanic deposits of Cenozoic age which reach a maximum thickness of 10,500 ft. The depth to bedrock in the outer graben along both sides of the narrow depression ranges from 1000 to 5000 ft. This basin structure indicates that Dixie Valley subsided along a complex system of step faults rather than along single boundary faults. Velocities ranging from 5000 to 8000 ft/sec are associated with unconsolidated to semi-consolidated clastic sediments of Pleistocene and Recent age. A seismic velocity boundary below which the velocity increases to an average of 10,000 ft/sec is characteristic of the entire Dixie Valley region; this higher velocity is correlated with volcanic rocks in the upper part of the Miocene to Pleistocene section that partly caps the Stillwater Range to the west. This boundary is found at depths ranging from 300 ft in the outer graben to 3500 ft in the inner graben. An average basement velocity of 16,000 ft/sec measured in the southern part of the valley is associated with limestones, slates and metavolcanic rocks exposed in the adjacent mountains, and with the granitic rocks that intruded this Mesozoic section. Farther north, velocities as high as 20,700 ft/sec are characteristic of gabbroic rocks included in a Jurassic complex that is exposed in the northern parts of the Stillwater and Clan Alpine ranges. A special study was made of side refractions in a reversed profile parallel to the outcropping fault zone bounding the Stillwater Range west of Humboldt Salt Marsh. The study shows that this fault zone dips 45° to the east, and its sharp changes in strike are conserved to a depth of at least 2500 ft. The geometric constraints of the fault pattern argue against large scale strike-slip faulting in Dixie Valley, and other geophysical evidence supports an interpretation of primarily dip-slip displacements. The average displacement rate during the life of the basin is on the order of one ft per thousand years.

ACKNOWLEDGEMENTS

The writer wishes to express his gratitude to Professor George A. Thompson for his supervision and guidance throughout this work.

Special thanks are due to L. C. Pakiser of the U. S. Geological Survey for the loan of a seismic recording truck during part of the summer of 1964.

Sincere appreciation is expressed to the late Professor Joshua L. Soske for his counsel, to Professor Benjamin M. Page for geologic information concerning the Stillwater Range, Nevada, and to Gerry H. Cabaniss, Air Force Cambridge Research Laboratories, for his cooperation throughout this project.

The writer is indebted to Alan T. Herring and Thomas E. Smith for assisting in the field and to the Chester B. Knittle family for providing food and lodging at the Crazy K Ranch.

This report is based on a Ph.D. thesis submitted to the Department of Geophysics, Stanford University.

TABLE OF CONTENTS

	<u>Page</u>
ABSTRACTiii
ACKNOWLEDGEMENTS	v
TABLE OF CONTENTSvii
LIST OF ILLUSTRATIONS	ix
LIST OF TABLES	xi

Chapter

I. INTRODUCTION	1
A. Introduction and Purpose	1
B. Previous Work	3
C. Field Work	3
II. GEOLOGIC SETTING	5
A. Physiography	5
B. Major Rock Units	5
C. Major Faulting of the Stillwater Range	9
III. SEISMIC REFRACTION INVESTIGATION RELATING TO HYDROLOGY . .	11
A. Instrumentation and Field Procedure	11
B. Interpretation of the Measurements and Conclusions . .	11
IV. FIELD PROCEDURE FOR DEEP SEISMIC REFRACTION STUDY	19
A. Instrumentation	19
B. Seismic Energy Sources	19
V. SEISMIC REFLECTION RESULTS	22
VI. REDUCTION OF DATA AND INTERPRETATION	23

<u>Chapter</u>	<u>Page</u>
VII. ANALYSIS OF SEISMIC PROFILES	25
Profile 1: West Road	25
Profile 2: Central Road	28
Profile 3: IXL Canyon	30
Profile 4: Crazy K Ranch	32
Profile 5: Dixie	34
Profile 6: Dixie Meadows	36
Profile 7: East Road	38
Profile 8: Horse Creek	38
Profile 9: Pirouette Mountain	41
Profile 10: Salt Marsh	43
Profile 11: Bernice Canyon	47
Profile 12: Seven Devils	49
Profile 13: Boyer Ranch	52
Profile 14: Hyder Springs	54
VIII. CORRELATION OF SEISMIC VELOCITIES WITH STRATIGRAPHY .	57
A. In Situ Velocity Measurements	57
B. Correlation of Seismic Velocities with Stratigraphy	60
IX. STRUCTURAL IMPLICATIONS	65
X. CONCLUSIONS	68
BIBLIOGRAPHY	70

LIST OF ILLUSTRATIONS

FIGURE	TITLE	PAGE
1.	Location Map. Historical faults of 1903 and later are shown. After Slemmons (1957).	2
2.	Geological Map showing locations of seismic profiles.	6
3.	Locations of seismic profiles shot for the investigation of the water table.	17
4.	Position of the water table below the surface of the alluvial fan east of IXL Canyon.	18
5.	Total charge required for good record quality as a function of distance between shot and end of seismic spread.	21
6.	Time-distance curves and cross-section of the West Road Profile.	26
7.	Time-distance curves and cross-section of the Central Road Profile.	29
8.	Time-distance curves and cross-section of the IXL Canyon Profile.	31
9.	Time-distance curves and cross-section of the Crazy K Ranch Profile.	33
10.	Time-distance curves and cross-section of the Dixie Profile.	35
11.	Time-distance curves and cross-section of the Dixie Meadows Profile.	37
12.	Time-distance curves and cross-section of the East Road Profile.	39
13.	Time-distance curves and cross-section of the Horse Creek Profile.	40
14.	Time-distance curves and cross-section of the Pirouette Mountain Profile.	42
15.	Time-distance curves and cross-section of the Salt Marsh Profile.	44

FIGURE	TITLE	PAGE
16.	Detailed Map showing the layout of the Salt Marsh Profile and the Dixie Meadows Profile.	46
17.	Time-distance curves and cross-section of the Bernice Canyon Profile.	48
18.	Time-distance curves and cross-section of the Seven Devils Profile.	50
19.	Time-distance curves and cross-section of the Boyer Ranch Profile.	53
20.	Time-distance curves and cross-section of the Hyder Springs Profile.	55
21.	East-West cross-section along Mud Springs Road.	66

LIST OF TABLES

TABLE	TITLE	PAGE
1.	Seismic data related to the study of the water table.	13
2.	Seismic data related to the study of the water table.	15
3.	Summary of seismic velocities and layer thicknesses.	58
4.	Estimated maximum dilatational wave velocities in Pliocene (?) water-saturated non-marine sediments.	61

I. INTRODUCTION

A. Introduction and Purpose

The Basin and Range Province of the western United States may be viewed as part of the worldwide rift system which lies mainly along ocean ridges (Menard, 1964). Deep seismic exploration in the western United States has revealed that the earth's crust is unexpectedly thin and the upper mantle velocity is anomalously low (Pakiser and Steinhart, 1964). This unusual property, associated with others such as regional Cenozoic volcanism and high heat flow, match the characteristics of the ocean ridges. Gravity measurements in the same area show that the Basin and Range Province is in regional isostatic balance and that great thicknesses of Cenozoic sediments fill the basins (Thompson, 1959).

However, little is known of the internal structure and rates of deformation of these deeply alluviated basins. Seismic exploration, combined with aeromagnetic and gravity surveys, has been needed to establish the detailed internal structure of a typical rift valley. Measurements of the depth and attitude of the deeply buried surface of pre-Tertiary rocks and of the layers within the valley fill may in turn reveal the pattern of faulting and the history of subsidence which can be related to the surrounding geologic features. The conclusions of such a study may be helpful in understanding the rifting mechanisms in the African rifts, the Oslo and Rhine grabens, and the oceanic rift zones.

Dixie Valley, which is located in west central Nevada, was chosen for this study because it lies along the most active seismic belt in the Basin and Range Province. Large earthquakes accompanied by displacements of the ground surface occurred in 1903, 1915, and 1954. The epicenters of these shocks and the historical faults are shown in Figure 1 (Slemmons, 1957). The strike-slip component of the 1954 faults is often invoked in recent literature as evidence of strike-slip fault control of Basin-Range structure. (Shawe, 1965). The detailed study of the geometry of the western side of Dixie Valley presented in this report has a strong bearing on this theory.

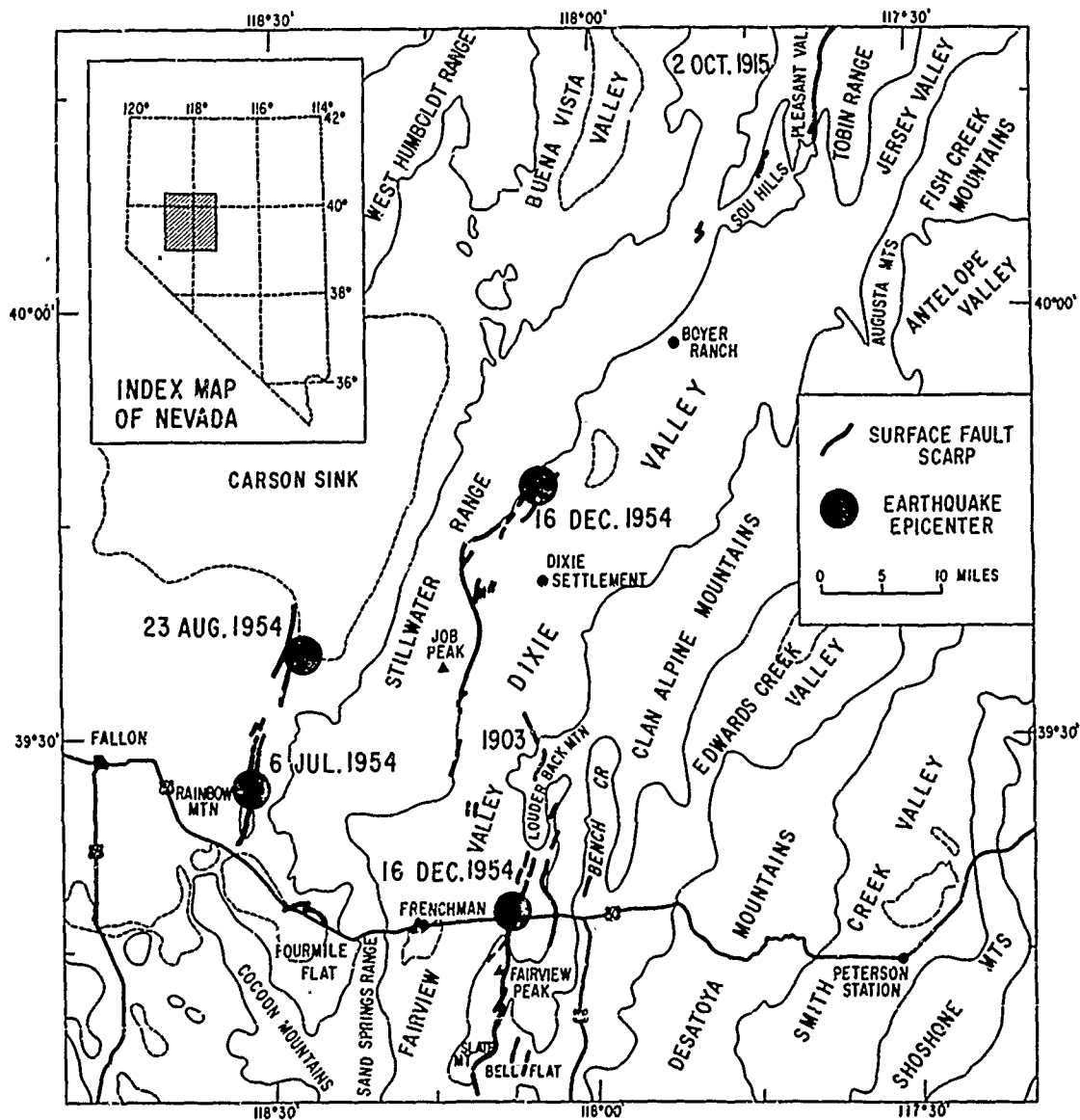


Figure 1. Location Map. Historical faults of 1903 and later are shown. After Slemmons (1957).

Moreover, the seismic velocities measured during this study will be useful for velocity calibration of microearthquake monitoring stations which are operating in the area (Ryall, oral communication, 1966).

B. Previous Work

Earlier published work in the Dixie Valley-Carson Sink region has been primarily of a geologic nature, the subsurface studies being limited to hydrologic investigation from shallow well data (Cohen et al., 1963). The stratigraphy and structure of the extreme north end of the project area have been discussed by Muller and others (1951). Most useful to the present project has been the recent mapping of the Stillwater Range and parts of the West Humboldt and Clan Alpine Ranges by Page (1965) and Speed (1963).

Geophysical work in and near the area under study consists of a reconnaissance gravity survey along U. S. Highway 50 between Hazen and Austin and across the Stillwater Range west of Dixie Settlement (Thompson, 1959), a recent gravity survey of the Carson Sink-West Humboldt region (Wahl, 1965), and a complete geological-geophysical investigation of the Sand Springs Range-Fairview Valley-Fourmile Flat area to the south of the present project (University of Nevada, 1962).

To supplement the present seismic work, an aeromagnetic survey of the Dixie Valley-Carson Sink area (Smith, 1965) and a study of side refractions at Mud Springs (Herring, 1966) were made. An extensive gravity survey of the Dixie Valley-Fairview Valley area is in progress (Thompson, 1966).

C. Field Work

The seismic refraction survey of Dixie Valley was undertaken during the summers of 1964 and 1965. Because of the lack of access roads, it was generally impossible to select locations which would yield the most nearly ideal information for the seismic profiles. The geometric requirement of extending each profile to obtain reversed apparent velocities was not possible in the east-west direction because of the narrow width of the valley. North of Dixie Settlement, the central part of the basin was inaccessible because the sticky-wet surface near and on the Humboldt Salt Marsh would not support vehicles. Consequently most of the seismic lines were

located along both sides of the valley far enough from the mountain fronts to avoid side refraction.

During the 1965 field season numerous cloudbursts inundated the central part of the valley, washing out most of the roads and creating serious delays in the field work.

It was possible to shoot large explosive charges in the air because the population is sparse throughout the project area.

II. GEOLOGIC SETTING

A. Physiography

The Dixie Valley area displays typical physiographic features of the Basin and Range Province i.e., elongated north to northeast-trending mountain ranges separated by narrow valleys. The ranges bordering Dixie Valley--the Stillwater to the west and Clan Alpine to the east--are deeply dissected, complex fault-block mountains rising as much as 5,000 ft above neighboring valleys (Fig. 2). The mountains are generally bounded by steeply-dipping north to northeast-trending normal faults.

The mountain ranges in the project area are flanked by broad alluvial fans which slope gently toward the valley floor, the lowest area of which is occupied by the Humboldt Salt Marsh. The generalized geological map shown in Figure 2 outlines the structural elements of the area. Most of the information used in the following description was taken from the geologic map of part of the Stillwater Range published by Page (1965).

B. Major Rock Units

1. Triassic Rocks: The most important rock unit in the central map area is a large expanse of gray-black slate and phyllite. Slaty cleavage throughout this unit generally parallels bedding except near axial parts of folds where it approaches the axial plane. For the most part, only incipient recrystallization is evident; however, near granitic contacts, andalusite has been observed (Page, 1965).

Complex deformation of the unit prohibits direct measurement of the slate-phyllite-limestone sequence, but Page estimates its thickness as 5000 to 10,000 ft, of which only about 10% is metaquartzite and limestone.

Fossil identification has placed the age of this unit as Late Triassic.

A large body of allochthonous black to gray Upper Triassic limestone is present in the southern part of the project area. Fossil evidence indicates this unit is of the same age as the Upper Triassic slate upon which it rests, implying significant lateral transport of rocks formed in a different sedimentary environment. Triassic limestone is also present in the

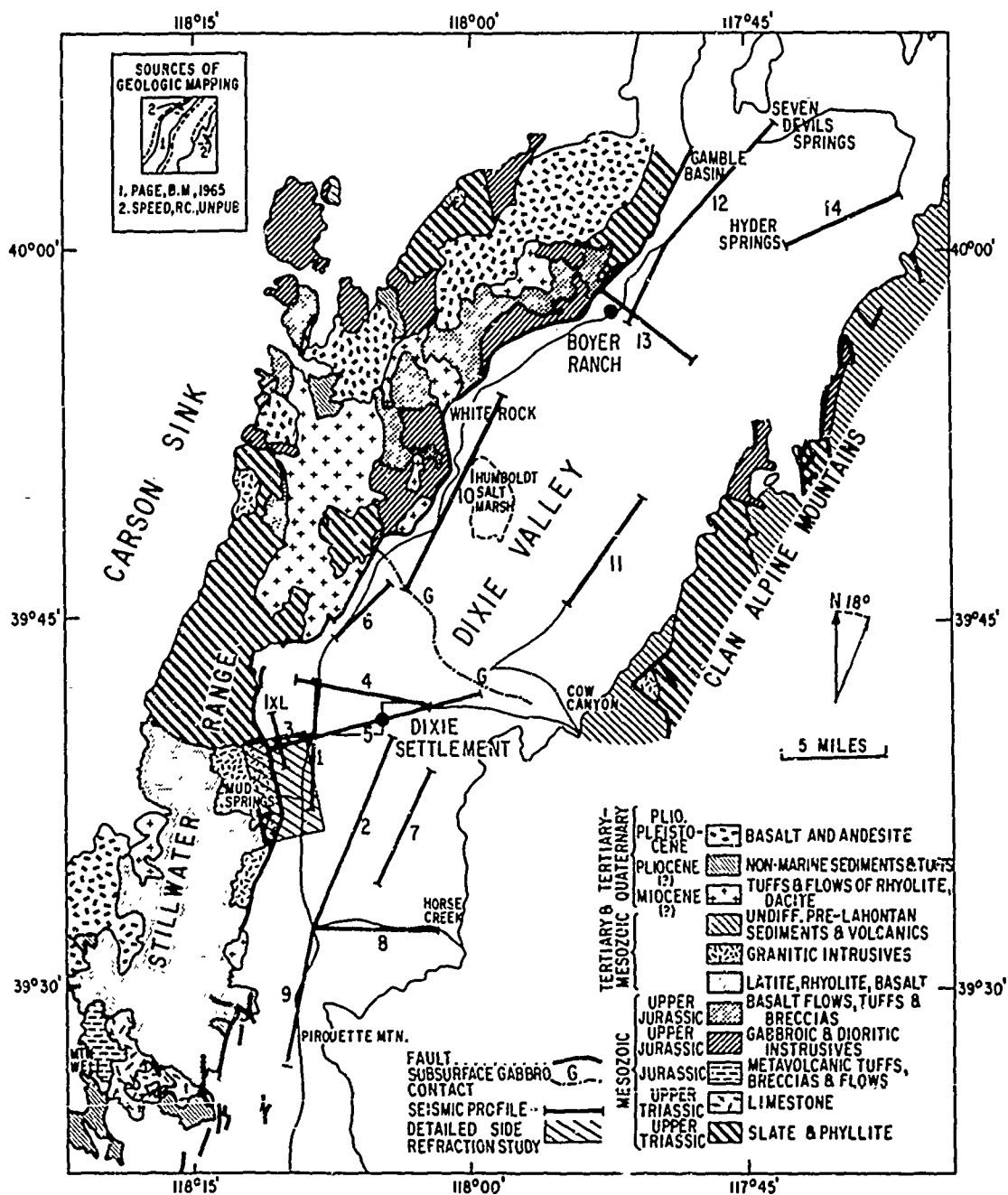


Figure 2. Geological Map showing locations of seismic profiles.

northern part of the Stillwater Range a few miles north of Boyer Ranch in thrust contact with the Triassic slates, the slates forming the upper plate and the limestones the lower one (Speed, written communication, 1966).

2. Jurassic Rocks: Bordering the Triassic limestone to the west in the southern end of the Stillwater Range is a sequence of altered and locally schistose metavolcanic rocks. They consist mainly of the fine-grained slaty andesitic tuffs, breccias, thin andesitic flows, quartzite, and calcareous sandstones. The volcanics are almost completely altered, but display certain relict textures. The sedimentary rocks are better preserved and unfossiliferous. This unit is in excess of 5000 ft thick, rests unconformably upon the allochthonous Triassic limestone and is thought to have been transported in as part of the La Plata thrust sheet (Page, 1965).

Of great importance to the present seismic study is the Humboldt Gabbroic Complex which covers large areas in the northern part of the Stillwater, Clan Alpine, and West Humboldt Ranges. One part of this unit is composed of extensive basalt flows, lapilli tuffs, and breccias. Alteration is common, epidote and chlorite imparting a distinct green color. Normally associated with the Upper Jurassic gabbroic intrusions, these rocks are quite possibly contemporaneous with and may represent an extrusive equivalent of the gabbro.

The intrusive rocks of the gabbroic complex are represented by a large, seemingly tabular complex of gabbroic and dioritic intrusions. These rocks form an igneous unit which includes hornblende gabbro, diorite, anorthosite, keratophyre, and gabbroic pegmatite. Distinct layering is evident in the earlier parts of the suite along intrusive margins. This unit has been carefully studied by Speed who considers it to have been emplaced at very shallow depths, in places penetrating to the surface and forming the extrusive basalts discussed earlier. A potassium-argon date from the West Humboldt Range indicates an age of about 140 million years, placing it chronologically in Late Jurassic time. Profound alteration including albitization and dolomitization is common in this unit. The gabbroic complex was mapped as two distinct units in Figure 2: the extrusive rocks as basalt flows, tuffs, and breccias, and the intrusive rocks as gabbroic and dioritic intrusives.

3. Tertiary and Mesozoic Rocks: In the area of the Stillwater Range near Mud Springs and to the south, blue-gray weathered latite is abundant. Some of the latite shows fine flow layering. Rhyolitic tuffs and latite breccias are locally present with the flows. Exposed sections of the unit show a thickness of 2000 to 6000 ft. Near intrusive contacts with Oligocene or Lower Miocene granite, recrystallization and darkening are common.

Farther south, much of the exposed rock consists of devitrified welded tuff whose composition probably ranges from latite through silica-rich rhyolite. Curiously resembling porphyries, these gray to brown weathered rocks are extremely competent. Megascopically, only the presence of angular lithic fragments of Triassic slate, latite, and other volcanics attests to the pyroclastic origin of the unit. This entire sequence, varying in thickness from 2000 ft to possibly 10,000 ft, rests unconformably on Upper Triassic slate and limestone and on Jurassic meta-volcanics. Along the east side of the Stillwater Range, the devitrified tuff has been intruded by Miocene or Oligocene granitic rocks and white felsite dikes.

A third unit of extrusive and intrusive rocks is grouped under the same heading. The intrusive rocks of this group are represented by basaltic andesites that invade the devitrified welded tuff and older formations near the center of the Stillwater Range. Extrusives of similar composition totaling about 8000 ft in thickness are exposed west of IXL Canyon. The latter three groups of rocks are mapped as a latite-rhyolite-basalt unit (Fig. 2).

Scattered plutons of Late Cretaceous or Tertiary granite, quartz monzonite, and granodiorite are exposed near the center of the map area. The latter two intrude latite and devitrified tuff near Job Peak, where they form a composite unit consisting of several successive intrusions. A potassium-argon date on biotite from the granodiorite in IXL Canyon indicates an age of about 28 million years. These rocks are mapped as granitic intrusives in Figure 2.

4. Rocks Younger than the Granitic Plutons: Capping much of the Stillwater Range is a sequence of post-granitic Miocene (?) volcanics including tuffs, breccias, and flows which vary in composition from latites through dacites and rhyolites. Intensive local alteration is common, although the silicic members retain fresh biotite and glass. Dissection has exposed only 1800 ft; however, total thicknesses may be on the order of 3000 to 4000 ft. These rocks are grouped under the heading: Tuffs and Flows of Rhyolite, Dacite. In other parts of the area, rocks belonging to this unit are included within the undifferentiated pre-Lahontan sediments and volcanics (Fig. 2).

Pliocene (?) sediments and tuffs cover a minor part of the map area; they are prevalent only in the southern Stillwater Range, where a sequence of 1500 ft is exposed in dissected pediment slopes and low hills. Of lacustrine and fluvial origin and locally including ash beds, this unit is probably equivalent to the Truckee Formation farther to the west.

In places overlying the Pliocene (?) sediments and other earlier units along the length of the Stillwater Range are flows of olivine basalt, and basaltic andesite. Individual flows vary in thickness from 20 to 100 ft, although locally aggregate thicknesses of 1600 ft have been noted.

5. Late Cenozoic Lake Sediments: The late Cenozoic valleys of the Basin-Range Province contain great thicknesses of essentially unconsolidated lake and stream sediments. These range in age from Plio-Pleistocene to Recent and include alluvial fan detritus, stream channel deposits, and lacustrine sediments. The latter consist for the most part of silt and clay, although shoreline deposits of gravel and sand exist locally.

C. Major Faulting of the Stillwater Range

1. Thrust Faults: An apparent structural base of the Triassic slate is exposed in the central part of the Stillwater Range. There, a shale member of the slate rests discordantly on quartzite, and a distinct zone of brecciated shale defines the contact. South of Cox Canyon, the quartzite overrides Jurassic (?) metavolcanics which in turn are thrust upon an undated limestone. Apparently, these units form a section of an imbricate thrust zone. Page (1965) suggests that this zone may underlie all slates of the Stillwater Range.

North of Dixie Meadows, another thrust fault structurally higher than the previous zone is apparent. It is well exposed in Cottonwood Canyon near Boyer Ranch where quartzite of unknown age and Late Jurassic gabbroic rocks have overridden Upper Triassic slate. Speed and Page (1964) have suggested that the shallow intrusion of the molten gabbroic complex may have propelled the thrust sheet. The gabbroic rocks of the upper plate extend across the entire northern end of the region, covering an area of about 500 square miles. The Late Jurassic date of the gabbroic rocks implies a similar age for the thrusting.

2. Cenozoic Faulting: Typical of late Basin-Range structure, the Stillwater Range is essentially an uplifted horst of narrow, elongate, north-trending blocks separated by Cenozoic normal faults. Deformation of the Plio-Pleistocene basalts attests that some tilting accompanied block faulting, but these tilted flows rarely dip more than 12° . In some cases, normal faults interior to the range become the bordering fault where they extend to the range margins.

III. SEISMIC REFRACTION INVESTIGATION RELATING TO HYDROLOGY

The superficial sedimentary materials in Dixie Valley range from the poorly sorted debris of the high alluvial fans to the silts and clays of the Humboldt Salt Marsh; therefore, it is logical to expect large lateral variations in seismic velocity of the shallow, low-velocity zone. The thickness of this uppermost layer, which lies above the water table, was determined from the shallow well data in the central part of the valley (Cohen and Everett, 1963); but had to be investigated by seismic refraction on the alluvial fans. A detailed study of the velocity distribution in the near surface material was made on the alluvial fan west of Dixie Settlement and on most of the refraction profile sites.

A. Instrumentation and Field Procedure

A GT-2 Interval Timer built by the Geo Space Electrodynamic Corporation was used for this shallow refraction investigation. The instrument is carried in a suitcase and records on Polaroid film. The recording time is limited to 0.4 second. We used six channels; the geophones were fixed on a line at 50-ft intervals. This enables us to use a maximum spread length of 250 ft. The largest offset of the shot point with respect to the spread was 500 ft. Small charges ranging from 1/4 to 1 lb of 40% dynamite were used as sources of seismic energy. The charges were placed at a depth of one foot.

B. Interpretation of the Measurements and Conclusions

A total of 25 seismic profiles were recorded with the GT-2 Interval Timer. Six of these seismic lines were reversed. All data related to this investigation are summarized in Table 1. All apparent velocities that cannot be associated with reversed data are assumed to be true velocities and are used as such in the interpretation.

The first linear segments of the travel-time curves of eight of the long refraction lines recorded with the SIE seismic system (Chapter VII) represent velocities lower than 4500 ft/sec. These velocities are listed in the V_0 column of Table 2.

The V_{oo} and V_o velocity layers form the "weathered" zone above the V_1 velocity layer which was associated with the water table. The reversed velocity which corresponds to V_1 is listed in the V_1' column (Table 1).

H_1 is the depth of the recorded refractor V_1 and was computed from the observed velocities by the conventional intercept-time method. In general a two-layer interpretation was made. Along two profiles, three different velocities were observed and an intermediate depth H_o to the top of the second layer was computed.

When the velocity V_{oo} of the upper layer was not observed, a velocity listed in the V_{oo} column was assumed. Each of these assumed velocities is shown in parentheses in Table 1. A three-layer interpretation was then made, which yielded a depth H_v to the top of the V_1 velocity layer (Table 1).

If the intermediate velocity V_o was not observed, its presence was assumed as a blind zone and another depth H_B was computed to the upper boundary of the V_1 velocity zone. The assumed velocity in parentheses in column V_o and the nomograms of Hawkins and Maggs (1961) were used for the interpretation. The nomograms yield, in terms of the calculated depth H_1 , the thickness of the blind zone and the depth H_o to the top of the blind zone. Comparison of H_1 , H_v , and H_B shows the range of uncertainty in the determination of the depth of the V_1 velocity layer.

The velocities in column V_{oo} range from 1000 to 1300 ft/sec; they are associated with the aerated sands and gravels which form the surface of the ground. The thickness of this surface layer varies from a few feet in the central part of the valley to about twenty feet on the high alluvial fans. For IXL-5 profile, an abnormally high thickness of 47 ft was found indicating that large lateral variations in thickness of the surface layer exist within the alluvial fans.

V_o includes velocities ranging from 1700 to 3300 ft/sec. This intermediate layer is probably composed of the same material as the superficial layer but may be more consolidated. It is well developed on the alluvial fans.

TABLE 1
SEISMIC DATA RELATED TO THE STUDY OF THE WATER TABLE

Profile	Location	Elevation (ft)	Velocities (ft/sec)				Depths (ft)			
			V _{oo}	V _o	V ₁	V ₁ '	H ₁	H _B	H _V	H _O
1	NW of Dixie Settlement	3400	1100	(2500)	5000	5250	6	8		5
2	NW of Dixie Settlement	3400	1250	(2500)	4750		4	5		3
3	NW of Dixie Settlement	3400	1100	(2100)	4000		6	7		4
4	NW of Dixie Settlement	3420	1100	2850	5880		15			5
5	SW of Salt Marsh	3380	1000	(2500)	4000	3320	3	4		3
6	SW of Salt Marsh	3380	1000	(2500)	4500		3	4		3
7	Alluvial Fan SW of Salt Marsh	3500	(1100)	2100	4550				64	2
8	Alluvial Fan SW of Salt Marsh	3500	(1100)	1850	5900				63	1
9	Low Alluvial Fan SW of Salt Marsh	3420	1150	(2100)	7150		34	45		22

TABLE 1 (continued)

Profile	Location	Elevation (ft)	V _{oo}	V _o	V _l (ft/sec)	V _l '	H _l	H _E	H _V	H _O
10	Low Alluvial Fan SW of Salt Marsh	3420	1050	(2100)	5900		29	39		20
11	East of Mud Springs	3520	1100	1700	5000		45	*41		14
12	W of Dixie Settlement	3450	1200	(2000)	5250		24	31		16
13	W of Dixie Settlement	3840	1250	(2500)	5000		30	49	*28	17
14	W of Dixie Settlement	3840	1000	(1850)	5400		21	33		11
15	E of Salt Marsh	3670	(1250)	3300	5000		*128		107	11
16	W of Cow Canyon	3450	(1250)	2200	4350				51	2
17	Cow Canyon	3680	(1250)	2800	5550	5550			135	23
18	SW of Cow Canyon	3600	(1250)	2400	7700				82	11
19	SW of Cow Canyon	3580	(1100)	2400	5000	5400			70	4
20	IXL-1	3490	1300	(2300)	5250	5250	34	44		23
21	IXL-2	3510	(1300)	2350	6250	6250			71	1
22	IXL-3	3550	(1300)	1750	5900				64	1
23	IXL-4	3600	(1300)	2300	5900				103	4
24	IXL-5	3660	(1300)	2950	4550				117	47
25	IXL-6	3850	(1300)	2800	5000				146	23

*Depth from Well Data

TABLE 2
SEISMIC DATA RELATED TO THE STUDY OF THE WATER TABLE

PROFILE	LOCATION	ELEVATION (ft)	V_c (ft/sec)	V_1 (ft/sec)	H_1 (ft)
8	HORSE CREEK	4400	2000	4600	40
9	PIROUETTE MOUNTAIN	3870	2000	4500	100
12	SEVEN DEVILS	3500	2500	5700	70
13	BOYER RANCH	3435	2000	5400	18
14	HYDER SPRINGS	3600	3000	6000	150
3	IXL CANYON	3850	2500	5000	130
A10	NW OF SALT MARSH	3750	2300	5000	100
E51	IXL CANYON STUDY	4010	2350	5000	150

The velocities in column V_1 , ranging from 4000 to 7150 ft/sec, are related to unconsolidated, water-saturated sediments. The top of this velocity layer is correlated with the water table; therefore H_1 , H_B , and H_V can be considered as depths to the water table at the profile location. As the composition of the clastic deposits below the water table may vary from clays and silts in the central part of the valley to gravel and sands on the alluvial fans, a wide range of velocities can be expected for the V_1 layer.

Along three profiles, velocities higher than 6000 ft/sec were measured. These velocities probably represent horizons below the water table which are partially cemented. The water table was a blind zone and could not be observed. Three refraction lines were shot close to water wells. The depths computed from seismic data agree within 10% with the depths to the water table measured in these wells (Table 1).

Figure 3 shows the locations of the profiles and the depths H_1 , H_B or H_V to the water table determined by seismic refraction.

An E-W cross-section of the alluvial fan in front of IXL Canyon shows very clearly the near-parallelism of the surface of the ground and the water table (Fig. 4). The attitude of the water table was deduced from 9 N-S refraction profiles shot along this cross-section.

In conclusion, it should be noted that the GT-2 Interval Timer proved to be very efficient for such a seismic investigation because it permitted the rapid collection of a large amount of information on the general attitude of the water table in Dixie Valley.

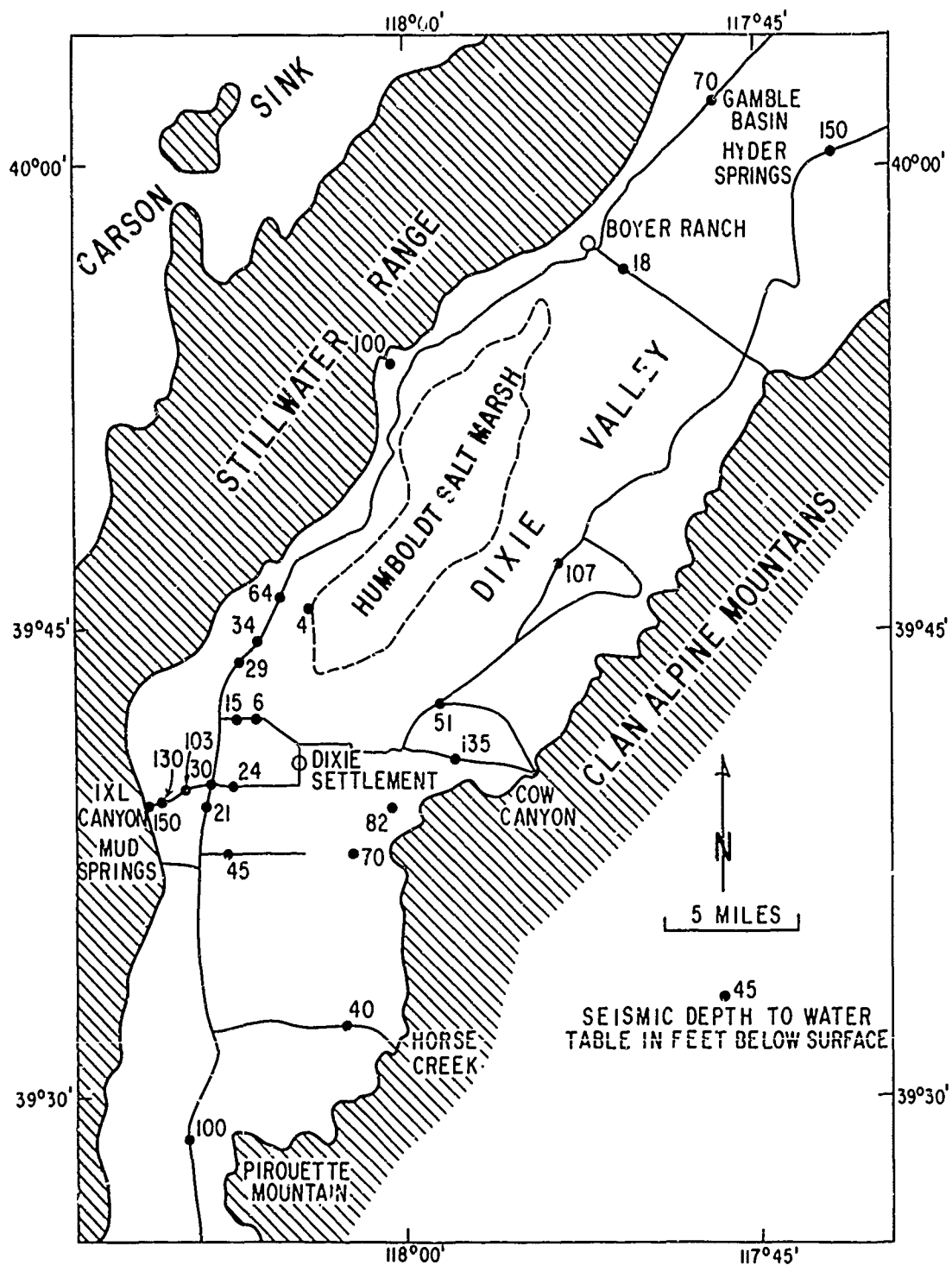


Figure 3. Locations of seismic profiles shot for the investigation of the water table.

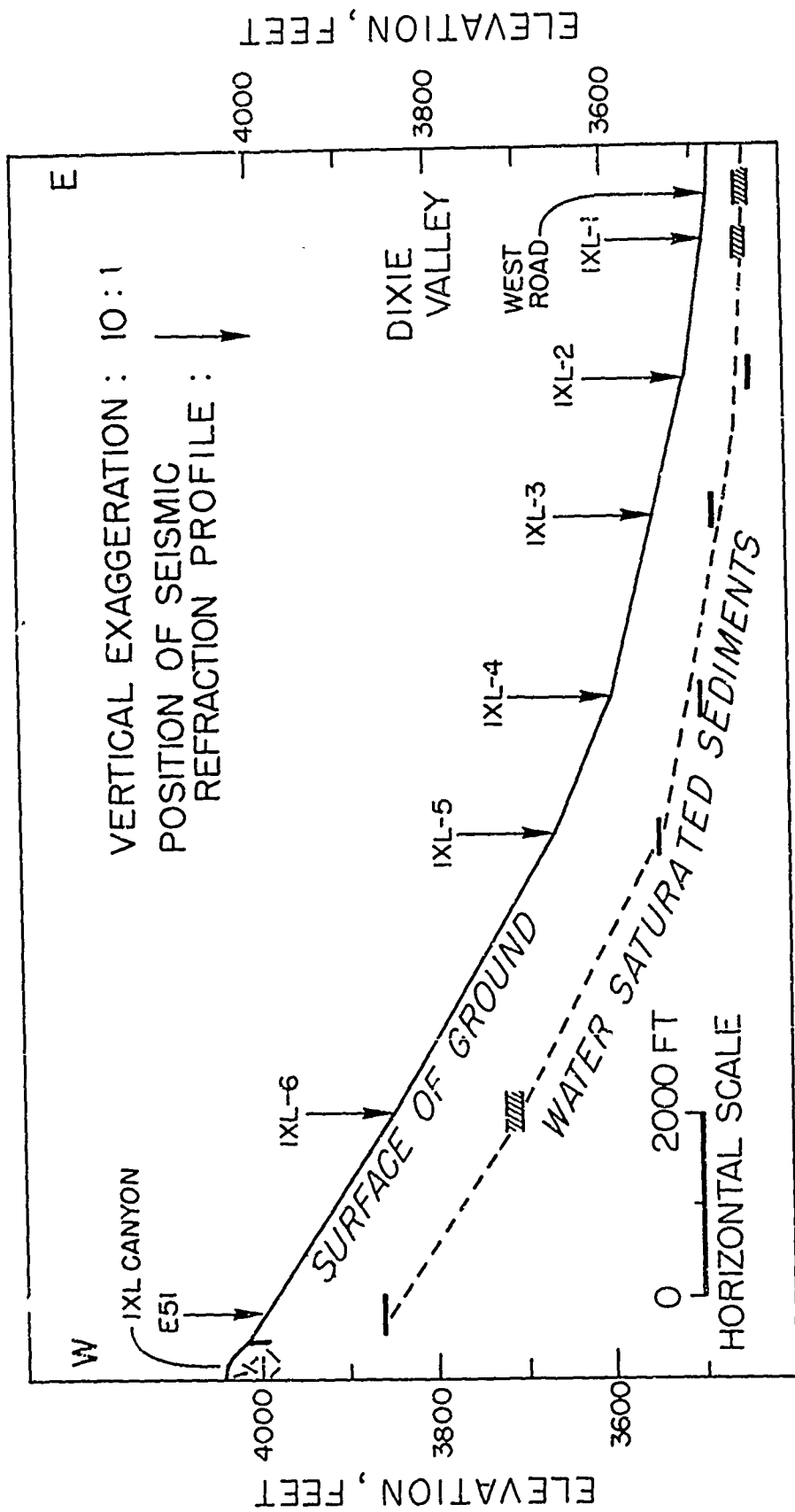


Figure 4. Position of the water table below the surface of the alluvial fan east of IXL Canyon.

IV. FIELD PROCEDURE FOR DEEP SEISMIC REFRACTION STUDY

A. Instrumentation

Four of the fourteen seismic refraction profiles recorded in Dixie Valley, were set up in an east-west direction, transverse to the topographic outline of the valley, and the others in a northeast direction (Fig. 2).

During the summer of 1964 two recording units were used. One was a six-channel 7000 B seismic system manufactured by Texas Instruments, Inc. with 4.5 cps geophones from Hall Sears, Inc. This unit was loaned by L. C. Pakiser of the U. S. Geological Survey. The spread used with this unit was 8200 ft long. The second unit consisted of twelve-channel amplifiers made by Southwestern Industrial Electronics (Model GA-33D) and geophones having a natural frequency of 4.5 cps from Hall Sears, Inc. This SIE recording unit was used with 2200 to 4600 ft spreads.

The recording instrumentation used during the 1965 field season consisted of a 24-channel amplified unit (Model GA-33D) made by the Southwestern Industrial Electronics Company and a 4600-ft spread composed of 24 geophones having a natural frequency of one or two cps from Hall Sears, Inc.

The latter recording setup proved to be the most efficient for our reconnaissance survey.

Radio transceivers manufactured by the General Radio-Telephone Company (Model VS-4) were used for communication and transmission of the shot instant. Shot times were estimated to have an accuracy of ± 0.002 sec for close shots and ± 0.005 sec for distant shots.

B. Seismic Energy Sources

Two types of explosive were used during the field work: Giant Petrogel (60% gelatin dynamite) in 1964 and Nitramon S-EL manufactured by Dupont de Nemours and Co. in 1965.

In order to get the maximum possible information in areas where drilling conditions were poor, shots in hot springs and in the air were used as means of converting energy to seismic waves. Shot holes drilled by hand or dug with shovels were not efficient.

Twenty-one shot holes were drilled with a rotary drill in the central part of the valley where the water table was near the surface. The drilling was easy but the use of drilling mud was necessary to prevent cave-ins. These shot holes, from 25 to 100 ft deep, provided excellent energy coupling and were used as many as three times. They were located at both ends of the longest profiles where suspended shots would have a poor shot efficiency. Charges up to 130 lbs were required for these distant shots. Those shots in hot springs were fired under 5 to 30 ft of water and had a good energy coupling.

An attempt was made during the first field season to obtain information on the attitude of the bedrock under the high alluvial fans near the mountain fronts. Shots were fired in 20-ft holes drilled in bedrock and recorded in the valley at distances of 2000 to 15,000 ft. The efficiency of these shots was very poor.

Since it is impossible to obtain a satisfactory shot hole in the poorly sorted debris and large boulders of the high and low alluvial fans, air shooting, a technique adopted by Buffet and Layat (1960) for refraction work in the Sahara, was used extensively. Buffet and Layat studied the influence of different parameters on the shot efficiency for small (less than 50 lbs) suspended charges. Their conclusions were extended to total charges as high as 180 lbs, and the following shot pattern was adopted: an individual charge of 20 lbs was fixed on a wood lath at the top of a 7-ft high steel post. For large shots, the 20-lb charges were positioned approximately 50 ft from each other in triangular or hexagonal patterns, similar to those used by T. C. Poulter (1950).

Air shooting was also successfully used in the central part of the valley at all shot points whose distances from the spread were less than 14,000 ft, and on the west side of the Humboldt Salt Marsh where the ground surface could not support drilling equipment. In the latter area, good first breaks from air shots with offset distances as great as 29,000 ft from both sides of the spread were recorded. Figure 5 shows how the total charge size of air shots was increased as the shot point was moved away from the end of the spread.

Energy coupling was better on the salt marsh, where the water table was near the surface, than on the high alluvial fans. This observation may be specific to the area under consideration, since Buffet and Layat (1960) observed the opposite in the Sahara.

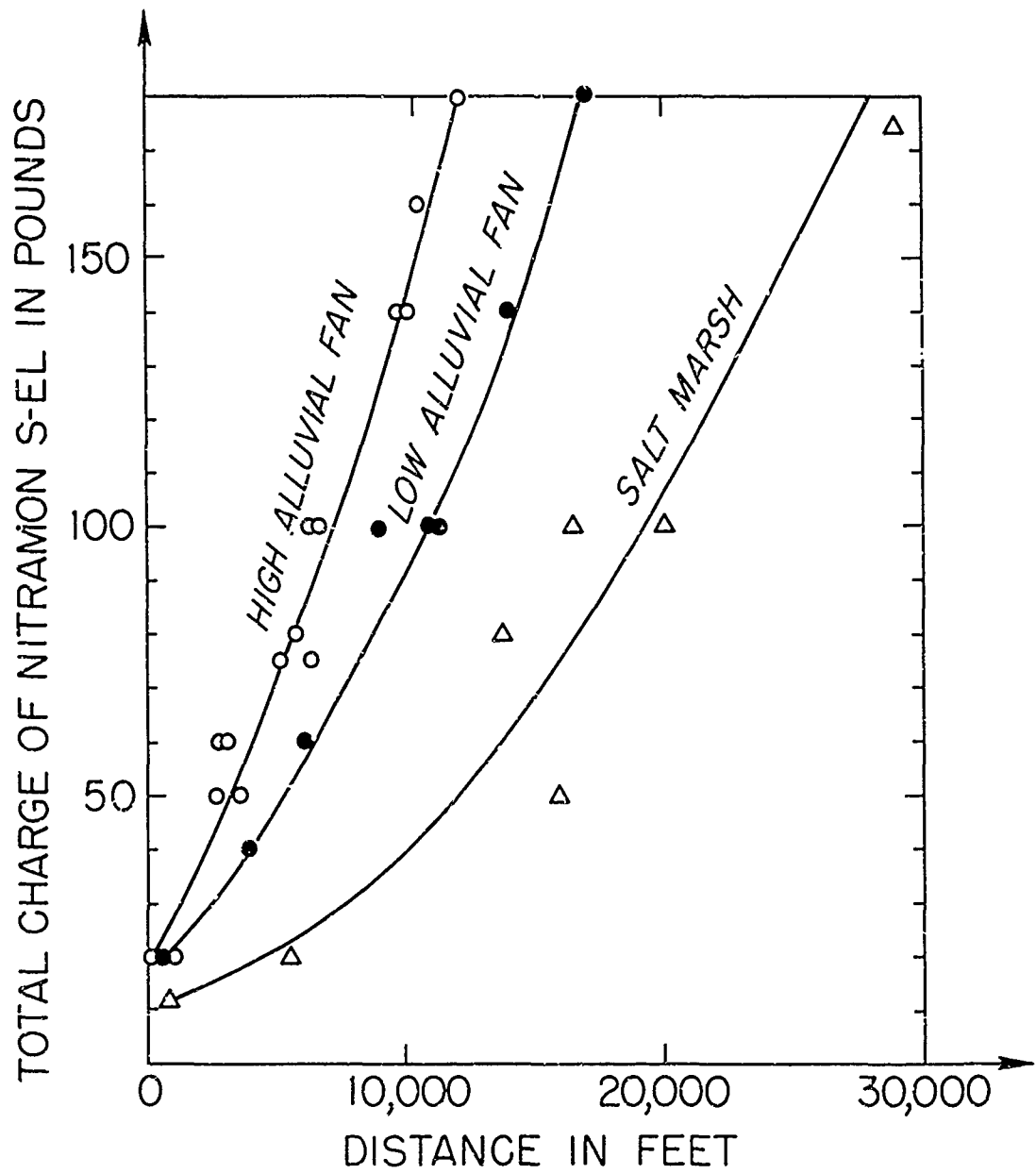


Figure 5. Total charge required for good record quality as a function of distance between shot and end of seismic spread.

V. SEISMIC RELECTION RESULTS

At the beginning of the 1964 field season an evaluation of the reflection technique was attempted in an area three miles east of the west end of profile 4 (Fig. 9), where the water table was shallow and the basement was expected to be deep. Ten-foot holes were drilled with a hand auger and small charges were used. The recording instrument was the 12-channel SIE seismic system with 35 cps geophones.

The only good and consistent events observed arrived at about 0.680 sec. This reflection corresponds to a horizon 2200 ft deep associated with the shallowest volcanic flow of the upper part of the Miocene to Pleistocene section. The fact that this horizon is situated at about the same depth as the 10,000 ft/sec velocity zone of profile 4, may confirm the assumption made later in this study that the apparent velocity of 13,000 ft/sec observed in this area by refraction is due to an east sloping 10,000 ft/sec velocity zone.

A combination of reflection and refraction techniques was also tried during the 1964 field season. Each time a shot was fired in one of the six 50-ft shot holes drilled in the center of the valley; two units were recording. The 12-channel SIE seismic system, set up near the shot point, recorded possible reflections from horizons deeper than the volcanic flows; the 6-channel 7000 B seismic system, located some distance away from the shot point, recorded energy refracted from some horizon inside the sedimentary section. Charges as heavy as 50 lbs were fired, but no coherent event which could be correlated with a bedrock reflection was recognized.

It is concluded that larger charges of explosives in deeper holes or complicated patterns of suspended shots are needed in order to by-pass the volcanic flows and record reflections from the basement.

VI. REDUCTION OF DATA AND INTERPRETATION

The method of refraction profiling which proved to be efficient for previous reconnaissances of basin structures (Pakiser, Press, and Kane, 1960; Kane and Pakiser, 1961; Pakiser and Kane, 1963; Kovach, Allen, and Press, 1962; Zbur, 1963; Healy and Press, 1964) was used. The geophone spread was held fixed and the shot points were moved away from both ends of the spread to distances as great as 30,000 ft.

The seismic velocity layering beneath the geophone spread was determined with this technique by applying the usual assumptions pertinent to seismic refraction computations. In order to extend this information along the entire profile the following additional assumption was made: when the same apparent velocity of first arrivals across the spread came from two successive shots situated on the same side of the spread, it was assumed that the seismic energy was refracted from the same interface below the spread. As the Miocene to Pleistocene section is composed of numerous volcanic flows interbedded in non-marine sediments such a hypothesis may be unlikely and furthermore numerous small velocity reversals may be present. Nevertheless it is the only way one can obtain additional control on the depths and attitudes of the different velocity layers between the spread and the different shot points.

The apparent velocities observed from shots lying on one side of the spread were associated with reversed apparent velocities obtained from shots fired on the other side of the spread to give a true velocity section beneath the spread. When a new velocity zone was observed a corresponding average depth was computed by the conventional intercept time method (Nettleton, 1940). This depth was assigned to the part of the profile between the spread and the shot point and is called the normal depth.

If the same apparent velocity was observed from a more distance shot-point the geophone delay time corresponding to the normal depth previously determined was subtracted from the new intercept time to yield a shot point delay time. For conversion of this last delay time into depth, the velocity layering above the refractor at the shot point had to be known. The velocity layering under the spread was assumed to be continuous under the entire profile, unless additional information on the shot point area was available from another profile.

The position and depth of the refractor corresponding to a given delay time is represented on each seismic cross-section by a short line without continuity, since the information is valid only at this point. All dashed lines on the sections represent velocity layering assumptions. When velocity reversals are expected in the sedimentary section the range of uncertainty of the position of the basement is represented by shaded zones on the seismic cross-sections.

The preceding conclusions are well-grounded only if there are no horizontal velocity variations along the refractor.

Depths to seismic discontinuities along the profile can also be obtained by making use of the reciprocity principle (Ewing et al., 1937, Dix, 1952 p. 263). The apparent velocity measured for a given layer at the spread is compared with the apparent velocity obtained by plotting a travel time curve for which the shot points whose energy was refracted from this layer are considered as geophone locations and one of the geophones of the spread becomes the shot point. This last apparent velocity indicates the average dip of the interface between the two shot points. From the normal depth obtained at the shot point which is close to the spread, it is possible to compute a depth for the other shot point. Although the two methods are equivalent, the first has been used during the present study because no reciprocity principle must be assumed in its application.

The accuracy of the seismic refraction method has been studied in detail by Steinhart and Meyer (1961). They showed that it is difficult to obtain estimates of uncertainty for refraction depth calculations and even when obtained, these estimates may be suspect.

The interpretation of the data as presented in the following study is not unique and the model chosen to fit each set of travel time curves represents the simplest solution consistent with the seismic data and geology.

VII. ANALYSIS OF SEISMIC PROFILES

The location of the seismic profiles is shown on the geologic map (Fig. 2).

The major graben structures were initially assumed to be parallel to the physiographic trend of the valley with a corresponding thickening of the sedimentary section toward the center of the valley. Therefore it was considered illogical to make a classical interpretation of any transverse profile because of the lateral changes in velocity layering. Accordingly, three profiles were shot in a NNE-SSW direction (profiles 1-3) where only small lateral velocity changes were expected. This information was carried over to two sub-parallel transverse profiles (profiles 4 and 5). By delay time analysis, the transverse structure of the valley under Dixie Settlement was then determined.

Similarly, the information from profile 12, shot between Seven Devils and Boyer Ranch, was used for the analysis of the Boyer Ranch profile shot across the west side of the valley.

PROFILE 1: West Road Profile

The West Road profile was shot in a north-south direction on the west side of the valley along the main road of Dixie Valley. Recordings were made on three 4600-ft geophone spreads. The only air shots along this profile were S4 and S2; two shots were fired in most of the drilled holes. The travel-time curves and the seismic cross-section corresponding to the West Road profile are shown in Fig. 6.

All times were corrected to a 3500-ft datum. The superficial velocity of 5200 ft/sec was taken from Table 1 and corresponds to that measured in sediments lying below the water table.

Below the 6300 ft/sec layer an 8000 ft/sec layer was observed which was based on distinct breaks in the travel time curve. The horizontality and continuity to the south of the 10,000 ft/sec layer are controlled by the two geophone setups B9 and B11. It is assumed that this layer is also continuous to the north. The two apparent velocities 14,000 ft/sec and 17,000 ft/sec recorded on spread B9 from shot points N3 and N4 respectively

were correlated as down-dip and up-dip velocities of the bedrock with a calculated true velocity of 15,400 ft/sec.

The arrival times from the common shot point N3, which show an apparent speed of 14,000 ft/sec, on spread B11 line up with those of the wave refracted from the basement on spread B9. This alignment of arrival times proves that the basement can be represented between B9 and B11 by a plane dipping 4 degrees to the south. The normal depth to bedrock was computed using formulas for a dipping layer for the part of the profile between spread B11 and shot point N2.

The apparent speed of 16,600 ft/sec observed across spread B10 and the corresponding geophone delay time, show that the attitude of the basement between shot points N2 and N3 is in continuity with the one deduced from the observations made on spreads B6 and B11. The apparent velocity of 23,000 ft/sec which was observed across spread B11 was associated with a change in dip of the basement.

The seismic energy of shot S4 is believed to have been laterally refracted from bedrock at the Stillwater Range which is only 6000 ft west of the southern end of the profile. The information obtained from this shot completes the detailed study of Herring (1966) and determines the attitude of the basement at the eastern side of the cross-section shown in Fig. 21.

The line at the bottom of the shaded zone on Fig. 6 is the position of the pre-Tertiary bedrock as computed on the assumption that the 10,000 ft/sec layer continues downward to the 15,400 ft/sec basement. If the 10,000 ft/sec layer is only a thin high-velocity zone within the 8000 ft/sec layer, the basement could be as shallow as the top of the shaded zone. Since a 13,000 to 14,000 ft/sec layer was observed to exist between the 10,000 ft/sec layer and the basement in several places in the valley, a similar layer may exist along this profile as a blind zone. If that is the case, the calculated depth to the 15,400 ft/sec layer would be increased. The uniform velocity of 10,000 ft/sec assigned to the layer just above the basement can therefore be regarded as an average for a heterogeneous sedimentary section containing small velocity reversals and high velocity blind zones. Consequently the dark line on Figure 6 and on all following cross-sections represents the most reasonable attitude of the pre-Tertiary bedrock.

PROFILE 2: Central Road Profile

Seismic profile 2 (Fig. 7) was shot along a NNE-SSW trending road in the central part of the valley just south of Dixie Settlement. We recorded on a 4600-ft spread; shots N4 and S5 were fired in drilled holes; the other shots, in the air.

A water table velocity of 5000 ft/sec was assumed in order to compute a depth for the 6400 ft/sec velocity layer using intercept times at shot points S1 and N1. A velocity of 8600 ft/sec for the third layer was computed from the two apparent velocities, 8700 ft/sec and 8500 ft/sec.

The slight northward dip of the 8600 ft/sec interface under the spread is consistent with an abrupt increase in shot point delay time between N2 and N3, which was interpreted as a down-drop of the 8600 ft/sec velocity boundary and a consequent thickening of the 6400 ft/sec layer.

Constant thickness was assumed for the 8600 ft/sec layer under both shot point and spread, in order to calculate depths to the 10,000 ft/sec layer from the intercept time of the corresponding segment of the time-distance curve at shot point N3. This layer is a blind zone for the refracted arrivals from shot point S3.

The depth to the 16,000 ft/sec bedrock was computed from the intercept time at shot point S3.

The 25 msec offsets in the basement arrivals from shot points S4 and S5 were associated with a fault which uplifts the southern bedrock block about 350 ft. Depths to basement at shot points S4 and N4 were computed assuming continuity of the 10,000 ft/sec velocity layer from S1 to S4 and from N3 to N4 respectively. If the 10,000 ft/sec velocity layer proved to be thin, the basement would be about 500 ft shallower.

The apparent velocities observed along profiles 8 and 9 show a velocity layer between the 10,000 ft/sec layer and the basement. From the information of profile 8 and with the assumption of a true speed of 13,000 ft/sec, this layer should be about 4900 ft deep at the south end of profile 2. This information was carried over to the latter profile and yielded a maximum depth to bedrock of 6600 ft near shot point S5 (lower boundary of the shaded area in Fig. 7).

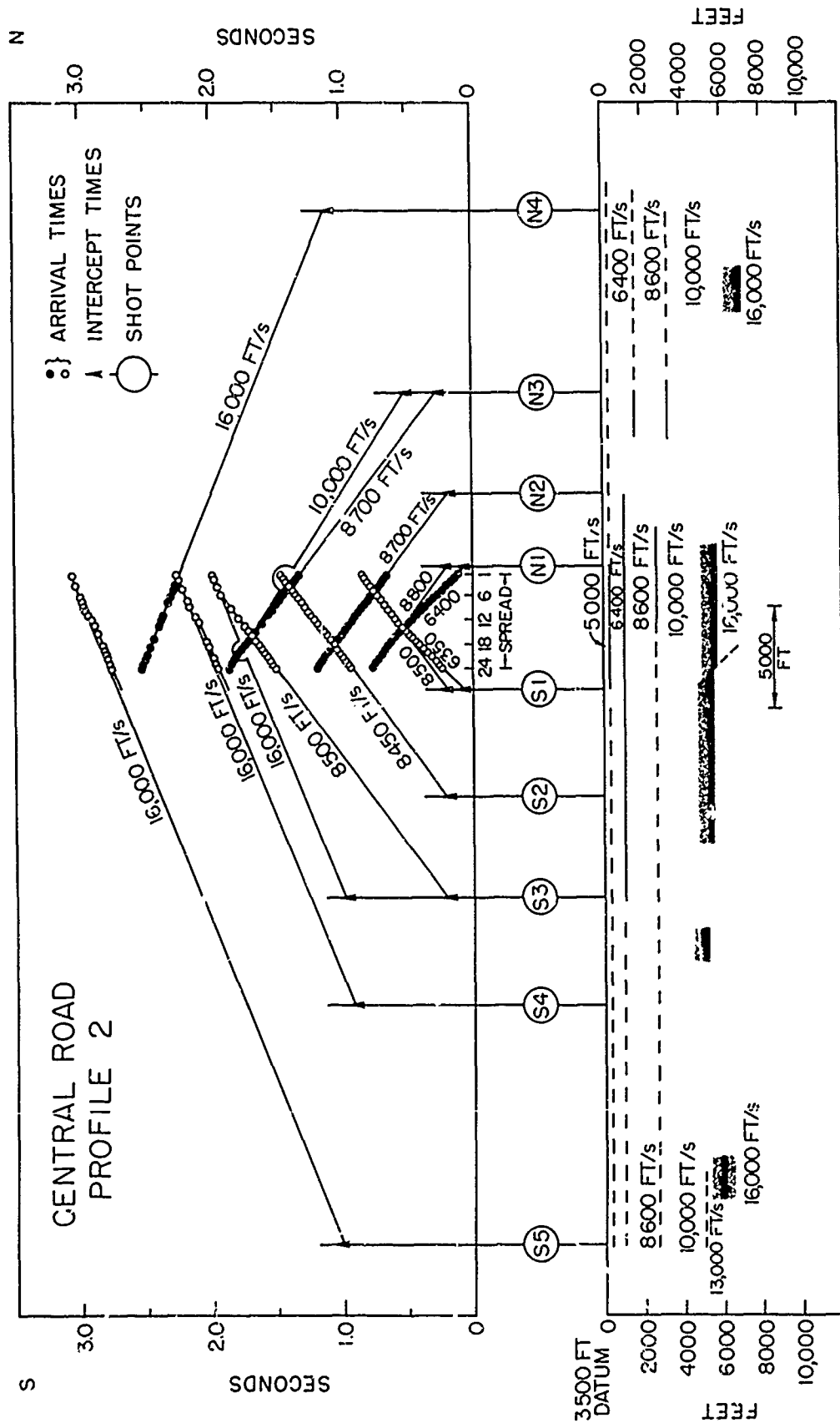


Figure 7. Time-distance curves and cross-section of the Central Road Profile.

PROFILE 3: IXL Canyon Profile

The main purpose of the IXL Canyon profile (Fig.8) was to test the efficiency of the air shooting technique on high alluvial fans. The profile was shot in a N-S direction one-half mile east from the mouth of IXL Canyon. The total length of this refraction line was 14,000 ft and the maximum average velocity observed was 11,300 ft/sec. No basement arrivals were recorded along the 2200 ft spread.

The gradual increase in velocity with depth from 5000 ft/sec to 11,300 ft/sec was conventionally interpreted as two velocity layers of 8000 ft/sec and 9300 ft/sec. The normal depth to the 11,300 ft/sec velocity boundary was computed from the intercept time at shot point N3. From the shot point delay times associated with the shots N4, N5, and S4 we deduced a down-drop of the 11,300 ft/sec horizon in the northern part of the profile and a rise of this same velocity boundary at the southern end of the profile.

The only control on superficial layering along the refraction lines of this entire study was obtained under the geophone spreads and this information was extrapolated to the entire profile. Any change in shot point delay time was then associated with a change in basement depth. But the profile 3 data show the existence of important structural features in velocity boundaries within the Cenozoic sedimentary section.

Therefore, with the assumption of continuity of these horizons, false structures may have been introduced in the basement. Consequently the structures of the 11,300 ft/sec horizon along this profile could also have been exaggerated by the assumption of continuity of the 5000 and 8000 ft/sec velocity layers.

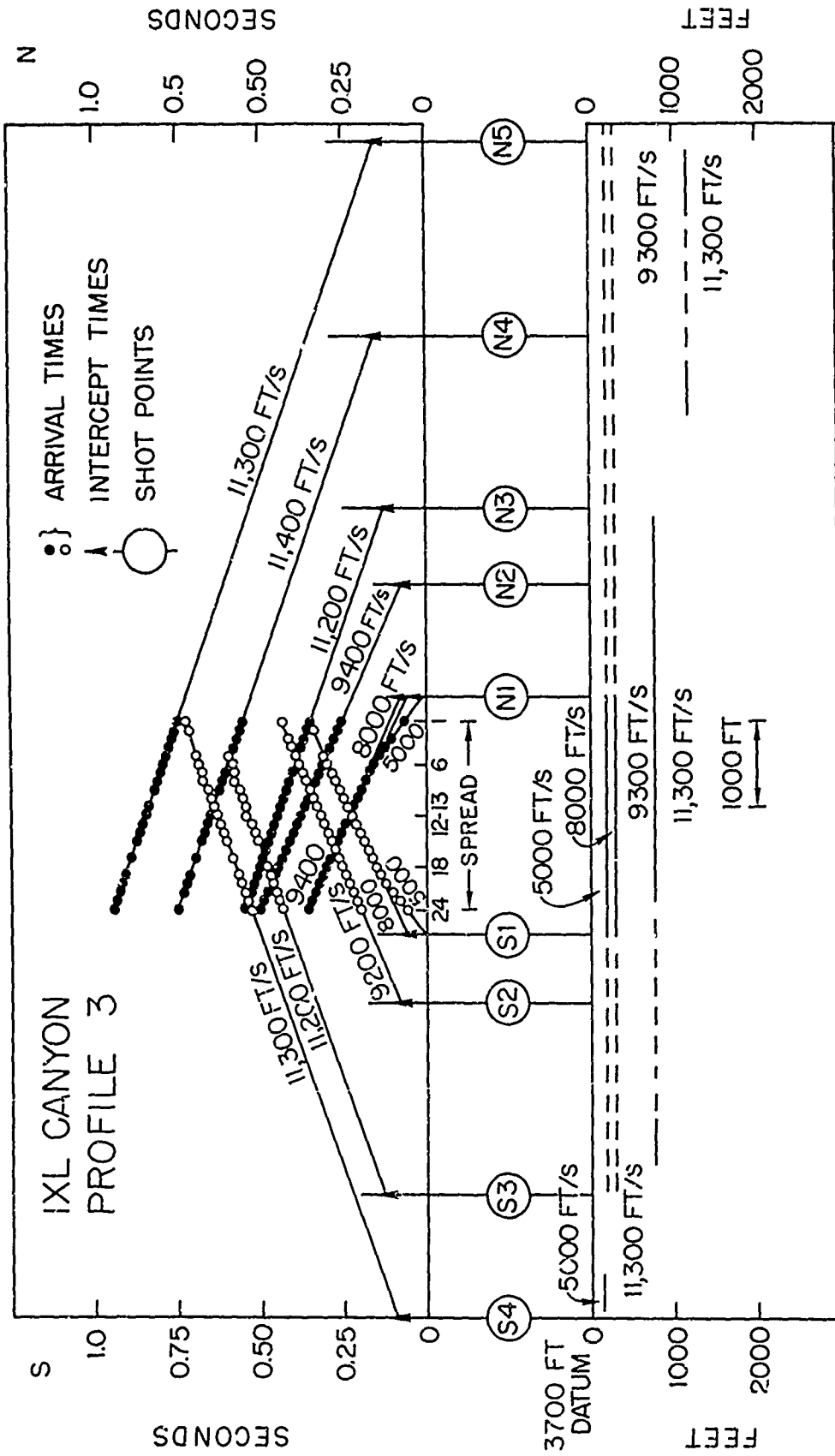


Figure 8. Time-distance curves and cross-section of the IXL Canyon Profile.

PROFILE 4: Crazy K Ranch Profile

Profiles 4 and 5 are the two E-W trending refraction lines across Dixie Settlement. They have shot point DP in common. The western end of profile 4 crosses the West Road profile at the northern end of spread B10, and the western end of profile 5 intersects the same line at shot point N1. The travel time curves for both profiles were corrected to allow for the slight offset of the shot points with respect to the general direction of the profiles.

The Crazy K Ranch profile (Fig. 9) consists of four individual spreads. On each setup energy arrivals were recorded from shots fired at point DP. All data were corrected to a 3500 ft datum. The superficial velocity of 5000 ft/sec represents an average of all speeds measured near Dixie Settlement in connection with the hydrogeologic study. In making the calculations it was assumed that this velocity is constant along the profile.

The depth to the 6000 ft/sec velocity layer determined under spread D3 was extended to the east. The apparent velocity of 8300 ft/sec measured along the D3 geophone setup was associated with a horizontal velocity layer whose lower boundary extended to the west to shot point CR. The 8500 ft/sec segment recorded on spread A105 from shot point 4 was correlated (profile 5) as an apparent up-dip velocity, with the 11,500 ft/sec layer dipping 10° to the west. This interpretation was preferred, primarily on geologic grounds, to the alternate interpretation based on the assumption that the apparent velocities were true velocities of horizontal layers.

The information obtained in the northern part of the West Road profile was carried over under spread B14. The 10,000 ft/sec segment recorded along B14 from shot point CR was assumed to be refracted from the 10,000 ft/sec velocity layer determined under spread B9 of the West Road profile. By subtracting the corresponding geophone delay time from the intercept time at shot point CR, the depth to the 10,000 ft/sec boundary under shot point CR was obtained.

The 13,000 ft/sec apparent velocity recorded along spreads A26 and A34 from shot point DP can be interpreted as a down-dip velocity of a west-dipping basement, as a true velocity of a horizontal velocity layer, or as

Figure 9. Time-distance curves and cross-section of the Crazy K Ranch Profile.

an up-dip velocity of a 10,500 ft/sec layer. The latter alternative seems to be the most probable since similar apparent velocities were recorded along the west side of profile 5 where a deepening of the 10,000 ft/sec horizon was observed from the data of profiles 1 and 3. All reflections obtained east of Crazy K Ranch came from the top of the 10,000 ft/sec velocity layer (Fig. 9).

The sole arrivals refracted from the basement were recorded along spread B14 from shot point DP. The apparent velocity of 20,000 ft/sec was associated with a 15,400 ft/sec basement with an apparent dip of 10° to the east whose depth was determined from the West Road profile. As a true bedrock velocity of 16,000 ft/sec was observed along the Central Road profile, an average velocity of 15,700 ft/sec was used as characteristic of the pre-Tertiary basement below Dixie Settlement. This average speed and the information under spread B14 yield a delay time at shot point DP and the depth to basement at this point.

PROFILE 5: Dixie Profile

The Dixie profile (Fig. 10) consisted of six spreads which were 8200 ft long and composed of six geophones each. All shots were fired in holes, four of which were drilled in valley sediments and one in granitic bedrock at the mouth of IXL Canyon. The energy from shots fired in welded tuff at Cow Canyon, which would have completed the information at the east end of this profile, was presumably absorbed in concealed low-density breccias and ash beds which underlie the welded tuff.

The information on superficial velocity layering obtained from the IXL profile, the West Road profile and the Central Road profile was carried over to the Dixie profile. These three north-south profiles show a deepening of the 10,000 ft/sec horizon from the west side towards the center of Dixie Valley. This suggests that the most plausible interpretation of the 12,800 ft/sec segments and the 8000 to 10,000 ft/sec segments recorded along A101 and A102 spreads is to associate them with apparent velocities of an 11,000 ft/sec velocity layer dipping to the east. The 12,700 ft/sec velocity recorded on spread A103 suggests that this 10,500 to 11,300 ft/sec velocity zone continues toward the center of the valley. Because of the

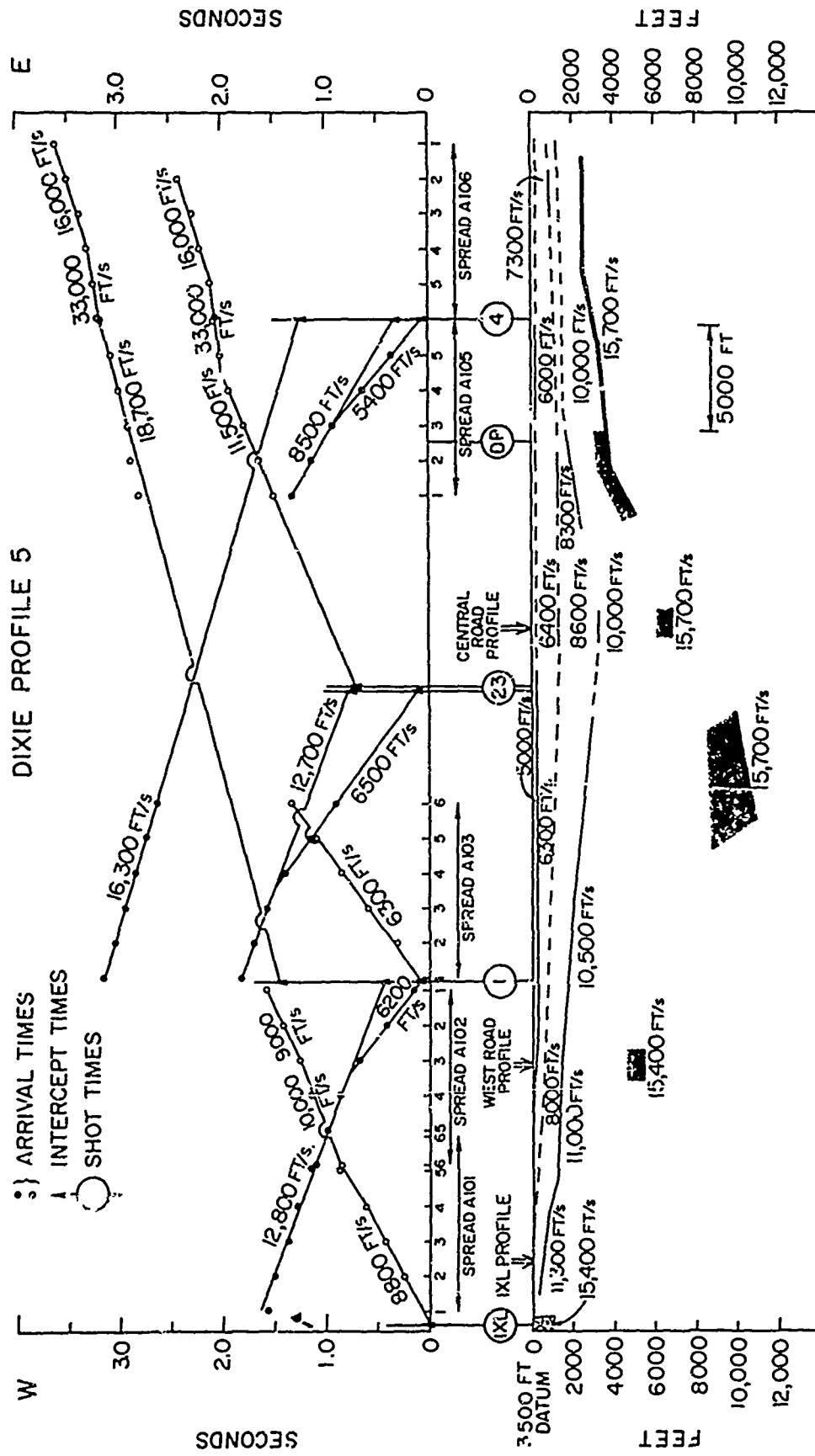


Figure 10. Time-distance curves and cross-section of the Dixie Profile.

similarity with the west side, the 11,500 ft/sec and the 8500 ft/sec velocities recorded on spread A105 were assumed to be apparent velocities of a 10,000 ft/sec velocity boundary dipping west.

All velocities higher than 15,000 ft/sec observed along Dixie profile were interpreted as basement refractions. An average basement velocity of 15,700 ft/sec was assumed for the depth computations using delay times. As the depth to bedrock under shot point DP was determined from the profile 4 data, a geophone delay time could be computed for spread A105. From the 18,700 ft/sec velocity segment recorded on the same spread from shot point 1, a delay time was determined at this point. The corresponding depth to basement is 10,500 ft if there are no velocity reversals in the 10,500 ft/sec velocity layer; it is the maximum depth measured during the survey.

The apparent basement velocity of 16,300 ft/sec recorded on A103 corresponds to a basement dipping to the west rather than to the east. This slope of the bedrock is due to the fact that the delay time is increased by the thickening of the 6,300 ft/sec and the 8000 ft/sec velocity layers toward the center of the valley. Depths to the 15,700 ft/sec layer under spread A106 and under shot point 3 were similarly computed.

The velocity layering beneath the geophone spread A106 was assumed to be similar to the one measured under the East Road profile (Fig. 12). A horizontal basement in the north-south direction under Dixie Settlement is indicated by the equality of the delay times at shot point N4 of the Central Road profile and shot point 3 of the Dixie profile.

PROFILE 6: Dixie Meadows Profile

The Dixie Meadows profile (Fig. 11) was shot about three miles north of West Road profile along the main north-south road on the west side of Dixie Valley. Conventional refraction techniques were used: three shots were fired in the same hot spring and the seismometer spread was moved away from the shot point.

The shallow velocity structure at the south end of the profile was determined from spread E50 data. This velocity layering is similar to that determined beneath the Salt Marsh profile (Fig. 15), which is situated

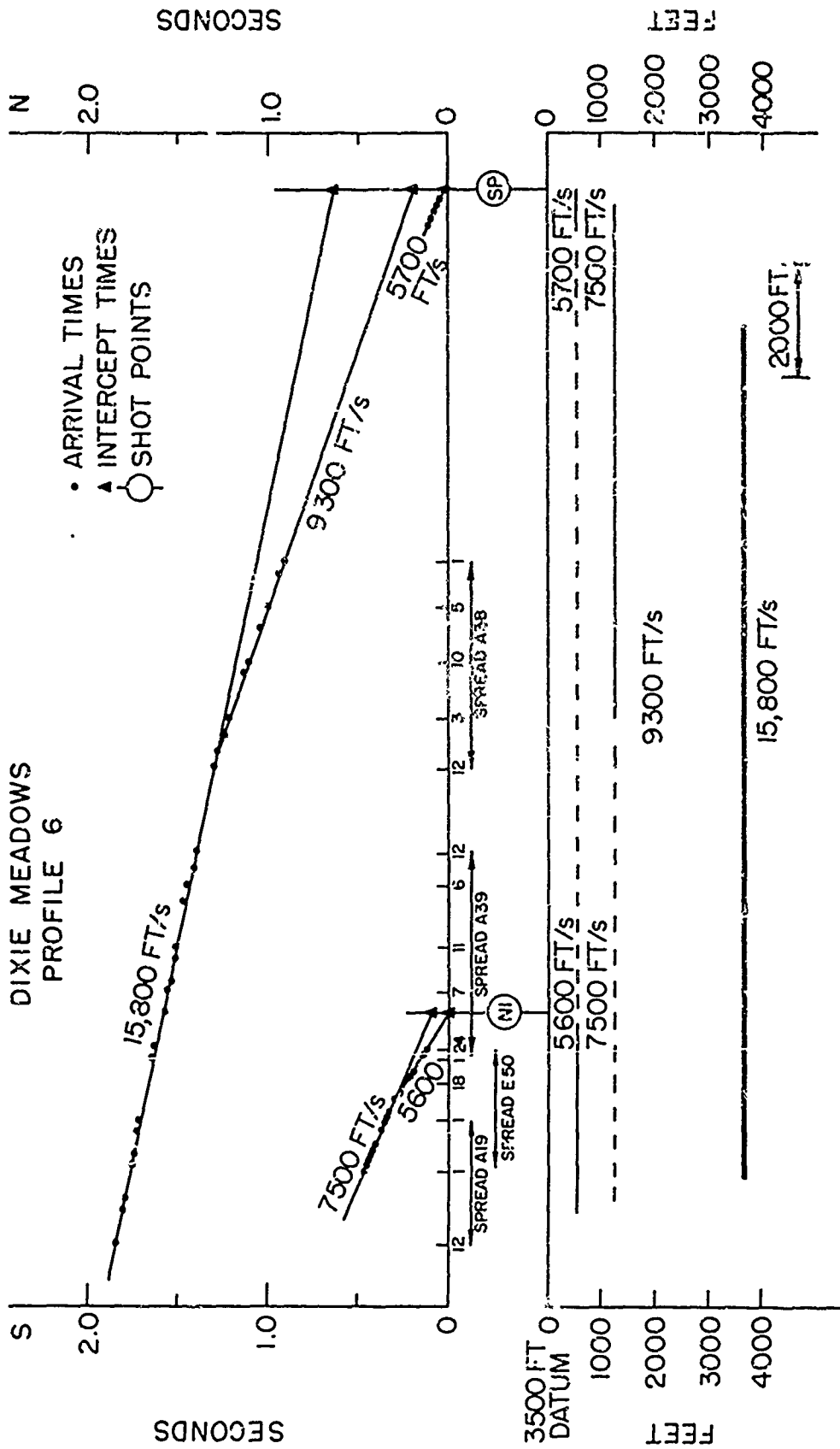


Figure 11. Time-distance curves and cross-section of the Dixie Meadows Profile.

along the west side of Humboldt Salt Marsh, as is shot point SP. Despite the difference in surface conditions between the northern and southern part of the Dixie Meadows profile, a similarity in seismic velocity layering justifies the assumption that the lateral velocity changes along this profile are small.

Since no reversal data were obtained all observed velocities were assumed to be true velocities. The depths of the three horizontal velocity boundaries were determined by conventional intercept-time methods.

PROFILE 7: East Road Profile

Suspended air shots were used exclusively as sources of seismic energy for the East Road profile (Fig. 12). All data were reduced to a 3650-ft datum and the velocity of 5000 ft/sec for the surface layer was taken from Table 1. The velocity boundary between the 7300 and 8300 ft/sec layers was computed to be horizontal between shot points S3 and N3; this boundary was assumed to remain horizontal along the rest of the profile.

The true velocity of the 14,700 ft/sec layer was obtained from the association of the apparent velocity of 24,800 ft/sec recorded from shot point S3 with the 11,000 ft/sec recorded from shot point N4. The attitude of the 14,700 ft/sec layer in the central part of the profile was determined from the intercept time of the 11,000 ft/sec velocity segment at shot point N3; the depth of this same layer below shot points S3, S4, N4, and N5 was determined from the delay times associated with these points.

PROFILE 8: Horse Creek Profile

Horse Creek profile was shot in an area where the gravity measurements (Thompson, 1966) suggested that the gravity low, associated with the deepest part of the graben around Dixie Settlement, is trending toward Horse Creek Canyon.

In order to minimize the weathering corrections all data were reduced to an inclined datum plane on the eastern side of the profile (Fig. 13).

The attitude of the 9300 ft/sec velocity layer below the geophone spread was determined from the intercept times of the 9700 and 8900 ft/sec apparent velocity segments and was assumed to be the same below shot points W2 and W3.

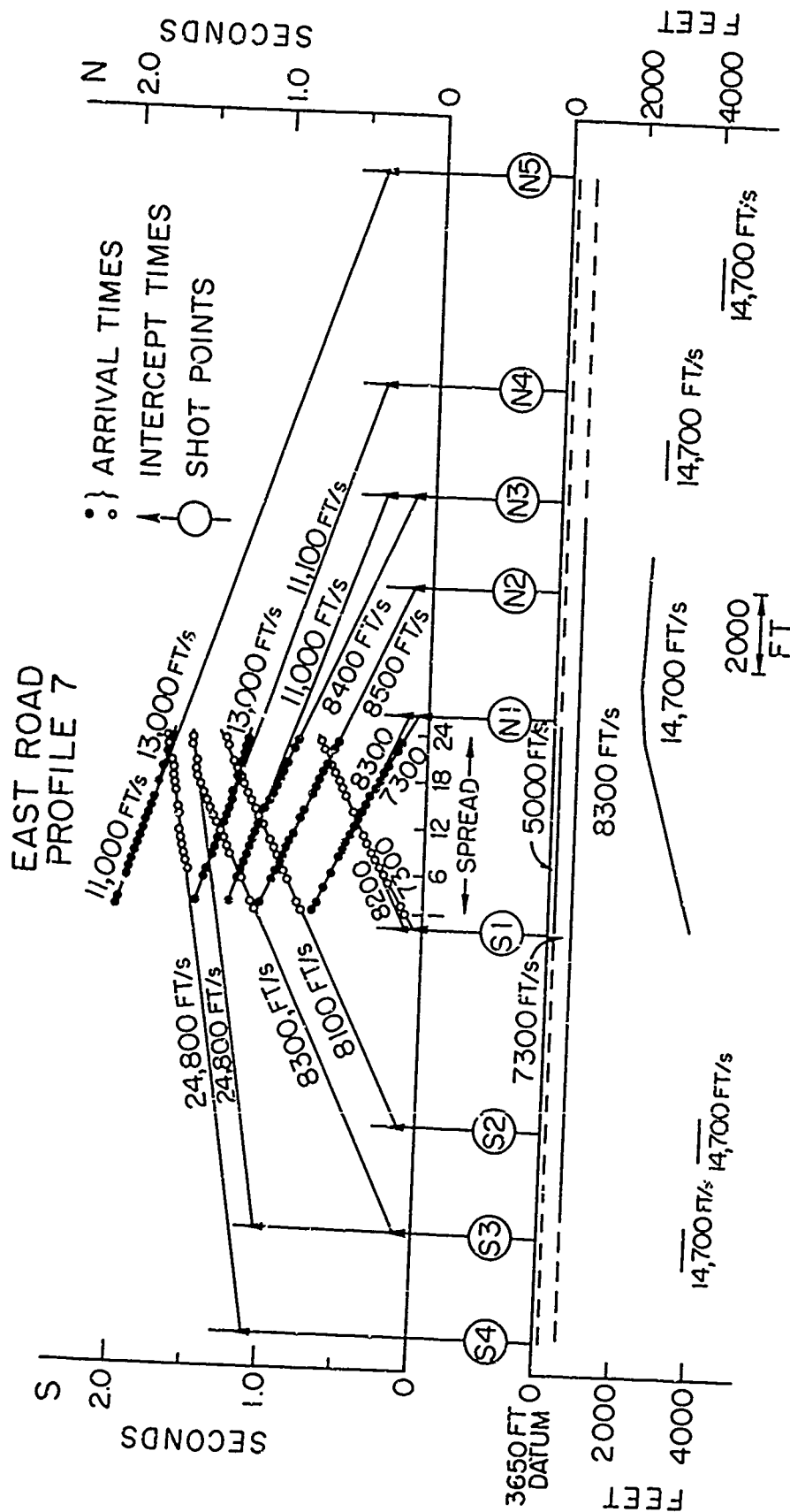


Figure 12. Time-distance curves and cross-section of the East Road Profile.

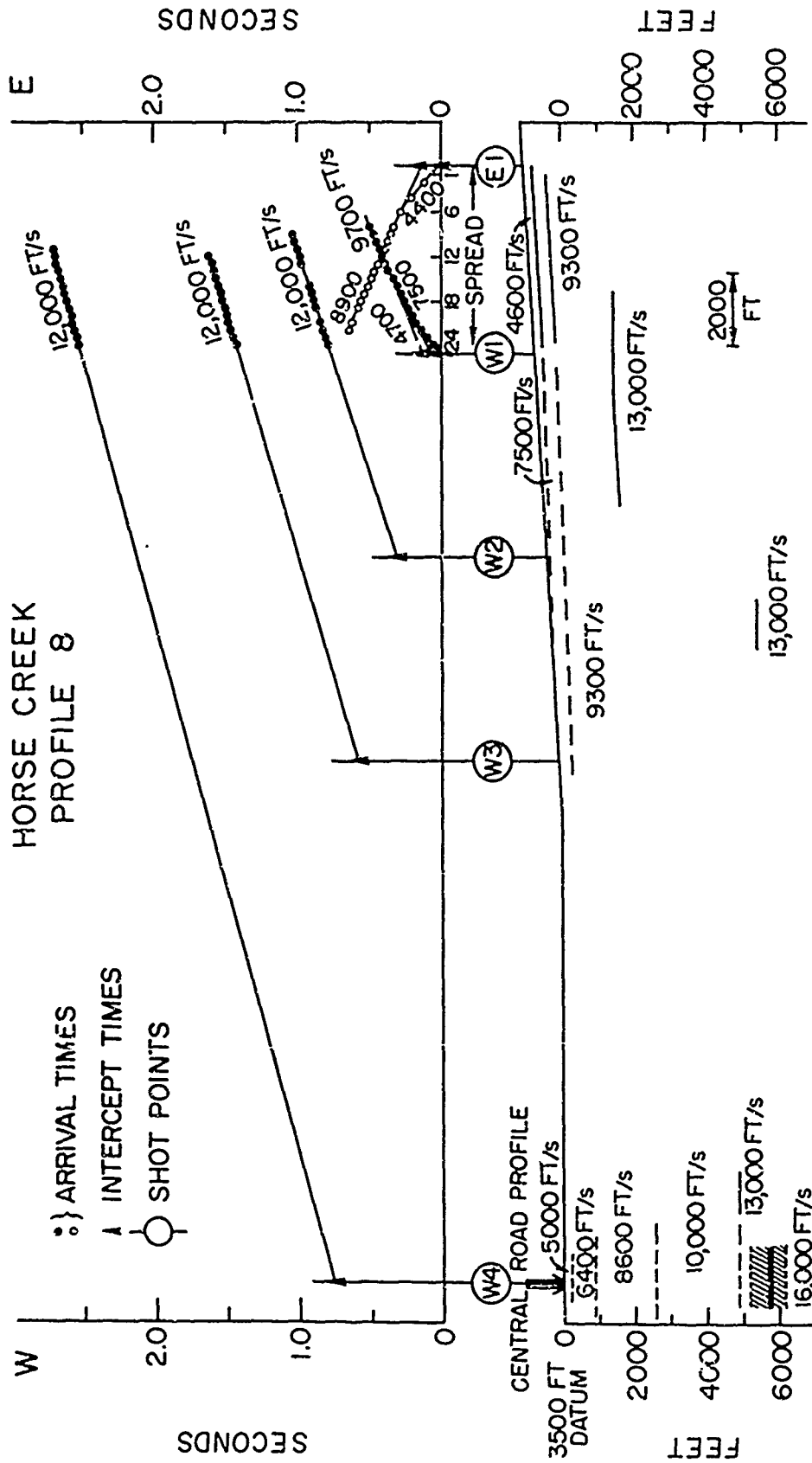


Figure 13. Time-distance curves and cross-section of the Horse Creek Profile.

The maximum apparent velocity recorded along Horse Creek profile was 12,000 ft/sec. In a first interpretation this velocity can be considered as the down-dip velocity of a portion of a 16,000 ft/sec basement dipping east. The delay time at shot point W4 would be about 0.2 sec larger than the one determined for this same shot point from the Central Road profile (Fig. 7), thus indicating a deepening of the valley floor to the east of W4 comparable to that observed along the Dixie profile (Fig. 9).

As the gravity gradient along the east side of the present profile (Thompson, 1966) indicates instead a west dipping basement, the following interpretation was preferred (Fig. 13): the 12,000 ft/sec apparent velocity is associated with an intermediate 13,000 ft/sec velocity zone situated between the 9300 ft/sec layer and the basement. Similar velocity zones were observed along Pirouette Mountain and East Road profiles (Fig. 14 and Fig. 12) and seem to be characteristic of the southern part of Dixie Valley. The normal depth to the 13,000 ft/sec layer is calculated from the intercept time of the 12,000 ft/sec segment at shot point W2. The depth below shot point W3 is computed from the increased delay time at this point and must be considered as a maximum since the continuity of the 9300 ft/sec layer is assumed across a discontinuity in the structure of the 13,000 ft/sec layer. An increase in depth of the 9300 ft/sec layer is more probable across this discontinuity; this increase would decrease the computed depth to the 13,000 ft/sec horizon. The superficial velocity layering determined along Central Road profile (Fig. 7) was used to compute the depth of this same horizon below shot point W4.

Since no basement refractions were observed, according to this last interpretation, the basement must be at least 6000 ft deep below the eastern end of Horse Creek profile.

PROFILE 9: Pirouette Mountain Profile

The shallow velocity layering below the 4600 ft spread of Pirouette Mountain profile (Fig. 14) was determined from the data recorded along this spread. The interpretation of the northern part of this profile was carried over from the Center Road profile (Fig. 7).

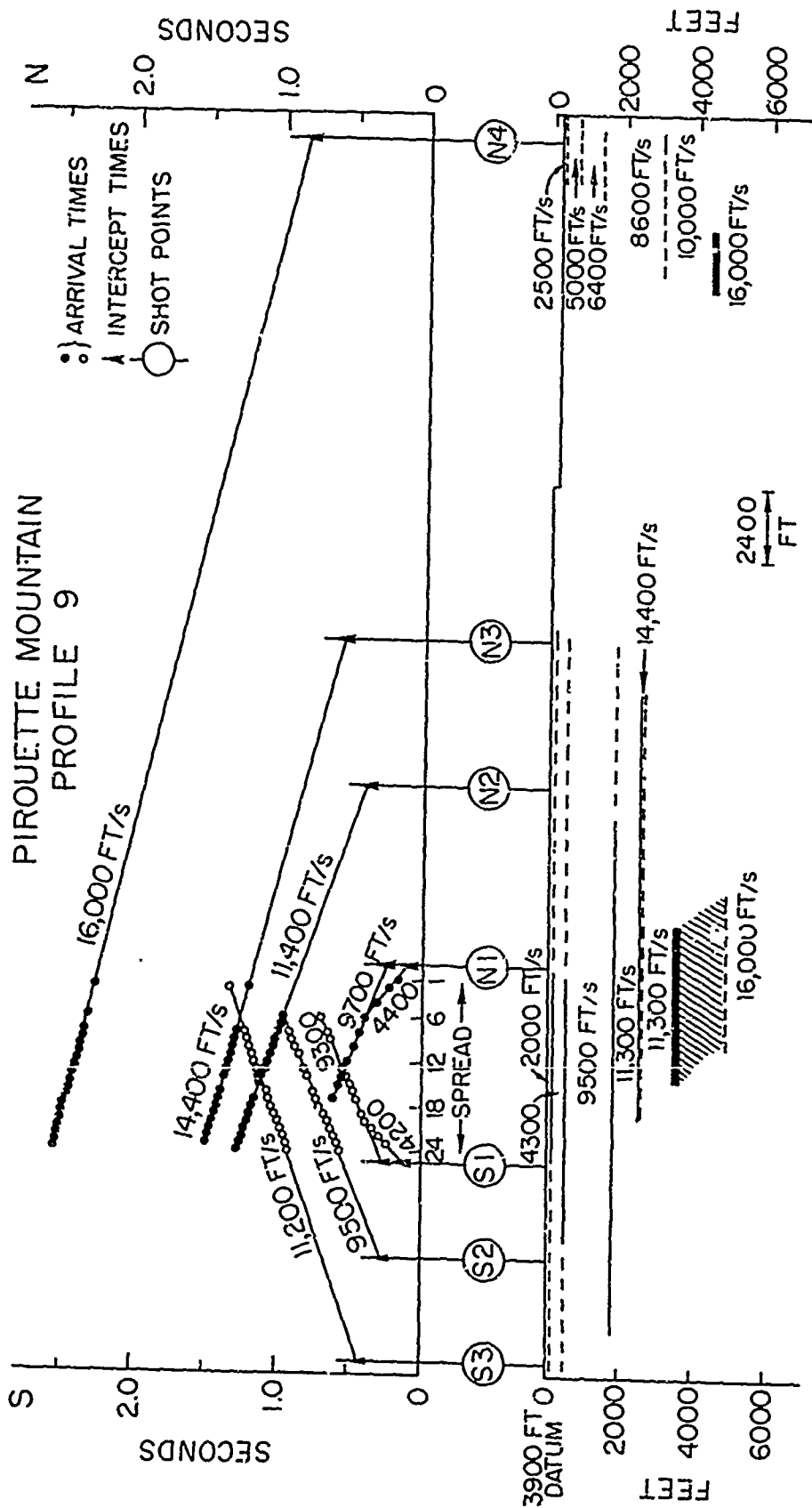


Figure 14. Time-distance curves and cross-section of the Pirouette Mountain Profile.

The attitude of the 11,300 ft/sec layer was determined from the intercept times of the 11,200 ft/sec and the 11,400 ft/sec segments at shot points S3 and N2. The small intercept time of the 14,400 ft/sec velocity segment at shot point N3 implies that part of the energy arrivals which form the 11,400 ft/sec velocity segment recorded from shot point N2 must be second events. No detectable arrivals refracted from the 14,400 ft/sec layer were received from shot point N2.

The apparent velocity of 16,000 ft/sec was assumed to be the true velocity of the basement below Pirouette Mountain profile. If the 14,400 ft/sec velocity segment represents only first arrivals, the 16,000 ft/sec layer must be at least 1000 ft below the 14,400 ft/sec layer in the southern part of the profile. From this minimum depth to basement (represented by a heavy line in Fig. 14) it is possible, through the intercept time at shot point N4, to determine a maximum depth to basement below this point. The 14,400 ft/sec layer was assumed to be thin in the previous calculation. In the absence of a velocity reversal below this layer, the basement may be as deep as the lower boundary of the shaded area in Fig. 14.

PROFILE 10: Salt Marsh Profile

Salt Marsh profile (Fig. 15) was shot along a 54,000-ft line oriented in a NNE-SSW direction on the west side of Humboldt Salt Marsh. Recordings were made on a single 4600-ft spread. Suspended air shots were used exclusively as sources of seismic energy. All data were reduced to a 3400-ft datum plane and the velocity of 4000 ft/sec for the surface layer was obtained from Table 1. Below this layer, velocities of 6100 ft/sec and 7600 ft/sec were measured and this layering was assumed to be continuous between shot points S4 and N2.

The velocity of 5700 ft/sec for the uppermost layer at shot point S5 was carried over from Dixie Meadows profile where this superficial layer was determined at shot point SP. The attitude of the 10,000 ft/sec layer is not well defined since only a small segment of the time distance curve obtained from shot N2 corresponds to this velocity. The attitude of the 9300 ft/sec layer from the Dixie Meadows profile was transferred to the area around shot point S5.

Figure 15. Time-distance curves and cross-section of the Salt Marsh Profile.

The apparent velocity of 19,800 ft/sec recorded from shot point N2 was associated with the 14,800 ft/sec velocity recorded from shot point S2 to yield a true basement velocity of 16,800 ft/sec. The normal depth to the 16,800 ft/sec layer was determined by correlating the 19,800 ft/sec velocity with a dipping plane solution between shot point N2 and the spread. Delay times related to all other shot points were computed on the assumption that the basement velocity is constant and equal to 16,800 ft/sec along the entire profile. Any lateral decrease in basement velocity will result in a decrease in computed depths to basement. Delay times at N3 and N4 are equal and are of the same order of magnitude as the one obtained for shot point 6 east of Boyer Ranch profile (Fig. 19). This indicates an abrupt deepening of the valley floor under N3 and N4 which must be accompanied with a change in superficial velocity layering. Consequently, the velocity distribution obtained for the eastern end of Boyer Ranch profile was used to compute the depths corresponding to the delay times of shot points N3 and N4.

A detailed layout of the Dixie Meadows and Salt Marsh profiles is shown in Fig. 16. Assuming basement continuity between shot points S4 and S1, a comparison of basement attitude determined between S4 and N2 with the corresponding distance of the Stillwater front to the profile, shows a striking similarity. This leads to the conclusion that the energy recorded along this profile is refracted from the east side of the Stillwater Range and that the front of the range must be continuous to the depth where side refraction takes place.

The interpretation of the Salt Marsh profile was made with the assumption that the ray paths are in the vertical plane of the profile. This vertical plane is represented by a dashed line in cross-section A-B of Fig. 16. The refractor is a plane perpendicular to this vertical plane through point N. The depth of this point was determined from the delay time associated with geophone 24 (Fig. 15). If the energy is side refracted, the refractor will lie tangent to the curve SN (cross-section AB of Fig. 16) which is the locus of points having the same geophone delay time.

Herring (1966) determined a parametric equation for this locus for a model formed by two horizontal layers bounded by a dipping high velocity

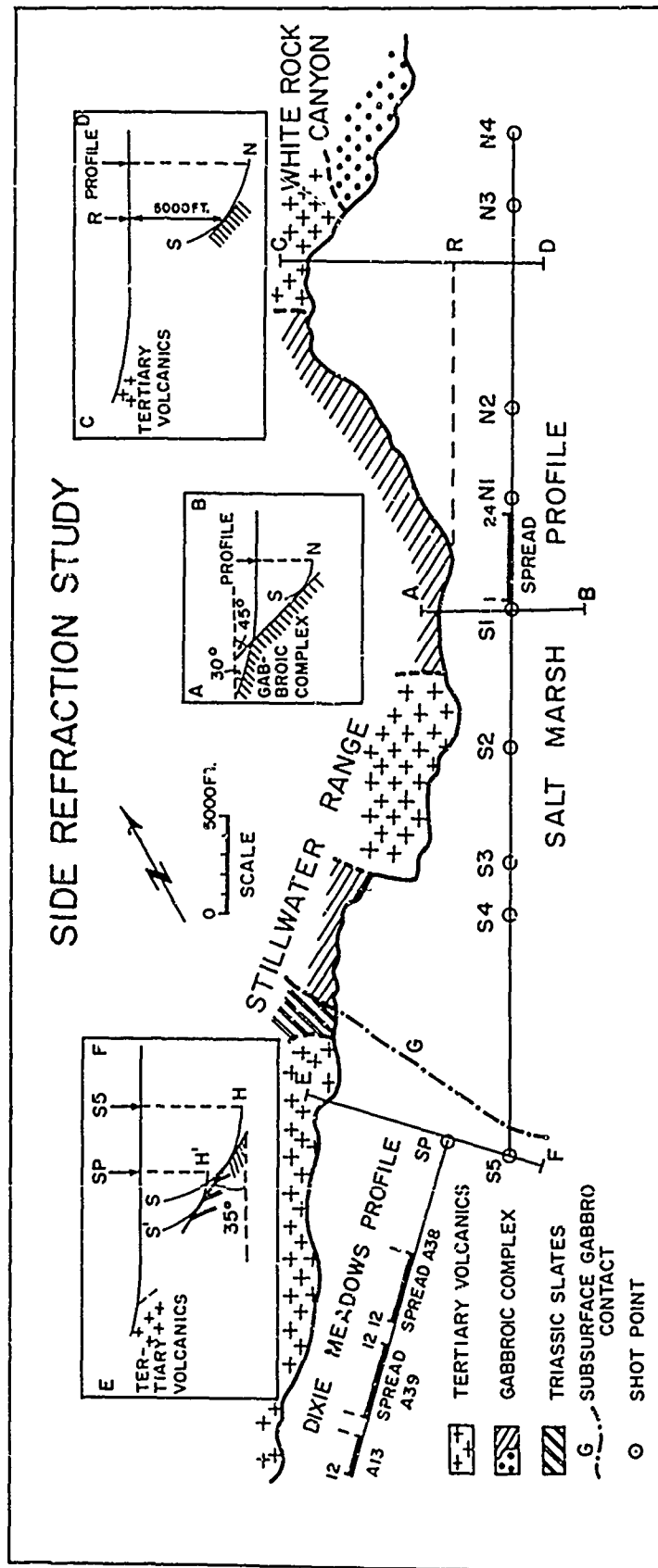


Figure 16. Detailed Map showing the layout of the Salt Marsh Profile and the Dixie Meadows Profile.

refractor whose strike is parallel to the line of the profile. All four side refraction curves SN shown in the three cross-sections of Fig. 16 were constructed by applying Herring's formula to the seismic data determined along the Salt Marsh and Dixie Meadows profiles.

Cross-section AB of Fig. 16 shows that the energy recorded at the geophone spread of the Salt Marsh profile is side refracted at a depth of 2500 ft from a plane dipping 45° to the east. The change from a topographic slope of 20° on the east side of the Stillwater Range to a bed-rock dip of 45° beneath the alluvial fan supports the conclusion that this refracting surface is a fault zone rather than an erosional surface.

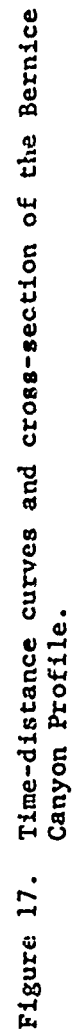
Cross-section CD shows that the basement is at least 5000 ft deep 1.5 miles southeast of White Rock Canyon. This reentrant of the Stillwater Range is therefore controlled by high angle faults which strike approximately at right angles to each other, or by one fault which bends through a right angle.

It is reasonable to assume that the energy of shot SP and shot S5, recorded respectively along Dixie Meadows and Salt Marsh profiles, is side refracted along the same basement plane; therefore this plane has an apparent dip of 35° to the southeast (cross-section EF of Fig. 16) and is 4300 ft below shot point SP.

PROFILE 11: Bernice Canyon Profile

Bernice Canyon profile (Fig. 17) was shot in order to clarify the structure associated with a large positive magnetic anomaly on the eastern side of Dixie Valley. The profile was 31,000 ft long and consisted of three 4600 ft spreads. All shots offset by more than 500 ft from the spreads were fired in drilled holes; they provided poor energy coupling, which is probably a result of high attenuation in the alluvial fan in this part of the valley.

The upper boundary of a 9000 ft/sec zone, at a depth of 160 ft, remains horizontal between spread B5 and spread D6. A 7200 ft/sec layer, recognized along spread D1 below the 4500 ft/sec layer, resulted in an increased depth to the 9000 ft/sec layer.



The velocity of the 14,500 ft/sec layer was calculated from reversed data of the B5 setup. This layer is horizontal between spreads D6 and D1 on the basis of the intercept times of the 14,200 to 15,000 ft/sec velocity segments recorded on the same spreads.

The depth to the 14,500 ft/sec layer, computed beneath shot point N4 using the increased delay time at this point, must be considered a maximum since a horizontal 9000 ft/sec layer north of the profile was assumed. In reality this layer may be deeper under N4 to correlate with the increase in depth of the 14,500 ft/sec layer. The 15,000 ft/sec velocity segment shown on spread D6 was recorded from a shot which was fired at N4 without time break.

The maximum average velocity measured along this 31,000 ft profile was only 14,500 ft/sec and a depth penetration of about 8000 ft was reached. This leads to the conclusion that the 14,500 ft/sec arrivals are refracted from the basement.

PROFILE 12: Seven Devils Profile

The subsurface structure of Gamble Basin between Boyer Ranch and Seven Devils Springs was investigated from data obtained along Seven Devils profile (Fig. 18). Seismograms were recorded from shots fired in Seven Devils Springs on three 8200 ft spreads of six geophones each. These spreads were placed end to end. Reversed data in the same part of the profile were measured along the 4600 ft spread B8 of twenty-four geophones. Information on the southern part of the profile was deduced from the apparent velocities recorded along spread D4.

An apparent velocity of 7700 ft/sec was measured around Seven Devils Hot Springs and was associated with the weathered siliceous sinter dome deposited by the hot springs. These rocks were assigned a true velocity of 10,000 ft/sec. Beneath spread B8 a true velocity of 5700 ft/sec was observed for the uppermost layer. The apparent velocity of 6900 ft/sec was assumed to be the true velocity of the second layer.

The 10,000 ft/sec velocity segments recorded from shot point S2 along the north end of spread B8 and from shot point SD along spread A115 were interpreted separately as representing true velocities of horizontal layers whose depth was computed using intercept times at shot points S2 and SD.

Figure 18. Time-distance curves and cross-section of the Seven Devils Profile.

The 13,700 ft/sec and 20,700 ft/sec layers were defined by association of the apparent up-dip velocities of 14,600 and 24,800 ft/sec recorded along spread B8 with the apparent down-dip velocities of 13,000 and 18,200 ft/sec recorded along spreads A116 and A117. Intercept formulas for a dipping layer were used to compute the normal depths to the 13,700 ft/sec layer between shot point S3 and spread B8.

There are two possible ways to compute the depth to 20,700 ft/sec basement from the intercept time of the 24,800 ft/sec velocity segment at shot point S4. Assuming that the basement is a plane dipping 7° between S4 and spread B8, a depth to basement at S4 is obtained which is much larger than the horizontal distance from the profile to the front of the Stillwater Range. Any side refraction along this boundary will then result in earlier arrivals than those actually observed. Consequently, the 7° dip was considered to be a local attitude of the basement below spreads A117 and B8 and depths below shot point S4 and these spreads were computed using delay time formulas and a constant basement velocity of 20,700 ft/sec.

If the 13,700 ft/sec layer were a thin high velocity zone inside the 10,000 ft/sec layer, then the basement, below spreads B8 and A117 and shot point SD, would be as deep as the top of the shaded area in Fig. 18. The 13,700 ft/sec layer in the southern part of the profile was not observed but may exist as a blind zone in that area and along Boyer Ranch profile (Fig. 19). In both regions the depth to basement was computed for a continuous 11,000 ft/sec layer because the effect of any velocity reversal in this layer would be compensated by the presence of the blind zone.

The energy recorded on spreads B8 and A117 was refracted from the bottom of Gamble Basin just below the spread but may have been side refracted just north of shot point S4 where the front of the Stillwater Range is 6000 ft west of the profile.

The 6600, 8800, and 11,300 ft/sec velocity segments recorded at geophone setup D4 were interpreted as the true velocities of three horizontal layers situated between the 5400 ft/sec layer and the basement. The 20,000 ft/sec segment represents an apparent down-dip velocity of the 20,700 ft/sec basement with a local apparent dip of 2° to the south. The depth to the 20,700 ft/sec basement was calculated using the conventional intercept-time method for horizontal layers for the part of the profile between spread D4 and shot point S4.

PROFILE 13: Boyer Ranch Profile

Boyer Ranch profile (Fig. 19) was shot along a road trending east from Boyer Ranch across Dixie Valley. All data were reduced to a 3500 ft datum. All three geophone setups recorded an apparent velocity of 9700 ft/sec from shots fired in 20-ft holes drilled in the basement at shot point CW. At points 5 and 6 the shots were fired in 50-ft holes. The southern end of Seven Devils profile crosses Boyer Ranch profile 3400 ft west of shot point 5.

Intercept times at shot points 5 and 6 of the 6600 and 6500 ft/sec velocity segments control the thickness of the 5400 ft/sec velocity layer along the profile. The apparent velocity of 8000 ft/sec recorded along spread A110 was assumed to be the true velocity of a horizontal layer between shot point 6 and this spread. The interpretation of the southern part of Seven Devils profile showed an 8800 ft/sec layer whose attitude is carried over to Boyer Ranch profile. The upper boundary of this layer was correlated with that of the 8000 ft/sec layer determined along spread A110.

The 9700 ft/sec and the 13,100 ft/sec velocity segments given in the travel time curves of spread A109 and A110 were associated respectively with down-dip and up-dip apparent velocities of a 10,900 ft/sec velocity layer. The depth to this layer below spread A109 was calculated from the intercept time at shot point 5 using the intercept formula for a dipping layer; the continuation of the 9700 ft/sec velocity segment along the geophone setup A110 led to the determination of the attitude of the 10,900 ft/sec layer beneath this spread. The depth of the 10,900 ft/sec velocity zone below shot point 6 was calculated from the intercept time of the 13,100 ft/sec velocity segment at that point.

The true velocity of 20,700 ft/sec determined for the basement along Seven Devils profile was assumed to be characteristic of the bedrock beneath Boyer Ranch profile. The depth to basement determined from the data of Seven Devils profile was used to compute a one-way delay time for geophone 5 of spread A109 and a delay time for shot point 6. These delay times in turn lead to a basement depth below this latter point.

The high apparent velocity recorded between geophones 3 and 4 of spread A109 indicates the existence of a fault in the bedrock just west of

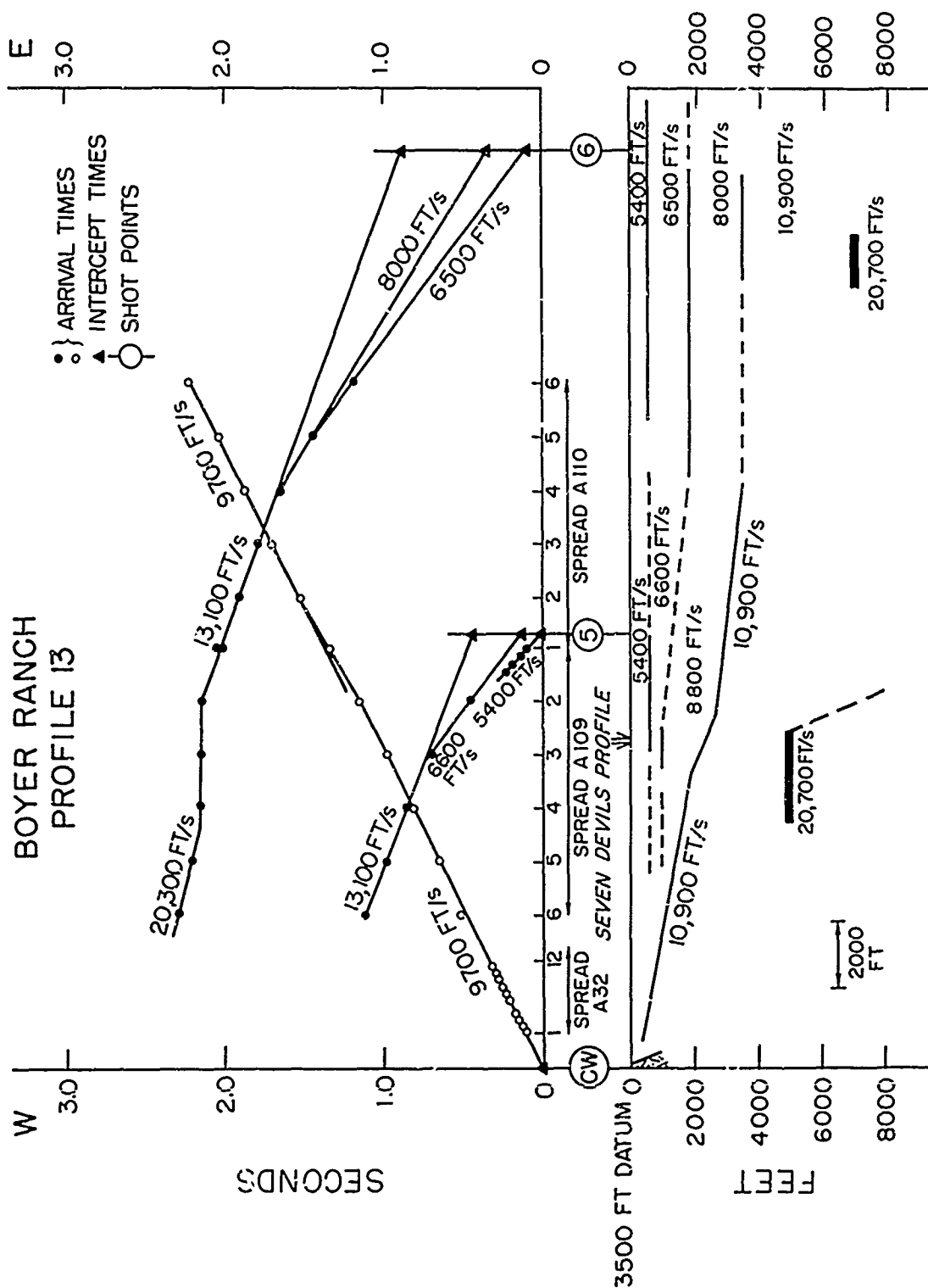


Figure 19. Time-distance curves and cross-section of the Boyer Ranch Profile.

shot point 5. The minimum step down observed in the time distance curve caused by the vertical displacement of the fault is 0.180 second which corresponds to a 2300-ft vertical down-throw of the basement on the east side of this fault. Such an attitude of the basement below spread A110 would cause the energy from shot point CW refracted from the bedrock to arrive as a first break around 2 sec at geophone 6 of spread A110. Unless these early arrivals were weak and the 9700 ft/sec velocity segment is a second event, the vertical offset along the fault is more than 2300 ft. The basement is therefore deeper below shot point 5 than beneath shot point 6.

PROFILE 14: Hyder Springs Profile

The three individual spreads of profile 14 (Fig. 20) were laid out NE of Hyder Springs (Fig. 2). Shots W1 and W5 were fired in Hyder Hot Springs and shots E4 and E3 were fired in drilled holes.

The depth to the top of the 10,500 ft/sec layer was determined below spread B7 and assumed to be constant along the northeastern end of the profile.

The depth to the 6000 ft/sec velocity layer below point E1 associated with spread D5 was calculated with a superficial velocity of 3000 ft/sec.

The 8200 ft/sec velocity segment recorded along the same spread was associated with a horizontal velocity layer.

Two apparent velocities of 11,200 ft/sec and 9000 ft/sec were recorded on spread D5 and associated as apparent up-dip and down-dip velocities of a NE dipping 10,000 ft/sec velocity layer. Depth below shot point W1 was computed from the intercept time of the 9000 ft/sec velocity segment.

The apparent velocity of 22,500 ft/sec recorded from shot point W2 was associated with the 12,500 ft/sec velocity recorded from shot point E2 to yield a true basement velocity of 16,000 ft/sec.

The 16,400 ft/sec velocity segment recorded along spread A119 from shot W5 shows the lack of significant structure in the basement between shot point W2 and spread B7. The normal depth to basement was therefore computed from the intercept time of the 16,400 ft/sec velocity segment at W2.

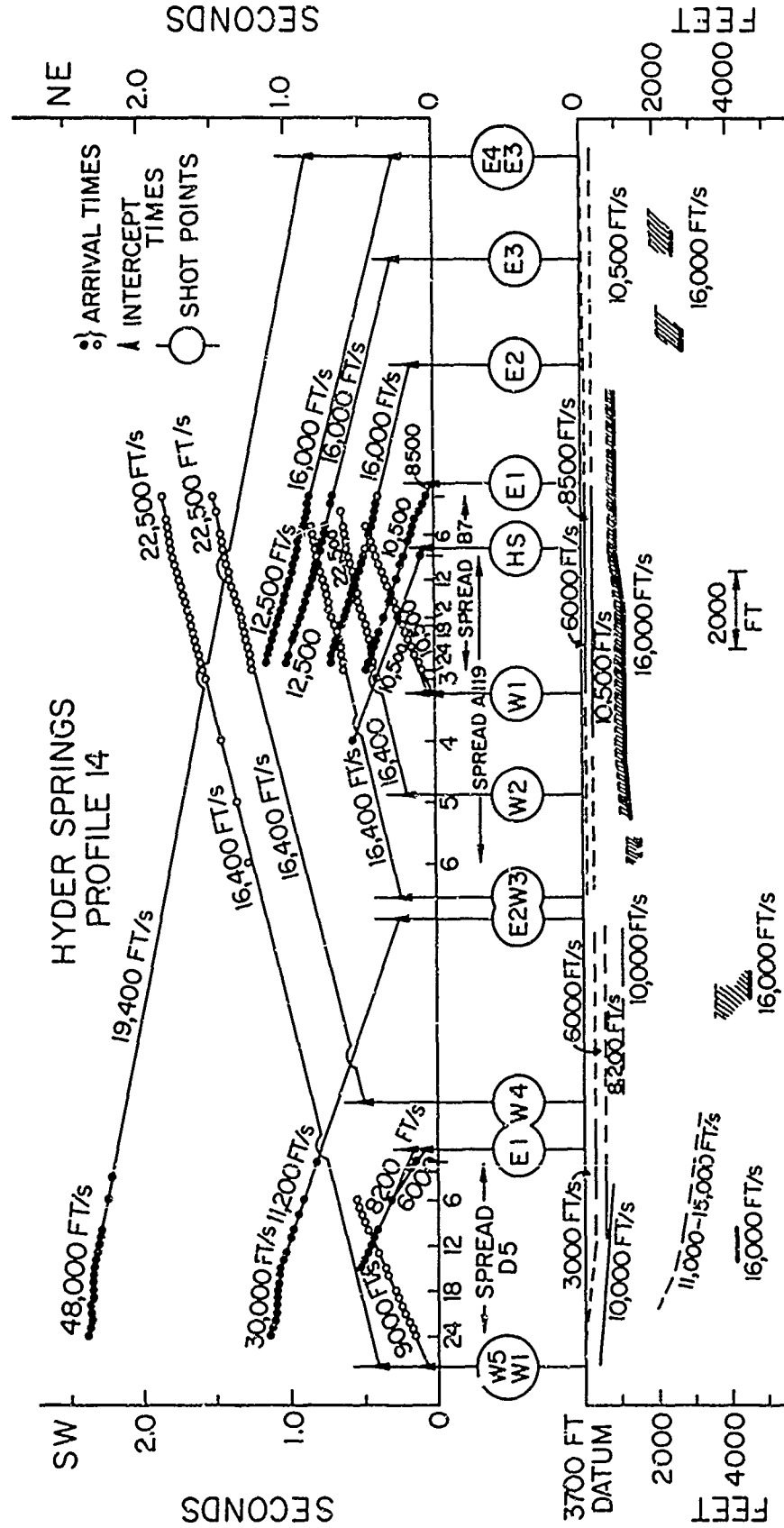


Figure 20. Time-distance curves and cross-section of the Hyderabad Springs Profile.

The increase in delay times associated with shot points E3, E4, W3, W4, and W5 was correlated with a deepening of the basement on both sides of the horst outlined below spreads A119 and B7.

The geophone delay time associated with the 48,000 and 19,400 ft/sec velocity segments recorded along spread D5 from shot point E3 corresponds to a refractor which is shallower than the basement determined from the shot point delay time at W5. This leads to the conclusion that the energy was refracted from the side of a siliceous sinter cone which exists below Hyder Hot Springs and whose attitude at depth is represented by the dashed line below spread D5.

Hot springs with associated siliceous sinter domes are convenient shot points and were used on Seven Devils and Hyder Springs profiles. Unfortunately they represent high velocity zones whose detailed structure is unknown. Therefore they may introduce significant errors in the interpretation of refraction data around them.

VIII. CORRELATION OF SEISMIC VELOCITIES WITH STRATIGRAPHY

A. In Situ Velocity Measurements

Table 3 summarizes the seismic compressional wave velocities and thicknesses of each velocity layer observed below the water table along the fourteen profiles studied in the previous chapter. It is difficult to relate these velocity layers to the stratigraphic units exposed in the ranges surrounding Dixie Valley because of the wide range of speeds with which seismic waves travel in the sedimentary or igneous rocks present in the area under study. To support the conclusions drawn below, additional information was obtained through side refraction measurements along outcrops of geologic units. These measurements are of greatest importance to the present study.

A true velocity of 15,400 ft/sec was calculated from two apparent velocities of 12,000 and 22,000 ft/sec measured along the granitic rocks exposed at the mouth of IXL Canyon. The data from the detailed side refraction study reported by Herring (1966) indicate an average velocity of 16,500 ft/sec for this same granitic pluton at Mud Springs. A 16,800 ft/sec velocity characterizes the gabbroic and dioritic rocks which form the front of the Stillwater Range just west of the Salt Marsh profile (Fig. 15).

The Cenozoic deposits which form most of the valley fill are composed of sedimentary and igneous material. Seismic velocities were measured for both kinds of rocks. A velocity of 10,000 ft/sec was obtained using side refraction for the Tertiary volcanics, mainly rhyolites and dacites, exposed in the White Rock Canyon. Herring (1966) associated the 10,000 ft/sec velocity zone found close to the surface below the southern part of profile E53 with a nearby outcrop of rhyolitic tuffs found about 1000 ft east of the fault scarp which runs along the base of the Stillwater Range.

Four refraction profiles were recorded with the GT-2 Interval Timer (described in Chapter III) in the Pliocene (?) non-marine sedimentary rocks at the southern end of the Stillwater Range near Mountain Well. Along exposures of semiconsolidated sands and clay beds which were above the water

TABLE 3

A. SUMMARY OF SEISMIC VELOCITIES

Profile	Location	Velocities (ft/sec)						
		V ₁	V ₂	V ₃	V ₄	V ₅	V ₆	V ₇
1	West Road	5200	6300	8000		10,000		15,400
2	Central Road	5000	6400	8600		10,000		16,000
3	IXL Canyon	5000		8000	9300	11,300		15,700
4	Crazy X Ranch	5000	6000	8300		10,500		15,700
5	Dixie	5000	6300	8300		10,500		15,800
6	Dixie Meadows	5600		7500	9300		14,700	
7	East Road	5000		7300, 8200			13,000	
8	Horse Creek	4800		7500	9300			16,600
9	Fromette Mt.	4300			9500	11,300	14,400	16,800
10	Salt Marsh	4000	6100	7600		10,000		14,500
11	Bernice Canyon	4500		7200	9000			20,700
12	Seven Devils	5700	6900			10,000	13,700	20,700
13	Boyer Ranch	5400	6500	8000		10,900		16,000
14	Hyder Springs		6000	8500		10,500		

TABLE 3 (continued)

B. SUMMARY OF LAYER THICKNESSES

Profile	Location	h_1	h_2	h_3	h_4	h_5	h_6	h_{Total}
1	West Road	90	510	870		3000-4600		4470-6070
2	Central Road	260	650-1350	1700		2200-3500		4810-6800
3	IXL Canyon	140-190		0-120	0-870	1700		3800
4	Crazy K Ranch	90-450	1000-1200	300-1900		2000-8000		2500-10,500
5	Dixie	250	1000-1290	1700				3650
6	Dixie Meadows	550		660	2440			
7	East Road	170		460, 1600-3500				
8	Horse Creek	200		380	1600-5000			
9	Pirouette Mt.	340			1300	700		3500-4300
10	Salt Marsh	200	330	1200				6000
11	Bernice Canyon	65-160		440	2640			2800
12	Seven Devils	1100	1600			1200	2300	6200
13	Boyer Ranch	500	1400	1700		3400		>7000
14	Hyder Springs		85-3000	210		7000		1000-4000

table, velocities ranging from 4000 to 5000 ft/sec were measured. Arrivals refracted from the upper boundary of an 8300 ft/sec layer which was 160 ft deep were observed by extending two of the refraction lines. This velocity was associated with non-marine sedimentary rocks lying below the water table and having a composition similar to the sand and clay beds exposed at the surface.

The 8300 ft/sec velocity which is a function of overburden pressure was measured under a pressure of 160 psi since 1 psi corresponds to about the pressure created by 1 ft of sediments of density 2.2 gr/cm^2 . The influence of liquid saturation and overburden pressure on the compressional wave velocity in sedimentary rocks has been determined experimentally by a number of workers, such as Wyllie, et al. (1962), and King (1966). They have found that an increase in hydrostatic confining pressure increases the dilatational wave velocity. Most of the samples studied were sandstones saturated with salt water.

The increase in velocity to be expected in the sands and clay beds of the Pliocene (?) sedimentary section when these rocks are buried under Pleistocene and Recent alluvium was determined by assuming that the rate of increase found by King (1966) for the Bandera sandstone could be applied to these Pliocene (?) rocks. Since the sandstones are more consolidated than the sands and clay beds observed in the Mountain Well area, the velocities listed have to be considered as maxima. Table 4 contains these velocities and the depths at which they may be observed.

B. Correlation of Seismic Velocities with Stratigraphy

All observed velocities were classified into seven categories. The velocities in columns V_1 , V_4 , V_5 , and V_7 are in general based on distinct changes in slope in the travel time curves while the velocities listed in columns V_2 and V_3 , especially, may sometimes be the result of replacing a continuous increase of velocity with depth by a series of layers of constant velocity.

Velocities listed in columns V_1 through V_3 are associated with unconsolidated to semi-consolidated clastic sediments of Pleistocene and Recent ages. The two velocity discontinuities reported here are similar to those

TABLE 4
ESTIMATED MAXIMUM DILATATIONAL WAVE VELOCITIES
IN PLIOCENE (?) WATER-SATURATED NON-MARINE SEDIMENTS

Depth of Burial (ft)	Maximum Velocity (ft/sec)
160	8300
1000	9000
2000	9700
4000	10500
5000	10700
8000	11000

observed by previous workers in the sedimentary basins along the eastern front of the Sierra Nevada (Zbur, 1963; Healy and Press, 1964; Pakiser et al., 1964) and in the Colorado Delta Region (Kovach et al., 1962).

Velocities ranging from 4000 to 5700 ft/sec represent unconsolidated sediments just below the water table. It is important to note that the intermediate 6000-6900 ft/sec velocity zone can be identified only in the central part of Dixie Valley and is absent or exists as a blind zone along the margins. Therefore, this layer is believed to be composed of clays and silty material, common in the lower parts of closed basins.

The layers with velocities ranging from 7200 to 8500 ft/sec may represent more consolidated sands along the sides of the valley. Toward the center of the valley these layers are found at depths up to 1900 ft and may indicate an increase in velocity in the 6000-6900 ft/sec layer due to the increase in overburden pressure.

Mabey's (1956) seismic velocity tests on salt outcrops on the Searles Lake plays in southern California indicated a velocity of 10,000 ft/sec for surface salt. Where the salt body was covered by mud there was no crust and the test indicated a velocity of only 7700 ft/sec. From these observations it can be concluded that the V_3 velocity layers recorded in Dixie Valley near the center of the basin could also represent a zone of concentration of saline minerals. The combined thickness of the V_1 to V_3 velocity layers ranges from 300 ft north of Hyder Springs to 3500 ft beneath Dixie Settlement and east of Boyer Ranch. This indicates that a maximum thickness of 3500 ft of sediments were deposited in the Dixie Valley basin since Plio-Pleistocene time.

A seismic velocity boundary below which the velocity increases to an average of 10,000 ft/sec is characteristic of the entire Dixie Valley region and represents a distinct stratigraphic horizon within the valley fill. Since we measured similar velocities in rhyolitic tuffs and flows at White Rock Canyon and at Mud Springs, this higher velocity is correlated with the tuffs and flows of rhyolite of the Miocene to Pleistocene stratigraphic unit.

The non-marine sediments included in this section should create velocity reversals in the V_4 or V_5 velocity layers. Knowing the depth of these layers, it is possible to determine from the data of Table 4 the

speed of the seismic waves in this low velocity zone. These data indicate that the velocity in the sediments can reach 10,000 ft/sec at a depth of 3500 ft and therefore no velocity reversals are likely below this depth. On another hand, the existence of an 8000 ft/sec layer at a depth of 3000 ft beneath Dixie Settlement where normally the Pliocene (?) sediments would have a velocity of 9 to 10,000 ft/sec, strongly suggests that clastic sediments of post-Pliocene age exist at that depth.

A maximum thickness of the Miocene to Pleistocene section of 8000 ft was measured below Dixie Settlement and is of the same order of magnitude as the thickness reported by Page (1965).

The presence of a 13,000 to 14,700 ft/sec velocity layer observed between the 10,000 ft/sec zone and the basement along the East Road profile, Pirouette Mountain profile, and inferred from the data of Horse Creek profile, is correlated with a competent volcanic flow interbedded in the Miocene to Pleistocene section. This flow seems to be present only in the southern part of Dixie Valley. Velocities ranging from 15,400 to 16,500 ft/sec measured south of Dixie Meadows are correlated with the Mesozoic limestones, slates and metavolcanic rocks exposed north of IXL Canyon and with the granitic rocks which intruded this Mesozoic section.

The southern subsurface margin of the Gabbroic complex was determined from the data of the aeromagnetic survey completed by Smith (1965)(Fig. 2). Along the Salt Marsh profile, which was shot just north of the gabbro contact, a basement velocity of 16,800 ft/sec was measured by side refraction on gabbroic and dioritic rocks. These rocks are considered to be the intrusive part of the Gabbroic Complex.

The 20,700 ft/sec velocity measured between Boyer Ranch and Seven Devils was also correlated with the intrusive rocks of the Gabbroic Complex while the 13,700 ft/sec layer found below the 10,000 ft/sec zone probably represents Mesozoic basalt flows, tuffs, and breccias associated with the gabbroic and dioritic rocks of the Gabbroic Complex. From the data of Seven Devils profile it can be concluded that rocks from the Gabbroic Complex form at least part of the bedrock below Gamble Basin and that the attitude of the pre-Tertiary basement is represented by the upper boundary of this 13,700 ft/sec velocity layer.

The 14,500 ft/sec velocity measured below Bernice Canyon profile was correlated with the extrusive rocks of the Gabbroic Complex. The seismic waves reached a depth of penetration of about 8000 ft and no higher velocity was recorded. Therefore the minimum depth for the intrusive rocks of the Gabbroic Complex below this profile is 8000 ft and any magnetic model which may be constructed to fit the positive anomalies in this area must accommodate the boundary conditions set forth by the seismic model.

Seismic velocities in the Gabbroic Complex range from 13,700 ft/sec and 14,500 ft/sec in the extrusive rocks to as high as 20,700 ft/sec in the intrusive rocks. This wide spread reflects the heterogeneity of composition of the Gabbroic Complex and makes it impossible to differentiate the nature of the basement for velocities less than 17,000 ft/sec without the support of the magnetic data. Another consequence of this inhomogeneity is that the delay time method used for the interpretation of the refraction data is less reliable in the northern part of the valley. The northwestern part of the subsurface contact of the Gabbroic Complex lies approximately north of Gamble Basin, but it is not possible to define from seismic data the northeastern part of this contact since the 16,600 ft/sec velocity recorded along Hyder Springs profile can be correlated with both the Mesozoic slates and the extrusive part of the Gabbroic Complex.

IX. STRUCTURAL IMPLICATIONS

From the attitudes of the velocity boundaries determined by the seismic profiles, it is now possible to describe the subsurface structural configuration of Dixie Valley. It is a long trough showing a "graben in graben" structure controlled by normal faulting.

The inner graben whose detailed structure can be seen in Fig. 10, is about 5 miles wide beneath Dixie Settlement and lies slightly to the west of the topographic center of the valley. Its depth just west of Dixie Settlement was found to be 10,500 ft and two miles east of Boyer Ranch, at least 7000 ft.

The following depths to bedrock were determined for valley blocks bordering the trough to the west:

- a. Five miles southwest of Dixie Meadows the basement is 3500 ft. deep;
- b. About two miles east of IXL Canyon, the valley floor is 5400 ft deep;
- c. At Boyer Ranch the basement is 4900 ft deep.

Fig. 21 is an east-west cross-section along Mud Springs Road; it combines the results obtained by Herring (1966) with the information of the southern end of West Road profile. It shows how the basement drops step-by-step valleyward from the topographic escarpment of the Stillwater Range. Three high-angle faults were detected between the west side of the valley and the west side of the inner graben. The dip of these faults was found to be 55° to 70° eastward.

Below shot point SP of Dixie Meadows profile (Fig. 16), the floor of the outer graben is 4300 ft deep and has a dip component of 35° to the southeast.

About 1.5 miles southeast of the mouth of White Rock Canyon, in the basin formed by the reentrant of the Stillwater Range, the basement is at least 5000 ft deep (Fig. 16). Finally, the floor of Gamble Basin is 4000 ft deep and has a dip component of 3° to the south.

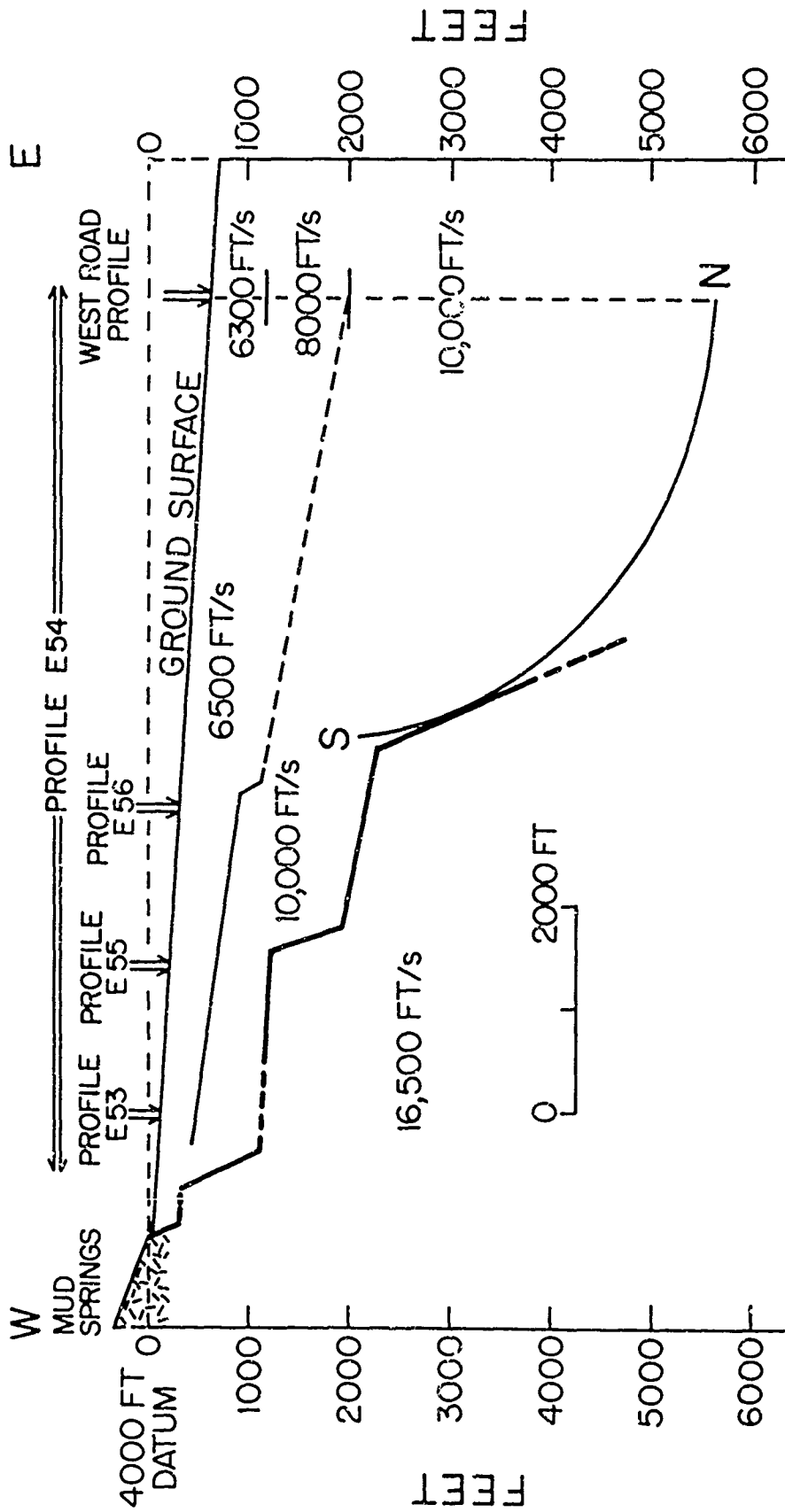


Figure 21. East-West cross-section along Mud Springs Road.

Below Dixie profile the floor of the outer graben rises eastward from a depth of 3800 ft to 2500 ft. Further north, the floor on the east side of this narrow depression is 2800 ft deep at Bernice Canyon profile and 1000 ft deep at Hyder Springs profile.

The continuity of the inner graben between Boyer Ranch and Dixie Settlement could not be verified in the present study but is inferred from the aeromagnetic survey (Smith, 1965) and from the gravity map of the Dixie Valley area (Thompson, 1966). West of Dixie Settlement, a maximum vertical offset of 5500 ft in the basement was determined along the western bounding fault of the inner graben. Similarly at the Boyer Ranch profile there is at least 2300 ft of offset.

From Dixie Settlement the southward continuation of the eastern fault zone of the inner graben can be deduced from the abrupt valleyward drop of the 13,000 and 14,700 ft/sec horizons observed along the western part of Horse Creek profile and the southern end of the East Road profile.

The northward continuation of this same zone cannot be determined from the present seismic data since the high-angle fault at the southwestern end of Hyder Springs profile is not necessarily related to the longitudinal trough but may represent the northeastern boundary of a transverse structure. The shallow depth of the bedrock determined below the Pirouette Mountain profile indicates either that the main longitudinal trough ends as a closed basin at the southern end of Dixie Valley or that its axis turns to the east below the Louderback Mountains.

The comparison of the depth of the pre-Tertiary basement obtained in the northern part of Pirouette Mountain profile with the depth at the southern end of the Central Road profile shows a structural relief of the bedrock of 1500 ft over a north-south horizontal distance of one mile. This structural relief forms the southwestern boundary of the Dixie Valley trough.

IXL Canyon profile and East Road profile show minor transverse structures in the velocity boundaries within the Cenozoic section, but it was not possible to establish their continuity across the valley. The layers which form the upper part of the Miocene-to-Pleistocene unit have been much less displaced by faults than the pre-Tertiary interface (Fig. 10). This leads to the conclusion that faulting was continuous or repeated at short intervals concurrently with deposition of the Cenozoic rocks.

X. CONCLUSIONS

The seismic refraction investigation of Dixie Valley revealed several structural features which are significant in the understanding of the structural history of the Basin and Range Province and supply new constraints on the theories of its formation.

The subsurface structural configuration of Dixie Valley is summarized in Fig. 10, which shows a concealed complex of normal faults forming a long subsurface trough with a "graben in graben" structure. The inner graben, situated beneath the west side of the valley floor, is as narrow as five miles and contains an accumulation of sedimentary and volcanic deposits of Cenozoic age which attain a maximum thickness of 10,500 ft. The last 3500 ft of this section were deposited since late Pliocene time.

The Dixie Valley and Rainbow Mountain fault scarps, which were formed during the 1954 earthquakes, each lie along the western side of a narrow trough. One of these troughs is the composite graben of Dixie Valley, which reaches a depth of 10,500 ft, and the other lies on the west side of the Stillwater Range and is 10,000 ft deep (Wahl, 1965). The Stillwater Range forms a horst rising 15,000 ft above the floors of these two grabens. Thus the most active seismic area in the Basin and Range Province is characterized by a total structural relief of three miles over a breadth of twelve miles.

The fault zone bounding the Stillwater Range west of the Humboldt Salt Marsh dips at least 45° to the east; its zig-zag pattern is conserved to a minimum depth of 2500 ft. The geometry of this fault zone is such that no large-scale strike-slip movement is possible along the zone.

At Mud Springs the western boundary fault of Dixie Valley has 4000 ft of throw (Fig. 21), whereas the western fault zone of the inner graben has a vertical offset of 5500 ft west of Dixie Settlement and at least 2300 ft at Boyer Ranch. This interior concealed fault may be more nearly straight than the Stillwater frontal fault and may therefore allow strike-slip displacement.

The following observations limit the amount of horizontal movement which could have taken place since the beginning of the Cenozoic:

- a. The maximum possible strike-slip displacement of the southern subsurface contact of the gabbroic complex across Dixie Valley cannot be more than two miles (Smith, 1965).
- b. Zbur (1963) observed en echelon normal faults in the sediments of Indian Wells Valley, California. He associated these features with right lateral strike-slip movement along a fault in the pre-Tertiary bedrock. However Burke (1966), who studied in detail the geomorphology of the Dixie Valley floor, did not see any such normal faults in the sediments above the west side of the inner graben.

Geophysical evidence thus strongly suggests that the maximum possible strike-slip displacement in Dixie Valley cannot be more than two miles. Therefore it is believed that all bounding and interior faults which form the structural framework of this basin are normal faults along which mainly dip-slip movement occurred.

From the present study it is possible to obtain average displacement rates for two successive intervals of geologic time. On one hand, the 15,000 ft of vertical deformation which took place in the last 15 million years would suggest an average displacement rate on the order of 1 ft per thousand years. On the other hand, it was found that depths of the volcanic rocks of Plio-Pleistocene age range from 300 ft in the outer graben to 3500 ft in the inner graben. Assuming original continuity the difference of 3200 ft implies also an average displacement rate of 1 ft per thousand years.

Therefore it can be concluded that the Dixie Valley region was deformed over the last 15 million years at a rate of about 1 ft per thousand years with dip-slip exceeding strike-slip movement.

BIBLIOGRAPHY

- Buffet, A., and Laya, C.H., 1960, Nouvel Aspect de la Sismique Refraction au Sahara: Tirs non Enterrés; Geophysical Prospecting Vol. 8, pp. 47-67.
- Burke, D.B., 1967, Aerial Photograph Survey of Dixie Valley, Nevada; A. F. Cambridge Research Labs. Final Scient. Rpt. Part IV, AFCRL-66-848.
- Cohen, P., and Everatt, D.E., 1963, A Brief Appraisal of the Ground Water Hydrology of the Dixie-Fairview Valley Area; Dept. Conserv. and Nat. Res., State of Nevada, Report No. 23.
- Dix, C.H., 1952, Seismic Prospecting for Oil; New York, Harper and Brothers 414 pp.
- Ewing, M., Crary, A.F., and Rutherford, H.M., 1937, Geophysical Investigation in the Emerged and Submerged Atlantic Coastal Plain, Part 1: Methods and Results; Bull. Geol. Soc. Am., Vol. 48, pp. 753-802.
- Hawkins, L.V. and Maggs, D., 1961, Nomograms for Determining Maximum Errors and Limiting Conditions in Seismic Refraction Survey with a Blind Zone Problem, Geophysical Prospecting, Vol. 9, No. 4.
- Healy, J.H., and Press, Frank, 1964, Geophysical Studies of Basin Structures Along the Eastern Front of the Sierra Nevada, California; Geophysics, Vol. 29, pp. 337-359.
- Herring, A.T., 1967, Seismic Refraction Study of a Fault Zone in Dixie Valley Nevada, A. F. Cambridge Research Labs. Final Scient. Rpt. Part II AFCRL-66-848.
- Kane, M.F., and Pakiser, L.C., 1961 Geophysical Study of the Subsurface Structure in Southern Owens Valley, California; Geophysics, Vol. 26, pp. 12-26.
- King, M.S., 1966 Wave Velocities in Rocks as a Function of Changes in Overburden Pressure and Pore Fluid Saturants; Geophysics, Vol. 31, pp. 50-73.
- Kovach, R.L., Allen, C.R., and Press, Frank, 1962, Geophysical Investigations in the Colorado Delta Region, Jour. Geoph. Res., Vol. 67, pp. 2845-2871.
- Mabey, D.R., 1956 Geophysical Studies in the Intermontane Basins in Southern California, Geophysics Vol. 21, pp. 839-853.

- Menard, H.W., 1964, Marine Geology of the Pacific; New York, McGraw-Hill, pp. 117-152.
- Muller, S.W., Ferguson, H.G., and Roberts, R.J., 1951, Geology of the Mount Tobin Quadrangle, Nevada; U. S. Geol. Survey Geol. Quadrangle Map CQ-7.
- Nettleton, L.L., 1940, Geophysical Prospecting for Oil; New York, McGraw-Hill, 444 pp.
- Page, B.M., 1965, Preliminary Geologic Map of a Part of the Stillwater Range, Churchill County, Nevada; Nevada Bureau of Mines Map 28.
- Pakiser, L.C., Press, Frank, and Kane, M.F., 1962, Geophysical Investigation of Mono Basin, California; Bull. Geol. Soc. Am., Vol. 71, pp. 415-448.
- Pakiser, L.C., and Kane, M.F., 1962, Geophysical Study of Cenozoic Geologic Structures of Northern Owens Valley, California; Geophysics, Vol. 27, pp. 334-342.
- Pakiser, L.C., Kane, M.F., and Jackson, W.H., 1964, Structural Geology and Volcanism of Owens Valley Region, California--A Geophysical Study; U. S. Geol. Survey Prof. Paper 438.
- Pakiser, L.C., and Steinhard, J.S., 1964, Explosion Seismology in the Western Hemisphere; Research in Geophysics, Vol. 2, (Odishaw, Ed.) M.I.T. Press, pp. 123-147.
- Poulter, T.C., 1950, The Poulter Seismic Method of Geophysical Exploration; Geophysics, Vol. 15, pp. 181-207.
- Shawe, D.R., 1965, Strike-Slip Control of Basin-Range Structure Indicated by Historical Faults in Western Nevada; Bull. Geol. Soc. Am., Vol. 76, pp. 1361-1378.
- Slemmons, D.B., 1957, The Dixie Valley-Fairview Peak, Nevada, Earthquakes of December 16, 1954: Geological Effects; Bull. Seism. Soc. Am., Vol. 47, pp. 353-375.
- Smith, T.E., 1967, Aeromagnetic Measurements in Dixie Valley, Nevada: Implications Regarding Basin-Range Structure; A. F. Cambridge Research Labs. Final Scient. Rpt. Part III, AFCRL-66-848.
- Speed, R.C., 1963, Unpublished progress map of parts of West Humboldt, Stillwater, and Clan Alpine Mountain Ranges, Nevada.
- Steinhart, J.S., and Meyer, R.P., 1961, Minimum Statistical Uncertainty of the Seismic Refraction Profile; Geophysics, Vol. 26, pp. 574-587.

- Thompson, G.A., 1959, Gravity Measurements Between Hazen and Austin, Nevada: A Study of Basin-Range Structure; Jour. Geophys. Res., Vol. 64, pp. 217-229.
- Thompson, G.A., 1966, Unpublished Gravity Survey of Dixie Valley, Nevada.
- University of Nevada, 1962, Geological, Geophysical, and Hydrological Investigations of the Sand Springs Range, Fairview Valley, and Four Mile Flat, Churchill County, Nevada; Report to Atomic Energy Commission for Shoal Project, Vela Uniform Program, 127 pp.
- Wahl, R.R., 1965, An Interpretation of Gravity Data from the Carson Sink Area, Nevada; M. S. Research Project, Stanford University.
- Wyllie, M.R.J., Gardner, G.H.F., and Gregory, A.R., 1962, Studies of Elastic Wave Attenuation in Porous Media; Geophysics, Vol. 27, pp. 569-589.
- Zbur, R.T., 1963, A Geophysical Investigation of Indian Wells Valley, California; U. S. Naval Ord. Test Station Techn. Publ. 2795.

PART II.

SEISMIC REFRACTION STUDY OF A FAULT ZONE
IN DIXIE VALLEY, NEVADA

by

Alan T. Herring

ABSTRACT

Seismic refraction was used in Nevada to study the fault zone bounding the alluvium on the west side of Dixie Valley and the crystalline basement on the east side of the Stillwater Range. Seismic refraction profiles utilizing patterns of air charges were successful on the high alluvial fan where, a year previously, charges planted up to a hundred feet below the surface in the dry fan material failed to yield usable refraction records. Profiles were shot parallel to the strike of the fault zone so that a special method of interpreting side refractions had to be derived. The derived technique should be useful in studying faults in the Nevada Basin and Range province or anywhere that similar geometry is suspected. Four normal faults with dips between 55 and 70 degrees were found and delineated. Rather than a single steep drop-off, the faults form a series of steps descending to the deepest part of the valley.

ACKNOWLEDGEMENTS

The writer wishes to thank the Chester B. Knittle family of Dixie Valley, Nevada, for their assistance both with work on the project and in providing food and lodging.

Laurent Meister taught the writer how to use the equipment and suggested the problem discussed in this paper. The advice of Professor George A. Thompson and of the late Professor Joshua L. Soske was appreciated.

TABLE OF CONTENTS

	<u>Page</u>
ABSTRACT	ii
ACKNOWLEDGEMENTS	iii
TABLE OF CONTENTS	iv
LIST OF ILLUSTRATIONS	v

Chapter

I. INTRODUCTION	1
II. FIELD WORK, EQUIPMENT, AND TECHNIQUE	3
III. ENERGY SOURCE--AIR SHOOTING	4
IV. SIDE REFRACTION	6
V. INTERPRETATION	15
A. Correction of Data and Sources of Error	15
B. Special Techniques Used in Interpretation	16
C. Profile E53	18
D. Profile E54	20
E. Profile E55	20
F. Profile E56	23
VI. CONCLUSIONS	25
BIBLIOGRAPHY	27

LIST OF ILLUSTRATIONS

	<u>Page</u>
Figure 1. Location of seismic profiles and shot points for side refraction study.	2
Figure 2. Side refracted ray path in three dimensions	7
Figure 3. Expanded geometry of Figure 2.	9
Figure 4. Two-dimensional approximation of Figure 2.	12
Figure 5. Cross-section of Figure 4	13
Figure 6. Time-distance curves and cross-section, Mud Springs Profile E53.	19
Figure 7. Time-distance curves and cross-section, Mud Springs Profile E54.	21
Figure 8. Time-distance curves and cross-section, Mud Springs Profile E55.	22
Figure 9. Time-distance curves and cross-section, Mud Springs Profile E56.	24
Figure 10. Cross-sections along scarp showing basement contact . . .	26

I. INTRODUCTION

A section of a major fault zone partially exposed on the west side of Dixie Valley (Fig. 1, Part I) was studied in detail with seismic refraction techniques. Both the valley and faulting appear typical of the Basin and Range Province. The latter is of particular interest because of recent displacements associated with the 1954 Dixie Valley earthquake. The interpretation of the survey is noteworthy because the velocity structure limits the applicability of classical seismic refraction methods of analysis.

The pre-Tertiary granitic and metamorphic rocks on the west side of the fault are well exposed in the rugged Stillwater Range. The geology (Fig. 2, Part I and Fig. 1) is taken from Page's 1965 map. On the east side of the fault a seismically perverse boulder and pebble conglomerate overlies interbedded volcanic flows, ash, and sediments of Miocene through Recent age.

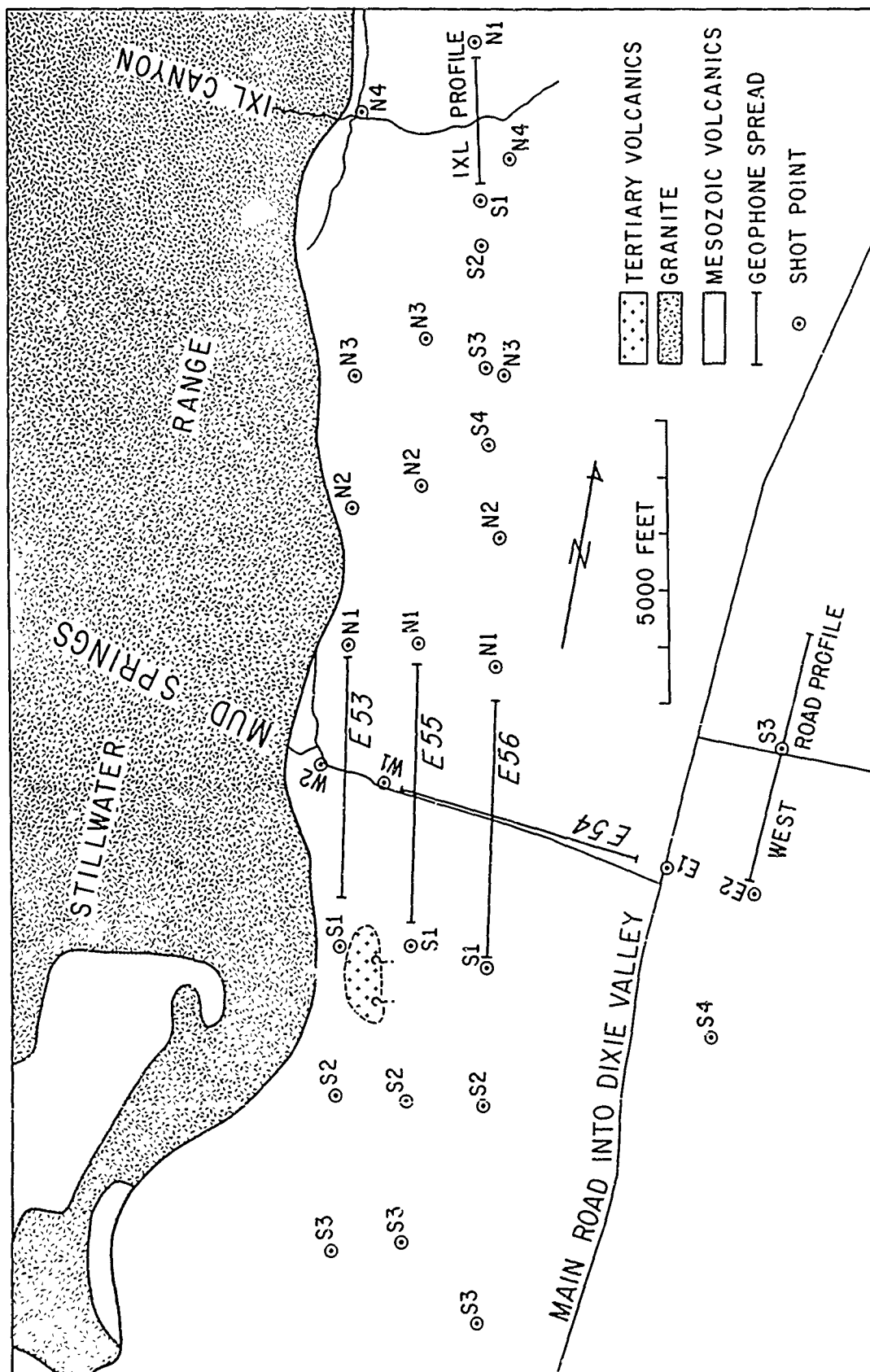


Figure 1. Location of seismic profiles and shot points for side refraction study.

II. FIELD WORK, EQUIPMENT, AND TECHNIQUE

The field work for this paper was done in the summer of 1965. The geophones used were nine 1-cycle geophones and sixteen 2-cycle geophones manufactured by Hall Sears, Inc. The recording equipment (amplifiers and camera) was a SIE GA 33D, 24-trace, seismic system. The unit was built into a cabinet that was bolted semi-permanently to the inside of a Chevrolet four-wheel-drive Carryall. Four 1200-ft, 24-conductor cables were used; two manufactured by Vector, the others by Tesco. All of the shots made for this study were air shots using Dupont Nitramon.

The shot instant was transmitted on a radio frequency of 27 megacycles by means of Citizen's Band transceivers. A steady, 700-cycle-per-second, audio signal was generated by a specially built "shot-point modulator," which emanated a steady audio signal until the electric pulse detonating the charge caused the audio signal to abruptly cease. The audio signal was transmitted to the recording truck where the steady signal and the abrupt cut were recorded on the seismic record. Shot times determined in this fashion were estimated to have an accuracy of ± 2 to ± 5 milliseconds, depending on radio noise conditions.

III. ENERGY SOURCE--AIR SHOOTING

Energy coupling was a major problem. In the field season of 1964 it was found that drilling in the alluvial fan was difficult because of the many large granite boulders. Once a hole had been drilled in the fan and a charge buried and detonated, the energy coupling was unsatisfactory, particularly as the water table was never reached on the fans. An attempt was also made in 1964 to map the fault by setting charges into holes drilled in the outcropping granitic basement rock on the west side of the fault, and recording with the geophones placed on the alluvial fan in a line perpendicular to the fault. This too was unsuccessful. It should be added, however, before all credit for the good records obtained in 1965 is given to the method of air shooting used that year, that in 1965 the 1- and 2-cycle geophones were first used. In 1964 smaller 4 1/2-cycle geophones were used and apparently (from comparable profiles shot in the two different years) had an appreciably lower output than the former.

The use of multi-charge air shooting was suggested to L. Meister and the author by "The Poulter Method of Geophysical Exploration" (Poulter, 1950). Buffet and Layat (1960) discussed the energy coupling problem and air shooting as they apply to refraction work (Poulter was concerned mainly with reflection problems). The following procedure was used by the author: charges were suspended eight feet above the ground on wooden stakes tied to steel fence posts. As many as seven 20-pound charges were suspended on poles, each 50 ft from any adjacent pole; the smallest charge found to produce satisfactory results on the high alluvial fans was 20 pounds. Care was taken to suspend the charge at least a foot above the steel post in order to avoid damage to the post so that it could be re-used. Two 20-pound charges spaced about 50 ft apart were found to be more efficient than a single 40-pound charge. A similar observation was made by Buffet and Layat (1960). The blast from a 20-pound charge suspended eight feet above the ground causes practically no permanent distortion of the ground immediately beneath it. A 40-pound

charge suspended at the same height makes a wide, shallow crater. It was further observed that air shooting was superior to shooting in holes only where there was a considerable thickness of porous, loosely compacted, and often poorly sorted surface materials. A charge placed below the water table in a drilled hole would generally be expected to give a better record than the same charge detonated in the air.

IV. SIDE REFRACTION

Ordinarily, seismic refraction profiles can be interpreted as if the ray paths of the refracted energy all lie in a single vertical plane which contains the line of the profile. This interpretation is correct provided the refractors are all either flat lying or are striking perpendicular to the direction of the profile. Due to the nature of the problem under study, it is necessary to consider the case of energy refracted from an interface that strikes roughly parallel to, and dips toward, the line of the profile; this case is hereafter referred to as a side refraction.

Fig. 2 illustrates that the problem is not easily reduced to a single plane. The figure simplifies the situation somewhat in the sense that interfaces are not expected to be so nearly planar, but it illustrates an important difference between normal and side-refracted ray paths. Although the diagram is intended to illustrate a general case, it was constructed to fit closely the situation being considered: the velocities used in the construction of the diagram are $V_0 = 6000$ ft/sec, $V_1 = 10000$ ft/sec, and $V_2 = 16000$ ft/sec. The dip of the fault is 60° .

Energy refracted from the V_1V_2 interface ($FF'GG'$, which dips at an angle of θ_F and strikes parallel to the line of the profile) travels in two planes. These planes can be determined from the law of refraction stating that the refracted ray lies in the plane formed by the incident ray and the normal to the surface at the point of incidence.

The ray segment CD, which is the portion of the ray path along the V_1V_2 interface, is defined by the intersection of the interface and some plane which passes through the line of the profile. That is, CD is parallel to the line of the profile.

The ray segment BC must lie in a plane perpendicular to the V_1V_2 interface which passes through the ray segment CD (i.e. the plane $DD'RR'$). The angle θ_c is measured from a line perpendicular to the V_1V_2 interface and is the critical angle $\theta_c = \sin^{-1} (V_1/V_2)$.

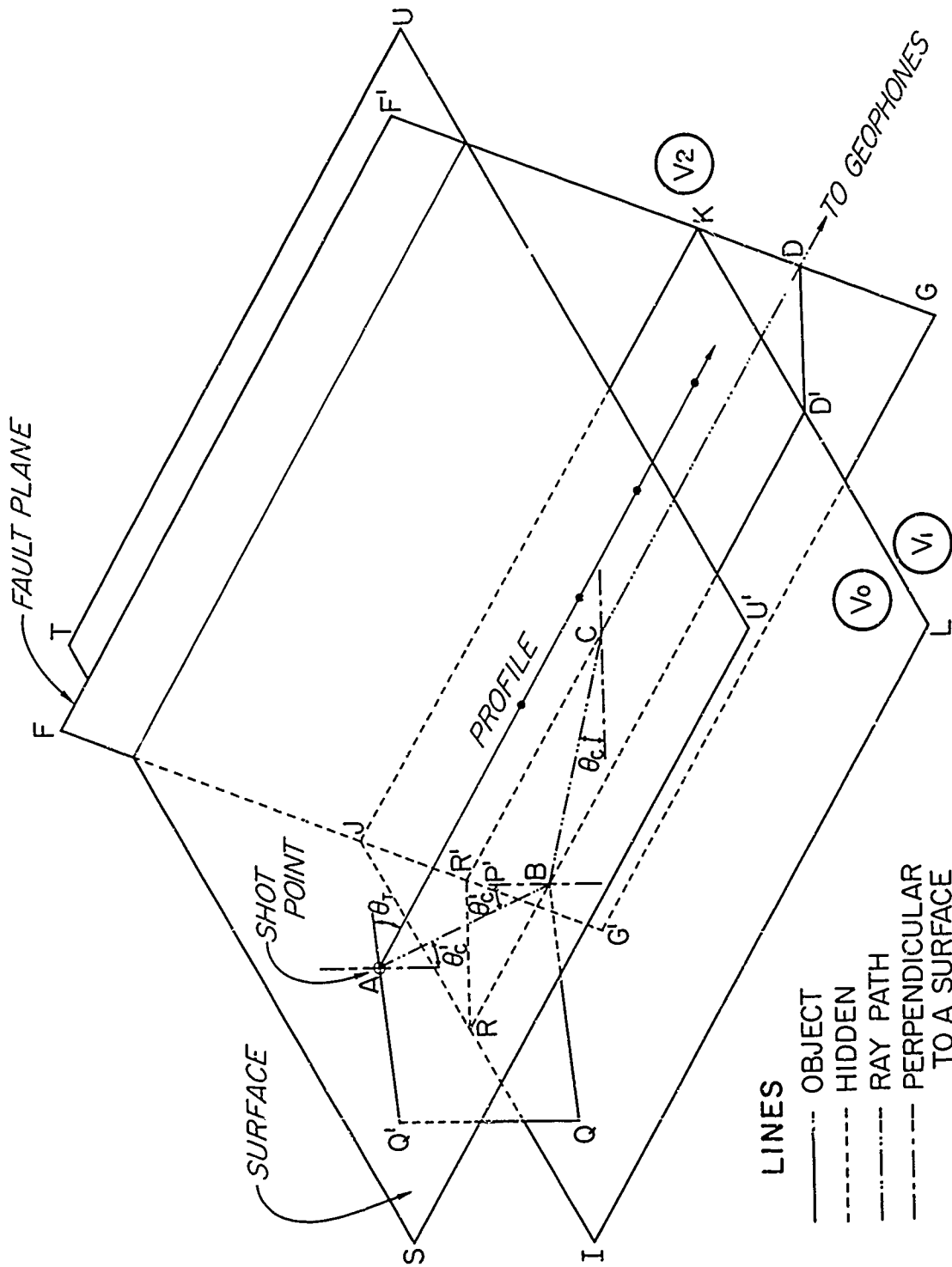


Figure 2. Side-refracted ray path in three dimensions.

Now consider the V_0V_1 interface, IJKL. The ray AB must lie in a plane determined by BC and a perpendicular to the interface erected at B (i.e. ABQQ'). The angle θ_R is measured in this same plane, and can be expressed in terms of θ_c and the dip of the fault, θ_F . Fig.3 shows an expanded portion of Fig.2 that can be used to find an expression for θ_R . Consider the following:

$$\begin{aligned}
 \theta_F &= \text{Dip of } V_1V_2 \text{ interface or fault} \\
 \theta_c &= \sin^{-1} V_1/V_2 \\
 \theta_T &= \text{Acute angle formed by Q'A and the line of the profile (see Figs.2 and 3)} \\
 \sin \theta_F &= b/h \quad \cos \theta_F = z/h \\
 \cos \theta_c &= h/y \\
 \sin \theta_R &= z/y \quad \cos \theta_R = z/y \\
 \frac{\cos \theta_R}{\cos \theta_c} &= \frac{h}{h} = \cos \theta_F \\
 \cos \theta_R &= \cos \theta_c \cos \theta_F \\
 \sin \theta_R &= \sqrt{1 - \cos^2 \theta_c \cos^2 \theta_F} \\
 \sin \theta_T &= b/z \\
 \sin \theta_F \cos \theta_c &= b/y \\
 \sin \theta_T &= \frac{\sin \theta_F \cos \theta_c}{\sin \theta_R} \tag{2}
 \end{aligned}$$

Clearly now, the angle θ_c' will depend on θ_R according to Snell's law.

$$\begin{aligned}
 \frac{\sin \theta_c'}{\sin \theta_R} &= \frac{V_0}{V_1} \\
 \sin \theta_c' &= \frac{V_0}{V_1} \sin \theta_R
 \end{aligned}$$

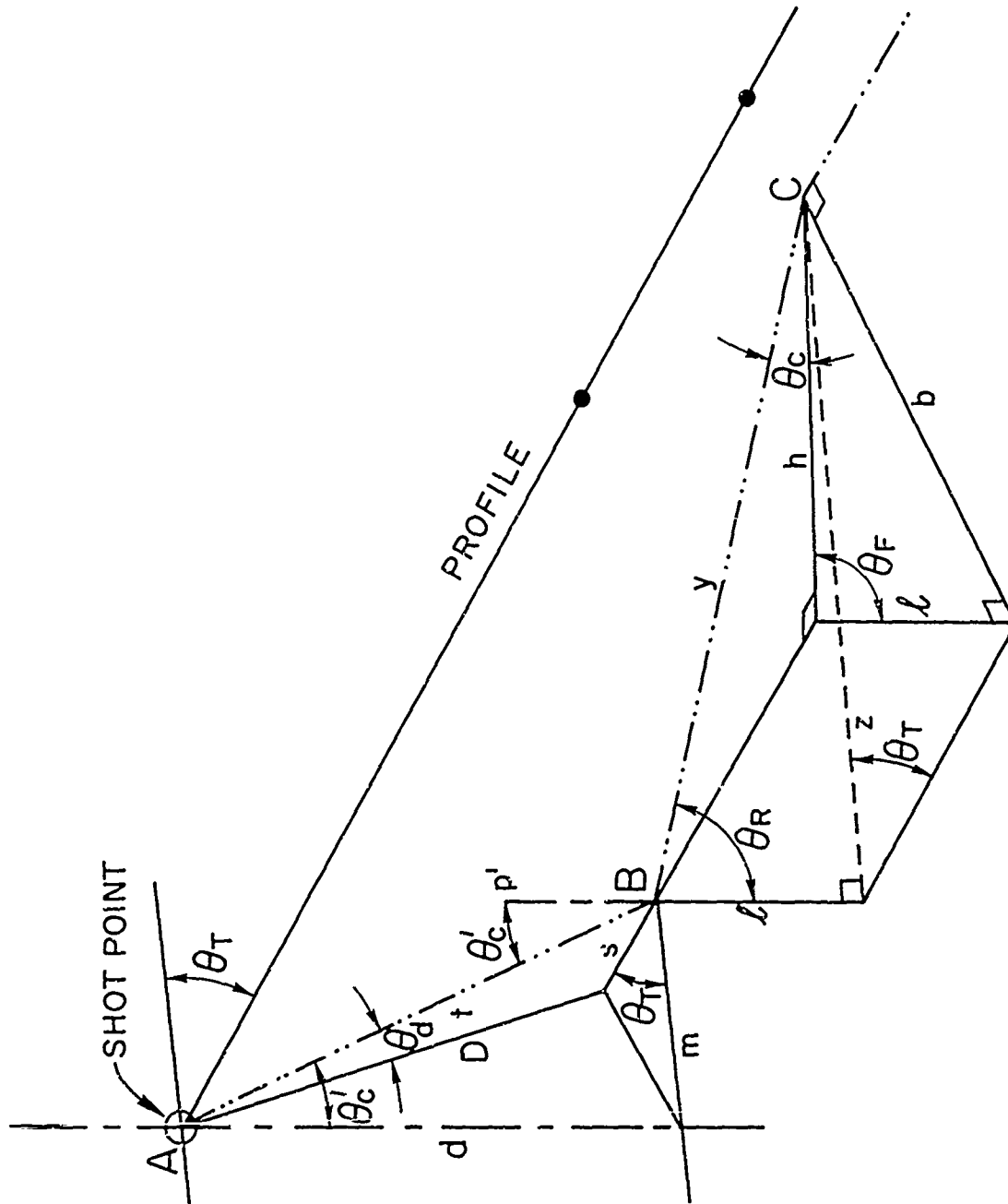


Figure 3. Expanded geometry of Figure 2.

$$\sin \theta_c' = \frac{V_0}{V_1} \sqrt{1 - \cos^2 \theta_c \cos^2 \theta_F'}$$

Alternatively, it can be easily seen that the velocity at which a plane wave, perpendicular to AB, moves down the geophone line will depend on V_0 , θ_T , and θ_c : the velocity, V can be expressed as

$$V = \frac{V_0}{\cos \theta_T \sin \theta_c'}$$

As the $V_1 V_2$ interface is parallel to the line of the profile, V should equal V_2 .

From equations 1 and 2

$$\begin{aligned} \cos^2 \theta_T &= 1 - \frac{\sin^2 \theta_F \cos^2 \theta_c}{1 - \cos^2 \theta_c \cos^2 \theta_F} \\ &= \frac{1 - \cos^2 \theta_c \cos^2 \theta_F - \sin^2 \theta_F \cos^2 \theta_c}{1 - \cos^2 \theta_c \cos^2 \theta_F} \\ &= \frac{\sin^2 \theta_c}{\sin^2 \theta_R} = \left(\frac{V_1}{V_2 \sin \theta_R} \right)^2 \end{aligned}$$

$$\cos \theta_T = \frac{V_1}{V_2 \sin \theta_R}$$

$$\sin \theta_c' = \frac{V_0}{V_1} \sin \theta_R$$

$$V = \frac{V_0}{\frac{V_0 \sin \theta_R}{V_1} \cdot \frac{V_1}{V_2 \sin \theta_R}}$$

$$V = V_2$$

As $V = V_2$, it is concluded that the ray path previously derived is correct.

The important conclusion to be drawn here is that a side refraction problem of this type cannot be reduced to two dimensions without error. The magnitude of the error will, of course, depend on the particular problem. Figs. 4 and 5 illustrate the amount of error that would be incurred if a simplification were made whereby the line of refraction from the V_1V_2 interface is assumed to lie along the intersection of the fault plane and a plane perpendicular to the fault plane (dipping $90 - \theta_F$ or 30° in this case) which passes through the geophone line ($D_1D_1'R_1R_1'$). For purposes of depth calculation this assumption would be convenient. The refractor would be assumed to lie tangent to a circle with its center on the line of the profile and a radius determined from the standard intercept time formulas. In Figs. 4 and 5, $F_1F_1'G_1G_1'$ is the position of the plane $FF'GG'$ that would be obtained if such an interpretation were made.

The magnitude of the error encountered in making this simplifying assumption would, in practice, depend on the thickness of the low speed material lying above the V_1 refractor as well as the angle of the fault. Given thickness d and R (Fig. 5) and the velocity of the three media, it is possible to calculate, as a function of the dip of the V_1V_2 interface, the locus of points where first arrival of energy would be expected to be refracted from the V_1V_2 interface at various angles of dip. The concept of delay time (Nuttleton, 1940) is central in the following reasoning. Consider Fig. 3 and the following: the delay time in the V_0 medium is

$$D_t = \frac{t}{V_0} - \frac{S}{V_2}$$

$$D_t = \frac{d}{V_0 \cos \theta_c'} - \frac{D \tan \theta}{V_2}$$

Where θ_c' can be seen from previous discussion to be an angle that varies with the angle θ_F . θ_d can be related to θ_c' and θ_T by using Fig. 3:

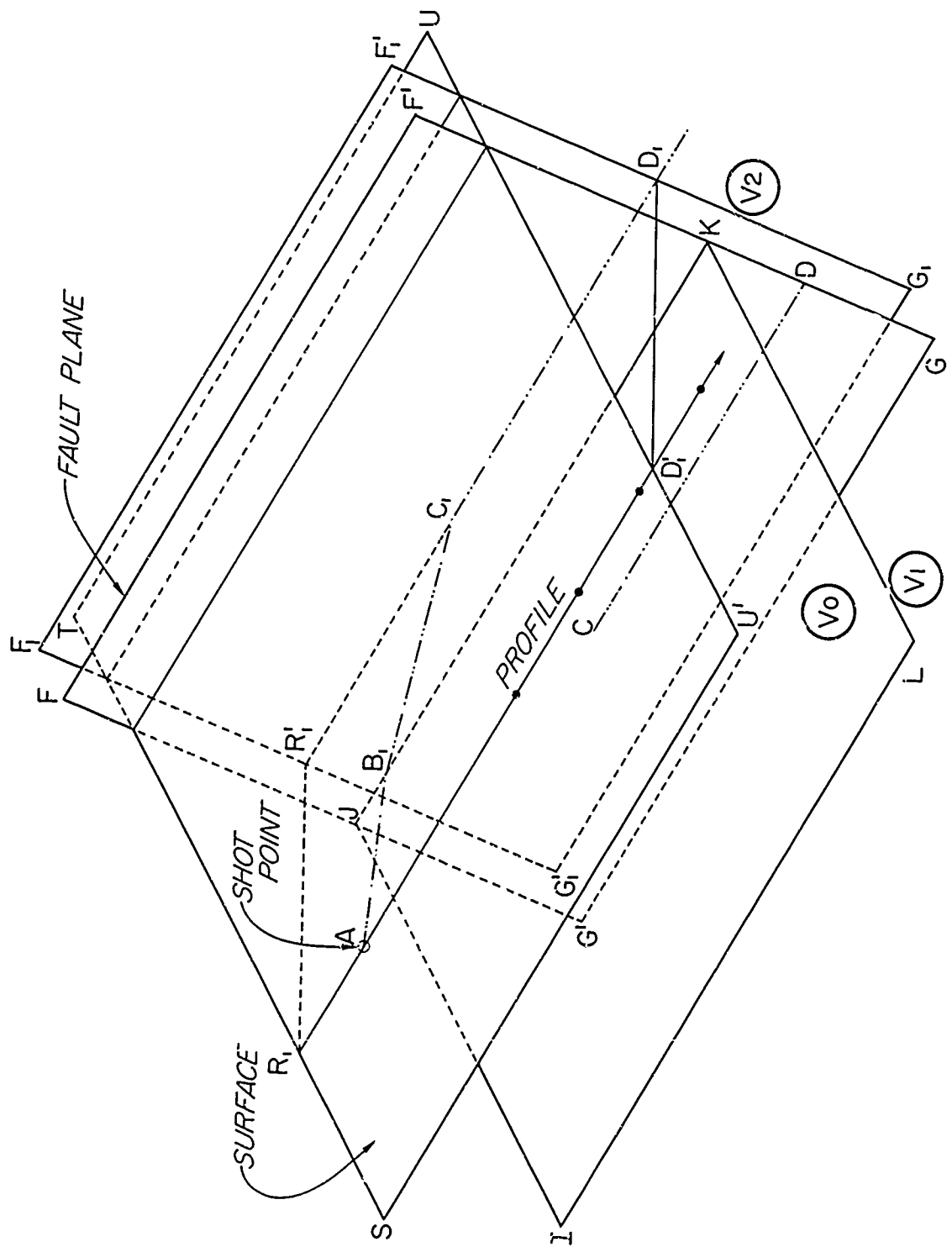


Figure 4. Two-dimensional approximation of Figure 2.

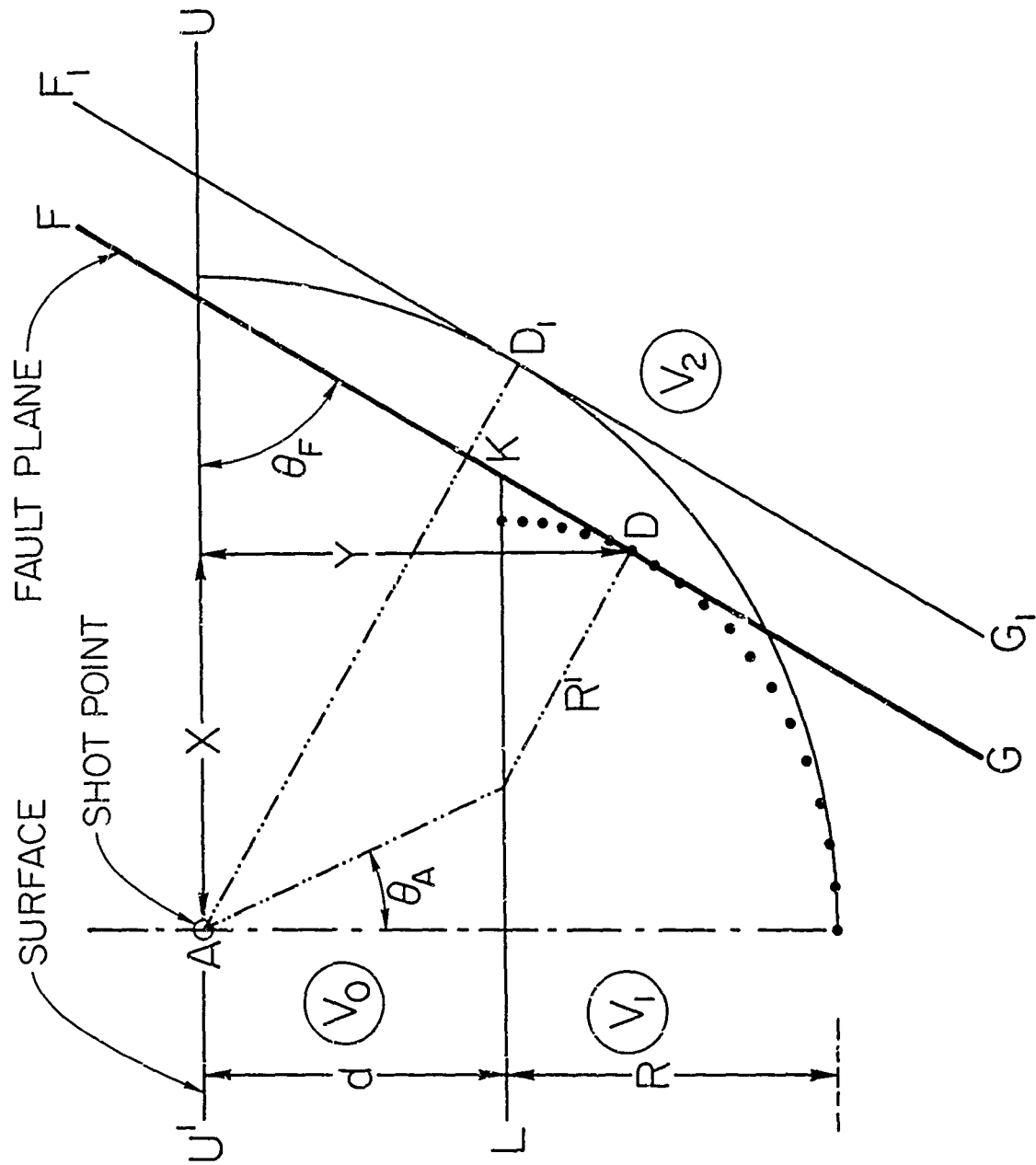


Figure 5. Cross-section of Figure 4.

$$\frac{\sin \theta_d}{\cos \theta_c'} = \frac{s}{d}$$

$$\cos \theta_T \tan \theta_c' = \frac{s}{d}$$

$$\sin \theta_d = \cos \theta_c' \tan \theta_c' \cos \theta_T$$

$$\sin \theta_d = \sin \theta_c' \cos \theta_T$$

$$\tan \theta_d = \sin \theta_d \sqrt{1 - \sin^2 \theta_d}$$

If $\theta_F = 0$, then we have the standard case of three horizontal layers. The delay time in the first medium is

$$d_{n02} = \frac{D_t}{V_0} \sqrt{V_2^2 - V_0^2/V_2}$$

except in the case where $\theta_F = 0$ ($D_{02} = D_{n02}$), D_{02} is greater than D_{n02} due to the greater distance traveled in the V_0 medium. R' will therefore be less than R (Fig.5) and using the form of the expression for depth in the second medium (i.e. $Z = D_{12} V_1 / \cos \theta_c$) and noting that D_{12} is diminished by an amount $(D - D_n)$, we can write

$$R' = R - \frac{(D_{02} - D_{n02}) V_1}{\cos \theta_c}$$

From Fig.5 it is evident that the locus of side refraction points for varying angles of dip can be written as parametric equations in x and y where y is positive downwards.

$$\begin{aligned} x &= d \tan \theta_A + R' \sin \theta_F & \text{where } \tan \theta_A &= \sin \theta_c \tan \theta_c' \\ y &= d & + R' \cos \theta_F \end{aligned}$$

A simple computer program has been written to calculate the points on the locus for angles of dip ranging from 0 to 90 degrees in 5-degree increments, given three velocities, d , and R . Extremely useful templates can then be made for solving side refraction problems.

V. INTERPRETATION

A. Correction of Data and Sources of Error

Fig. 1 shows the location of six seismic profiles. The interpretations of the IXL profile and the West Road profile were made by Meister (1967). Interpretations of E53, E54, E55, and E56 were made by the writer. Profiles E53, E55, and E56 were positioned as nearly parallel to the 1954 earthquake fault scarp as was possible. Care was taken to keep the shot points of a given profile on a straight line with the geophone line.

The survey data is sufficiently accurate for the problem being considered. Locations of geophones at the middle of the line where the spread crosses the road are known within approximately ± 10 ft. Geophone spacing averaged 198 ± 2 ft. Near the ends of the spread geophones may be off line by as much as 15 ft. Distant shot points may be off line by as much as 50 ft. Distances were measured using stadia and are probably accurate within 2 per cent. Some elevation differences were taken with an altimeter and may be in error by as much as 5 ft. Perhaps the greatest source of error is the incomplete knowledge of velocity distribution above the 16,500 ft/sec basement.

With the exception of the West Road profile, all the profiles shown on Fig. 1 rest on a topographically irregular high alluvial fan. Work done by Meister and Cabaniss in 1965 near IXL Canyon using a small, six-trace "GeoSpace Corp." seismic interval timer suggests that the "weathered" layer is commonly somewhat irregular in thickness and velocity. In general, however, the thickness of low velocity material increases toward the west with the increasing elevation of the fan (Fig. 4, Part I).

Using available weathering and sub-weathering data, E53, E55, and E56 have been corrected to flat datum planes resting on 6500 ft/sec sub-weathering alluvium. E54 was corrected to a sloping datum in order to avoid large corrections. Weathering corrections were performed using the standard formulas of Nettleton (1940). The sub-weathering layers are assumed, for purposes of calculation, to rest on a 10,000 ft/sec layer

which should be roughly equivalent to the top of the Tertiary section of interbedded volcanic and sedimentary rock. It is realized that neither the 6500 ft/sec layer nor the 10,000 ft/sec layer are as seismically homogeneous as the model suggests. Velocity reversals almost certainly occur in the Tertiary section because of its interbedded nature. Also, higher velocities than the model velocity have been observed in both layers: as much as 8000 ft/sec in the sub-weathering and up to 13,000 ft/sec in the interbedded Tertiary section. The simplification made in assuming these two average velocities is both expedient and, with the information available, reasonable. The granitic basement velocity has been reversed several times in the map area of Fig. 1 and found to be 16,500 ft/sec. When attempting to obtain a true velocity, care was taken that the segments of the travel time curve being considered actually represented the same segment of the refractor. This generally involved drawing ray paths and using segments of the two time-distance curves from opposite ends of the spread.

The method of shooting should be evident from Fig. 1. The geophone spread remained fixed and shot points were placed on straight lines extending from the spread at increasing distances from the geophones. The method of delay times was used in making the interpretation. Error due to possible structure in the space between shot points is expected to be no more serious than other sources of error inherent in seismic refraction work. Preliminary interpretation of each profile was made as if the refracting rays traveled in a vertical plane through the line of the profile (Figs. 6, 7, 8 and 9). Side refraction templates were then constructed as described in the previous section and cross-sections such as Figs. 7 and 10 were then drawn.

B. Special Techniques Used in Interpretation

As three of the profiles considered here were overlapped by a fourth (i.e. E54), it was, in many cases, possible to overcome some of the uncertainty inherent in the method of dividing the intercept time in half and

calculating a depth to an interface as if the depth were the same beneath the shot point and the geophone. The interdependent nature of all six of the profiles shown in Fig. 1 affected the delay times found for some of the southern shots of both E53 (Fig. 6) and E54 (Fig. 7). The shallowing of the 10,000 ft/sec material at shot N3 of E56 (Fig. 9) is supported by the IXL profile and an anomalous delay time.

Another technique that has been found to be helpful is to superimpose, on a light table, the time-distance curves associated with different shots on one side of a particular profile. In this way the points on a particular time-distance curve could be more easily associated with their proper refractors. The reasoning used in doing this is as follows: as the spread remains stationary, refraction arrivals for a given plane interface will always give the same time-distance curve, plus or minus a constant time due to the difference in distance of the shot point from the spread. Therefore a systematic approach to separating refractors is to begin with a time-distance curve of a distant shot which in most cases would be known to show entirely basement arrivals. This curve could then be superimposed on a curve made from a shot on the same side of, but closer to the spread; points associated with a lower velocity refractor would then be easily recognized. This method is especially useful when the surfaces between refractors are irregular and cause irregularly shaped time-distance curves. Also, it should be noted that what amounts to second arrival refraction times can be found using the same method of superimposing time-distance curves.

Intercept times associated with delay times of the geophones nearest the shot can then be found for the close-in shots, which show basement first arrivals only on the most distant phones. When this is the case, the delay time for one or all of the close-in geophones must be just half the intercept time. Sometimes a ray path construction is necessary to find the particular geophone with a delay time theoretically equal to that of the shot point.

C. Profile E53

Fig. 6 is the interpretation of profile E53 which was first made as if the refracted energy of all the shots of E53 traveled to the geophones in the same vertical plane. The energy arriving from the 16,500 ft/sec material was clearly side refracted and in Figs. 7 and 10 suitable corrections have been made using the method of handling side refractions.

The depth to the 10,000 ft/sec layer is based on the assumption that the 13,000 ft/sec arrivals from shot N1 represent a 10,000 ft/sec layer dipping toward the shot. Possibly there is a 13,000 ft/sec layer below the 10,000 ft/sec layer and no dipping layer, but the following evidence favors a 10,000 ft/sec dipping layer: on profile E55 a 10,000 ft/sec velocity is observed and reversed. Its depth agrees with the depth calculated for the 9000 ft/sec velocity shown on profile E54 where again a 10,000 ft/sec true velocity is assumed, but not reversed. The dipping 10,000 ft/sec layer assumed on E54 ties well with the depths calculated at E53, E55, and E56.

The irregularity in the top of the basement (16,500 ft/sec layer) was calculated from the amount of departure of the basement first arrival times from a straight line (16,500 ft/sec) drawn through them. The similarity in the time-distance curves for a given side of the spread suggests that the irregularity in the time-distance curves is due to irregularity in the basement or in the thickness of overlying layers rather than poor first breaks. The northward deepening of the 10,000 ft/sec layer was considered in calculating the configuration of the 16,500 ft/sec interface.

Since basement arrivals were observed on both S1 and N1, there was little ambiguity in the depth to basement beneath the geophones. Once this depth had been calculated, geophone delay times were available to be subtracted from the intercept times of shots more distant from the spread, thus yielding shot point delay times from which a depth to basement beneath the shot could be calculated.

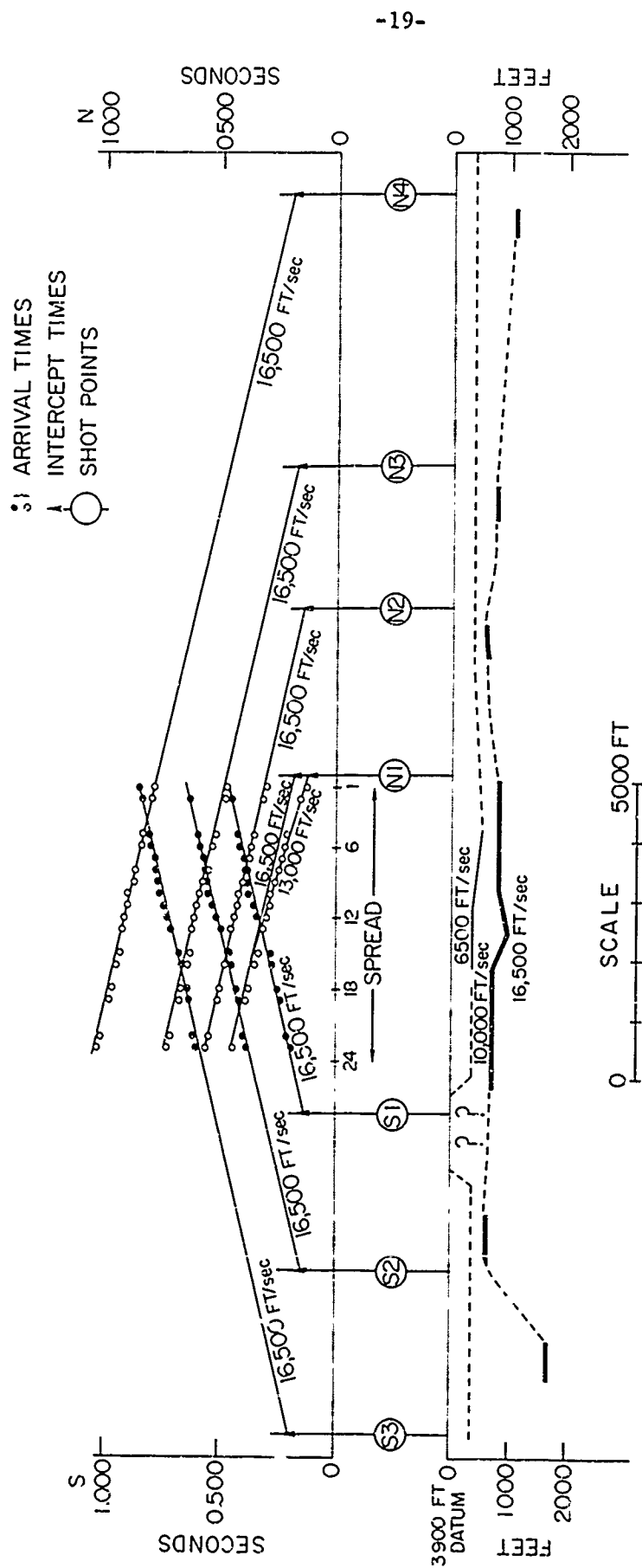


Figure 6. Time-distance curves and cross-section, Mud Springs Profile E53.

D. Profile E54

The data obtained from profile E54 and that of the other four profiles shown in Fig. 7 were combined to construct a cross-section along E54. The arrival times observed on E54 were corrected to a sloping datum which very nearly approximated the ground surface. The sloping datum used is marked "GROUND SURFACE" in Fig. 7.

The 7500 ft/sec velocity observed on the record of shot point W1 is believed to be a thin, discontinuous interbed below the water table but above the 10,000 ft/sec layer. The existence of such an interbed is unimportant in the determination of a depth to basement. The 9000 ft/sec velocity observed on the record of both W1 and W2 is a down-dip apparent velocity on the 10,000 ft/sec layer.

The 13,000 ft/sec velocity is a down-dip apparent velocity of the 16,500 ft/sec basement. On both E1 and E2 the water table velocity of 6500 ft/sec is observed as well as two early arrivals on the most distant phones which show an apparent velocity of 34,000 ft/sec. These high speed arrivals are most likely basement arrivals and may be the result of diffraction from the fault directly under E55. Total travel times calculated from both E1 and E2, using the interpretation shown in Fig 7 and assuming the high speed arrivals were basement arrivals, were within 20 milliseconds of the actual observed arrival times.

E. Profile E55

Profile E55 (Fig. 8) is parallel to and about 1600 ft east of E53. The small intercept times noted at S1 and N1 indicate a shallow basement. After considering the position of E55 in cross-section (Figs. 7 and 10) and the intercept times at the six shot points and the depth they imply, it was concluded that side refraction does not occur on this profile. The method of interpretation was very similar to that of E53 except that side refraction corrections were not necessary.

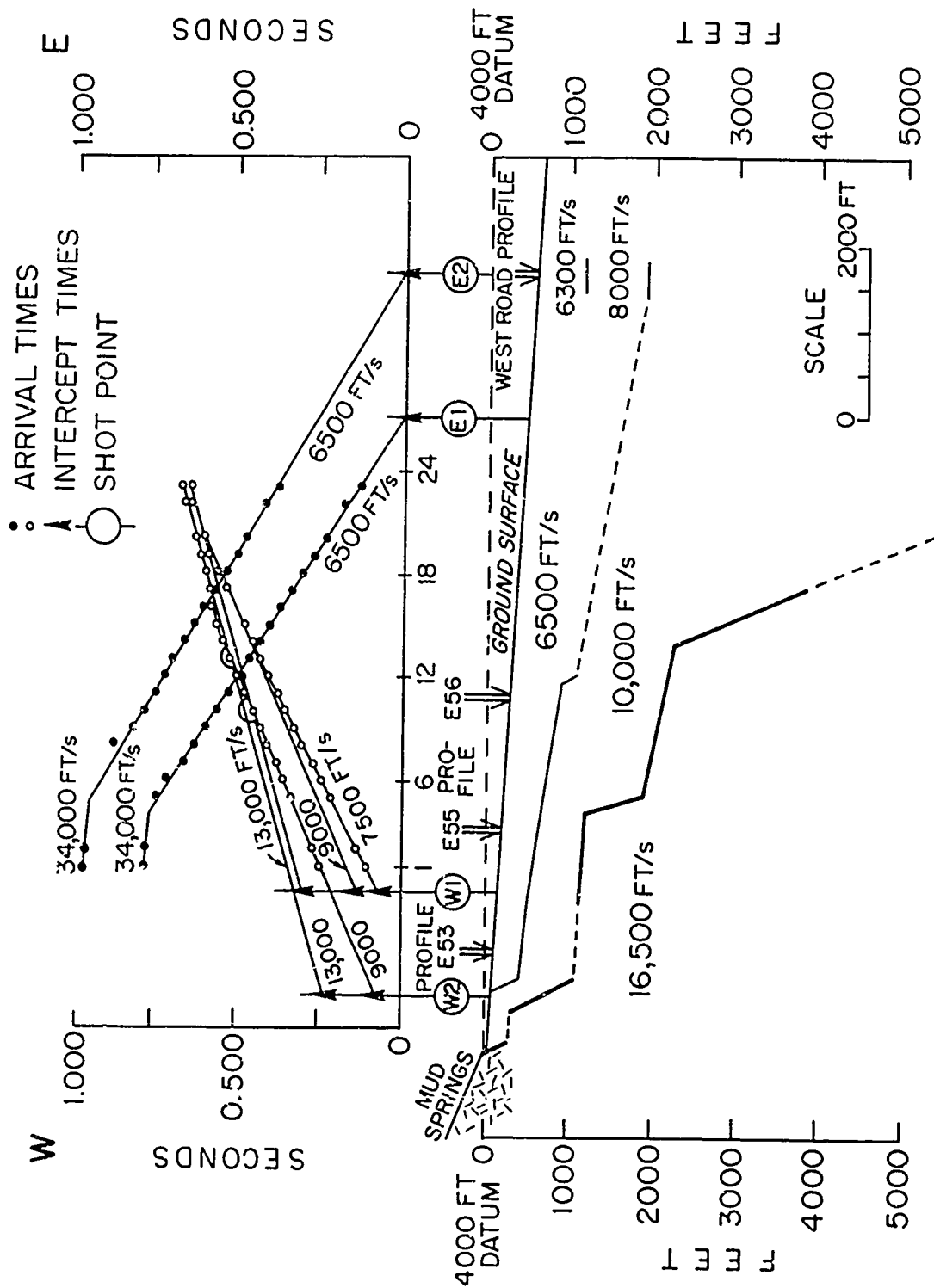


Figure 7. Time-distance curves and cross-section, Mud Springs profile E54.

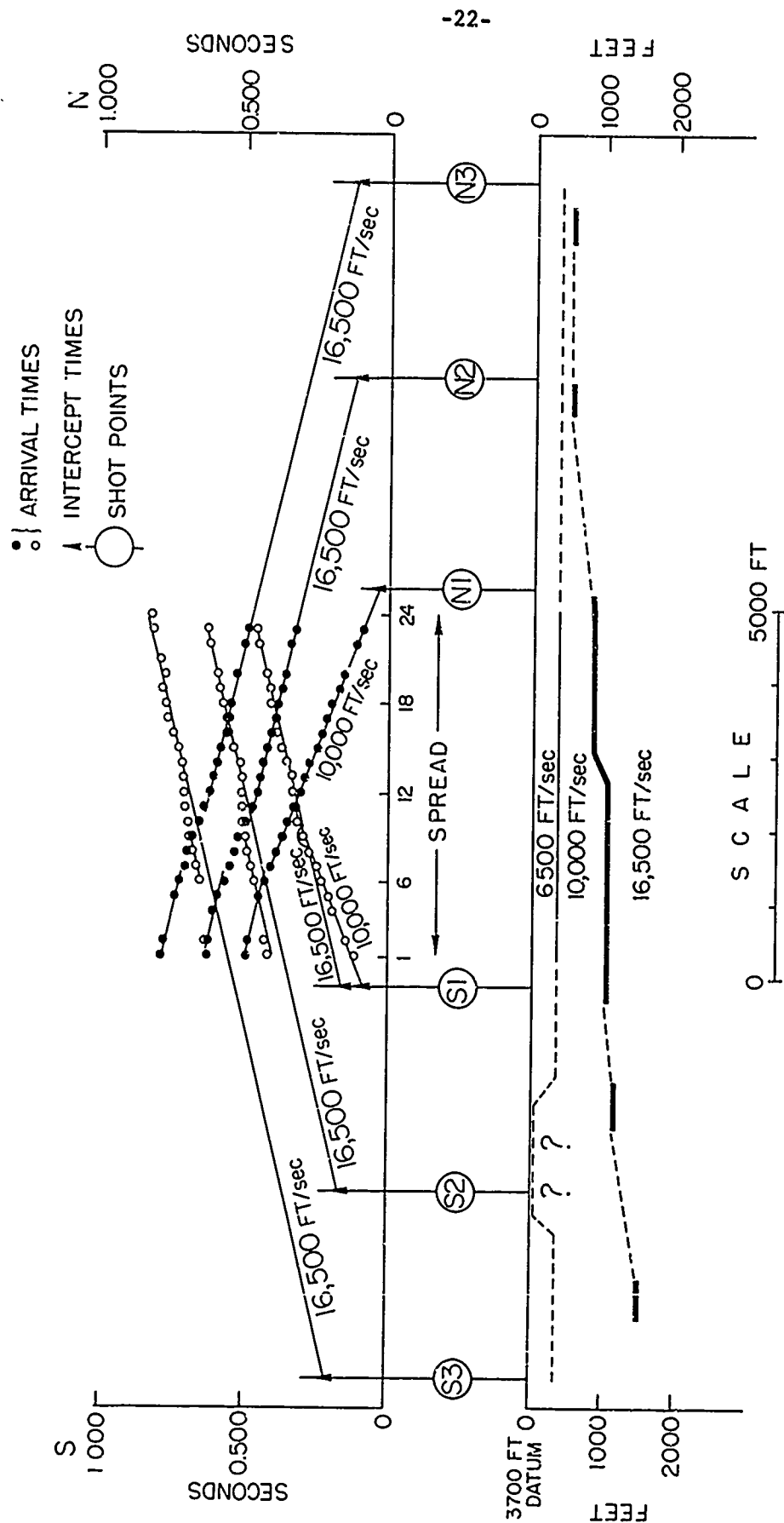


Figure 8. Time-distance curves and cross-section, Mud Springs Profile E55.

F. Profile E56

The interpretation of E56 is complicated by the structure in the layers above the basement. Delay times in the three layers above the basement were calculated at several points along the profile before the solution shown in Fig. 9 was reached.

It is not certain if side refraction occurs under the geophone line of E56. The interpretation given in Fig. 7 assumes that it does not. As interpreted in Fig. 7, first arrivals must come from the basement directly under E56, but if the fault directly under E55 were moved 200 ft east, first arrival side refractions would be possible. In either case (i.e., the energy is or is not side refracted), the geophone delay times at E56, combined with the data from E55 and the West Road profile, place sharp constraints on the possible basement configuration below E56.

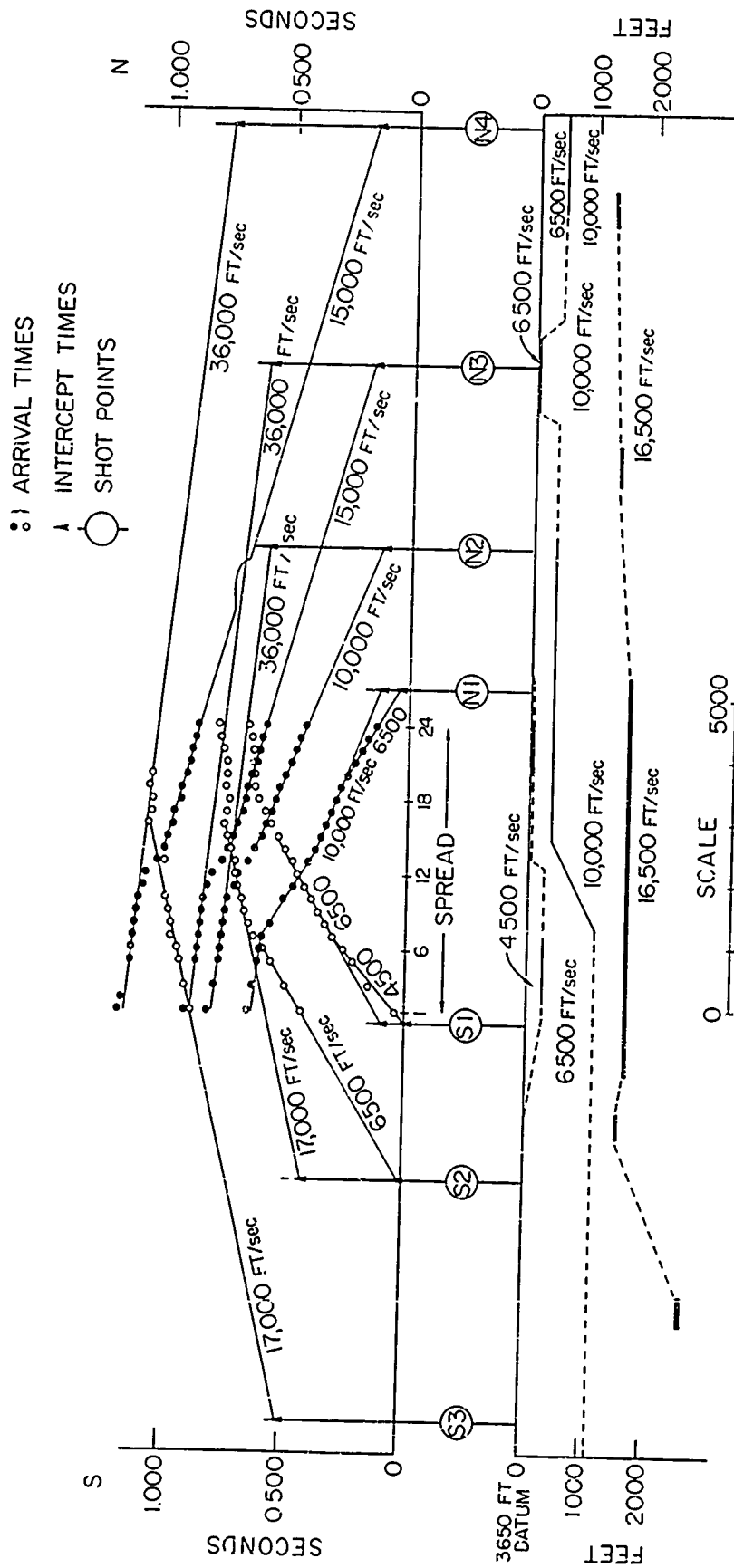


Figure 9. Time-distance curves and cross-section, Mud Springs Profile E56.

VI. CONCLUSIONS

The technique of air shooting proved to be rapid, relatively inexpensive, and effective. The blasts cause no pain to the ears of the shooter, so air shooting is not an unpleasant or excessively dangerous technique to use.

The theory developed on side refractions was effectively used in constructing the cross-sections shown in Fig. 7 and Fig. 10. The templates that can be made using the computer program should be useful in any situation where side refractions are likely.

From the point of view of structural geology, it is significant, although perhaps not surprising, that four major faults in the basement were found rather than only the one evident at the surface. The dips of the faults are steep. Within the restrictions of the data as it has been interpreted, the dips may range from 55 to 70 degrees. Dips outside this range would not fit the data.

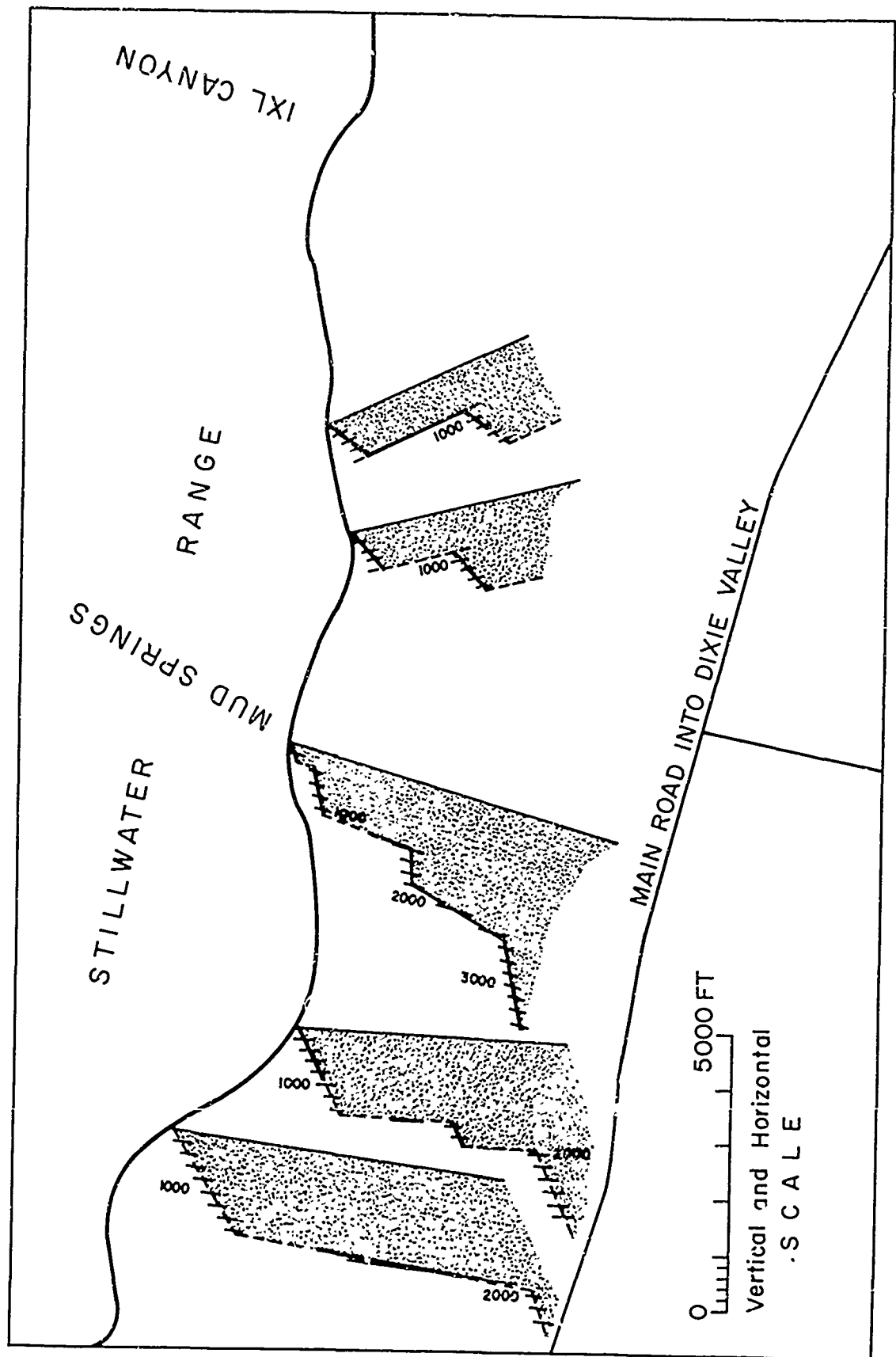


Figure 10. Cross-sections along scarp showing basement contact.

BIBLIOGRAPHY

- Buffet, A., and Layat, C. H., 1960, Nouvel Aspect de la Sismique Refraction au Sahara: Tirs non Enterrés; Geophysical Prospecting, Vol. 8, pp. 47-67.
- Meister, L. J., 1967, Seismic Refraction Study of Dixie Valley, Nevada; A. F. Cambridge Research Labs. Final Scient. Rpt. Part I, AFCRL-66-848.
- Nettleton, L. L., 1940, Geophysical Prospecting for Oil; New York, McGraw-Hill, 444 pp.
- Page, B. M., 1965, Preliminary Geologic Map of a Part of the Stillwater Range, Churchill County, Nevada; Nevada Bureau of Mines Map 28.
- Poulter, T. C., 1950, The Poulter Seismic Method of Geophysical Exploration; Geophysics, Vol. 15, pp. 181-207
- Smith, T. E., 1967, Aeromagnetic Measurements in Dixie Valley, Nevada; Implications Regarding Basin-Range Structure; A. F. Cambridge Research Labs. Final Scient. Rpt. Part III, AFCRL-66-848
- Soske, J. L., Unpublished notes on seismic refraction.

PART III.

AEROMAGNETIC MEASUREMENTS IN DIXIE VALLEY, NEVADA:
IMPLICATIONS REGARDING BASIN-RANGE STRUCTURE

by

Thomas E. Smith

ABSTRACT

Interpretation of an aeromagnetic survey flown during 1964 suggests that the pre-Tertiary magnetic basement under Dixie Valley, Nevada, forms an asymmetric, composite graben. The deepest component block is approximately 5 km wide and lies under the western half of the valley at an average depth of 2 km. Bordering "shelf" blocks are downthrown with respect to adjacent ranges, but to a lesser degree. Depth estimates imply, in addition, that the eastern shelf block is broken by several NW-trending transverse faults of 300 to 600 meters displacement.

The magnetic expression of contacts between a Jurassic gabbroic complex and other basement rocks is traceable across both northern and southern Dixie Valley. An absence of appreciable horizontal offset of this contact across the major Basin-Range faults indicates that post-Jurassic displacements have been primarily dip-slip. An apparent right lateral offset of 2-3 km may exist along the eastern side of the deepest graben block, however.

Models computed from anomalies over the southern gabbro contact tend to verify earlier geologic inferences that this intrabasement complex is of lopolithic form. The apparent northward displacement of the gabbro contact in the Clan Alpine Range from the subsurface contact in eastern Dixie Valley may reflect an uplift of the range, relative to the Valley block, with subsequent erosional stripping of the tapered lopolith.

Satisfactory alternative solutions of an equidimensional anomaly in southeastern Dixie Valley are either a volcanic cone or an equidimensional volcanic remnant. Both computational models overlie the gabbroic complex and require a high total magnetization.

* Now at Mackay School of Mines, University of Nevada, Reno, Nevada.

ACKNOWLEDGEMENTS

The writer is indebted to Sheldon Breiner of Varian Associates for the use of a magnetometer and for monitoring of total intensity background. Dr. R. C. Speed of Jet Propulsion Laboratory has been extremely helpful in providing an additional magnetometer; both he and Dr. Ben M. Page of Stanford University have generously contributed geologic information concerning mountain ranges adjacent to Dixie Valley. Sincere gratitude is expressed to the late Professor J. L. Soske and to Professor G. A. Thompson for their counsel and suggestions.

TABLE OF CONTENTS

	<u>Page</u>
ABSTRACT.....	ii
ACKNOWLEDGEMENTS.....	iii
TABLE OF CONTENTS.....	iv
LIST OF ILLUSTRATIONS.....	v
<u>Chapter</u>	
I. INTRODUCTION.....	1
II. COLLECTION AND REDUCTION OF DATA.....	3
III. GENERALIZED GEOLOGY AND MAGNETIC UNITS.....	5
IV. DETERMINATION OF MAGNETIC PARAMETERS.....	9
V. INTERPRETATION OF MAGNETIC DATA.....	12
A. Qualitative Inference.....	12
B. Basement Topography.....	15
C. Model Representations of the Magnetic Units.	18
VI. CONCLUSIONS.....	21
APPENDIX.....	22
BIBLIOGRAPHY.....	23

LIST OF ILLUSTRATIONS

FIGURE	TITLE	PAGE
1.	Generalized geologic and geophysical map of the West Humboldt, Stillwater, and Caln Alpine Ranges, Nevada. Surface geology adapted from Page, 1965, and Speed, 1963. Subsurface structures inferred from geophysical data.	6
2.	Generalized geologic section and observed total intensity anomaly along the Stillwater Range, Nevada.	7
3.	Magnetic total intensity and second vertical derivative maps of Dixie Valley, Nevada. Boundary of this map shown on Fig. 1.	13
4.	Topographic map of magnetic basement (compiled from depth estimates).	16
5.	Alternative solutions satisfying equidimensional anomaly in southeastern Dixie Valley.	19

I. INTRODUCTION

Dixie Valley and the adjacent mountain ranges considered in this paper are located in the western part of the Basin-and-Range structural province and are bounded approximately by latitudes $39^{\circ}20'$ N. and $40^{\circ}15'$ N., and by longitudes $117^{\circ}30'$ W. and $118^{\circ}30'$ W. (Part I, Fig. 1).

Following the earthquake of December 16, 1954, Dixie Valley and surrounding areas have been the foci of numerous investigations. Effects of that dynamic display of tectonic activity and the availability of supplementary information contributed by investigators in the various disciplines renders Dixie Valley particularly advantageous for geophysical studies of Basin-and-Range structural problems.

Magnetic data were collected in Dixie Valley during 1964 to help determine the structural history and subsurface geometry of that basin. Of primary concern in this investigation was the establishment and tracing, by means of magnetic measurements, of a geologic contact which is intersected by the major fault systems of Dixie Valley. The magnetic expression of displacements on this contact establishes whether shallow crustal faulting throughout the Cenozoic era has been principally of a normal sense as the 1954 scarps and strain data suggest (Slemmons, 1957, Meister, personal comm., 1966) or, alternatively, whether movement in a strike-slip sense has been of major significance (Sales, 1966, Romney, 1957).

A secondary objective was to examine, through gradient analyses, the general configuration of magnetic basement under Dixie Valley, both as an aid to programming subsequent seismic refraction work, and as a means of extrapolation between seismic profiles. An additional aspect, investigated through computational models, was the intrabasement geometry of a gabbroic complex exposed in adjacent mountain ranges.

Previous geological work in Dixie Valley and adjacent mountains has been primarily concerned with surface mapping, subsurface studies being limited to hydrologic investigations from shallow well data (Cohen et al., 1963). The stratigraphy and structure of the extreme

north end of the project area have been discussed by Muller and others (1951). Of particular value to the present project has been recent mapping of the Stillwater Range and parts of the West Humboldt and Clan Alpine ranges by Page (1965) and Speed (1963). Previous geophysical studies in and near the region of interest have been limited to a gravity survey of Dixie Valley (Thompson, 1959, unpublished), a recent gravity survey of the Carson Sink-West Humboldt area (Wahl, 1965), a complete geological-geophysical investigation of the Sand Springs Range, Fairview Valley, and Fourmile Flat area to the south of Dixie Valley (Nev. Bur. Mines, et al, 1962), and to seismological investigations of the December, 1957 earthquake (Romney, 1957, Cloud, 1957)

II. COLLECTION AND REDUCTION OF DATA

Magnetic total intensity measurements were taken with a Varian Model M-49 nuclear precession magnetometer adapted for aeromagnetic use. The instrument package, mounted in a light aircraft, was connected through 31 meters of suspension and transmission line to the sensing unit. It was found that this cable length effectively eliminated magnetic interference of the airplane, regardless of flight orientation. Actuation of the polarization-readout cycle was effected manually by an operator at ten second intervals determined by a stop watch. Station values accurate to ± 5 gammas and pertinent location information were recorded by a third person in the aircraft.

Positioning of flight lines was controlled by establishing a series of ground reference points over which the pilot would fly, indicating to the recorder when they were crossed. In the subsequent plotting of data, station points were distributed linearly between reference locations, compensating for variations in groundspeed. Locations accurate to approximately ± 100 meters were obtainable by this method. With minor exceptions, flight lines were flown at a barometric elevation of 1280 ± 15 meters above sea level. This elevation corresponds to an approximate height of 215 meters above the valley floor. Departures from this elevation were necessary only over isolated alluvial fans at the basinal margin.

During periods of aeromagnetic measurements, a continuous monitor of total intensity was recorded by Varian Associates in Palo Alto, California (37°30' N., 122°05' W.). Diurnal and transient variations appearing on those records were compensated for in all survey data.

A linear gradient of 1.2 gammas/km in the direction N30E was assumed as a regional corrective factor for all magnetic data (U.S.C. & G.S., 1955). After application of space and time dependent corrections, crossing profiles generally agreed to within 15 gammas. This value closely approaches the inherent standard deviation error in the survey,

- 4 -

and in view of the 50-gamma map contour interval desired, no further statistical adjustments were made to data within the survey grid.

III. GENERALIZED GEOLOGY AND MAGNETIC UNITS

A comparison of the total intensity isoanomalic map (Fig. 3a) and of a profile flown along the crest of the Stillwater Range (Fig. 2) with mapped geology (Fig. 1) reveals that the numerous rock units mapped by Page (1965) and Speed (1963) in that and other ranges from these includes sedimentary rocks of Upper Triassic age and overlying welded tuffs, latite, and rhyolite. An average total intensity anomaly over this unit is approximately 200-gammas above the magnetic base level of 53,150 gammas observed in the area farther south (U.S.C. & G.S., 1955). Bordering these rocks on the north, a second magnetic unit, of late Jurassic age, is composed of heterogeneous gabbroic intrusive rocks and basalt, which generate a strongly undulatory anomaly averaging approximately 500 gammas. The third magnetic unit of significance, unexposed in the ranges, borders the aforementioned gabbroic suite on the north. The magnetic expression of this mega-unit, of comparable magnitude but lower relief, suggests it is more homogeneous than the gabbroic complex.

Triassic rocks of the southern magnetic unit in the Stillwater Range are exposed generally south of latitude $39^{\circ}50'$ N. They occur as gray-black, grayish-weathering slates and phyllites. Over the greater part of the exposure, only incipient recrystallization is evident although exceptions do occur near granite contacts. Complex deformation of these rocks precludes direct measurement of their thickness; however, estimates are between 1500 and 3000 meters (Page, 1965). Fossils collected in this marine unit indicate that it is of Upper Triassic age.

South of latitude $39^{\circ}40'$ N., the Triassic slates are unconformably overlain by a number of magnetically similar volcanic units. These are shown as undifferentiated devitrified welded tuffs, rhyolite, and latite on Fig. 1. Of nonmarine origin, these rocks may range in age from late Jurassic through early Tertiary. The composite thickness of this sequence is as much as 4800 meters (Page, 1965).

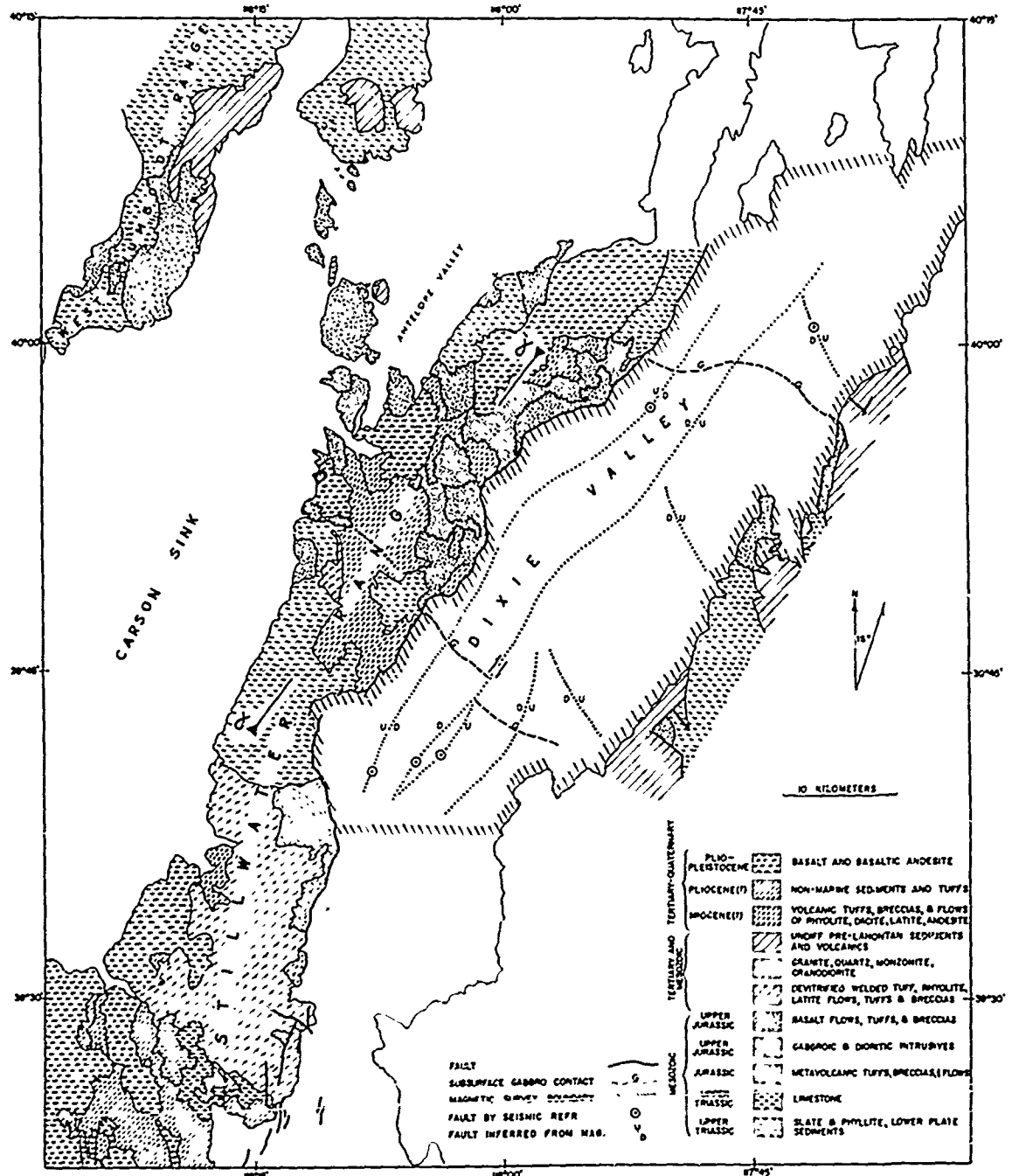


Figure 1. Generalized geologic and geophysical map of the West Humboldt, Stillwater, and Clan Alpine Ranges, Nevada. Surface geology adapted from Page, 1965, and Speed, 1963. Subsurface structures inferred from geophysical data.

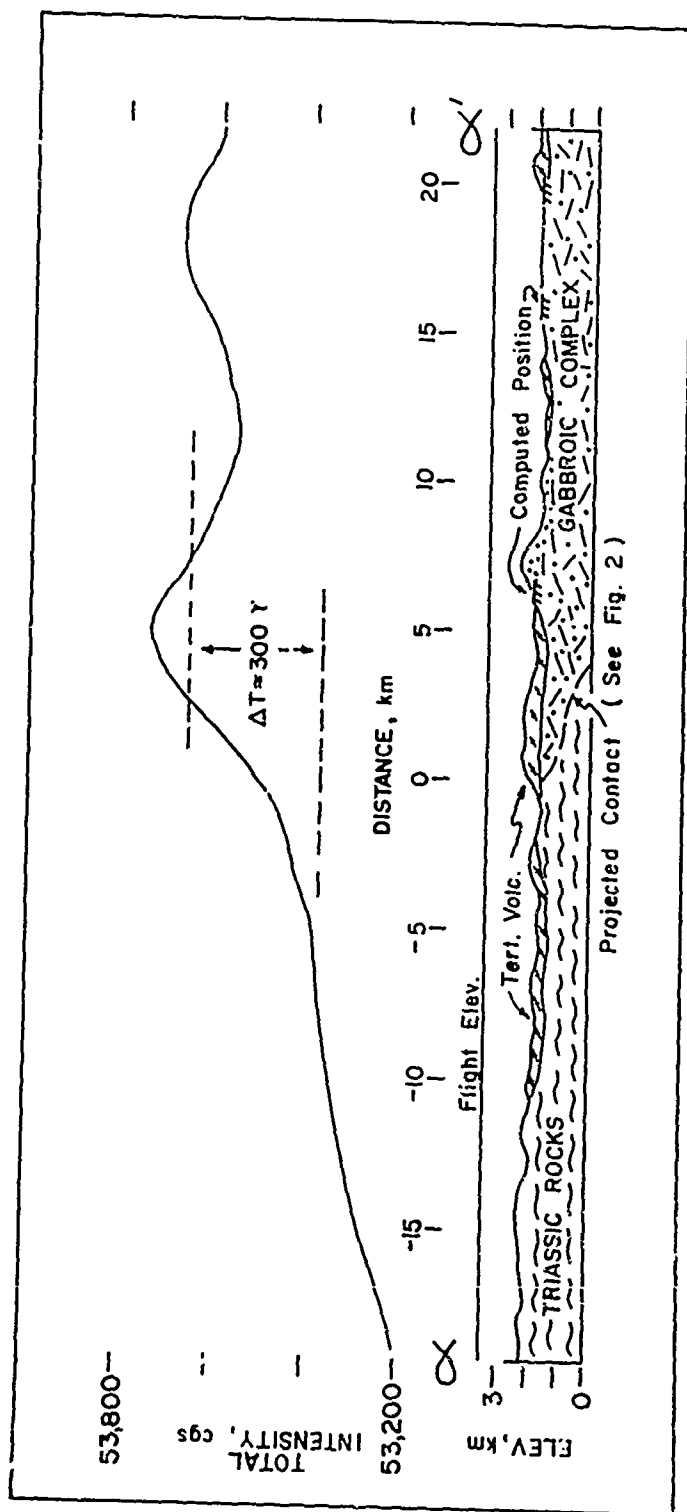


Figure 2. Generalized geologic section and observed total intensity anomaly along the Stillwater Range, Nevada.

The second magnetic mega-unit is exposed north of latitude 39°50' in the Stillwater Range. Intrusive rocks of this unit form a heterogeneous gabbroic assemblage which includes diorite, gabbro, picrite, anorthosite, diabase, keratophyre, and gabbroic pegmatite. Along margins of the intrusion, differentiation layering has been noted. A potassium-argon age determination from similar rocks in the West Humboldt Range indicates the complex is probably of Late Jurassic age (Speed, 1962 a, b). Closely associated with the intrusive gabbroic complex are large areas of altered basalt which appear to be co-genetic and perhaps contemporaneous with the intrusive suite. Speed suggests the entire complex, of lopolithic form, was emplaced at shallow depth, locally erupting to form the associated effusives

Along much of the Stillwater crest, the gabbroic unit is capped by Tertiary flows and pyroclastics of rhyolite, dacite, latite, and andesite. Dissection of the flows exposes a total thickness of about 550 meters. Approximating a thin plate geometry, these rocks exhibit an apparent magnetic transparency.

In Dixie Valley proper, as in many other valleys of the western Basin-and-Range, great thicknesses of late Cenozoic lake and stream deposits have accumulated. These range in age from Pliocene to Recent and include alluvial fan detritus, channel deposits, and lacustrine sediments. For the most part, the lake sediments consist of silt and clay although shoreline deposits of gravel and sand exist locally. For the purpose of this investigation, complexities in this sequence are ignored; it is considered as essentially non-magnetic valley fill.

IV. DETERMINATION OF MAGNETIC PARAMETERS

In order to assign representative parameters to the various magnetic units, methods of approach were employed which depend both on inferences derived from total intensity profiles and on individual rock samples from the region. A limited number of samples were collected by the writer and by R. C. Speed from the Clan Alpine, West Humboldt, and Stillwater Ranges. From cores of these specimens, volume susceptibility, magnitude of remanent magnetization, and density were determined (Appendix A). High average values of remanence, particularly in the gabbroic complex, dictated the application of methods which consider that property. The general method adopted has its basis in techniques discussed by Green (1960), and Hays and Sharon (1963) which establish an equivalent susceptibility contrast between adjoining magnetic units.

Resulting magnetization $\vec{J}_{1,2}$ over contiguous units 1 and 2 can be expressed by

$$\vec{J}_1 = \vec{P}_1 + K_1 \vec{T}_0 \quad (1)$$

$$\text{and} \quad \vec{J}_2 = \vec{P}_2 + K_2 \vec{T}_0 \quad (2)$$

where K = volume susceptibility, \vec{P} = remanent magnetization, and \vec{T}_0 is the geomagnetic field intensity. A relative contrast of magnetization is then given by

$$\vec{J}_t = (\vec{P}_1 - \vec{P}_2) + (K_1 - K_2) \vec{T}_0 \quad (3)$$

This relative intensity contrast is equivalent to that produced by a volume susceptibility contrast of

$$\Delta K_t = \frac{\vec{J}_t}{\vec{T}_0} \quad , \text{ in the particular case of } \vec{J}_t \text{ and } \vec{T}_0 \quad (4)$$

The value ΔK_t is referred to as an equivalent susceptibility contrast.

Application of this expression in the present study assumes components of magnetization in all units are parallel to the present inducing field, and further, that reversal of permanent components is not of importance in the area of interest. These assumptions are necessary in the absence of detailed sampling. In addition, the Triassic slate is assumed to have negligible remanence. With these constraints on the method, equation (3) becomes

$$\vec{J}_t = \vec{P}_{gb} + (K_{gb} - K_{so}) \vec{T}_0 \quad (5)$$

where the subscripts gb and so refer to the gabbroic and southern magnetic units respectively.

Using only the average anomaly over the magnetic units, a lower limiting value of either K or ΔK may be established by use of the following expressions (Redford, 1964):

$$K_t = \frac{\Delta \vec{T}}{2\pi \vec{T}_0 \sin^2 i} \quad (6a)$$

$$\Delta K_t = \frac{\Delta \vec{T}}{2\pi \vec{T}_0 \sin i} \quad (6b)$$

where i is field inclination. Equation (6a) determines a minimum equivalent susceptibility over an infinite magnetic basement, whereas equation (6b) provides a minimum equivalent susceptibility contrast between two semi-infinite magnetic bodies of differing magnetizations. The former was used in this investigation to determine a value of $K_{so} = 700 \times 10^{-6}$ cgs for the southern magnetic mega-unit. Because this value clearly represents a minimum, a K_{so} value of 1000×10^{-6} cgs was assumed for calculation of an equivalent contrast between the southern magnetic unit and the gabbroic complex. Insertion of this K_{so} -value and an average of measured gabbro susceptibility and remanence (Appendix) into (5) yields $K_{gb-so} = 2700 \times 10^{-6}$ cgs.

If equation (6b) and a ΔT value of 300 gammas (Figs. 2 and 5) are used to determine K_{gb-so} , a minimum value of 1050×10^{-6} cgs is

obtained. The best typical value of K_{gb-so} most probably falls between this and the value determined using rock sample analyses; model computations in this investigation assume, therefore, an equivalent susceptibility contrast of 2500×10^{-6} cgs across this contact.

V. INTERPRETATION OF MAGNETIC DATA

A. Qualitative Interference

Dominating the center of the total intensity map (Fig. 3a) is a broad region of sharp anomalies exhibiting numerous closures of high magnetic relief. General characteristics of "fabric" and dipolar effects of this zone are even more discernible through an appropriate second vertical derivative filter (Fig. 3b). It should also be noted that the average magnetic base level over this region is approximately 300 gammas higher than over the adjoining area south of $39^{\circ}45'$ N (Figs. 2 and 3a). The southernmost margin of this undulatory magnetic "plateau" is marked by a linear gradient trending N 45 W at this latitude. Where the inflection line of this gradient intersects the Stillwater Range, it is nearly coincident with the mapped exposures of the gabbroic complex, suggesting that the high average level and magnetic topography to the north are correlative with the complex. Additional evidence of this correlation is furnished by a profile flown along the crest of the Stillwater Range, where a similar shift in magnetic level over the southern gabbroic edge is noted (Fig. 2). Figs. 1 and 3 show the position of the gradient inflection and inferred gabbro boundary across Dixie Valley.

Control on position of the northern contact of the complex is less exact in that a comparable shift in magnetic level is not observed. An approximate boundary can be established, however, by correlating the northernmost extent of the undulatory magnetic province with exposures of gabbro in adjacent mountains. A line indicating the inferred position of the contact trends roughly S 80 E from latitude $40^{\circ}00'$ in the Stillwater Range.

Extending northeasterly along the axis of Dixie Valley is a longitudinal, linear trend of anomalies of relatively high amplitude. To the west, approximately 4 km from and paralleling the east flank of the Stillwater is a second elongate anomalous

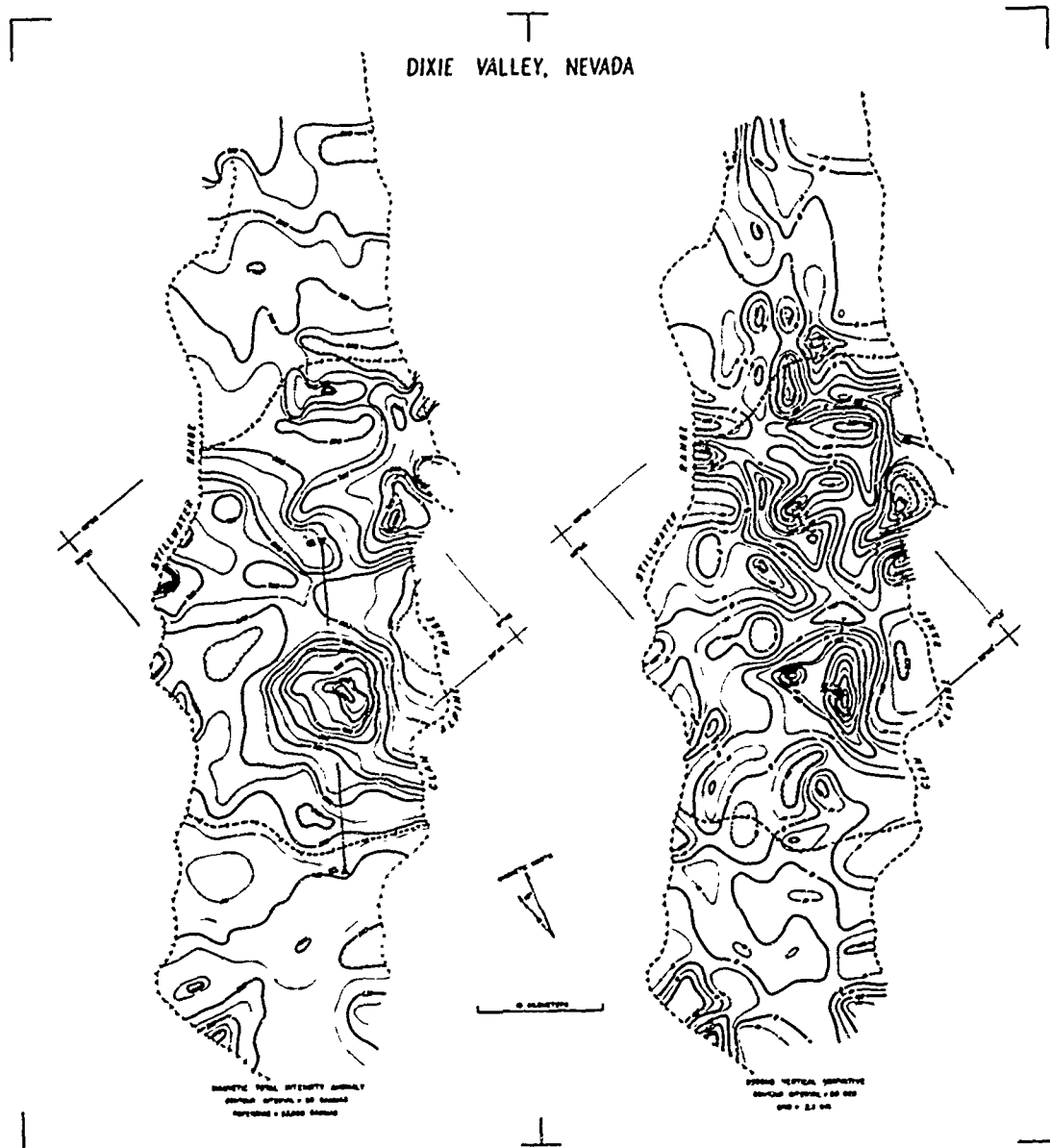


Figure 3. Magnetic total intensity and second vertical derivative maps of Dixie Valley, Nevada. Boundary of this map shown on Fig. 1.

trend which is more subdued than the first. Along these longitudinal zones, most prominent crosstrends are truncated or deflected. Coincidence of several such anomalies and their amplified counterparts on the filtered map with faults located by seismic refraction (Meister, 1967) implies they may be edge effects over major subsurface fault systems. Both seismically determined locations and extrapolations of the faults are shown on Fig. 1. By this interpretation, the basement under Dixie Valley is suggestive of a composite, asymmetric graben whose deepest component block is about 5 km wide and lies under the western half of the valley. Apparent "shelf blocks" bordering the main graben are downthrown with respect to adjacent ranges, but to a lesser degree.

In addition to the longitudinal trends, several transverse anomalies other than those discussed earlier are in evidence. They are located for the most part over the eastern "shelf" and trend obliquely (N 25 W) to the major features. Depth estimates on this block and coincidence with projections of faults in the Clan Alpine Range provide two lines of evidence that these anomalies are expressions of transverse faulting.

There is little magnetic indication of large strikeslip displacements along the longitudinal fault system of Dixie Valley. This is particularly true along the western bounding fault of the valley, where no appreciable offset is noted between the aforementioned magnetic inflection line and mapped exposures of the gabbroic complex, implying that post-gabbroic displacement (since Late Jurassic) has been primarily, if not entirely, of a normal sense.

Along the central fault zone, exceptions to this generality do exist; there, several anomalies of transverse strike are deflected 2 to 3 km in a right lateral direction (Figs. 1 and 3).

B. Basement Topography

In magnetic studies of sedimentary basins, techniques of depth estimation are generally employed in order to establish basement configuration. Most such methods operate on magnetic gradients and are usually independent of rock parameters, requiring only that they remain constant within the assumed geometric model. For the reconnaissance purpose of this study and in view of the numerous dike-like bodies exposed in the neighboring ranges, the method of Peters (1949) was applied to applicable profiles in Dixie Valley. The factor by which Peters' "half-slope" index is converted to depth was empirically determined from a control profile over the Stillwater Range; a value of 1.35 was found to give representative depths along the entire profile (Fig. 2).

Applying Peters' expression to depth indices from profiles parallel to useable gradients, it was possible to construct a topographic map of the magnetic basement (Fig. 4). Most striking of the features revealed by this map is a longitudinal trough whose axis is approximately 6 km from the parallel to the Stillwater Range. Close spacing of depth contours along the edges of the trough lends confirmation to the fault-bounded graben mentioned above. Both the longitudinal anomalous trends and seismic fault locations fall within these closely spaced contours (Figs. 4 and 5). This interpretation agrees well with those determined independently by gravity analysis (Thompson, unpublished) and by seismic refraction studies (Meister, 1967).

Secondary features of significance on this map are the apparent transverse "steps" in the eastern half of the valley. The most northerly of these steps trends approximately N 30 W and displays 300 to 600 meters of vertical offset. A similar deflection of depth contours is present about 20 km to the southwest, suggesting a second transverse fault with displacement in the same sense, but of approximately 300 meters.

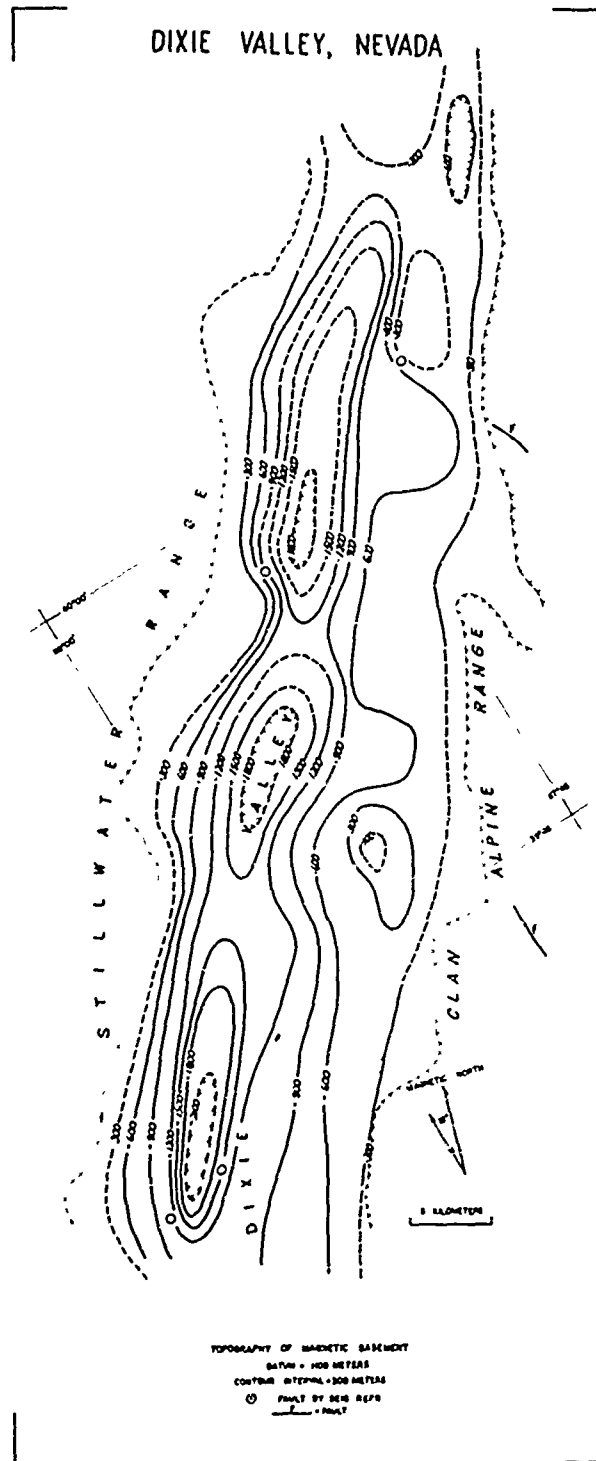


Figure 4. Topographic map of magnetic basement (compiled from depth estimates).

Finally, the basement map clearly delineates a roughly equidimensional high in the southeast part of Dixie Valley, which coincides precisely with a closed magnetic high of 500 gammas. Application of the depth expression to the extremely steep gradients over this feature indicates its top is between 60 and 150 meters below the valley surface. A comparable depth to a 2740 m/sec layer was subsequently obtained by seismic refraction (Meister, 1967). Total relief of the "buried mountain" above the mean level of the eastern valley block is roughly 600 meters.

C. Model Representations of the Magnetic Units

A secondary objective of this investigation was to test a hypothesis offered by Speed, who, on the basis of detailed surface mapping, has suggested the gabbroic complex forms an elongate, northwest trending body of lopolithic form (Speed, oral comm., 1964). To investigate this possibility, a computational analysis of a N-S profile ($\beta\beta'$ on Fig. 5) over the southern edge of the complex was performed using a Pirson graticule integrator for two-dimensional bodies (Pirson, 1940). Utilizing the previously calculated susceptibility contrast for this contact, a series of successive model assumption-curve comparison operations yielded the tabular model shown in Fig. 5. The associated intensity curve over this model accords well with the two-dimensional component of the observed anomaly.

Existence of such a tabular body is further substantiated by indirect indications on the east side of Dixie Valley. There, the magnetic expression of the subsurface contact is over 20 km southwest of the nearest surface exposure (Fig. 1). Strike-slip movement could produce a left-lateral displacement of this magnitude, although it may equally well be attributed to Clan Alpine uplift and subsequent erosional stripping of a lopolithic body. Northward extrapolation of the lower gabbro contact shown on Fig. 5 would place its depth between 3 and 5 km, implying a relative Clan Alpine uplift of comparable magnitude to produce the apparent offset.

A second investigative approach was used to study the dominant magnetic "high" in southeastern Dixie Valley. For purposes of computation, the three-dimensional component of profile $\beta\beta'$ (Figs. 3 and 5) was smoothed and reduced to vertical intensity amplitude. The resulting curve is similar to the anomaly induced by a vertical field except for the usual asymmetry of total intensity at this geomagnetic latitude i.e., a slight southward migration of the maximum and a discernible minimum on the north. At this magnetic latitude, the peak migration of either a point pole or point dipole

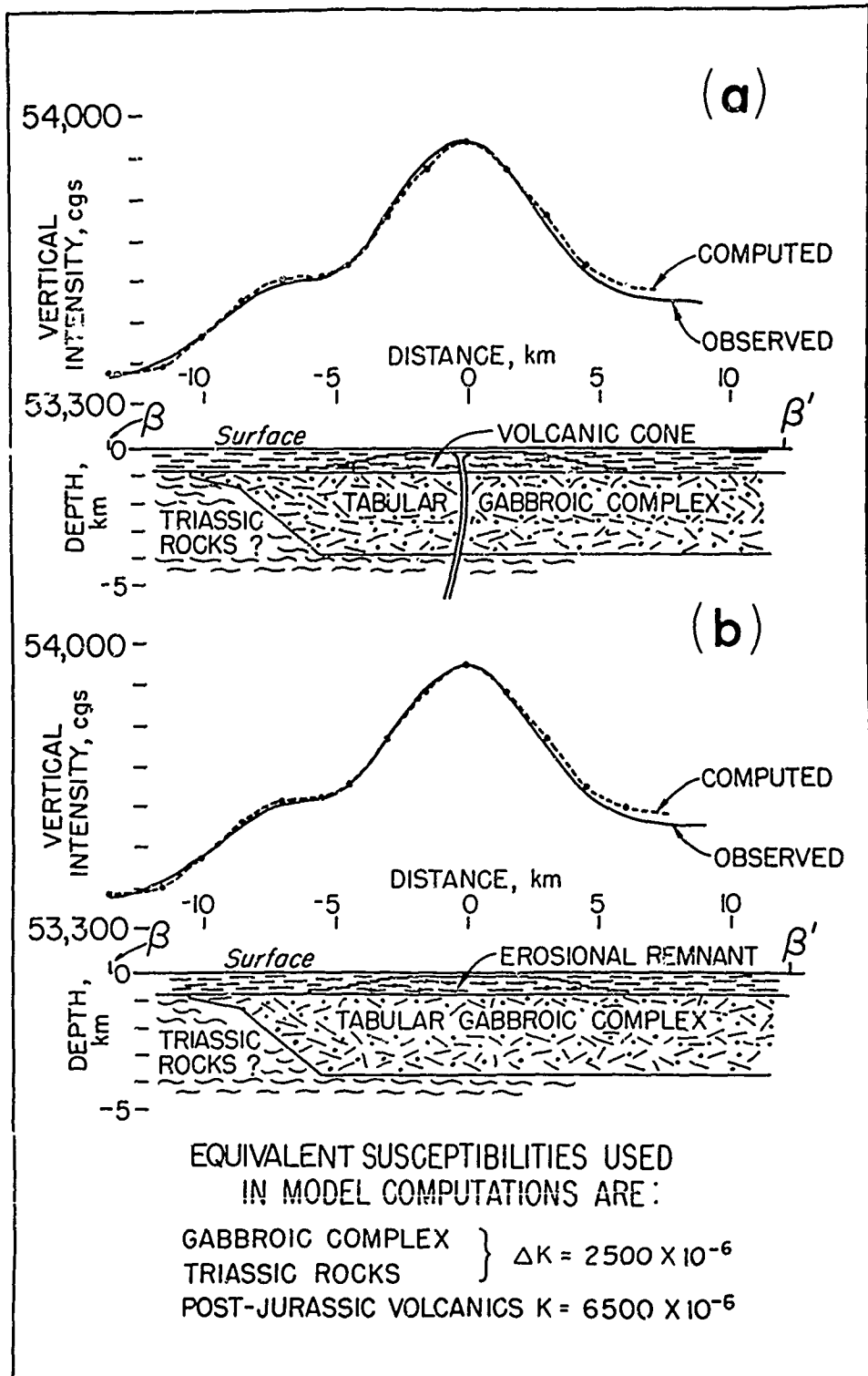


Figure 5. Alternative solutions satisfying equidimensional anomaly in southeastern Dixie Valley.

is only on the order of tens of meters (Smellie, 1956), a negligible quantity when compared to the observed anomaly width of 12 km. As a consequence, reduction to vertical intensity, while introducing no appreciable error in solution, facilitates use of solid angle charts developed by Nettleton for determining magnetic effects of buried vertical cylinders (Nettleton, 1942).

Three-dimensional models depicted in Fig. 5 with associated equivalent susceptibilities are constructed of superposed vertical cylinders. Either model generates magnetic effects which are in close agreement with the reduced observed anomaly. Fig. 5a attributes the equidimensional anomaly to a volcanic cone of high remanence and consequent equivalent susceptibility, whereas Fig. 5b represents an erosional volcanic remnant with similar total magnetization. The equivalent susceptibilities indicated for these models are those necessary to satisfy the reduced anomaly. In Fig. 5a, the feeder is assumed to contribute a negligible magnetic effect. Both models are in reasonable agreement with gravity and seismic measurements in this area (Thompson, unpublished; Meister, 1967).

VI. CONCLUSIONS

This investigation supports the interpretation that basement rocks under Dixie Valley form a composite, asymmetric graben, which is roughly parallel to the valley axis. The inner graben block is approximately 5 km wide and lies under the western half of the valley at an average depth of 2 km. Between the main graben and bordering mountain ranges are "shelf" blocks, also downthrown with respect to the ranges, but to a smaller extent. The eastern shelf is broken by a series of NW-trending normal faults with smaller displacements. This general configuration is in basic agreement with seismic refraction studies and gravity measurements in the area.

The contacts of an intrabasement gabbroic complex are traceable across both northern and southern Dixie Valley. No appreciable strike-slip displacements of the southern contact are in evidence, except along the eastern side of the inner graben, where a maximum offset of 2-3 km may be present. This implies that post-Late Jurassic movements on the major fault systems have been primarily dip-slip. It is suggested that dip-slip movement on a conical fault surface is responsible for minor en echelon structures observed at the surface.

A model computed from the anomaly over the southern gabbro contact lends confirmation to an earlier suggestion that the gabbroic complex is of lopolithic form. If a body similar to the computational model is vertically displaced on a Basin-Range fault, an apparent horizontal offset of the contact may result. This mechanism is suggested to explain the apparent gabbro offset along the eastern side of Dixie Valley, and requires a relative dip-slip displacement of 3 to 5 km.

Additional computational models suggest the three-dimensional anomaly in southeastern Dixie Valley may be generated by a volcanic cone, or alternatively, by an equidimensional volcanic remnant; either model requires a high equivalent susceptibility.

APPENDIX

Physical Properties of Rock Samples

Sample No.	Rock Type	Volume Suscep- tibility in cgs units $K \times 10^6$	Permanent Magnetization in cgs units $P \times 10^4$	Density in g/cc
<hr/>				
Southern Magnetic Mega-unit				
1	Latite	100	1.76	2.51
2	Latite	910	0.00	2.49
3	Welded tuff	<u>930</u>	<u>58.1</u>	<u>2.57</u>
Average		646	20.0	2.52
Gabbroic Complex				
4	Gabbro	2910	31.2	2.82
5	Gabbro	4120	21.9	2.74
6	Gabbro	680	17.3	2.82
7	Gabbro	160	0.017	2.87
8	Diabase	3570	9.79	2.81
9	Scapolitized Gabbro	3330	3.94	2.70
10	Gabbro	40	0.173	2.82
11	Albitized Gabbro	20	0.028	2.71
12	Anorthosite	1130	2.00	2.67
13	Peridotite	2790	12.5	2.99
14	Altered Gabbro	3700	12.6	2.87
15	Hydrated Basalt	<u>420</u>	<u>2.22</u>	<u>2.71</u>
Average		1906	9.47	2.79

BIBLIOGRAPHY

- Cloud, William K., 1957, Intensity Distribution and Strong-Motion Seismograph Results, Nevada Earthquakes of December 16, 1957; Bull. Seism. Soc. Am., Vol. 47, pp. 327-334.
- Cohen, Philip, and Everett, D. E., 1963, A Brief Appraisal of the Ground-Water Hydrology of the Dixie-Fairview Valley Area, Nevada; Dept. Conserv. and Nat. Res., State of Nevada, Report No. 23.
- Green, R., 1960, Remanent Magnetization and the Interpretation of Magnetic Anomalies; Geophysical Prospecting, Vol. 8, pp. 88-110.
- Hays, W. W., and Scharon, L., 1963, An Example of the Influences of Remanent Magnetization on Magnetic Intensity Measurements; Geophysics, Vol. 28, pp. 1037-1048.
- Meister, L. J., 1967, Seismic Refraction Study of Dixie Valley, Nevada; A. F. Cambridge Research Labs. Final Sci. Report Part I, AFCRL-66-848.
- Muller, S. W., Ferguson, H. G., and Roberts, R. J., 1951, Geology of the Mt. Tobin Quadrangle, Nevada; U.S. Geol. Survey Geol. Quadrangle Map GQ-7.
- Nettleton, L. L., 1942, Gravity and Magnetic Calculations; Geophysics, Vol. 7, pp. 293-310.
- University of Nevada, 1962, Geological, Geophysical, and Hydrological Investigations of the Sand Springs Range, Fairview Valley, and Four Mile Flat, Churchill County, Nevada; Report to Atomic Energy Commission for Shoal Project, Vela Uniform Program, 127 pp.
- Page, B. M., 1965, Preliminary Geologic Map of a Part of the Stillwater Range, Churchill County, Nevada; Nevada Bureau of Mines Map 28.
- Peters, L. J., 1949, The Direct Approach to Magnetic Interpretation and Its Practical Application; Geophysics, Vol. 14, pp. 290-340.
- Pirson, S. J., 1940, Polar Charts for Interpretation of Magnetic Anomalies; Trans. Amer. Inst. Min. Met. Eng., Vol. 138, pp. 173-185.
- Reford, M. S. and Sumner, J. S., 1964, Aeromagnetism, A Review Article; Geophysics, Vol. 29, pp. 482-516.
- Romney, C., 1957, Seismic Waves from the Dixie Valley-Fairview Peak Earthquake; Bull. Seism. Soc. Am., Vol. 47, pp. 301-319.

Sales, John K., 1966, Structural Analysis of the Basin-Range Province in Terms of Wrench Faulting; Unpub. Ph.D. dissertation, University of Nevada.

Slemmons, D. B., 1957, Geological Effects of the Dixie Valley-Fairview Peak, Nevada, earthquakes of December 16, 1954; Bull. Seism. Soc. Am., Vol. 47, pp. 353-375.

Smellie, D. W., 1956, Elementary Approximations in Aeromagnetic Interpretation; Geophysics, Vol. 21, pp. 1021-1040.

Speed, R. C., 1962a, Humboldt Gabbroic Complex (abs); Geol. Soc. Am., spec. paper 73.

_____, 1962b, Scapolitized Gabbroic Complex, West Humboldt Range, Nevada; Unpublished Ph.D. thesis, Stanford University.

_____, 1963, Unpublished progress map of parts of West Humboldt, Stillwater, and Clan Alpine Mountain Ranges, Nevada.

Thompson, G. A., 1959, Gravity Measurements Between Hazen and Austin, Nevada: A Study of Basin-Range Structure; Jour. Geophys. Res., Vol. 64, pp. 217-229.

_____, 1955, Unpublished Gravity Survey of Dixie Valley, Nevada;

Wahl, R. R., 1965, An Interpretation of Gravity Data from the Carson Sink Area, Nevada; M. S. Research Project, Stanford University.

PART IV.

AERIAL PHOTOGRAPH SURVEY OF DIXIE VALLEY, NEVADA

by

Dennis B. Burke

ABSTRACT

Large scale aerial photographs of Dixie Valley, Nevada record surface features in the alluvium that are associated with bedrock faulting. The photogeologic study reveals a complexity of sub-alluvial structure. Mapping of beach ridges of ancient Dixie Lake supplies a measure of tilting and offset in approximately the last 10,000 years.

The pattern of faulting and the geomorphology, together with data from geophysical investigations, indicate that the basin is a complex graben, subsiding along multiple step faults. The graben shallows and pinches out in the northern part of the valley. The structure is less clear in the southern part of the valley but involves a shallowing and possible change in trend of the graben.

Pronounced topographic asymmetry of the valley and adjacent ranges is believed to have been caused by slight tilting of the region, commensurate with normal faulting during crustal extension.

ACKNOWLEDGEMENTS

I would like to express my thanks to the many people with whom I have discussed Dixie Valley and its problems. My appreciation, especially, is owed to Dr. George A. Thompson and Dr. Arthur D. Howard, both of Stanford University; they have contributed many valuable insights into the problems of Basin-Range structure and development.

Dr. James G. Smith, of the U. S. Geological Survey, and Raymond L. Elliott, of Stanford University, critically reviewed the manuscript and offered many helpful suggestions.

All observations and conclusions, except where noted, are my own and for any errors I am solely responsible.

TABLE OF CONTENTS

	<u>Page</u>
ABSTRACT	ii
ACKNOWLEDGEMENTSiii
TABLE OF CONTENTS	iv
LIST OF ILLUSTRATIONS	v
 <u>Chapter</u>	
I. PURPOSE AND PROCEDURE	1
II. INTRODUCTION	2
III. PREVIOUS WORK	4
IV. METHODS	5
V. INTERPRETATION OF THE PHOTOGRAPHS	7
A. Faults	7
B. Lineaments	8
C. Beach ridges	9
VI. OBSERVATIONS AND INTERPRETATIONS	11
A. Age of Surface Features and Their Relation to Bedrock Structure	11
B. Pattern of Bedrock Faulting as Indicated from Surface Features	11
C. Nature of Basin Subsidence and its Relation to Present Topography	15
VII. CONCLUSIONS	20
APPENDIX	25
I. THE RECOGNITION OF SCARPLETS RESULTING FROM BEDROCK FAULTING	25
A. Scarplets Within Alluvium	25
B. Scarplets at the Bedrock-Alluvium Contacts	29
II. THE RECOGNITION OF NON-TOPOGRAPHIC TRACES RESULTING FROM BEDROCK FAULTING	32
III. THE RECOGNITION OF MOUNTAIN-FRONT SCARPS	34
BIBLIOGRAPHY	35

LIST OF ILLUSTRATIONS

Page

PLATES

1. Photogeologic map of Dixie Valley: surface features related to bedrock faulting in pocket
2. Photogeologic map of Dixie Valley: beach ridges and elevations in pocket

FIGURES

1. Relation of surface features to bedrock structure . . 12
2. Fence Diagram of Dixie Lake beach ridge elevations . . 16
3. Hypothetical sequence in basin development 19
4. Generalized zones of bedrock faulting in Dixie Valley 21
5. Generalized cross section of north-central Dixie Valley 22
6. Generalized block diagram of central and northern Dixie Valley 23
7. Development of troughs at mountain-front faults . . . 30

I. PURPOSE AND PROCEDURE

The purpose of this study was to determine, largely by the study of aerial photographs, as much as possible of the structural history and sub-alluvial bedrock structure of Dixie Valley, Nevada. This was accomplished by delineating surface features both in the alluvium and at the bedrock-alluvium contact which are interpreted as having resulted from bedrock faulting at depth. Although interpretation of aerial photographs was largely restricted to the alluvial fill of the valley, some historically active faults were mapped in the bedrock of the adjacent ranges.

The shoreline deposits of pluvial Dixie Lake were mapped and surveyed to determine the symmetry of post-pluvial displacement in the basin.

The study was undertaken to augment the investigations of Meister (1967), Smith (1967), Herring (1967), and Thompson (1966), who simultaneously studied the valley by geophysical methods.

II. INTRODUCTION

Dixie Valley, in west central Nevada, is a closed depression some sixty miles long and as wide as twelve miles. It trends north-northeast and is bounded by the Clan Alpine and Augusta Mountains on the east and by the Stillwater Range on the west. To the south, the valley¹ rises to an indistinct divide separating it from the smaller closed depression of Fairview Valley. At the northern end of Dixie Valley, the depression is bifurcated by the Tobin Range into Jersey Valley on the east and Pleasant Valley on the west. The low Sou Hills partially separate Dixie from Pleasant Valley, although the major drainage continues through them to the south.²

Like most of the Basin and Range province, the area has low and sporadic rainfall, sparse vegetative cover and wide daily and yearly temperature variations. Hot springs are common, especially at the foot of the ranges but occasionally well out in the valley. The valley has the characteristics of youthful topographic development, and its continuing rejuvenation is most clearly attested to by frequent earthquakes and faulting in historic time (summary by Page, 1965).

Greater steepness and linearity of the front of the Stillwater Range, smaller, steeper fans on that side of the valley and the west-of-center location of the playa combine to give Dixie Valley a marked lateral asymmetry. The Humboldt Salt March, at an elevation of 3363 ft, is the lowest area in northern Nevada.

¹Although incorrectly used in the geomorphic sense, the term "valley" will here be used for the negative landform to differentiate from the term "basin," applied to the sub-alluvial bedrock structure.

²The geographic names of the area have undergone a bewildering number of changes in the geologic literature. The former names are here listed in chronological order:

Dixie Valley: Osobb and Salt Marsh Valley

Stillwater Range: Pah Ute or Pah-Ute, Table Mountain and East Range

Clan Alpine Mountains: Augusta Mountains

Tobin Range: Havallah and Sonoma Range

In Late Wisconsin or Tioga time (Flint, 1961), Dixie Valley was occupied by a lake with a maximum depth of some 220 ft. Successively lower water levels are recorded in the form of beach ridge deposits, well preserved on fans along the east side of the valley. Dixie Lake was a separate body of water from the contemporaneous and far larger Lake Lahontan, which lay immediately to the west.

III. PREVIOUS WORK

Much of the material published on the Dixie Valley region deals with the earthquakes and faulting mentioned above. Literature of a more general geologic nature comprises only a small part of the total.

There have been some general geophysical investigations of the region (Thompson, 1959) and large-scale studies of the valley recently reached completion (Meister, 1967; Herring, 1967; Smith, 1967). Page (1965) mapped the Stillwater Range and the adjacent Dixie Valley alluvium south of lat. 40° N. Muller, Ferguson, and Roberts (1951) mapped the quadrangles north of 40° N. No recent published maps exist of the Clan Alpines south of 40° N. Some unpublished mapping has been done, however (Speed, 1963).

IV. METHODS

The aerial photographs, some 600 of which were used in this study, were taken by the United States Air Force in March of 1964 for this research project. Although frequently of low tonal quality and taken when the ground was abnormally wet from melting snows, the photographs comprise a coverage superior to previous ones because of their much larger scale (1:26,000 vs 1:75,000). Also, orientation of the flight lines at approximately N 30°E, along the trend of the valley, simplified study of the photographs and their compilation as mosaics.

Two sets of photographs were used. A grid system of 1° latitude and longitude lines with control points was taken from an enlargement of the Army Map Service Lovelock, Millet, Reno, and Winnemucca (1:250,000) topographic maps covering the Dixie Valley region. This grid system was further enlarged to the average scale of the photographs, and the photographs were triangulated onto this grid to form a controlled mosaic. The second set of photographs was used for study, and information obtained was then transferred to the modified A.M.S. enlargement. Because of the quality of the maps and the paucity of control points in the valley (mountain peaks and some culture were used), the positions of geologic features with respect to those on the base are occasionally askew. For the most part, however, the method was quite successful.

The photographs were first studied with a mirror stereoscope of low magnification, then with a lens stereoscope of higher magnification and greater vertical exaggeration. All photographs were studied more than once at separate times to check interpretation.

Because of the size of the area and the fact that much of it is inaccessible, not all features mapped could be checked in the field. Also, many of the more subtle features could not be recognized in the field even though their positions were known. Typical accessible features were visited and conclusions made there were extended to other features of similar appearance.

Since the start of this project, preliminary 7 1/2' topographic quadrangle maps of the northern and eastern portions of the valley have been prepared by the U. S. Geological Survey. It was from this base and from Coast and Geodetic Survey bench marks that beach ridge elevations were obtained. The others were determined by leveling from U. S. Geological Survey bench marks.

V. INTERPRETATION OF THE PHOTOGRAPHS

A. Faults

Photogeologic evidence for faulting in the Dixie Valley alluvium is quite varied, and no single set of criteria can be stated for the recognition of all mapped features. These features can best be divided into three main groups--(a) scarplets, (b) non-topographic traces and (c) linear mountain fronts--each with its own set of criteria and subdivided into varying degrees of assuredness of interpretation.

(a) Scarplets¹: On the photographs, the most obvious indication of faulting in the alluvium and at the mountain front is the presence of existing scarplets. Not all apparent scarplets, however, result from bedrock faulting. Edges of stream terraces, inner edges of beach ridges (depositional), shoreline nips (erosional), and slump scarplets can all appear much like fault scarplets within the alluvium. Rapid mass wasting of a properly striking non-resistant bed, bedrock undercutting by an intermittent stream at the bedrock-alluvium contact and even game and cattle trails at this contact may produce effect similar in appearance to basal scarplets at the mountain front (see the Appendix for a description of fault scarplets and for the criteria by which these other features are differentiated).

(b) Non-topographic traces: Linear features in the alluvium with no topographic expression at the limits of stereographic resolution are the most difficult to recognize and verify as indicative of faulting. All of those mapped in this study appear to be the result of thorough erosion of former scarplets. Lineaments of tone, texture, and vegetation were observed either alone in the alluvium or grading into faults with

¹The term "scarplet" is used here to identify small fault scarps observable in the alluvium and those caused by reactivation of a mountain-front fault. In Dixie Valley, none of these are over 20 ft in height and most are only 3-4 ft high. "Scarp" is used for the larger feature--the steep, linear mountain front--which resulted from continuing relative uplift, modified by erosion, along a mountain-front fault.

topographic expression. It is from the latter situation that criteria for the recognition of these traces were derived. The tonal and textural relations indicate that all such traces began as scarplets facing into the valley. Observations from a low-flying airplane under back-lighting conditions demonstrate that there remain a few inches of topographic relief on some of these.

The traces are not easy to distinguish from old roads, some game and cattle trails, or abrupt changes in grain size or color of the sediments. (See the Appendix for a full description of the traces and the criteria for differentiation).

(c) Linear mountain fronts: Scarplets at the bedrock-alluvium contact can usually be interpreted to represent recent reactivation of a major fault which forms the front of the range. With mass wasting and stream erosion, the scarplets disappear and only a steep, linear mountain front can be observed under the stereoscope. Blackwelder (1928) has cataloged criteria for the recognition of such major scarps and fault-line scarps, many of which are applicable here. Again, there may be other explanations for the development of this landform and only those lengths of mountain front which fulfill Blackwelder's criteria are mapped (see Appendix).

Lineaments

This "catch-all" classification includes diverse features of problematic origin. These features, most of which are on the valley-floor lake deposits, include abnormally linear lengths of stream channels, straight or evenly curving tone boundaries, dark lines, lines of vegetation and wide bands defined by changes in drainage density and grain size. The only unifying element among these phenomena is that the origin of none is understood. Since faulting cannot be disproved as a mechanism of formation, these lineaments are included on Plate 1 for completeness.

C. Beach Ridges

Only the older, higher beach ridges on the fans of Dixie Valley were mapped in this project. The braided and meandering streams on the fine-grained valley-floor lake deposits have destroyed most traces of the younger, lower shorelines. Ridges on the fans, not subject to lateral erosion, are destroyed only where washes from the mountains have breached them.

The appearance of these upper ridges is distinctive. The coarse-grained composition and high permeability have left them less disturbed by runoff and wind deflation than other features such as fault scarplets. What little deflation has occurred has left a desert pavement of coarse pebbles and cobbles, shielding the ridge from further deflation. The stability of this configuration is evidenced by a well developed desert varnish on the crests of the ridges as compared to adjacent, non-ridge sediments.

This desert varnish characterizes the ridges on the photographs; they are much darker than surrounding sediment. The ridges are also usually unvegetated immediately behind the crest, apparently because of low water content and lack of soil. Where small rivulets from the face of the ridges pond in the swales between, the water percolates down, leaving fine, light colored sediment in striking contrast to the desert varnish.

These ridges are thought to be formed by longshore drift of sediment from arroyos entering the former lake, i.e., the lateral spreading of what would have been deltas in an environment of lower wave energy. The sediment is spread as a coarse, nearshore veneer and concurrently piled up by waves as offshore bars.

Dune morphology and the orientation of sand sheets blown from dry arroyos verify meteorological observations that the present dominant wind direction is from the southwest. Assuming this same situation at the time of ridge development, the greatest fetch would have been toward the northeast. Many aspects of the ridges indicate this was the case:

the ridges are not well developed on the west side, in the lee of the Stillwater Range; the only delta-form accumulations of sediment are in the south; and the greatest complexity of bar morphology, a consequence of wave reflection, eddy currents, and the large amount of sediment, is in the northeast corner of the former lake area (Plate 2).

Because of the variety of sediment types, drainage densities, erosion mechanisms and sedimentation rates in Dixie Valley, there is a natural bias in the mapped data. Sediments of the valley floor do not retain topographic irregularities as long as fan deposits. The finer grain size and lower permeability of the valley floor allow a greater degree of surface runoff, and lateral erosion and rapid deposition more quickly destroy and bury scarplet and ridge traces. The greater degree of destruction of old roads and trails on the valley floor, compared to the fans, is evidence of this variation in erosion rates. On the valley floor also, drainage commonly runs parallel to the assumed structural trend, so that arroyo banks can easily mask the effects of small offsets.

Scarplets at the mountain fronts or within the ranges are also more quickly destroyed than those on the fans, because of greater surface runoff and mass wasting. Evidence for this conclusion was found in many places where a scarplet in the alluvium, when traced to the bedrock-alluvium contact, could be recognized there only as a linear mountain front.

When noting the infrequency of scarplets mapped on the valley floor sediments, the consideration that they are simply no longer observable must be borne in mind; the record of faulting on the valley floor and at the mountain front is a shorter one than on the fans. To highlight the inequality of the record, the bedrock-alluvium contact and the inner margins of fans are shown on Plate 1.

VI. OBSERVATIONS AND INTERPRETATIONS

A. Age of Surface Features and Their Relation to Bedrock Structure

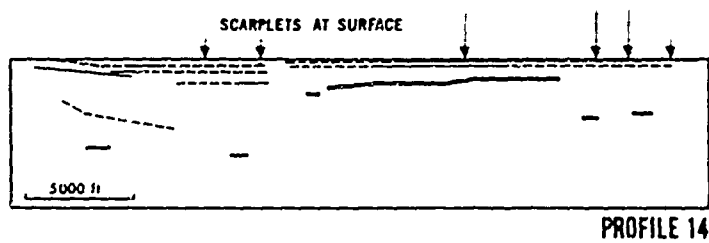
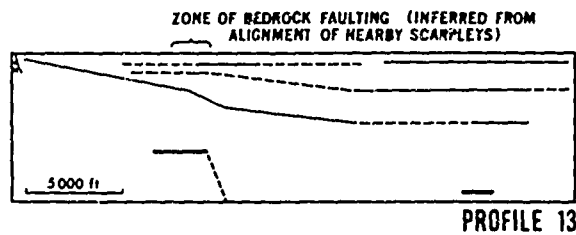
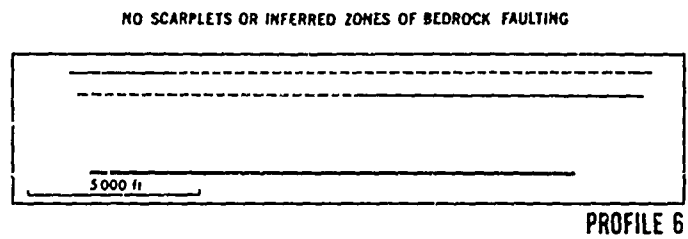
The record of faulting portrayed on Plate 1 is, at a maximum, some 10,000 years long. The oldest of the faults in Dixie Valley, now erode to the point where no topographic expression is evident under the stereoscope, cuts the higher Dixie Lake beach ridges ($39^{\circ}58'N$, $117^{\circ}47'W$). The age of the highest shoreline of Lake Lahonton, immediately to the west, has been dated at 10,000-11,000 B.P. (Morrison, 1964). This age is approximately the same for the highest beach ridge in Dixie Valley on the assumption that all the pluvial lakes of the region began to lower contemporaneously.

Locations of bedrock faults in fourteen seismic profiles of the valley (Meister, 1967; Herring, 1967) coincide well with zones of faults mapped on Plate 1 (Fig.1). Thus, faulting now evident in the alluvium, a record of about 10,000 years, is strongly indicative of that which has been active throughout the history of the basin. This history is given as some 15 million years by Thompson (1959), based on stratigraphic evidence. The existence of this important and somewhat surprising relationship allows many conclusions to be drawn concerning the sub-alluvial structure of the valley, based on surface features.

The following observations and conclusions concerning the bedrock structure of the basin include much of Meister's (1967) data. These two dissimilar approaches to the problem of basin structure contribute different parts of the total picture. Seismic studies supply depths to bedrock and general locations of bedrock faults in separate profiles through Dixie Valley; the photogeologic study shows the trends of bedrock faulting which tie these profiles together.

B. Pattern of Bedrock Faulting as Indicated from Surface Features

The pattern of faults on the two sides of the valley is quite dissimilar. The front of the Stillwater Range is bounded along much of its



PROFILES FROM MEISTER (1967)
LINES INDICATE LAYERS OF VARIOUS VELOCITIES
HEAVY LINE IS BASIN FLOOR
NO VERTICAL EXAGGERATION

Figure 1. Relation of surface features to bedrock structure.

length by a continuous fault, sinuous in plan. The surface record suggests another, straighter, subparallel fault beneath the alluvium of the fans. On the eastern side of the valley, however, the zones of bedrock faulting are numerous, straight, subparallel and at an angle to the main trend of the Clan Alpine Mountains. Faulting there exercises little control on the bedrock-alluvium contact, in contrast to the western margin of the valley.

The inner fault zones of the two sides converge to the north and meet south of the Sou Hills. The Stillwater mountain-front fault appears to curve eastward to form the southern boundary of the Sou Hills. Muller, Ferguson and Roberts (1951) have mapped a continuation of this fault to the north. Hence, the fault may branch at the Sou Hills. The more eastern fault zones diverge to the north and extend across Dixie Valley toward the Tobin Range. The easternmost of the faults mapped curves to form the eastern border of Jersey Valley.

The fault zones which extend toward the Tobin Range appear to cut off Jersey Valley as a separate structural unit from Dixie Valley. The alluvium in Jersey Valley is thin, hardly more than a pediment cover. Faults and deep drainage channels presently entrenching the middle of the valley have exposed Tertiary sediment types found in the east flank of the Tobin Range. Thus, the basin of Jersey Valley has not taken part in the great subsidence of the Dixie Valley basin since the deposition of these rocks. Surface indications of recent faulting are scarce on the west side of Jersey Valley and the topography indicates that the mountain front there is not fault controlled at present. As Page (1935) mentioned, the mountain blocks of the Tobin Range appear to be tilting eastward with uplift. Eastward dips in Tertiary volcanic rocks of the range (Muller, Ferguson, and Roberts, 1951) are additional support for this interpretation. Tilting may be subsequent to earlier, more symmetrical, uplift, for these authors state that the volcanics cover a formerly active mountain-front fault on the east side of the range.

In Pleasant Valley, the mountain-front scarplet of the Tobin Range dies out near the Sou Hills. Small scarplets branch into the alluvium where the mountain-front scarplet ends to the south. These small faults are subparallel but not consistent in displacement. Many are antithetic to the nearby mountain front and the appearance is one of numerous small graben in the alluvium.

The west side of Pleasant Valley resembles the west side of Jersey Valley. There are faults between the Stillwater Range and the Sou Hills, but farther north they are few and little influence topography. As in Jersey Valley, bedrock dips indicate eastward tilting of the structural blocks with major offsets occurring on the eastern margin of the valley.

The Sou Hills appear to be a structural block separated by faults from the main ranges. Both the Dixie Valley faults from the south and the Pleasant Valley faults from the north terminate at the bedrock of the hills. Subsidence has apparently been less here than to either the north or south. Dixie Valley appears to be the most rapidly subsiding area because the drainage from Pleasant Valley into Dixie Valley is deeply entrenched in the Sou Hills bedrock. Small streams flowing south from the Sou Hills into Dixie Valley are presently capturing many of those flowing north into Pleasant Valley.

In the southern portion of Dixie Valley, south of Lat. $39^{\circ}37'N$, the trend of the valley changes. The surface record at and south of this change suggests less continuous zones of suballuvial faults than farther north. On the western margin of the valley, the mountain-front fault of the Stillwater Range dies out to the south where many small faults branch into the alluvium, much like the Tobin Range fault in Pleasant Valley. South of this termination, eastward dips and many small faults in the Tertiary bedrock suggest that subsidence was taken up by flexure and small displacements of the bedrock and that the adjacent alluvial cover is thin. Evidence that the major subsidence occurred further north is found in high-level stream terraces bordering drainage that enters the valley from the south.

In southeast Dixie Valley, the surface record of bedrock faulting is a very recent one. Most of the scarplets mapped there have been formed in historic time (Slemmons, et al., 1959). Because the Clan Alpine Mountains have not been mapped in the area, the possible continuity of these southern faults with scarplets mapped to the north remains unknown.

Few faults in the southern portion of Dixie Valley exercise control on gross topography. Only those on the east side of Wonder Valley appear to be part of a long-active zone of major offset. It is difficult to evaluate the importance of these historic offsets to the overall structural history of the basin because of the lack of geophysical data.

C. Nature of Basin Subsidence and its Relation to Present Topography

The number and height of the scarplets on the two sides of Dixie Valley suggest that the basin has subsided an approximately equal amount on the two sides since beach ridge formation. Evidence to support this suggestion was found by leveling on the higher beach ridges. Leveling data demonstrate that the basin has been subsiding with little net tilting of the originally horizontal ridges in the past 10,000 years (Plate 2 and Fig. 2). A maximum of 14 ft of westward tilt was observed in a cross-valley profile taken near the southern end of the former lake area. Because absolute correlation could not be made between sets of ridges on the opposite sides, the lowest possible correlative ridge on the west was chosen for leveling. The actual amount of tilt may well be less than that measured. At the northern end of the beach deposits, a shorter cross-valley profile shows 8 ft of westward tilt. These values are no greater than variations in elevation found along the length of the ridges on the east side.

The ridges on the east side are crossed at a slight angle by post-ridge scarplets. Variations in ridge elevations there are explained by the fact that not all ridges and leveling stations are on the same

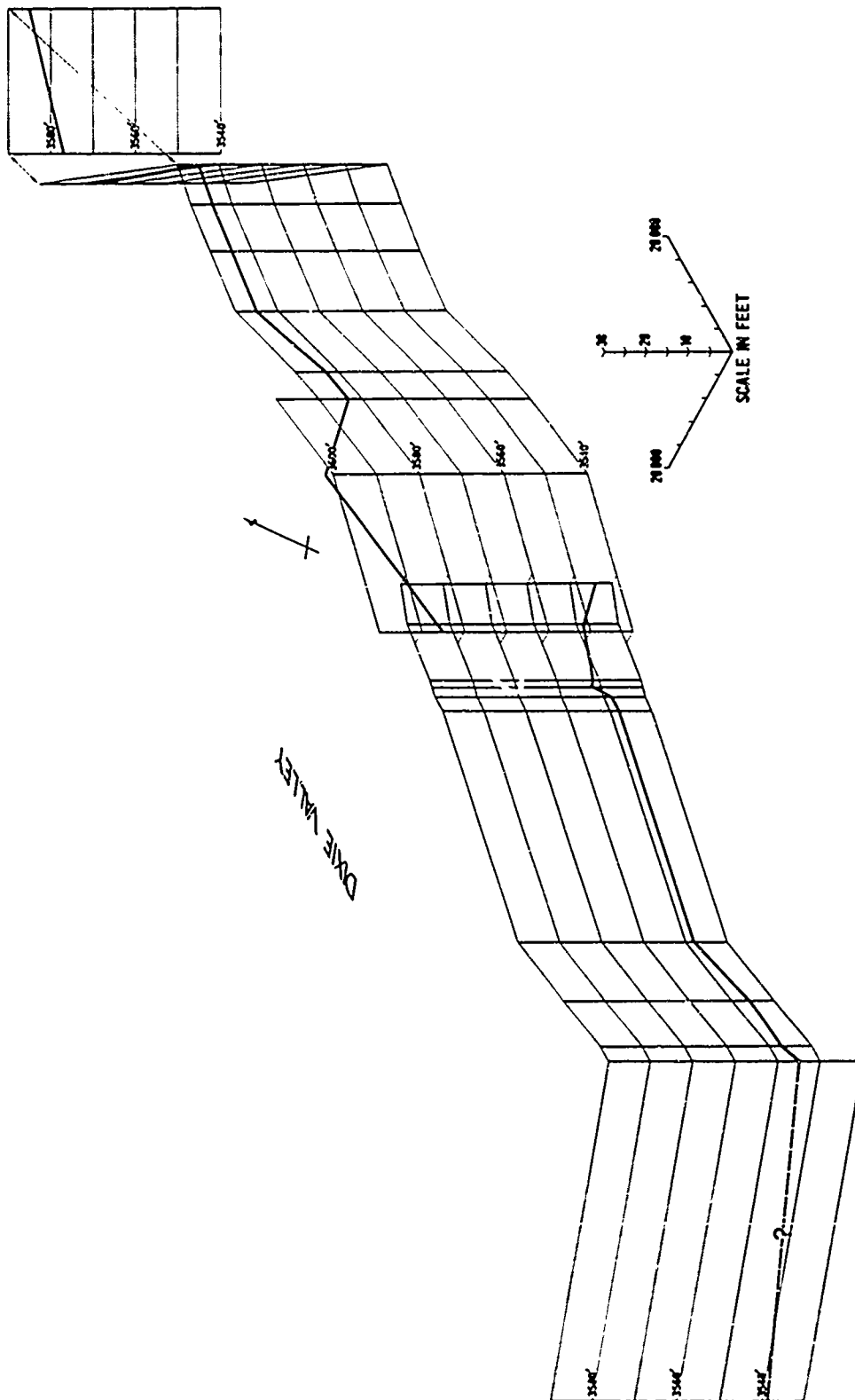


Figure 2. Fence diagram of Dixie Lake beach ridge elevations.

structural block. Varying amounts of post-ridge subsidence on the separate blocks has dropped the leveling stations correspondingly.

Seismic profiles taken in the valley indicate that the bedrock floor in the deepest portion of the basin has been subsiding nearly equally along faults on both sides. This is somewhat at variance with earlier theories of basin morphology, based on geomorphic considerations.

The work of Davis (1904, 1925), although it clarified many concepts regarding Basin-Range structure and geomorphology, failed to consider the possibility of major buried structure and topography. Simplicity of sub-alluvial structure is implicit in his text and diagrams. Davis interpreted a gentle bedrock slope on the opposite side of a range with a steep front as the tilted, dissected, unburied portion of the pre-faulting erosion surface. Early authors tacitly assumed this slope to continue at depth to the mountain-front fault of the next range. Valley asymmetry was explained by dissimilarity of consequent drainage on tilted fault blocks on the two sides of the valley.

The results of this study show that the situation in Dixie Valley is more complex than the classical concept. A suggested sequence of events in basin development must account for a number of present characteristics of the valley and adjacent ranges:

1. Offsets on both sides of the Dixie Valley basin are large and approximately equal.
2. The mountain fronts are markedly dissimilar. The eastern front of the Stillwater Range is closely controlled by faulting; the western margin of the Clan Alpine Mountains is not. It should be added here, incidentally, that the eastern flank of the Clan Alpines is similar to that of the Stillwater Range.
3. The valley is asymmetrical. The playa is located well west of center in the valley.

A possible sequence of events to account for these characteristics is outlined in Fig. 3. The initial development is like that envisioned by

Davis (1904, 1925). Offset on the Stillwater front fault and westward tilting of the structural blocks initiate very different drainage areas on the two sides of the embryonic basin. The result of this, as offset continues, is a steep western and gentle eastern mountain front with alluvium between. Subsequent faulting then occurs beneath the alluvial fill. So long as the rate of basin filling approximates the rate of relative subsidence, these major sub-alluvial offsets will affect topography only as evanescent scarplets in the alluvium. The present location of the playa is the result of continued tilting and/or greater relative subsidence on the western side of the basin in Quaternary time.

It can be argued that tilting is not a prerequisite for present valley appearance. If the basin developed without tilt and the preponderance of offset has taken place on the western margin during the Quaternary, valley asymmetry could result from the difference in geomorphic "age" of the two mountain fronts. The Clan Alpines would be farther advanced in the geomorphic cycle because of the lack of rejuvenation.

Evidence for the hypothetical sequence presented in Fig. 3 is admittedly circumstantial and open to further investigation:

1. The Clan Alpines have the appearance of a tilted block, as described by Davis (1904, 1925), with one steep, linear (eastern) flank and one gentle, irregular (western) flank.
2. Tilt is common in the region. The structural blocks of the Tobin range are tilting with relative uplift (Page, 1935). In the Carson Sink area to the west, Louderback (1904) found much evidence of tilting in the ranges.
3. The best oriented of Meister's (1967) cross-valley seismic profiles (Profile 5) shows the deepest portion of the basin to be tilted westward.
4. The surface record of faulting suggests as much offset on the east as on the west, in post-Dixie Lake time. The variations in beach ridge elevations also indicate movement of structural blocks on both sides of the valley. These are actually evidence against non-uniform subsidence, rather than evidence for tilt.

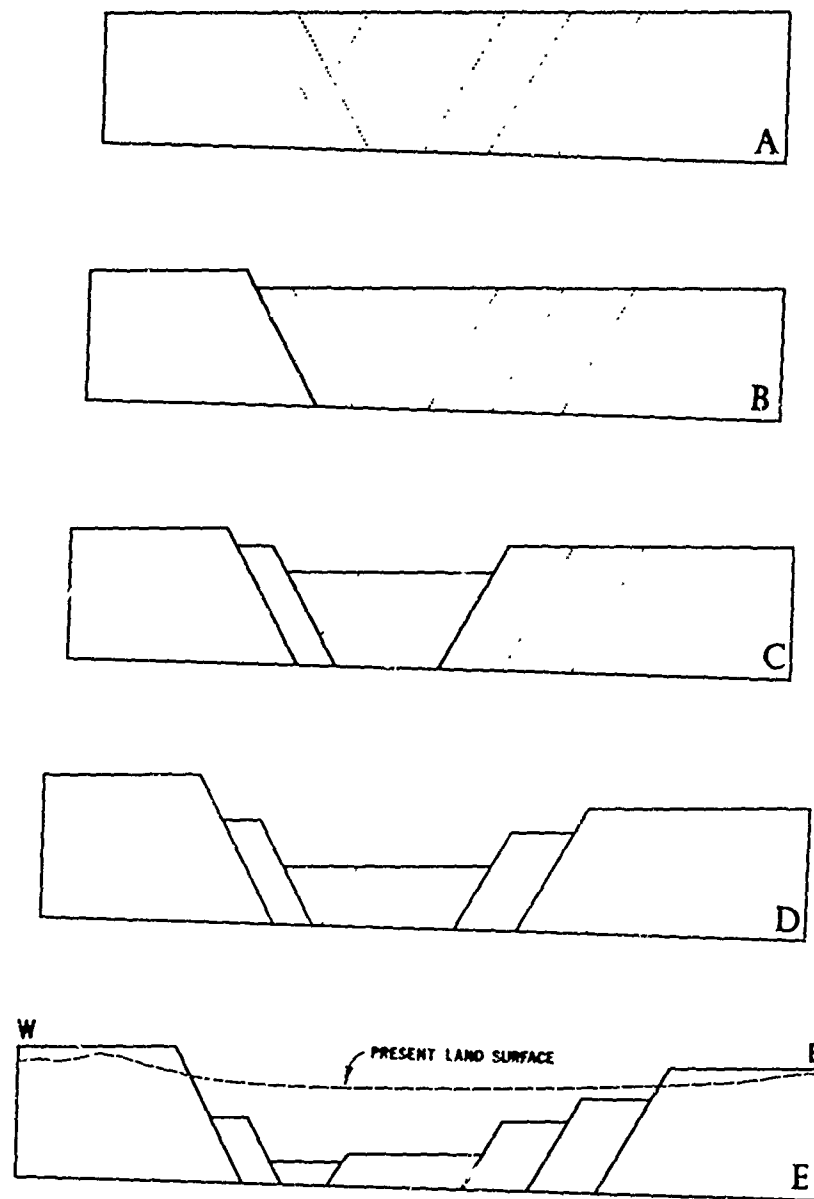


Figure 3. Hypothetical sequence in basin development.

VII. CONCLUSIONS

The conclusions gained from this study can best be summarized by the model of Dixie Valley presented in Figs. 4, 5, and 6. The structures portrayed are corroborated by the geophysical studies, which supplied the approximate depths to bedrock in these figures. The continuity of faults through bedrock areas was supplied by the geologic maps of the region (Muller, Ferguson, and Roberts, 1951; Page, 1965; Speed, 1963). An average near-surface fault plane dip of 60° was assumed from the data of Page (1935) and Meister (1967).

In its central and northern portions, the basin beneath the alluvial fill is a complex graben, bounded on the west by two normal faults of large displacements and on the east by multiple, sub-parallel faults of smaller displacements. The deepest portion of the graben is somewhat west of the central axis of the valley and the floor rises as the bounding faults die out to the north. Faulting was preceded or accompanied by westward tilting of the major structural blocks. North of the latitude of the Sou Hills, the tilt changes to an eastward one in all mountain blocks.

In southern Dixie Valley, the situation is more complex and less open to confident interpretation. The graben does not pinch out, as it does to the north. Rather, the amount of subsidence decreases and is taken up by flexure and numerous smaller faults. The central portion of the basin may well swing to a more north-south orientation as it shallows to the south.

One may speculate that the faulting in and near the Louderback Mountains and Wonder Valley is an unburied or less advanced analogue of the faulting farther north in the Clan Alpine Range. The recent faults in this area (Slemmons, et al., 1959) may be indicative of a number of blocks presently subsiding from the higher Clan Alpines. There is a marked topographic lineament in the range ($39^{\circ}28'N$, $117^{\circ}58'W$ to $39^{\circ}34'N$, $118^{\circ}00'W$) which forms the eastern border of Bench Creek Valley. If the lineament

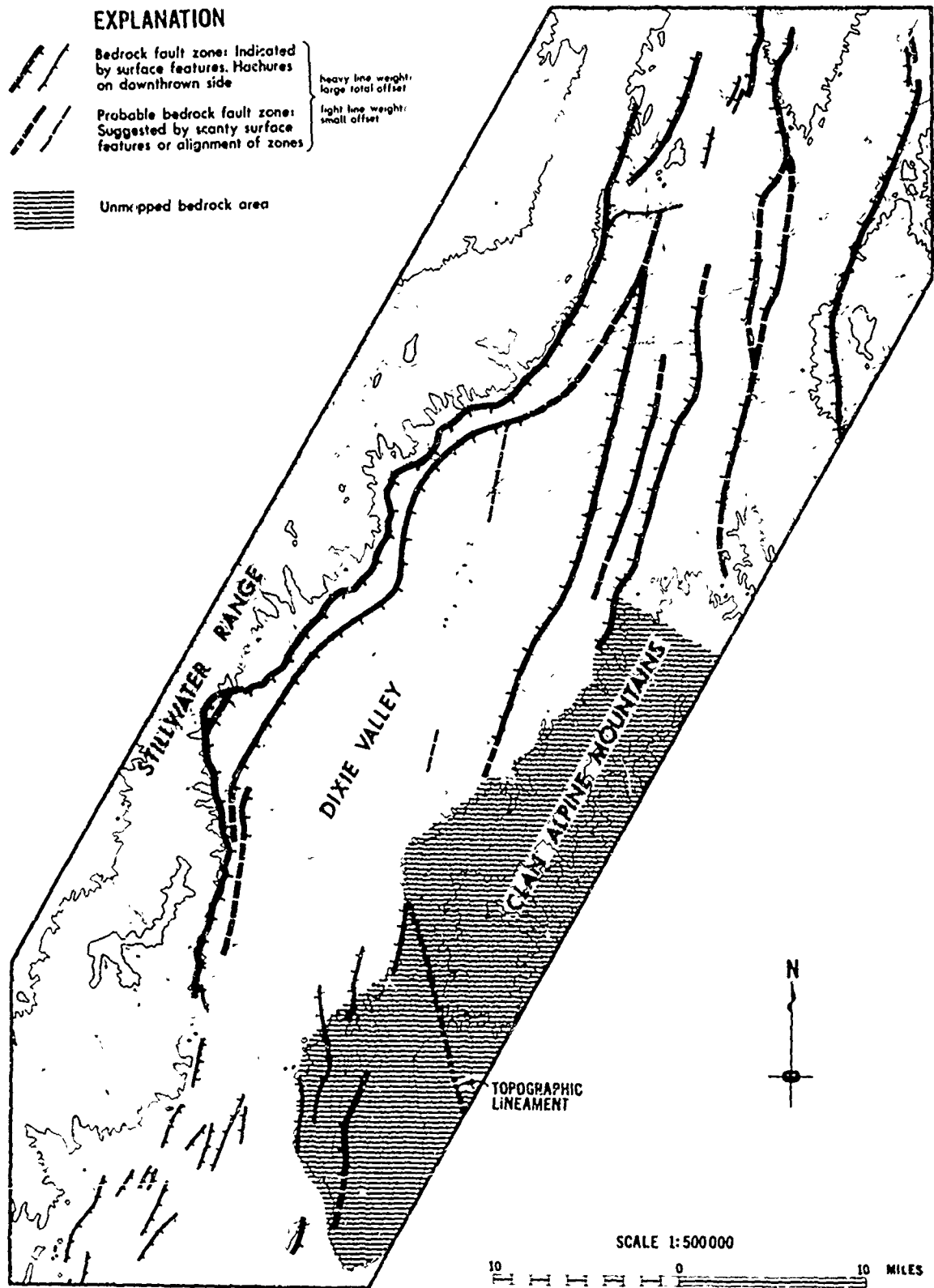


Figure 4. Generalized zones of bedrock faulting in Dixie Valley.

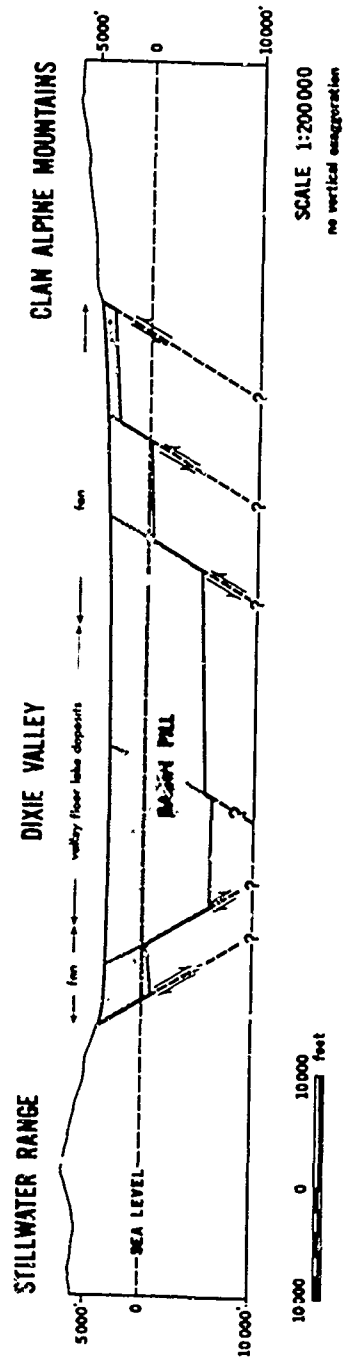
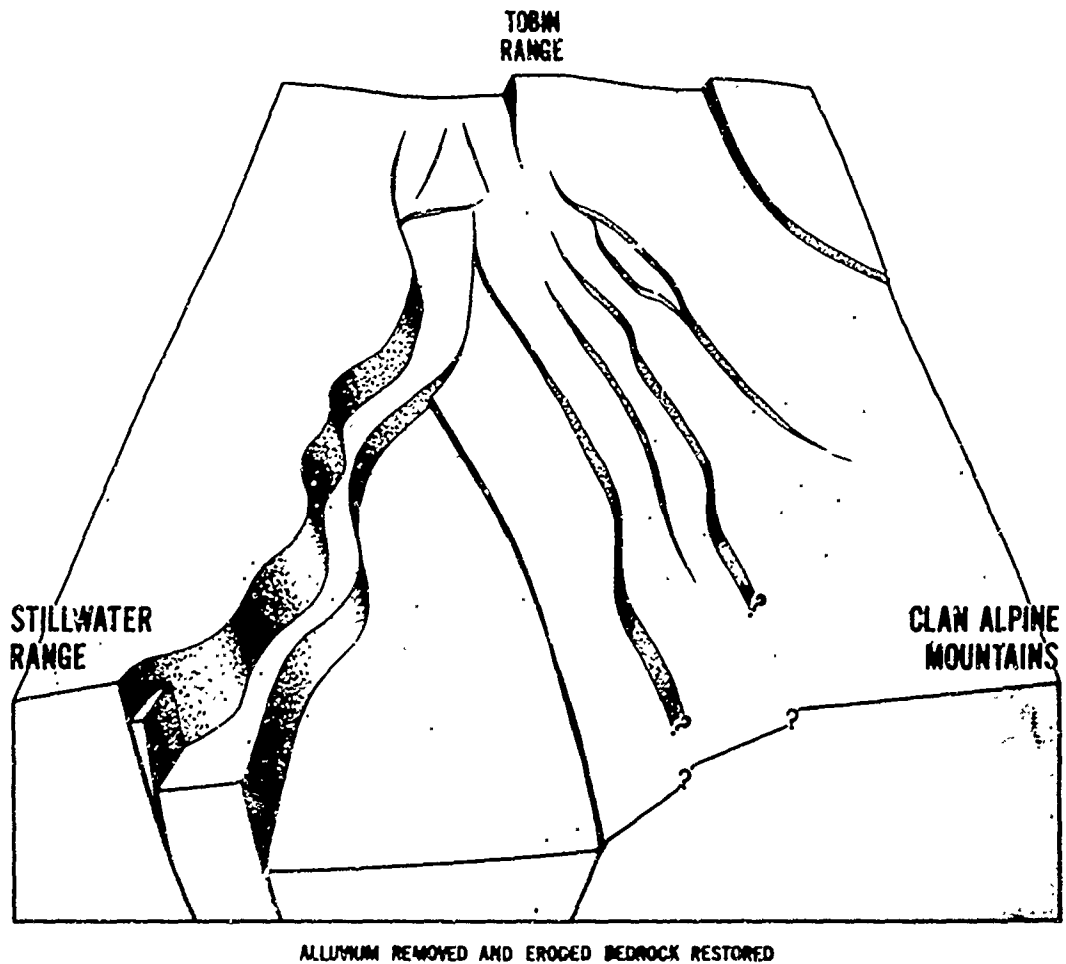


Figure 5. Generalized cross section of north-central Dixie Valley.



ALLUVIUM REMOVED AND ERODED BEDROCK RESTORED

Figure 6. Generalized block diagram of central and northern Dixie Valley.

is the expression of a major fault, the entire bedrock area west of it may be subsiding at the present time.

At the latitude of the Humboldt Salt Marsh, there has been, in this model, approximately 15-20 per cent extension in the crust during the past 15 million years. Strike-slip displacement may have occurred on the straighter faults but the geometry of the model here presented dictates that it be small. It is difficult to envision much consistent lateral displacement on the more sinuous faults in the basin.

In suggesting a mechanism for the sequence of events in basin development, it would be best to repeat Page's (1965) statement concerning the eastern margin of the Stillwater Range: "The normal faulting involved an east-west extension of the crust, and probably it was induced by a reduction in confining pressure in that direction . . . it looks as though the range sloughed off narrow subsidiary blocks during and after its uplift above the adjacent basins, mainly in response to gravity." This impression applies as well, if not better, to the appearance of the western margin of the Clan Alpine Mountains.

APPENDIX

I. THE RECOGNITION OF SCARPLETS RESULTING FROM BEDROCK FAULTING

A. Scarplets Within Alluvium

The photogeologic characteristics of fault scarplets in the alluvium of Dixie Valley vary widely as a function of degree of erosion and properties of the alluvium. However, generalizations can be made regarding the appearance of scarplets on the photographs.

Scarplets may be single but they typically die out along their lengths, and are replaced by others which are subparallel. Individual scarplets may branch. Where scarplets are multiple, not all necessarily face in the same direction. Single scarplets may also face a nearby mountain front.

The upthrown surfaces, scarplet faces and downthrown surfaces each vary in tone and texture as the scarplet is eroded. The relation between these tones and textures is consistent, and this relation is consistent with the form of the scarplet.

A steep, sharp, young scarplet face is typically very light in tone and smooth in texture. The up- and downthrown surfaces appear no different than the surrounding sediment in areas of fine-grained alluvium. With coarser grain size, the upthrown surface immediate to the upper edge of the face may be somewhat lighter than the surroundings (from lower water content?). Drainage is entrenched for a distance behind the scarplet.

The face is light and smooth on scarplets facing up-drainage because the washes are ponded by the face or much reduced in gradient. The downthrown surface may also be light and smooth, from deposited sediment. Larger channels which breach and entrench the upthrown side also leave light sediment on the downthrown surface. Derangement of many small channels outlines the position of a fault, even with little vertical offset.

The scarplet face becomes rounded and reduced in slope with continued erosion. The face darkens and develops a faint, vertically striate texture of small consequent drainage channels. The upthrown surface

remains as it appeared at the time of faulting. If additional sedimentation or reworking has occurred higher on the fans, this tone and texture near the face will be at variance with that prevailing in the alluvium. For example, a fault may occur in alluvium with a dark desert varnish; later reworking, which lightens the general tone of the alluvium, will not affect the upthrown surface near the scarp because the streams are there entrenched.

The downthrown surface becomes quite light at this stage of scarp-let destruction--lighter than the scarplet face--as the streams, entrenched in the upthrown side, lose their sediment on the downthrown surface. Rivulets on the scarplet face also deposit material on the downthrown surface.

Scarplets at a comparable stage of destruction, facing up-drainage, have rounded faces with less obvious consequent rivulets. The scarplets "V" downstream at major drainage channels. Tributary channels run at the base of the face, indicating that the scarplet no longer retains its initial position. The tributaries undercut the face and cause it to mass waste down-drainage. Streams along the scarplet base often exaggerate the height of the scarplet by entrenching the downthrown side.

The upper break in slope is lighter than the surroundings from continual mass wasting (and lower water content?). The downthrown surface is very light where streams occur at the base. The base is also characterized by larger, more verdant vegetation than elsewhere.

The final stage, before all topographic expression of faulting is removed, is typified by a return of the up- and downthrown surfaces to the tone prevalent in surrounding alluvium. The scarplet face is well rounded and gentle in slope. Its continuity is largely destroyed because formerly entrenched streams have now widened their channels. The original scarplet appears as aligned ends of projecting spurs of alluvium, with uniform height. The development of dark desert varnish on interfluves, by this stage, masks the possible effects of variations in moisture observable on fresher scarplets.

The scarplet faces, or spur ends, still possess a striation of small consequent channels. The lower gradient reduces the amount of erosion, and because of this, the lightness of the channels. Ridges between these

channels, however, have grown darker from desert varnish and the striate appearance is retained. Scarplet faces also do not possess the small, very light patches of wind-blown material found in depressions elsewhere in the alluvium.

Continuity of spur ends becomes more obscured as drainage channels widen in the upthrown side. At this stage of destruction, a scarplet face is no more steep or angular than the channel banks in the upthrown side. These banks are identical in tone and texture to the scarplet faces. The eye is continually drawn upstream when tracing scarplets along their lengths. It can be difficult to determine continuity from one interfluvium to the next if the scarplet is sinuous.

The tone and texture of scarplets facing up-drainage at this stage is much the same as described above. Desert varnish at the upper break in slope may be somewhat more uniform and the striae more obscure. Continuity of spur ends is harder to trace because the eroded scarplet curves down-drainage at each breaching channel. Small channels at the base of the face undercut greatest near through channels, destroying the linearity of the spur ends.

These characteristic tones, textures and forms are typical but not universal in Dixie Valley. Scarplets on valley-floor lake deposits, for example, do not follow this pattern and are recognized by form. They all appear to be quite recent in origin. The longevity of these features has already been discussed.

The characteristics do not apply well, or at all, where springs occur with scarplets in alluvium. Sapping and slumping destroy the scarplet form, vegetation and spring deposits mask the tones and textures. The presence of warm or hot springs at the base of a scarplet is here considered sufficient evidence for fault origin of that scarplet.

As mentioned in the initial discussion, scarplets in alluvium, particularly older ones, may be difficult to distinguish from other features. Over short sections of their lengths (a) stream terraces, (b) beach ridges, (c) shoreline nips and (d) slump scarplets can all possess characteristics on the photographs similar to fault scarplets.

An involved discussion of the tonal and textural properties of these other features is not necessary here. The origin of a feature in question can be resolved by a study of its geometry and position.

(a) Stream terraces: these are confined to only the largest streams in the area, entering the valley from the south. Smaller streams on the fans may have patches of low terrace within their high banks but these terraces are uncommon and easily recognized. The terraces of the large streams nearly follow the contours of the fans and there is no derangement of drainage at or near the scarplet. Where multiple, all terraces face toward the present drainage. Terraces do not branch and do not have springs at their bases.

(b) Beach ridges: these possess a definite ridge crest with slopes on both sides. There is much drainage derangement; a channel may be diverted hundreds of feet between ridges. The unvegetated back slopes and the very light, smooth areas in inter-ridge swales are distinctive. Ridges closely follow the contours.

(c) Shoreline nips: nips occur low on the fans or on the valley floor where sediment is fine-grained and cohesive. They follow the contours, do not branch, and do not derange drainage.

(d) Slump scarplets: slumping occurs at the toes of fans in Dixie Valley and appears to be triggered by the earthquakes which accompany faulting. Slump scarplets, however, are not the direct result of bedrock movement; location of bedrock faults cannot be inferred from the location of these scarplets.

Interbedded fan and pre-late Wisconsin lake deposits (Cohen and Everett, 1963) direct ground water movements to the margins of fans, causing seeps. The high water temperature of many seeps indicates a source in buried fracture zones beneath the present fan surface. The margins of fans are thus saturated with water and sapping by the seeps breaks the smooth slope from fan to valley floor. Here slumping occurs.

The position of slumps is their distinguishing characteristic. The tone, texture and form vary widely as a function of water content of the alluvium, amount of vegetation, presence of deposited carbonates and

degree of post-slumping destruction. Fresh slumps possess scarplet faces very similar to fresh fault scarplets. The two can be easily confused if only the faces are observed.

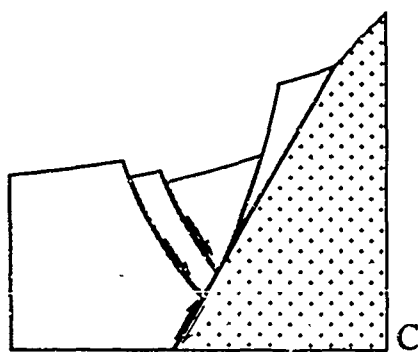
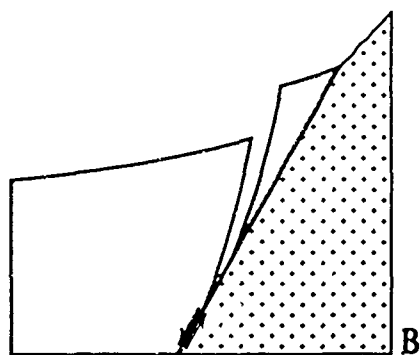
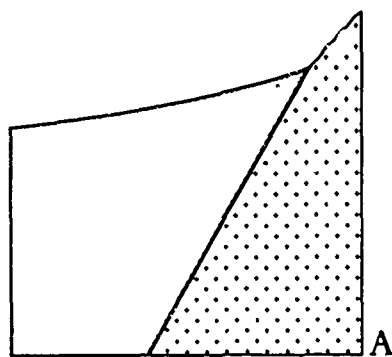
B. Scarplets at the Bedrock-Alluvium Contact

This category of fault features also includes, on Plate 1 as well as here, scarplets which are close and parallel to the bedrock contact but bounded on both sides by alluvium. It is common for mountain-front faults to carry a sliver of alluvium on the upthrown side during offset (Gilbert, 1890; Page, 1935).

Scarplets at the mountain front, where fresh, appear on the photographs as sharp, very light faces. The scarplets are commonly multiple and anastomosing or en echelon. Along lengths of scarplet where alluvium clings to the upthrown side, there is often a trench in the downthrown side immediate to the scarplet face. Because alluvium clings to the upthrown side, the dip of the scarplet face is steeper than that of the fault plane to which it clings. A gap must then be opened during offset. Slumping of alluvium of the downthrown side into this gap results in the trench-like appearance (Fig. 7). Vegetation is often larger and more verdant in this trench than elsewhere. The surface is light from wasting of material off the face. When offset has been so small that there is no topographic expression under the stereoscope, scarplets appear only as one or more light lines at the mountain front.

Mass wasting of material appears to be the dominant mechanism of scarplet destruction at the mountain front. The pre-faulting slopes are steep in the alluvium as well as in the bedrock. The striae of many small consequent drainage channels are not observed on the scarplet faces here.

Scarplets with bedrock exposed on the face and upthrown surface merge with the mountain front as the face darkens and develops the texture of higher bedrock. Where the upthrown side and scarplet face are alluvium, the face darkens but remains smooth. The upper break in slope becomes rounded and lighter. Mass wasting and stream erosion remove the alluvium from the upthrown side or reduce it to a series of discontinuous hummocks.



MODIFIED FROM GILBERT (1890)

Figure 7. Development of troughs at mountain-front faults.

The effects of other phenomena can appear much like mountain-front fault scarplets. The feature in question can be differentiated by following it along its length. Fault scarplets either directly cross the mouths of canyons or, because of erosion, do not appear there at all. The other, similar features react differently at canyon mouths.

(a) Mass wasting of a non-resistant bed: a bed subject to rapid mass wasting, if it outcrops just above and along the bedrock-alluvium contact between canyon mouths, can have the light tone and smooth texture of a mountain-front scarplet. At the canyons, however, the feature will curve upstream. Because of the complex structure of the ranges, beds rarely strike for long lengths with such consistency.

(b) Bedrock undercutting: this is also an uncommon situation. Drainage does not often run at the base of the mountain front. Where it does, the light band from mass wasting can be followed upstream.

(c) Animal trails: the herd animals of Dixie Valley leave light, smooth trails at the break in slope at the bedrock-alluvium contact. On the photographs, these trails are very similar to scarplets formed from slight offset. At the mouths of canyons, however, these trails curve upstream or branch and multiply as the animals separate to pick their individual paths down and up the steep channel banks.

II. THE RECOGNITION OF NON-TOPOGRAPHIC TRACES RESULTING FROM BEDROCK FAULTING

Lineaments of tone, texture and vegetation which result from bedrock faulting are varied in appearance but relations between these various appearances can be observed. Scarplets with topographic expression grade, on desert varnished older alluvium, into traces with no observable elevation change. These traces have different characteristics where they cross the lighter, reworked sediment of wide washes. Another change in characteristics is observed where traces cross beach deposits.

The appearance of traces in older alluvium is much like that of scarplets in the last stage of destruction. The trace is marked by a vaguely striate band within normal dark sediment. Vegetation on the striae may be darker (greener) than elsewhere. Any observable trace of this type must have originally faced down-drainage. Those scarplets which faced up-drainage have lost all linearity by this stage of destruction (Part I-A, above).

Where the traces continue into the lighter sediment of washes, they are characterized by bands of darker, larger plant growth. This is interpreted as due to ground water migration up the fracture zones. The traces here may be slightly ridged. This could be a result of soil retention by more extensive root systems of the larger plants or a greater cementation by material from solution in the fractures.

These traces, when crossing permeable beach deposits, often have slight topographic expression. The large, dark vegetation remains.

These fine details of morphology are not included in Plate 1. The entire length, in such a case, is mapped as a trace for simplicity.

Again, these characteristics are not universal and it is quite possible that other fault-produced traces could be recognized if their relation to scarplets were known. A case in point is the lineaments on the valley floor. These could be merely chance alignments of random features but they could equally well be an important part of the record of bedrock faulting in Dixie Valley. Lack of association with features of known origin makes a determination impossible.

Three other features in this study, under proper conditions, have appeared similar to fault traces.

(a) Old roads: dirt roads in Dixie Valley are graded on occasion and notch slightly into the gentle slopes of the fans. This slight change in slope across the road is apparently sufficient to pond or slow runoff and improve the growth of xerophytes. If a road is abandoned, it appears on the photographs as a light lineament with larger, darker vegetation than its surroundings.

These lineaments rarely curve sharply and they eventually join with obvious roads. Where they do curve, it is to avoid changes in topography such as large arroyos or beach ridges.

(b) Animal trails: on dark alluvium, trails of herd animals appear as vague lineaments, lighter in tone than the surroundings. The random network of these lineaments, and their continuation across arroyos, indicates their origin.

(c) Sediment grain size or color change: the uniform tone of a wind-blown covering is, in some cases, possessed of a very sharp boundary. This veneer obscures the fine texture of "normal" fan alluvium and can give the impression of a change in fine drainage type and density. The earlier discussion of scarplet destruction (Part I-A) included a stage in which the face and downthrown surface are lighter than elsewhere. The superficial appearance is similar in this situation.

The break in slope is lacking at a sand veneer edge and the zone of lightness is far wider than that of an aging scarplet. The source of a veneer can usually be traced upwind (southwest) to a specific arroyo or to the valley floor.

Wide bands of tone, texture and apparent drainage density are mapped as broad lineaments on Plate 1. These lineaments may be the result of wind erosion or deposition. However, they are at an angle to other features which are obviously of these origins, and no specific mechanism of formation is apparent.

III. THE RECOGNITION OF MOUNTAIN-FRONT SCARPS

Most linear lengths of the east front of the Stillwater Range are mapped on Plate 1 as having resulted from faulting. The straightness and imposing steepness of these lengths and their clear association with mountain-front scarplets makes obvious the interpretation that they are the result of faulting and post-faulting erosion.

At the western foot of the Clan Alpine Mountains, however, linear lengths of bedrock-alluvium contact often lack this intimate association with scarplets. Such contacts are often terminated by a return to a more typical fan-embayed and gently sloping front.

Processes of erosion can result in linear topography if bedrock attitude is properly predisposed. Cuestas of Cenozoic volcanics in the northern Clan Alpines, for example, possess steep and linear escarpments. Blackwelder (1928) pointed out that such linearity is not, per se, sufficient evidence for fault origin.

Blackwelder's discussion dealt with whole mountain fronts. However, his topographic criteria of faulting--such as the presence of triangular mountain-front facets, springs, "V"-shaped canyons and steepening stream gradients near mountain fronts--can be applied as well to the shorter lengths discussed here.

BIBLIOGRAPHY

- Blackwelder, Eliot, 1928, The Recognition of Fault Scarps; Jour. Geol. Vol. 36, pp. 289-311.
- Cohen, P., and Everett, D. E., 1963, A Brief Appraisal of the Ground-Water Hydrology of the Dixie-Fairview Peak Area; Ground-Water Resources-Reconnaissance Series, Report 23, Dept. Cons. and Nat. Res., State of Nevada, 40 pp.
- Davis, W. M., 1904, The Mountain Ranges of the Great Basin; Harvard College Bull. of the Mus. of Comp. Zoö., Vol. 42, pp. 127-178.
- _____, 1925, The Basin Range Problem; Proc. Nat. Acad. Sci., Vol. 2, pp. 387-392.
- Flint, R. F., 1961, Glacial and Pleistocene Geology; John Wiley and Sons, New York, 553 pp.
- Gilbert, G. K., 1890, Lake Bonneville; U. S. Geol. Survey Mono., Vol. 1, 438 pp.
- Herring, A. I., 1967, Seismic Refraction Study of a Fault Zone in Dixie Valley, Nevada; A. F. Cambridge Res. Labs. Final Scient. Rpt., Part II, AFCRL-66-848.
- Louderback, G. D., 1904, Basin Range Structure of the Humboldt Region; Bull. Geol. Soc. Am., Vol. 15, pp. 289-346.
- Meister, L. J., 1967, Seismic Refraction Study of Dixie Valley, Nevada; A. F. Cambridge Research Labs. Final Scient. Rpt., Part I, AFCRL-66-848.
- Morrison, R. B., 1964, Lake Lahontan: Geology of Southern Carson Desert, Nevada; U. S. Geol. Survey Prof. Paper No. 401.
- Muller, S. W., Ferguson, H. G., and Roberts, R. J., 1951, Geologic Map of the Mount Tobin Quadrangle, Nevada [with text]; U. S. Geol. Quadrangle Map CQ-7.
- Page, B. M., 1935, Basin-Range Faulting of 1915 in Pleasant Valley, Nevada; Jour. Geol., Vol. 43, No. 7, pp. 690-707.
- _____, 1965, Preliminary Geologic Map of a Part of the Stillwater Range, Churchill County, Nevada [with text]; Nevada Bureau of Mines Map 28.
- Slemmons, D. B., Steinbrugge, K. V., Tocher, D., Oakeshott, G. B., and Gianella, V. P., 1959, Wonder, Nevada, Earthquake of 1903; Bull. Seism. Soc. Am., Vol. 49, No. 3, pp. 251-265.
- Smith, T. E., 1967, Aeromagnetic Measurements in Dixie Valley, Nevada: Implications Regarding Basin-Range Structure; A. F. Cambridge Res. Labs. Final Scient. Rpt., Part III, AFCRL-66-848.

Speed, R. C., 1963, Unpublished progress map of parts of West Humboldt, Stillwater, and Clan Alpine Mountain Ranges, Nevada.

Thompson, G. A., 1959, Gravity Measurements between Hazen and Austin, Nevada: A Study of Basin-Range Structure; Jour. Geophys. Res., Vol. 64, No. 2, pp. 217-229.

_____, 1966, Unpublished gravity survey of Dixie Valley, Nevada.

PART V.

SURFACE STRAIN CHANGES AND STRAIN ENERGY RELEASE
IN THE DIXIE VALLEY-FAIRVIEW PEAK AREA, NEVADA

by

Laurent J.Meister, Robert O.Burford
George A.Thompson and Robert L.Kovach

ABSTRACT

Observations by the United States Coast and Geodetic Survey before and after the 1954 earthquakes in the Dixie Valley-Fairview Peak area have been reduced to surface strain patterns. The strain analysis shows a predominant NW-SE extension in the epicentral areas of the Rainbow Mountain and Fairview Peak earthquakes and NW-SE contraction in adjacent areas. The pattern of strain changes thus conforms to an elastic rebound model. A minimum energy release of 1.3×10^{23} ergs was estimated from the elastic strain changes. This value is comparable to the total energy released by the four large 1954 shocks as approximated by means of the magnitude-energy conversion. Net lowering of the ground surface during the earthquakes indicates a release of gravitational potential energy of about 4.3×10^{23} ergs. This energy possibly was dissipated as a minor, undetected uplift in a broad region surrounding the epicentral area.

TABLE OF CONTENTS

	<u>Page</u>
ABSTRACT	ii
TABLE OF CONTENTS	iii
LIST OF ILLUSTRATIONS	iv
LIST OF TABLES	v
<u>Chapter</u>	
I. ANALYSIS OF THE SURFACE STRAIN PATTERN	1
A. Introduction	1
B. Seismicity of the Area	3
C. Geodetic Measurements	4
D. Calculation of Surface Strain and Volumetric Dilatation	7
E. Interpretation of the Computed Strain Patterns	8
F. Accuracy of the Strain Analysis	14
II. STUDY OF THE STRAIN ENERGY RELEASE	17
A. General	17
B. Computation of the Strain Energy and Comparison with the Energy Inferred from the Earthquake Magnitude Scale	18
C. Gravitational Potential Energy	23
D. Conclusions	24
BIBLIOGRAPHY	26

LIST OF ILLUSTRATIONS

FIGURE	TITLE	PAGE
1.	Location Map. Historical faults of 1903 and later are shown. After Slemmons (1957).	2
2.	Displacement vectors in the Dixie Valley-Fairview Peak area. After Whitten (1957).	5
3.	Amplitude and direction of the principal strain axes in the Dixie Valley-Fairview Peak area.	9
4.	Volumetric dilatation in the Dixie Valley-Fairview Peak area. Positive values near the faults represent apparent dilatation due to slippage along the faults.	10
5.	Example of apparent strain in a triangle which crosses an active fault.	12
6.	Model used for strain energy computations.	19

LIST OF TABLES

TABLE	TITLE	PAGE
1.	Maximum Shear Strains and Orientations of Principal Strain Axes	16
2.	Magnitude-Energy Relations	22

I. ANALYSIS OF THE SURFACE STRAIN PATTERN

A. Introduction

Four earthquakes in the Dixie Valley-Fairview Peak area were accompanied by surface faulting in 1954. Immediately afterward, the United States Coast and Geodetic Survey revised the geodetic network in this area. The releveled data (Whitten, 1957) indicated a post-earthquake lowering of Dixie Valley relative to the surrounding area, and retriangulation showed a spreading in the vicinity of the active faults.

Analysis of the different components of fault displacements has stimulated in the last few years several hypotheses on the mechanics of deformation of the Basin and Range Province. Thompson (1959, 1960, 1965) has argued that the distension component of 5 in which occurred in 1954 in a direction normal to the strike of the faults is only the latest expression of a total distension estimated at 30 miles which took place in the last 15 million years throughout the province. On the other hand, Shawe (1965) believes that the strike-slip components of the 1954 fault displacements are strong evidence for an overall strike-slip control of the Basin and Range Province.

Although the analysis of relative surface displacements is a suitable representation for some purposes, a clearer picture of the details of crustal deformation can be obtained by computing strain components such as the orientation and magnitude of the principal strain axes, values of maximum shear, and dilatation. Unlike the displacement field, the strain pattern is independent of the frame of reference and is therefore uniquely determined.

One of the objectives of this research is to reduce the retriangulation data from the Dixie Valley-Fairview Peak area to surface strain components which may be analyzed to reveal details of the deformation that accompanied the 1954 earthquakes.

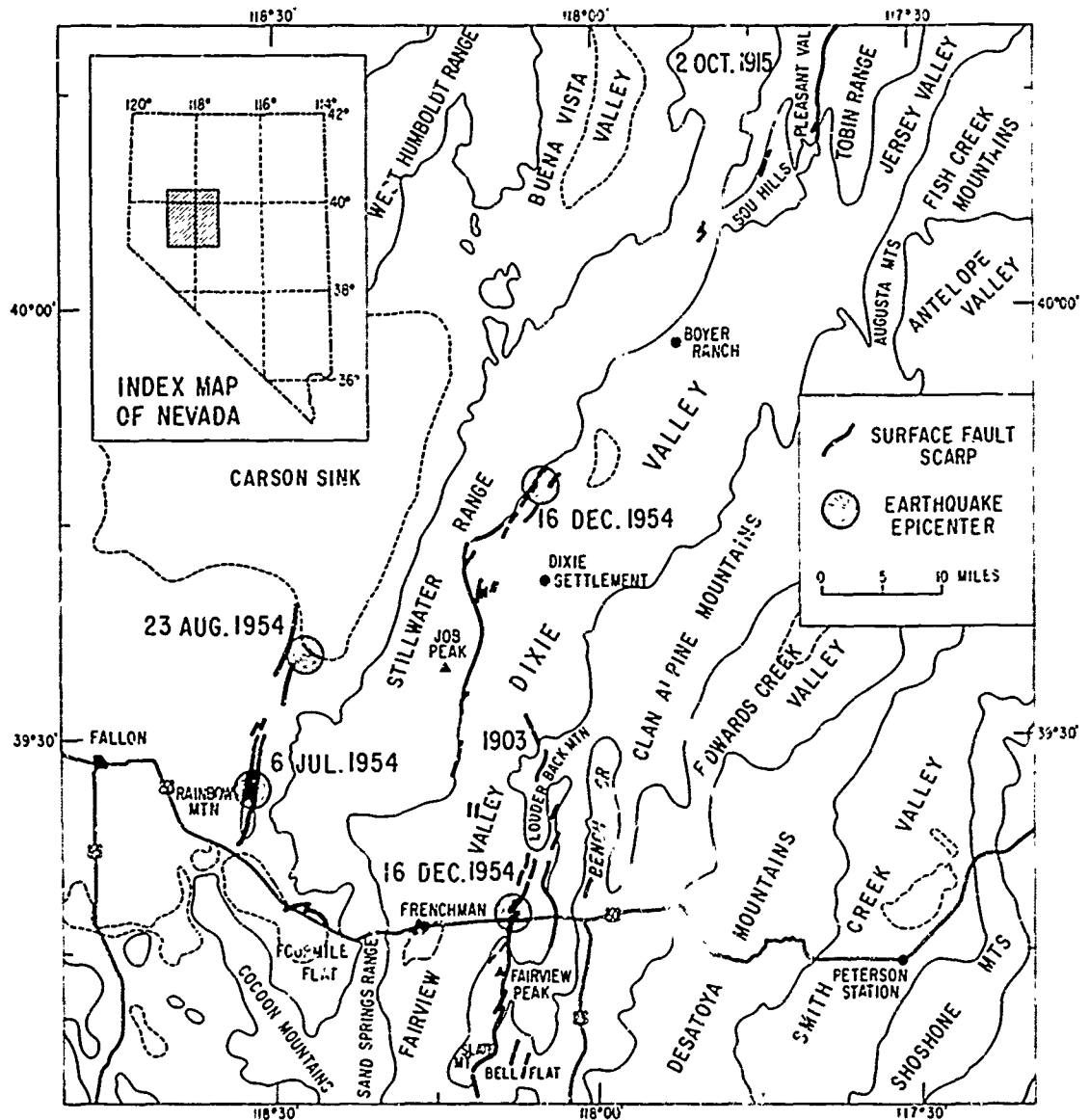


Figure 1. Location Map. Historical faults of 1903 and later are shown. After Slemmons (1957).

Computation of strain components from geodetic data of irregularly distributed triangulation stations was first discussed by Terada and Miyabe (1929) and used more recently by Kasahara and Sugimura (1964) and Burford (1965). Burford's method of analysis is used in the present study.

B. Seismicity of the Area

The Dixie Valley-Fairview Peak Area (Fig. 1) is at the center of the seismically most active region in western Nevada, a region extending from Pleasant Valley in the north to the Excelsior Mountains in the south. Historical faulting which occurred along the zone since 1903 has been summarized by Shawe (1965). Fig. 1 shows the faults and epicenters of the most recent seismic activity, consisting of the following earthquakes:

- a. The Fallon-Stillwater earthquake of July 6, 1954 had a magnitude of 6.6 (Tocher, 1958) and was accompanied by the development of a set of northerly aligned fault scarps on the east side of Rainbow Mountain.
- b. The Fallon-Stillwater earthquake of August 23, 1954, with an epicenter twelve miles northeast of the July 6 shock, had a magnitude of 6.8.
- c. The Fairview Peak earthquake occurred on December 16, 1954, near Fairview Peak and had a magnitude of 7.4.
- d. The Dixie Valley earthquake occurred only four minutes after the Fairview Peak shock and had a magnitude of 7.1.

The geological effects of these four earthquakes were described by Slemmons (1957), who mapped the fractures in the epicentral areas. The large circles on Fig. 1 show the epicenters of the four shocks (Romney, 1957). Romney estimated the focal depths from the pP-P times to be about 15 km for the Fairview Peak earthquake and 40 km for the Dixie Valley shock. According to Romney the focal fault causing the Fairview Peak main shock had a strike of N11°W and a dip of 62° to the east. Savage (1965) notes that a focal depth of 40 km for the Dixie Valley earthquake is

required to resolve a discrepancy in arrival times between P and S waves, but thinks that if the event identified as pP were instead a stopping phase the focal depth would presumably be less than 24 km and would then be about the same depth as the Fairview Peak earthquake. Eaton's (1963) seismic refraction data indicate that the crustal thickness in this part of the Basin and Range Province is about 24 km, so that it is possible that the foci for these shocks are located in the crust. During 1965, Westphal and Lange (1966) monitored seismic shocks of low magnitude in the Fairview Peak area. The measured foci were situated at depths ranging from 10 to 14 km. Later, the aftershocks of the April 13, 1965, earthquake were also recorded and were found to originate at depths between 6 and 10 km. Finally, the primary event of June 25, 1965, was located at a depth of 17.4 km, and the first aftershocks at depths between 12.3 and 14.9 km. These data together with the estimates of the focal depths for the 1954 shocks lead to the conclusion that nearly all the elastic strain must be released in the upper 20 km of the crust.

C. Geodetic Measurements

In the summer of 1954 a United States Coast and Geodetic Survey party extended an arc of first order triangulation eastward from Fallon to Ely, Nevada. In order to obtain information on the ground movement, especially during the Fairview Peak-Dixie Valley earthquakes, the same field party, in 1955, re-observed the entire network of triangulation stations from Fallon to Smith Creek Valley. After independent least-squares adjustment of the two sets of observed data, initial and revised geographic positions for each station were computed. Comparison of the two sets of geographic coordinates determined the horizontal component of movement of each station relative to control stations on the east and west ends of the network, which were assumed to be stable. The horizontal components of displacement are represented by vectors in Fig. 2 (after Whitten, 1957).

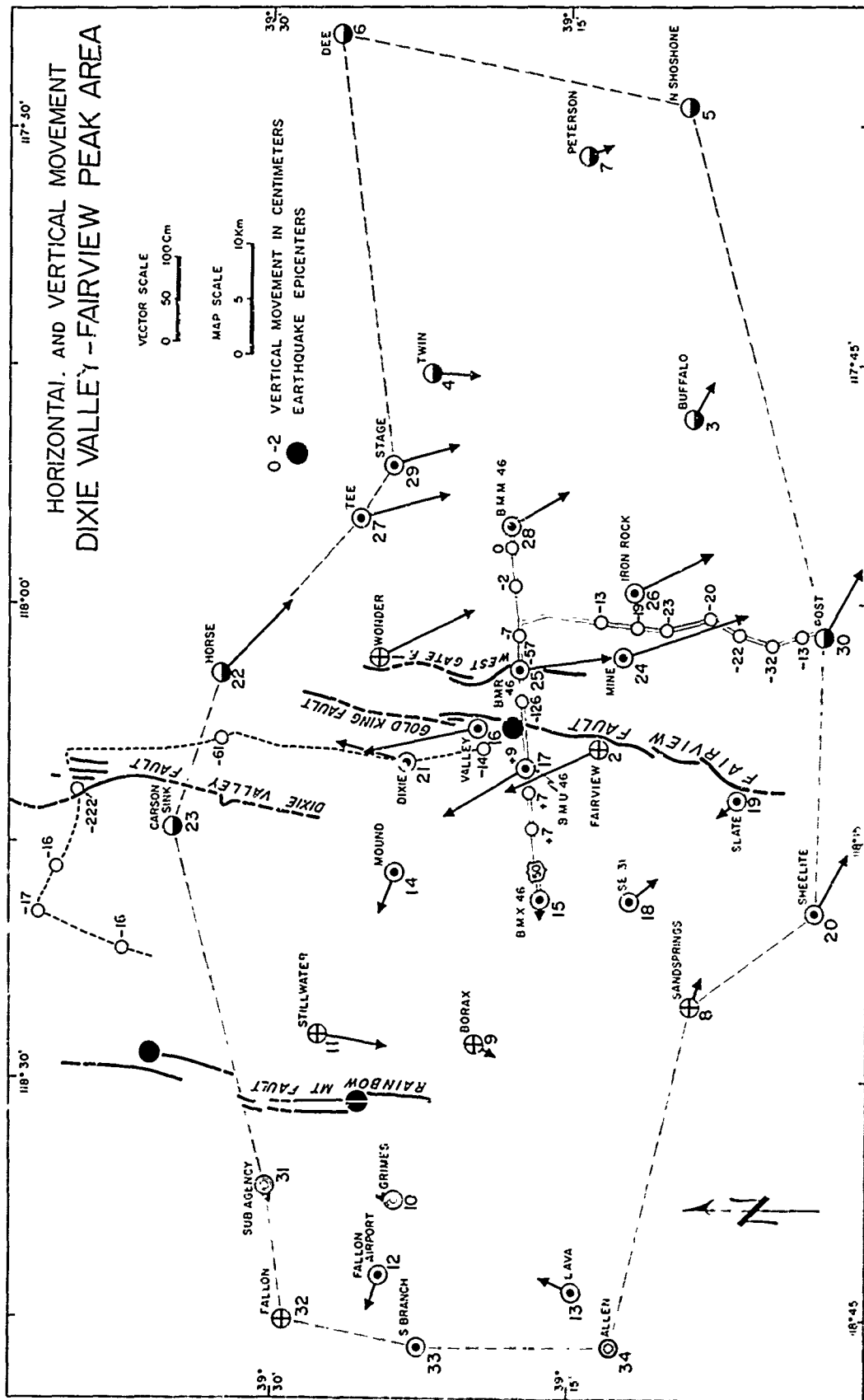


Figure 2. Displacement vectors in the Dixie Valley-Fairview Peak area. After Whitten (1957).

In addition to possible random errors introduced by non-tectonic displacement of the triangulation stations, systematic errors may be introduced into the data by slight undetected movement of control stations on the western and eastern ends of the surveyed area. Representations of systematic errors have been discussed by Burford (1965). Burford considered cases of finite pure shear with hypothetical baselines placed at various angles to the principal strain axes and concluded that the effect of possible systematic errors on the result of strain analysis is negligible.

Unfortunately the 1954 survey covered only part of the triangulation network which was observed in 1955. Some of the 1954 measurements were made after the July 6, 1954 earthquake and some after both Fallon-Stillwater earthquakes. Thus, the triangulation stations have been classified in the following four categories:

- a. Stations such as Grimes whose displacement vectors represent the sum of twenty years of creep plus movements which occurred during the four 1954 earthquakes (concentric circles in Fig. 2).
- b. Stations such as Lava which were surveyed in December 1953 and re-observed in May 1955 (black dot within circle in Fig. 2).
- c. Stations such as Carson Sink which were surveyed after the July 6, 1954 earthquake (half-black dot in Fig. 2).
- d. Stations such as Wonder whose displacement vectors represent only displacements at the time of the Fairview Peak-Dixie Valley earthquakes (cross within circle in Fig. 2).

This distinction between stations will bear especially on the interpretation of the map of principal strains

In addition to the retriangulation of the area, elevation benchmarks were releveled. Those extending across the Stillwater Range were originally leveled by the U. S. Geological Survey in 1907-1908, and those along Highway 50 and Road 23 east of Fairview Peak in 1934. These data, which are also shown in Fig. 2, show a general dropdown of the area and will be used in the strain energy calculations.

The leveling data are of poor reliability and represent the summation of the vertical components of all post-1908 tectonic movements for the Dixie-Stillwater area and post-1934 movements for the remainder of the surveyed area. In the present study it is assumed that these vertical displacements represent mainly movements which occurred during the Fairview Peak-Dixie Valley earthquakes.

The triangulation network re-observed by the U. S. Coast and Geodetic Survey comprises only the southern part of the region affected by the four earthquakes of 1954. Thus, the epicentral areas of the Dixie Valley shock and of the August 1954 Fallon-Stillwater shock are not completely covered by horizontal displacement data. These limitations must be considered in the interpretation of derived strain information.

C. Calculation of Surface Strain and Volumetric Dilatation

The displacement components u and v for each triangulation station were computed with respect to an orthogonal x, y coordinate system where the x and y axes were taken in the eastward and northward directions, respectively. Stations were grouped in such a way that they formed the smallest and most nearly equilateral triangles. Close approximations of the magnitudes and directions of the principal horizontal strains were calculated for each triangle under the assumption that strain is uniform within each triangle.

Kasahara and Sugimura (1964) assumed the displacement components to be given by

$$u = a_0 + a_1x + a_2y + a_3x^2 + a_4xy + a_5y^2,$$

and

$$v = b_0 + b_1x + b_2y + b_3x^2 + b_4xy + b_5y^2,$$

and therefore needed the data of six independent stations to determine the unknown constants. In the present study, we assume that the displacement

components u and v can be adequately approximated by linear functions of x and y so that three stations of a triangle are sufficient to determine the constants.

All strain components were calculated with a computer program written by Burford (1965). The magnitudes and directions of the principal strain axes are shown in Fig. 3 for each outlined triangular area.

Vertical strain and volumetric dilatation were also computed for each prism whose top is limited by the same triangle used to compute the horizontal strain and whose base was assumed fixed at a depth H (Fig. 6). The vertical changes of the surface of the ground were determined from the leveling data for the triangles nearest the leveling lines and the vertical movement was considered to be uniform over the entire surface of each triangle. Changes in elevation were not assumed within triangles for which releveled data were not available, and the vertical strain component was taken to be zero in these same areas. Volumetric dilatation was computed for H equal to 10, 15, and 20 km, a range of thicknesses based on estimates of focal depths discussed above. Fig. 4 shows the areal variation in volumetric dilatation for $H = 15$ km.

E. Interpretation of the Computed Strain Patterns

The region under study may be divided into several areas according to the directions and magnitudes of the principal strains and the values of dilatation.

The area east of the Fairview Peak-Dixie Valley fault zone is in general characterized by a predominant NW-SE contraction which is larger in magnitude than the NE-SW extension. The map of volumetric dilatation (Fig. 4) shows an overall contraction which decreases in magnitude eastward from the Fairview Peak-Dixie Valley fault zone.

The strain triangles which cross the Fairview Peak, Gold King, and West Gate faults, and the south end of the Dixie Valley fault, were subjected to discontinuous extension due to slippage on the fault planes, some of which showed surface offsets and ground breakage. Unfaulted material within these triangles on both sides of the fault, however,

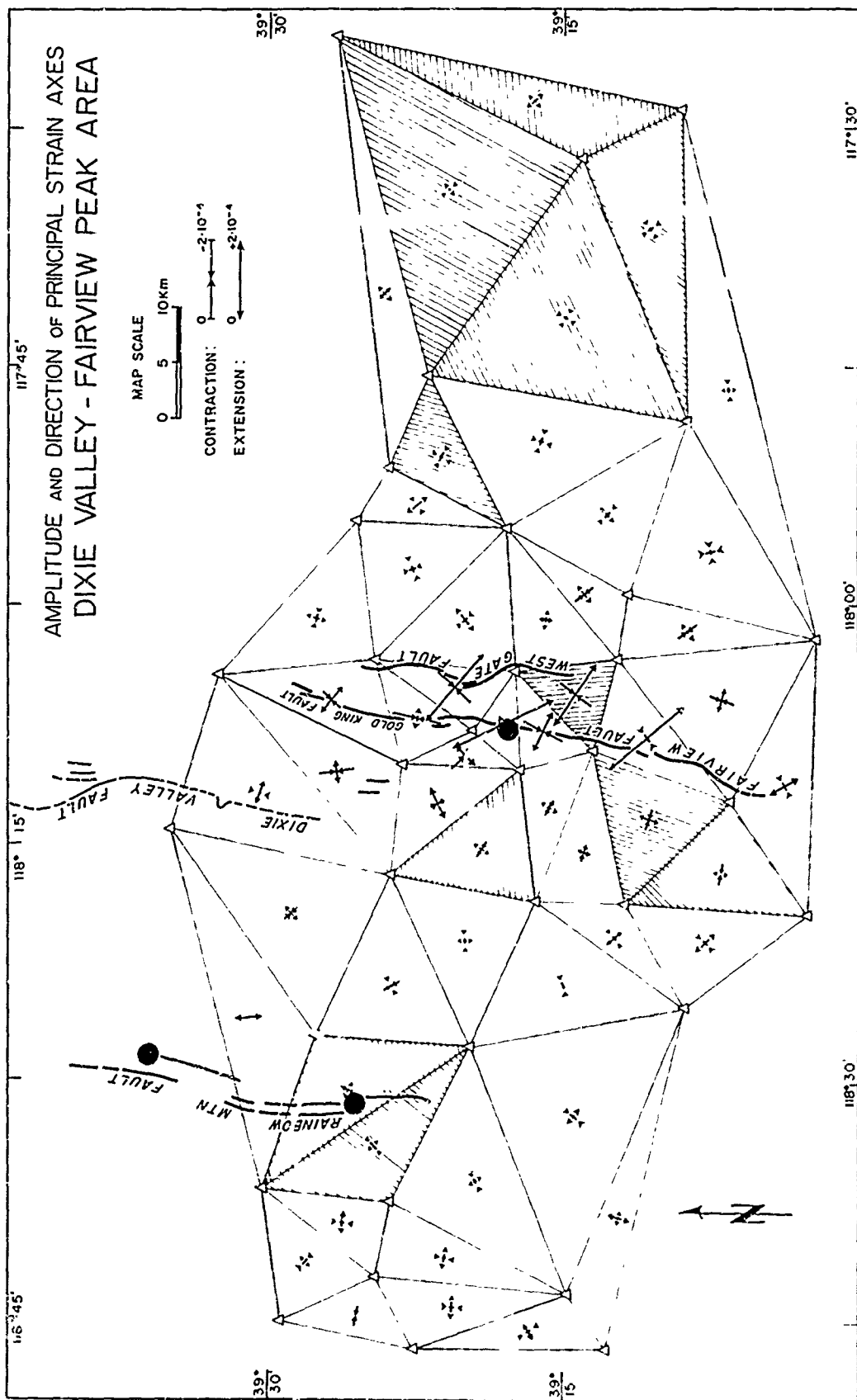


Figure 3. Amplitude and direction of the principal strain axes in the Dixie Valley-Fairview Peak area.

Figure 4. Volumetric dilatation in the Dixie Valley-Fairview Peak area. Positive values near the faults represent apparent dilatation due to slippage along the faults.

presumably underwent smaller, continuous elastic contraction much the same as that shown in triangles immediately to the east and west of the breaks. Computed strain results for triangles which cross faults are thus a composite of the two opposite effects, with the larger, discontinuous extension associated with fault slippage predominant over the contribution of elastic rebound (Fig. 5). The magnitude of the apparent strain in these triangles, treated as if the deformation were uniform over each triangle, varies from 6×10^{-5} to 3×10^{-4} . The values of the apparent volumetric dilatation associated with these triangles are all positive due to the fault slippage as shown in Fig. 4.

Principal axes of contraction in the region east of the Fairview Peak-Dixie Valley fault zone are generally parallel to the directions of maximum extension determined within triangles spanning the breaks (Fig. 3), reflecting the elastic rebound nature of the disturbance.

In order to analyze the strain pattern on the west side of the Dixie Valley-Fairview Peak fault zone, triangulation stations whose displacements represent movements of the crust during different time intervals were used in the calculations. Areas of similar strain distribution can, however, be distinguished.

A strain pattern comparable to that found on the east side of the Dixie Valley-Fairview Peak Fault is observed directly to the west of this fault.

The east side of the Sand Springs Range between stations "Sandsprings," "BM-X46," and "Sheelite" (Fig. 2) also shows predominant extension in the NW-SE direction associated with volumetric dilatation. Comparison of this observation with the apparent strain pattern obtained across the Fairview Peak fault leads to the suggestion that probably some movement occurred on a fault along the east base of the Sand Springs Range during the Dixie Valley-Fairview Peak earthquakes (Fig. 1). The only known surface expression that may be related to this movement is a small fissure which was observed (Fig. 1) at Frenchman's Station (Slemmons, 1957).

Kasahara (1959) noted that the rate of decrease of the N-S or E-W components of the displacement vectors shown in Fig. 2 is smaller to the

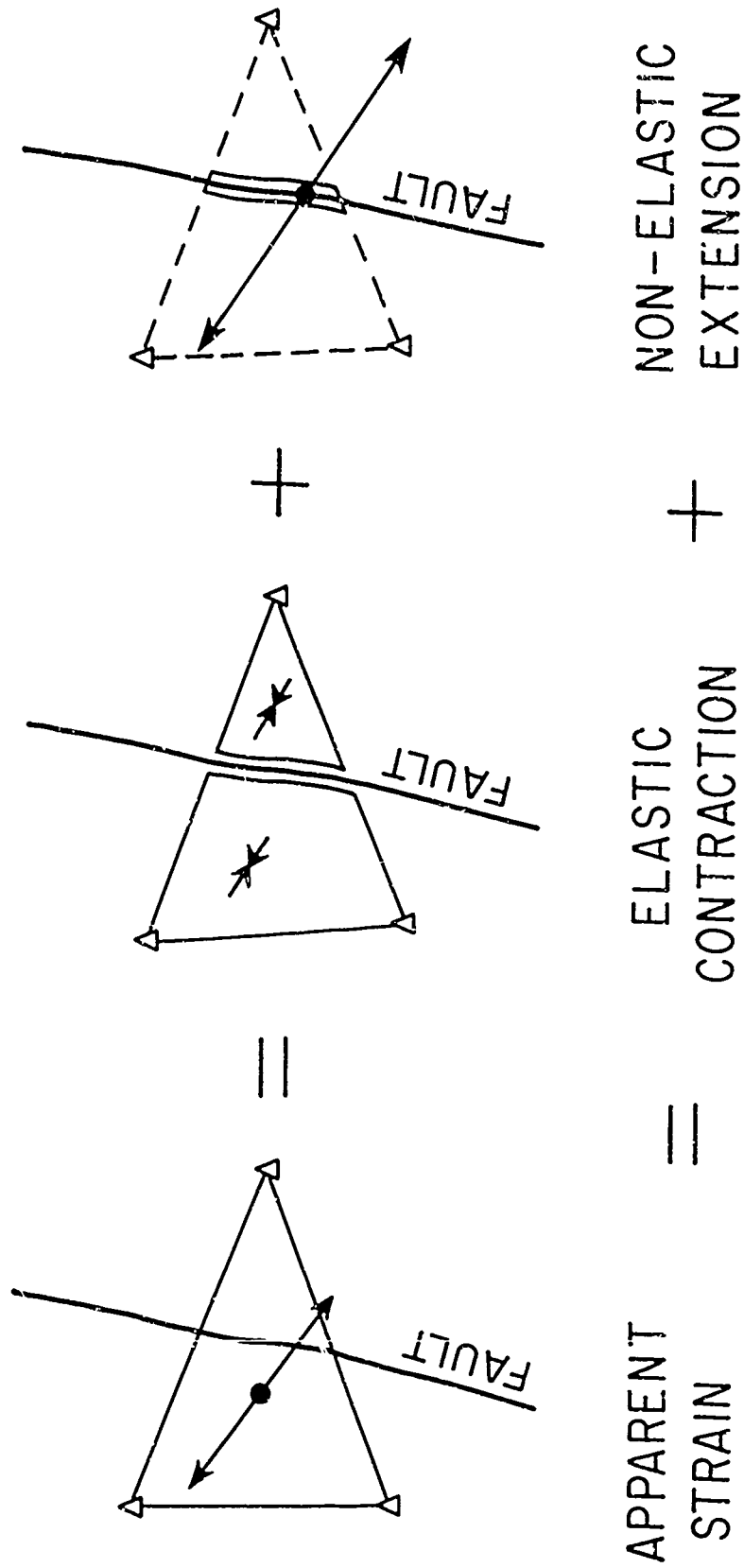


Figure 5. Example of apparent strain in a triangle which crosses an active fault.

east than to the west of the Fairview Peak fault. He suggested that this asymmetry may be due to an 80° eastward dip of the fault plane. However, from the present study it is seen that the rapid decrease on the west side of the fault may be due instead to slippage along the Sand Springs Range fault.

In the area which crosses the Rainbow Mountain fault zone the strain pattern is governed by a NW-SE apparent extension which is smaller in magnitude than the NE-SW contraction, resulting in an overall volume loss (Figs. 3 and 4). An explanation of this pattern is that the magnitude of the NW-SE elastic contraction associated with the Dixie Valley-Fairview Peak earthquakes reduced the NW-SE apparent extension which was associated with the activity on the Rainbow Mountain fault prior to the two large shocks on December 16, 1954. The sum of the two effects thus resulted in a residual volumetric contraction.

The apparent strain pattern across the Rainbow Mountain fault zone thus suggests significant components of right-lateral movement along this fault at the time of the 1954 earthquakes. Tocher (1954) reported only dip-slip displacement along the fault in this region.

In comparing the directions of the principal strain axes computed for the epicentral areas with the parameters of the fault plane solutions given by Fara (1964), one can note that the axes of minimum compression at the epicenters of the two Rainbow Mountain earthquakes and the Fairview Peak earthquake are roughly parallel to each other and parallel to the principal axes of extension in the epicentral areas, suggesting that the earthquake mechanism was similar for all three shocks.

Apparent E-W extension in the area west of the Rainbow Mountain fault coincides with a N-S band of positive dilatation (Fig. 4), suggesting possible dip-slip displacement along an unmapped N-S fault between stations "Grimes" and "Fallon Airport."

F. Accuracy of the Strain Analysis

The azimuths of the first order triangulation data are given to the nearest 0.01". Therefore, the largest error in the angular data of the survey is approximately $\pm 0.01''$. First order triangulation surveys are believed to be accurate to within $\pm 5 \times 10^{-6}$ (Pope, Stearn and Whitten, 1966).

All principal strain values less than 5×10^{-6} are therefore open to suspicion although it will be shown later that the strain values are probably known to better than 5×10^{-6} .

The volumetric contraction of the entire area to a depth of 15 km is 4×10^{-6} . Since the possible error is as much as 1.5×10^{-5} , this contraction is probably not significant and no conclusion can be drawn about the volumetric change of the entire region.

The present method of strain analysis is limited in several critical ways. In order to obtain magnitudes for the principal strains and dilatation, it is necessary to assume the existence of fixed baselines or stable points in one or more places in the triangulation net and the absence of significant earth motion during the periods of field observations.

Frank (1966) has pointed out recently that one can extract the local shear strains

$$\gamma_1 = (e_{11} - e_{22}) \quad \text{and} \quad \gamma_2 = (e_{12} + e_{21})$$

from the angle measurements of every triangle which was resurveyed without knowledge from adjoining areas and without a reference length.

To evaluate the accuracy of the present study, the maximum shear strain $\gamma = (\gamma_1^2 + \gamma_2^2)^{1/2}$ and the orientation of the principal strain axes given by $\tan 2\theta = \gamma_1/\gamma_2$ was calculated for the eleven hatched triangles shown in Fig. 3. The values obtained from the two independent methods are compared in Table 1.

Using Frank's expression for the maximum shear for an equilateral triangle, it is found that an angular error of 0.01" may produce a

spurious strain of only 2×10^{-7} . This value is the largest error of the maximum shear strain as deduced by Frank's method. The corresponding orientations of the principal strain axes are therefore accurate to two degrees.

By comparing Frank's values in Table 1 with the values deduced from the present study one can observe that they agree quite well. Since the maximum discrepancy between the strain data is only about 3×10^{-6} , it is concluded that the strain values of the present study are accurate to 3×10^{-6} instead of 5×10^{-6} as mentioned earlier. Similarly, possible errors for the orientation of the strain axes do not exceed 5° .

Frank's method utilizes data which are closer to actual observations and therefore the comparison of results from the two methods gives us an insight into the accuracy of the present analysis.

TABLE I
MAXIMUM SHEAR STRAINS AND ORIENTATIONS OF PRINCIPAL STRAIN AXES

TRIANGLE	PRESENT STUDY			FRANK'S METHOD	
	θ ₁ IN DEGREES	MAXIMUM SHEAR STRAIN	θ ₁ IN DEGREES	MAXIMUM SHEAR STRAIN	MAXIMUM SHEAR STRAIN
4	-34.7	7.00×10^{-5}	-33.4	6.97×10^{-5}	
13	-40.2	2.18×10^{-5}	-35.1	2.45×10^{-5}	
15	-35.2	1.09×10^{-5}	-32.4	1.01×10^{-5}	
16	41.8	0.96×10^{-5}	42.9	0.97×10^{-5}	
17	27.1	0.98×10^{-5}	29.3	0.94×10^{-5}	
22	44.8	3.18×10^{-5}	44.1	3.33×10^{-5}	
25	-34.1	6.56×10^{-5}	-32.9	6.69×10^{-5}	
41	-35.6	32.70×10^{-5}	-35.4	32.40×10^{-5}	
44	-12.5	6.29×10^{-5}	-11.5	6.49×10^{-5}	
45	-21.3	11.10×10^{-5}	-20.8	11.00×10^{-5}	
52	-45.3	3.19×10^{-5}	-42.6	3.15×10^{-5}	

II. STUDY OF THE STRAIN ENERGY RELEASE

A. General

Several estimates of strain energy released during earthquakes have been computed from geodetic observations and were each based on specific assumptions regarding the earthquake mechanism.

Byerly and De Noyer (1958) assumed that the strain energy released by a shallow earthquake is equal to the work done along the fault plane at the time of the break. They obtained 1.5×10^{22} ergs for the Dixie Valley-Fairview Peak earthquakes.

Knopoff (1958) attributed the cause of an earthquake to the formation of a crack in a material undergoing uniform strain and derived the following expression for strain energy:

$$e_k = 1/16 \pi \mu S^2 L$$

where

μ = the modulus of rigidity

S = the fault displacement at the surface

L = the length of the fault break

One of the boundary conditions imposed on these models is the vanishing of stresses on the fault plane, which ignores stresses set up by local rotation and dilatation of the material at the time of the earthquake.

Niazi (1964) computed the release of shear energy for a spherical focal model with a laminar displacement field in which the stresses across the fault plane after the earthquake are assumed to be discontinuous but finite. Taking 80 km as the length of the Dixie Valley-Fairview Peak fault and 370 cm as the maximum relative displacement along the fault break, he determined a strain energy release of 1.5×10^{22} ergs for the Dixie Valley-Fairview Peak earthquakes. Adopting Niazi's values ($\mu = 3 \times 10^{11}$ dynes/cm², $S = 370$ cm, $L = 80$ km) a strain energy release of 6.5×10^{22} ergs for these same earthquakes is obtained using Knopoff's formula. A representation of

faulting by dislocation theory has been used more recently by Press (1965) to compute the change in the strain field which accompanied the Alaskan earthquake of March 27, 1964. Press gave an estimate of the elastic strain energy released by this earthquake by evaluating the volume integral:

$$\int_V \left[\lambda \frac{\Delta^2}{2} + \mu \sum_{i,j=1}^3 e_{ij} e_{ij} \right] dV$$

where e_{ij} are the strain components, Δ is the dilatation, and λ and μ are Lamé's constants. He used the theoretical strain change which best fit the observed fault parameters.

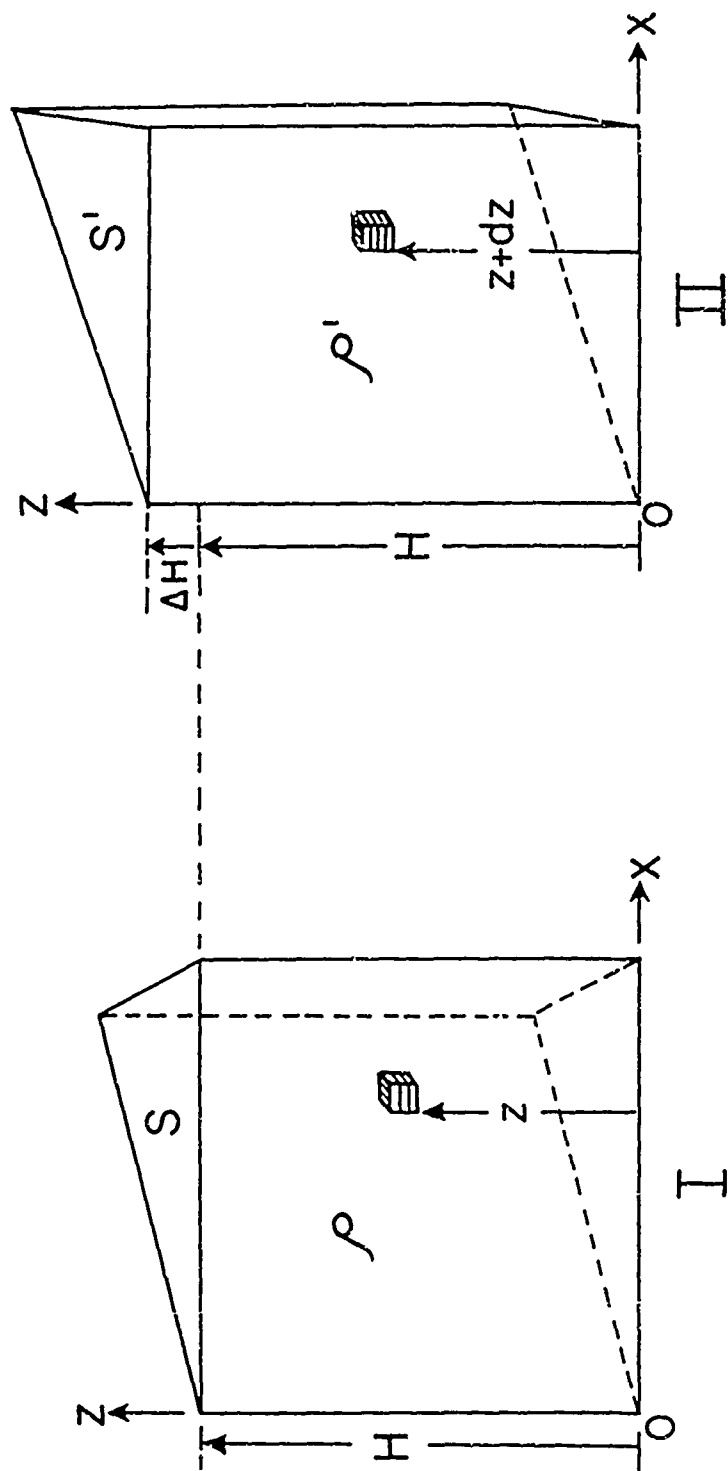
In this paper we evaluate the total strain energy released by the four large earthquakes which occurred in 1954 in the Dixie Valley-Fairview Peak area which are responsible for the previously observed changes in positions of survey stations.

The above volume integral was computed for each crustal prism. The sum of all these individual volume integrals thus yields an estimate of the strain energy released. The advantage of this method compared to previous estimates is that no assumption concerning the earthquake source mechanism is necessary. It is only assumed that the energy released was confined to the elastic part of the earth's crust. Since there is no way to estimate the residual strain field which existed after the 1954 earthquakes it is also assumed throughout the following calculations that the strain field dropped to zero at the time of faulting.

B. Computation of the Strain Energy and Comparison with the Energy Inferred from the Earthquake Magnitude Scale

To compute the strain energy released by a crustal prism as shown in Fig. 6 it is assumed that the crustal material is elastic and isotropic and therefore the directions of the principal axes of stresses and strains are identical.

Only a few data for level changes are available, and unfortunately these points usually do not correspond to triangulation stations. The representative value of vertical displacement, ΔH , chosen for each triangle is assumed to be uniform over its surface S (Fig. 6). Since the variation



Change in gravitational potential:

$$\Delta\phi = \phi_{\text{II}} - \phi_{\text{I}} = g \cdot \rho \cdot S \cdot H \cdot \Delta H / 2$$

Change in strain potential

$$\Delta W = \left\{ \frac{1}{2} \lambda \Delta^2 + \mu (e_{11}^2 + e_{22}^2 + e_{33}^2 + 2 e_{12}^2) \right\} S \cdot H$$

Figure 6. Model used for strain energy computations.

of strain with depth is unknown, computed horizontal strains and the vertical strain component given by $\Delta H/H$ are applied as constant throughout the volume of each prism down to the base, below which these strains vanish.

The following strain components are defined with the use of u , v , and w as the components of displacement at each station in an xyz coordinate system.

$$e_{11} = \frac{\partial u}{\partial x} ; e_{22} = \frac{\partial v}{\partial y} ; e_{33} = \frac{\partial w}{\partial z} ;$$

$$e_{12} = e_{21} = \frac{1}{2} \left(\frac{\partial u}{\partial y} + \frac{\partial v}{\partial x} \right) ;$$

$$e_{13} = e_{31} = \frac{1}{2} \left(\frac{\partial u}{\partial z} + \frac{\partial w}{\partial x} \right) ;$$

$$e_{32} = e_{23} = \frac{1}{2} \left(\frac{\partial w}{\partial y} + \frac{\partial v}{\partial z} \right) ;$$

W_p is the strain energy released by each crustal prism considered as an elementary volume; by expanding the volume integral mentioned above for each crustal prism and assuming $\lambda = \mu$ one obtains:

$$2W_p = (\mu(e_{11}^2 + e_{22}^2 + e_{33}^2) + 2\mu(e_{11}^2 + 2e_{12}^2 + 2e_{13}^2 + 2e_{23}^2 + e_{22}^2 + e_{33}^2))S \cdot H.$$

Due to the foregoing assumptions, $e_{13} = e_{23} = 0$, and $e_{33} = \Delta H/H$.

The expression for strain energy thus reduces to:

$$2W_p = (\mu(e_{11}^2 + e_{22}^2 + e_{33}^2) + 2\mu(e_{11}^2 + e_{22}^2 + e_{33}^2 + 2e_{12}^2))S \cdot H.$$

Usually the coefficient of rigidity is estimated to be about 5×10^{11} dynes/cm² at an earthquake focus. This estimate is based on information obtained from the propagation of seismic waves (Tsuboi, 1956; Press, 1965). However, Benioff (1951) suggested that μ may decrease sharply around a fracture zone. Byerly and De Noyer (1958), Knopoff (1958)

and Niazi (1964) followed this suggestion and assumed $\mu = 3 \times 10^{11}$ dynes/cm². In this study we applied a value of 4×10^{11} dynes/cm² for this coefficient.

The computer program used to obtain the horizontal strain components e_{11} , and e_{22} , and e_{12} was modified to compute W_p for each crustal prism.

The total apparent strain energy release obtained for the whole area, assuming $H = 15$ km, is 1.9×10^{23} ergs. The contribution to the total from all prisms not cut by active faults within the Dixie Valley-Fairview Peak fault zone was 0.7×10^{23} ergs, and represents an energy release due to elastic rebound. Only part of the remaining apparent strain energy release of 1.2×10^{23} ergs, computed for prisms situated along the Dixie Valley-Fairview Peak fault zone, is due to elastic strain rebound. The other part is meaningless, and results from non-elastic deformation. This apparent energy cannot be taken into account since only elastic strain changes are considered in the present analysis. An evaluation of the contribution to the total elastic strain energy release from the prisms containing active fault surfaces is necessary, however, since they comprise a significant volume of material within which the largest elastic changes occurred. It is possible to arrive at an estimate of this contribution by considering the areal distribution of energy density on the east side of the fault zone. This distribution was derived by dividing the energy contribution of each unfaulted prism by its volume.

It was found that the energy density within the area east of the Dixie Valley-Fairview Peak fault increased from east to west toward the fault zone. A linear extrapolation of this trend into the fault zone yields an estimated average of 6×10^3 ergs/cm³ for material within the faulted prisms. This density value was multiplied by the total volume of the faulted prisms, yielding a value of 0.6×10^{23} ergs for the estimated contribution from faulted prisms to the total elastic strain energy release.

Accordingly, the total strain energy release due to elastic rebound is approximately equal to $(0.7 + 0.6) \times 10^{23}$ ergs = 1.3×10^{23} ergs.

There are two major reasons for suggesting that the computed elastic strain energy represents only a lower bound for the total strain energy release:

A. The area investigated comprises only part of the region affected by the four earthquakes of 1954.

B. It is assumed that the strain field dropped to zero after the 1954 earthquakes and therefore the calculated strain energy release is minimum.

An estimate of the seismic wave energy released during each of the four 1954 shocks can be derived from the familiar Gutenberg-Richter relation:

$$\log_{10} E = 11.8 + 1.5 M$$

where M is the magnitude of the earthquake and E the seismic wave energy in ergs.

The seismic wave energy values contained in Table 2 have been calculated using the magnitudes given by Tocher (1958). The total wave

EARTHQUAKE	DATE	MAGNITUDE M	WAVE ENERGY in ergs
FALLON	July 6, 1954	6.6	0.5×10^{22}
FALLON	August 24, 1964	6.8	1×10^{22}
FAIRVIEW	Dec. 16, 1964	7.4	8×10^{22}
DIXIE VALLEY	Dec. 16, 1964	7.1	2.8×10^{22}

TABLE 2.
Magnitude-Energy Relations

energy dissipated by the four main shocks is 1.2×10^{23} ergs. Only 14% of this energy is due to the Fallon-Stillwater earthquakes.

The strain energy released by elastic rebound is approximately equal to the indicated seismic wave energy of 1.2×10^{23} ergs. It must be emphasized, however, that the computed elastic rebound energy may be

considered a minimum value and also that the transformation factor from elastic rebound energy to wave energy is less than unity.

C. Gravitational Potential Energy

The elastic strain energy is only part of the original potential energy stored in the rock, another part being gravitational potential energy. Any vertical change in the ground level occurring during an earthquake creates a change in gravitational potential energy; a regional downdrop may yield kinetic energy and any uplift may absorb it.

In order to devise an expression for this change in potential energy due to a vertical level change ΔH of the top of the crustal prism shown in Fig. 6 the gravitational potential energy of an elementary volume of this prism must be defined.

A volume $dv = dx \cdot dy \cdot dz$ at a height z above the reference plane is considered in the strain state of case I of Fig. 6. The potential energy of this elementary volume of rock is

$$d\phi = g z \rho dx dy dz$$

where g is the acceleration of gravity and ρ the density of the prism in state I. By integrating, one obtains the potential energy of prism I

$$\phi_I = g \rho S \int_0^H z dz = g \rho S \frac{H^2}{2}.$$

S and H are the cross-sectional surface and height of the crustal prism in state I.

During strain release, the crustal prism passes from state I to state II; the level of the elementary volume is changed by the amount dz and the top of the prism by ΔH . If S_1 and ρ_1 are the cross-sectional surface and the density of the prism in state II, the potential energy of prism II is:

$$\phi_{II} = g \rho_1 S_1 \frac{(H + \Delta H)^2}{2}.$$

Since it is assumed that the mass of the prism is not changed, the following relation applies:

$$\rho_1 = \frac{\rho H S}{(H + \Delta H)S_1} .$$

Therefore, one can readily obtain

$$\phi_{II} = \frac{g \rho S H (H + \Delta H)}{2} .$$

The difference between ϕ_{II} and ϕ_I gives the change in gravitational potential energy $\Delta\phi$ which occurs with the strain release of any crustal prism. $\Delta\phi$ is given by:

$$\phi_{II} - \phi_I = \Delta\phi = g \rho S H (\Delta H)/2 .$$

The change in gravitational potential energy is positive for an uplift of the crustal block, corresponding to an absorption of kinetic energy.

The change in gravitational potential energy was calculated for each crustal prism and all values were added to yield a total change in gravitational potential energy of -4.3×10^{23} ergs for $H = 15$ km. Out of the few bench marks which were releveled in the Dixie Valley-Fairview Peak area, only four showed a local uplift whereas most showed a regional drop, which leads to a net release of gravitational potential energy.

D. Conclusions

The total energy change which takes place during an earthquake includes both changes in strain energy and gravitational potential energy. The sum computed for the Dixie Valley-Fairview Peak earthquakes of 1954 is 5.6×10^{23} ergs for $H = 15$ km. Two-thirds of this energy was released by a change in gravitational potential and the rest is attributable to strain rebound.

Since the energy radiated from the earthquake sources in the form of elastic waves was found to be 1.2×10^{23} ergs, there is an excess of at least 4.4×10^{23} ergs which must have done mechanical work or was dissipated as heat at the moment of the earthquake.

Bomford (1962) states that the accuracy in leveling work is actually about ± 1 cm. Assuming a crustal thickness of 15 km, one thus finds that an uplift of 1 cm over an area of $25,000 \text{ km}^2$ would absorb 5×10^{23} ergs. This would mean that while the Dixie Valley-Fairview Peak area was undergoing an important subsidence, the region included in a 100 km radius around this epicentral area could have been affected by an uplift of about 1 cm at the time of the 1954 earthquakes, an uplift which was not detected because of the limited extent of the leveling survey and because of its accuracy. This suggestion is supported by observations throughout broad regions in Japan and especially by the vertical displacements which occurred albeit on a small scale during the Tzu Earthquake in 1930 (Inoue, 1960).

The areal distribution of surface strain accompanying the Dixie Valley-Fairview Peak earthquake illustrates the suggestions that volume changes accompanying large earthquakes in the Basin and Range Province are consistent with elastic rebound theory (Thompson, 1965). Furthermore, the energy study of these same earthquakes leads to a similar conclusion. Vertical displacements observed in the epicentral area and suggested in the surrounding area can be regarded as a Poisson bulge related to the observed surface strains. Interpreted in this way, the vertical displacements are consistent with an elastic rebound model.

BIBLIOGRAPHY

- Benioff, H., and Gutenberg, G., 1951, Strain Characteristics of the Earth's Interior; Chapt. 15, The Internal Construction of the Earth, New York: Dover Publications.
- Bomford, G., 1962, Geodesy; Oxford University Press.
- Burford, R. O., 1965, Strain Analysis Across the San Andreas Fault and Coast Ranges of California. Presented at the second symposium, Commission on Recent Crustal Movements, International Assoc. of Geodesy, International Union of Geodesy and Geophysics, Aulanko, Finland, August, 1965.
- Byerly, P., and J. DeNoyer, 1958, Energy in Earthquakes as Computed from Geodetic Observations; Contributions in Geophysics: In Honor of Beno Gutenberg, Pergamon Press, pp. 17-35.
- Eaton, J. P., 1963, Crustal Structure from San Francisco, California, to Eureka, Nevada, from Seismic-refraction Measurements; Jour. Geophys. Res., Vol. 68, pp. 5789-5806.
- Fara, H. D., 1964, A New Catalogue of Earthquake Fault Plane Solutions; Bull. Seism. Soc. Am., Vol. 54, pp. 1491-1517.
- Frank, F. C., 1966, Deduction of Earth Strains from Survey Data; Bull. Seism. Soc. Am., Vol. 56, pp. 35-42.
- Inoue, E., 1960, Land Deformation in Japan; Bull. Geographical Survey Inst., Vol. 6, pp. 73-133.
- Kasahara, K., 1959, Physical Conditions of Earthquake Faults II; Bull. Earthquake Res. Inst., Vol. 37, pp. 39-51.
- Kasahara, K., and A. Sugimura, 1964, Horizontal Secular Deformation of Land Deduced from Retriangulation Data, (1) Land Deformation in Central Japan; Bull. Earthquake Res. Inst., Vol. 42, pp. 479-490.
- Knopoff, L., 1958, Energy Release in Earthquakes; Geophys. Jour., Vol. 1, pp. 44-52.
- Niazi, M., 1964, Partition of Energy in the Focal Region of Earthquakes; Bull. Seism. Soc. Am., Vol. 54, pp. 2175-2183.
- Pope, A. J., Stearn, J. L., and Whitten, C. A., 1966, Surveys for Crustal Movement along the Hayward Fault; Bull. Seism. Soc. Am., Vol. 56, pp. 317-323.

- Press, F., 1965, Displacements, Stains and Tilts at Teleseismic Distances; Jour. Geophys. Res., Vol 70, pp. 2395-2412.
- Romey, C., 1957, The Dixie Valley-Fairview Peak, Nevada, Earthquakes of December 16, 1954: Seismic Waves; Bull. Seism. Soc. Am., Vol. 47, pp. 301-319.
- Savage, J. C., 1965, The Stopping Phase on Seismograms; Bull. Seism. Soc. Am., Vol. 55, pp. 47-58.
- Shawe, D. R., 1965, Strike-Slip Control of Basin-Range Structure Indicated by Historical Faults in Western Nevada; Bull. Seism. Soc. Am., Vol. 76, pp. 1361-1378.
- Slemmons, D. B., 1957, The Dixie Valley-Fairview Peak, Nevada, Earthquakes of December 16, 1954: Geological Effects; Bull. Seism. Soc. Am., Vol. 47, pp. 353-375.
- Terada, T., and N. Miyabe, 1929, Deformation of the Earth's Crust in Kwansai Districts and Its Relation to the Orographic Feature; Bull. Earthquake Res. Inst., Vol. 7, pp. 223-239.
- Thompson, G. A., 1959, Gravity measurements between Hazen and Austin, Nevada: A Study of Basin-Range Structure; Jour. Geophys. Res., Vol. 64, pp. 217-229.
- Thompson, G. A., 1960, Problem of Late Cenozoic Structure of the Basin Ranges; Internat. Geol. Congress, XXI Session, Part XVIII, pp. 62-68.
- Thompson, G. A., 1965, The Rift System of the Western United States; Internat. Upper Mantle Symposium, Ottawa, Geol. Survey of Canada Paper 66-14.
- Tocher, D., 1956, Movement on the Rainbow Mountain Fault; Bull. Seism. Soc. Am., Vol. 46, pp. 10-14.
- Tocher, D., 1958, Earthquake Energy and Ground Breakage; Bull. Seism. Soc. Am., Vol. 48, pp. 147-153.
- Tsuboi, C., 1956, Earthquake Energy, Earthquake Volume, Aftershock Area, and Strength of the Earth's Crust; Jour. of Physics of the Earth, Vol. 4, No. 2, pp. 63-66.
- Westphal, W., and Lange, A., 1966, Local Seismic Monitoring, Final Report, Project PHY-5043, Stanford Research Institute, Menlo Park, California.
- Whitten, C. A., 1957, The Dixie Valley-Fairview Peak, Nevada Earthquakes of December 16, 1954: Geodetic Measurements; Bull. Seism. Soc. Am. Vol. 47, pp. 321-325.

PART VI.

SEISMIC REFRACTION STUDY OF SMITH CREEK VALLEY, NEVADA

by

Alan T. Herring

ABSTRACT

Three reversed seismic refraction profiles were shot in Smith Creek Valley, Nevada, during September, 1966, to determine the depth and structure of the high-velocity basement. This work complements a gravity survey (Cabaniss, 1965) and an aeromagnetic survey (Salehi, 1965) in the same valley.

An interpretation of the seismic data exclusive of the gravity and aeromagnetic information indicates that the basement in both Smith Creek Valley and Dixie Valley (Meister, 1966) is similar in structural complexity. The maximum depth to basement in Smith Creek Valley ranges from 6500 ft. to 8000 ft. as compared to 10,000 ft. in Dixie Valley though a greater depth under the playa may be possible.

TABLE OF CONTENTS

	<u>Page</u>
ABSTRACT.....	ii
TABLE OF CONTENTS.....	iii
LIST OF ILLUSTRATIONS.....	iv
<u>Chapter</u>	
I. INTRODUCTION.....	1
II. ANALYSES OF PROFILES.....	4
A. Profile SC-1.....	4
B. Profile SC-2.....	6
C. Profile SC-3.....	8
III. SOURCES OF ERROR.....	10
IV. CONCLUSIONS.....	11
BIBLIOGRAPHY.....	12

LIST OF ILLUSTRATIONS

FIGURE	TITLE	PAGE
1.	Index Map	3
2.	Time Distance Curve and Cross Section, Profile SC-1	5
3.	Time Distance Curve and Cross Section, Profile SC-2	7
4.	Time Distance Curve and Cross Section, Profile SC-3	9

I. INTRODUCTION

In September of 1966, three reversed seismic refraction profiles were shot in Smith Creek Valley, Nevada, to determine the depth of the high-velocity basement. These profiles complemented a gravity survey by Cabaniss, 1965, and an aeromagnetic survey by Salehi, 1965. (The location of the valley can be seen in Fig. 1, Part I. The location of the three profiles is evident from Fig. 1.)

The first refraction line was located parallel to the probable structural trend; the other two lines were perpendicular to probable structure. A basement velocity of 16,500 ft/sec was reversed on two of the lines; the high apparent velocity observed on the third line is also believed to be from the basement refractor even though this line was not reversed. Basement depths relative to a 6000 foot datum approximating the altitude of the valley floor range from about 1000 feet to 8000 feet.

Surface charges were used as an energy source for all three lines. The charges were set up in a fashion suggested by Buffet and Layat (1960); twenty pound charges of Nitramon WW were placed on the surface fifty feet apart in square or rectangular patterns, the long axis of the rectangle always being parallel to the direction of the profile. When a multiple charge shot was detonated, all the charges on the side of the rectangular pattern farthest from the geophone line were detonated by Primacord which was tied at one end to cap-primed charges; the other end was inserted into the charges nearest the spread. Primacord inserted into a Nitramon WW booster was satisfactory for detonating the charges, so that caps were necessary only for the initial charges of a given shot. When the distance between charges was decreased to 30 feet, no change in the quality of record obtained was noted, although Buffet and Layat suggested a spacing of about 60 feet.

Detonating charges in this manner proved to be satisfactory both on the alluvial fan and the playa surface. Although no shots were fired in drilled holes general experience indicates that surface charges would

compare poorly in terms of record quality to an equal charge placed below the water table. A slightly better record can be obtained using a pattern of twenty pound charges suspended eight feet above the surface rather than an equal number of twenty pound charges resting on the surface. However, the primary advantage of surface charges over suspended charges is the reduction in set up time without significant loss in record quality.

The seismic equipment used for this survey was identical to that used in the 1965 survey of Dixie Valley. The method of transmitting the shot break is described in Part II.

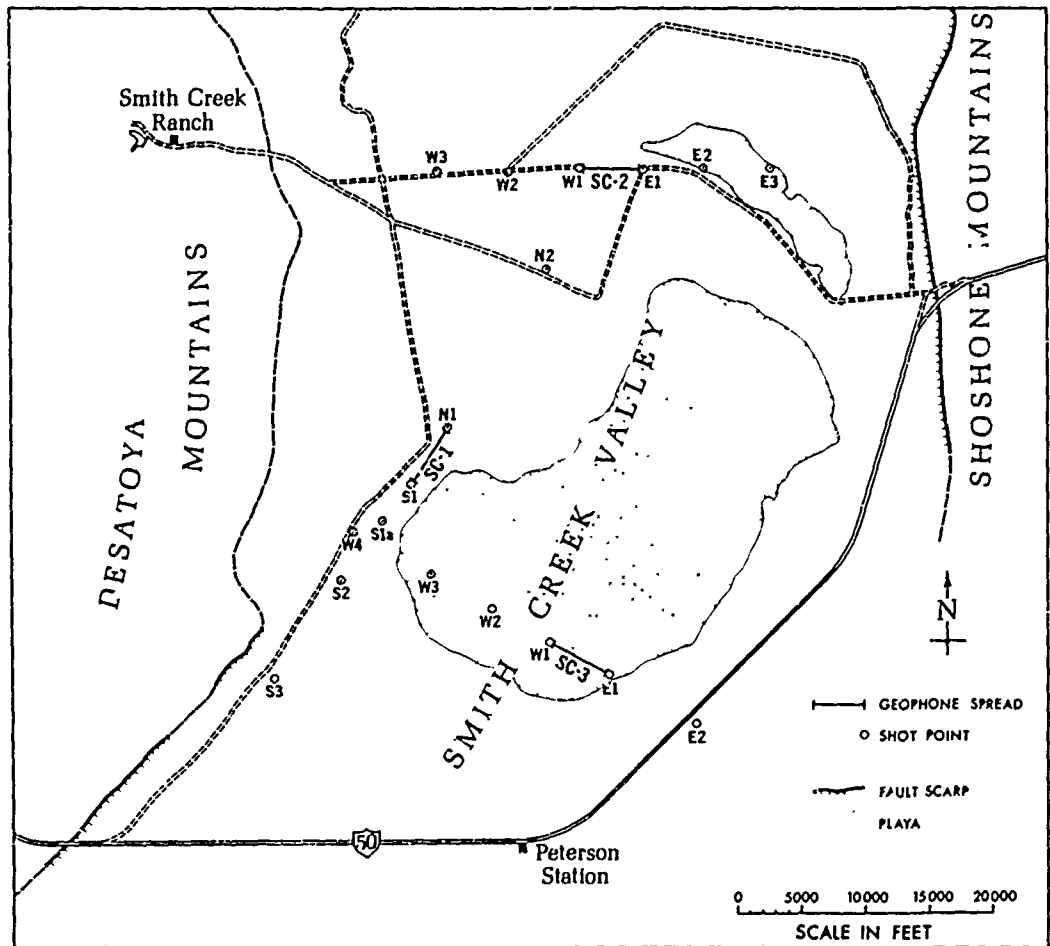


Figure 1. Index Map.

II. ANALYSES OF PROFILES

A. Profile SC-1

Contrary to expectation, Profile SC-1 proved to be structurally complicated, and the use of a simple intercept time method of interpretation is not valid. The delay time method (Nettleton, 1940) was used instead, and dips were determined using a method outlined by Soske (unpublished notes).

The structure in the 10,200 ft/sec material is suggested (Fig. 2) by the time-distance curve of S2. Similar intercept times at S1A and S1 suggest that the structure is channel-like.

As it is unreasonable to assume that the delay time at any shot point is equal to that at the geophones the delay time at some shot point or geophone must be assumed. The configuration shown in Fig. 2 is greatly constrained by the small intercept time observed at S3. Shot point S3 is about 3000 feet from a fault scarp at the base of the Desatoya Mountains (Fig. 1). The fault study in Part II of this report suggests a depth of 1000 feet to basement from the scarp on the west side of the valley. Note that the other shot points and the geophone line are much farther from the scarp.

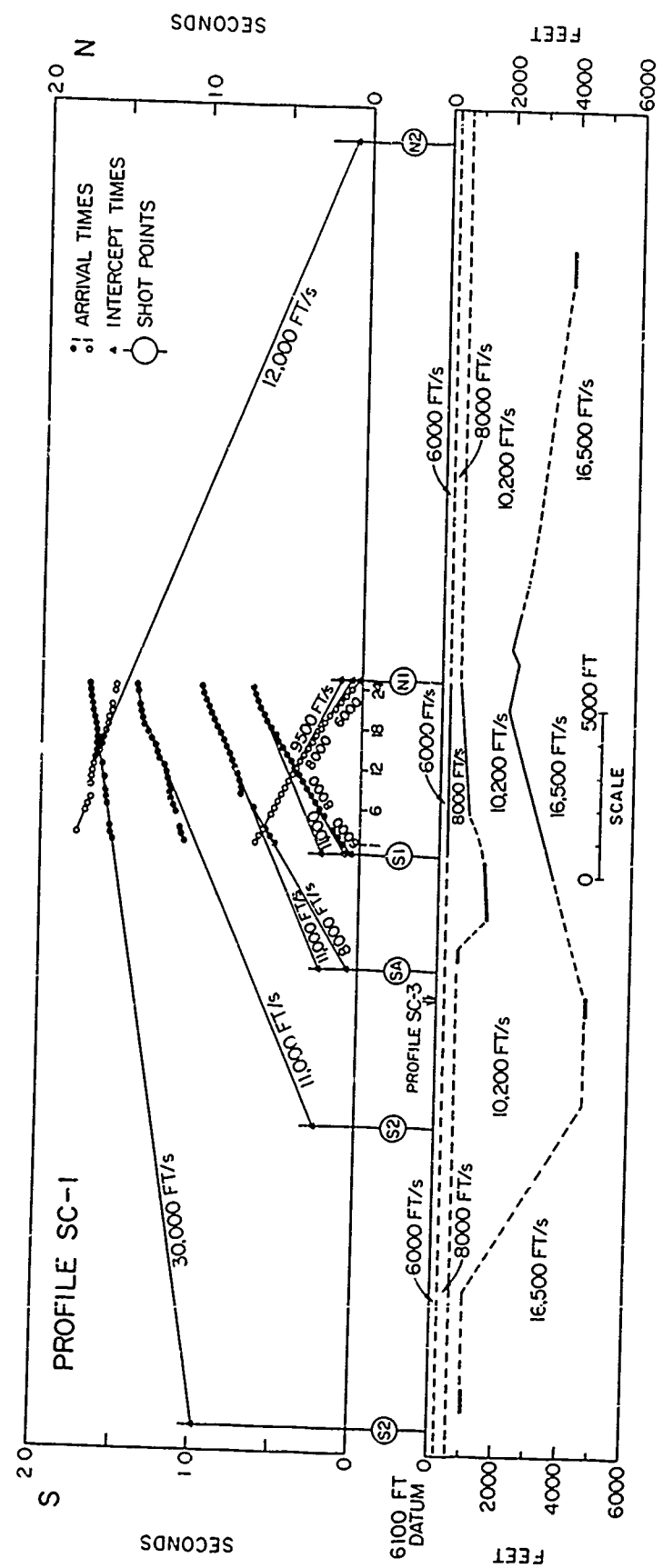


Figure 2. Time Distance Curve and Cross Section, Profile SC-1.

B. Profile SC-2

The record of shot W2 shows a velocity of 8200 ft/sec on the first part of the record, Fig. 3. There are basically three explanations of this velocity:

1. The refractor has a true velocity of 8200 ft/sec.
2. 8200 ft/sec is an up-dip apparent velocity from refractor with a down-dip apparent velocity of 7600 ft/sec, as observed on the first part of the record for shot E2.
3. 8200 ft/sec is a down-dip apparent velocity on a 12,000 ft/sec refractor. The dip of the refractor is less on the east side of the spread and yields an 11,000 ft/sec apparent velocity. The 7600 ft/sec velocity comes from a separate layer.

The first and second possibilities both place higher speed material (either 8200 ft/sec in the first case or 7900 ft/sec in the second case) so close to the surface as to be inconsistent with the records of shots W1 and E1. That is, if such material is indeed close to the surface, higher speed arrivals should have been observed on the records of W1 and E1. The third interpretation is both physically and geologically plausible.

The depth to basement was calculated using delay times. It is possible to change the distribution of total delay time to increase or decrease the depth to a refractor under the geophones and thereby decrease or increase it under the relevant shot points. Also, the 12,000 ft/sec velocity assumed for the entire thickness of material between the observed 12,000 ft/sec refractor and the basement refractor may be high. If it is assumed that the 12,000 ft/sec refractor is thin enough to be ignored in a calculation of depth to basement and that the average velocity between the 12,000 ft/sec refractor and the basement is 10,000 ft/sec, then the depth to basement would be decreased. The top of the shading indicates the depth to basement obtained using a 10,000 ft/sec average velocity instead of 12,000 ft/sec.

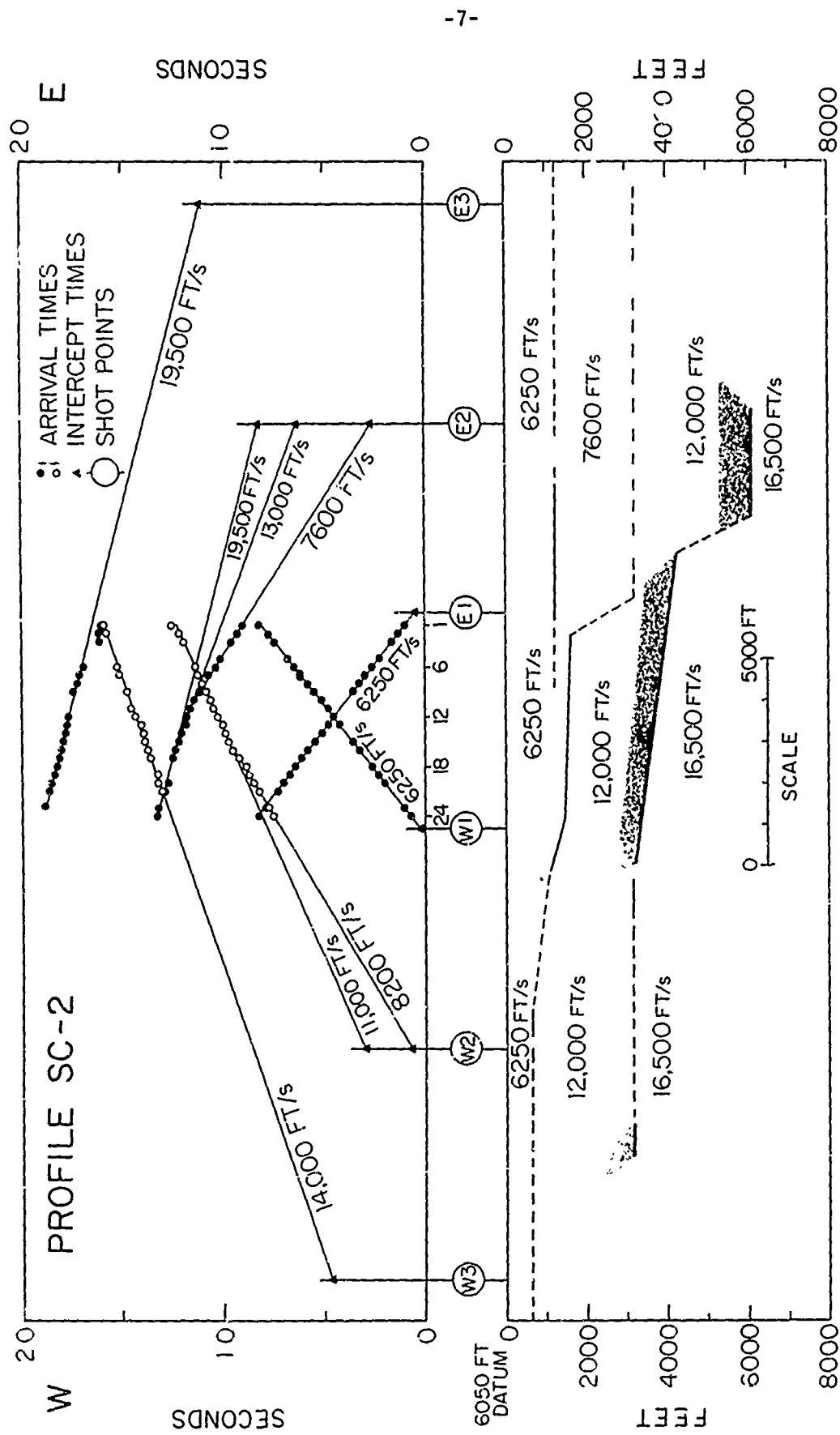


Figure 3. Time Distance Curve and Cross Section,
Profile SC-2.

C. Profile SC-3

A basement velocity of 16,500 ft/sec was observed on the record of shot point W4. It was not reversed. The interpretation as shown in Fig. 4 assumes that the observed velocity of 16,500 ft/sec is a true velocity. It is further assumed that the delay time to basement for shot point W4 is the same as that for shot point S2 of profile SC-1. The heavy line at the bottom of the shading is the position of the basement refractor assuming all of the intermediate material has a velocity of 12,000 ft/sec. The top of the shading indicates the depth to basement assuming an average intermediate velocity of 10,000 ft/sec.

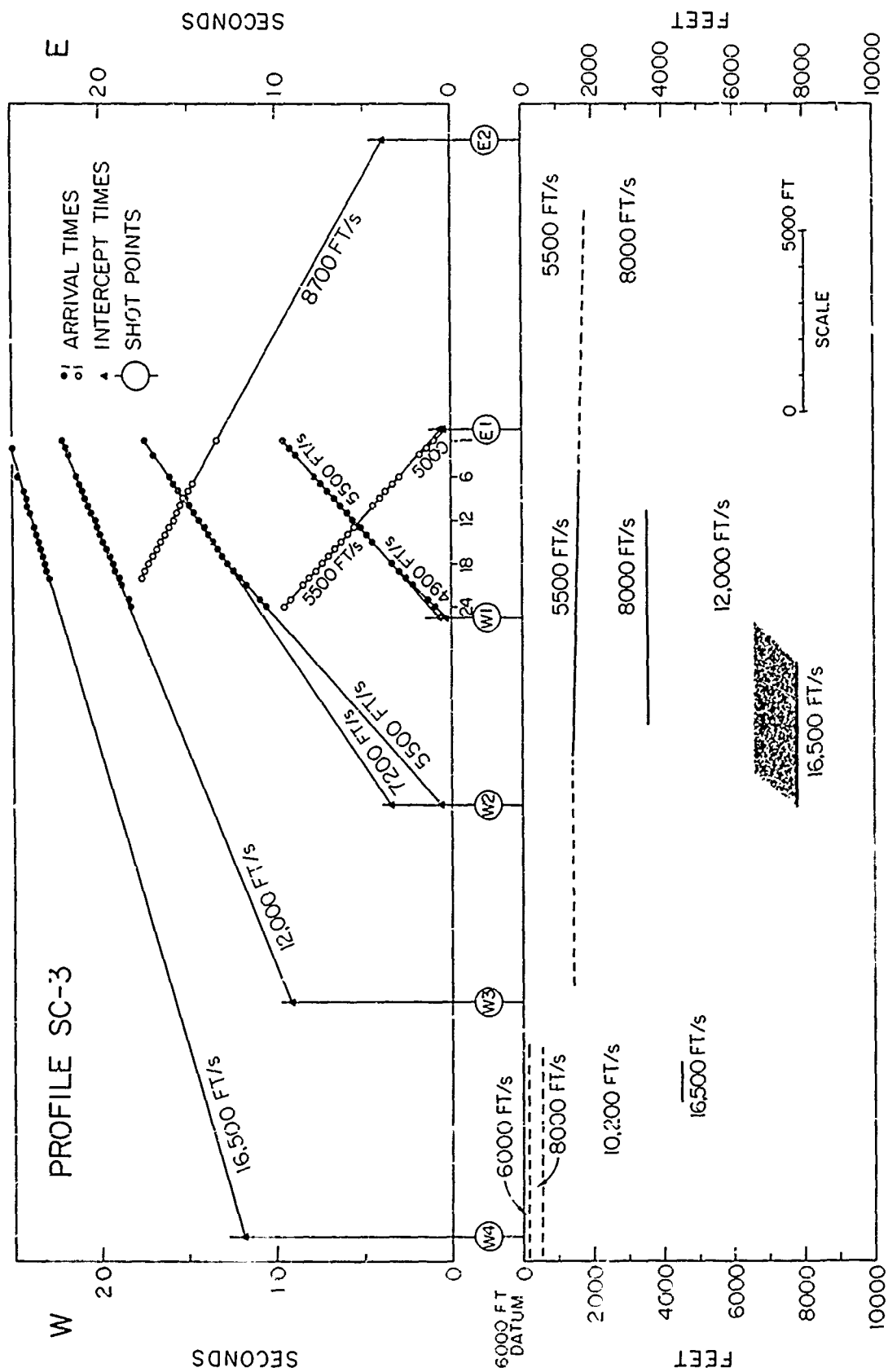


Figure 4. Time Distance Curve and Cross Section, Profile SC-3.

III. SOURCES OF ERROR

Distances on the playa were measured using a truck odometer. It was calibrated over a known distance with a precision better than ± 0.02 miles or about 100 feet. Other distances were scaled from air photos. For profile SC-2 it was possible to compare odometer and air photo distances. The two methods never disagreed by more than two percent.

All of the shots, with the exception of shots W3 of profile SC-2, were within two degrees of being on line. W3 was about five degrees south of profiles SC-2 (measured from the recording truck). Differences in shot point elevations were measured with an altimeter to within five feet.

Shot break times have a probable accuracy of 2 milliseconds. First breaks are accurately picked to within 2 to 5 milliseconds depending on the quality of the break.

The largest source of error in this survey is inherent in the refraction method. The change in velocity with depth is inferred from limited data. Possible depth errors due to poor velocity assumptions can be great, as is illustrated in Figs. 3 and 4. No weathering velocities were obtained for this survey. A weathering velocity of 2500 ft/sec was assumed for the thin, low speed layer which overlies the thicker subweathering layer observed to give velocities of 5500 ft/sec to 6250 ft/sec. Since the weathered layer is obviously quite thin, no important error is expected as a result of using an assumed velocity of 2500 ft/sec.

IV. CONCLUSIONS

The sediments and volcanics overlying the basement in Smith Creek Valley are 6500 to 8000 feet thick near the center of the valley. Much more work would be required to completely describe the subsurface basement in Smith Creek Valley, but it appears to be similar to Dixie Valley in the following ways:

1. Maximum depth to basement: Dixie Valley - 10,500 feet; Smith Creek Valley - 6500 to 8000 feet. More work might reveal deeper basement in part of Smith Creek Valley beneath the playa.
2. An intermediate layer with velocity 10,000 ft/sec to 12,000 ft/sec is present in both valleys.
3. Both valleys have a structurally complex basement.

BIBLIOGRAPHY

- Ruffet, A., and Layat, C. H., 1960, Nouvel Aspect de la Sismique Refraction au Sahara: Tirs non Enterres; Geophysical Prospecting, Vol. 8, pp. 47-67.
- Caboniss, G. H., 1965, Unpublished Gravity Survey of Smith Creek Valley, Nevada.
- Meister, L. J., 1967, Seismic Refraction Study of Dixie Valley, Nevada; A. F. Cambridge Research Labs. Final Scient. Rpt. Part I, AFCRL-66-848.
- Nettleton, L. L., 1940, Geophysical Prospecting for Oil; New York, McGraw-Hill, 444 pp.
- Poulter, T. C., 1950, The Poulter Seismic Method of Geophysical Exploration; Geophysics, Vol. 15, pp. 181-207.
- Salehi, A., 1967, Aeromagnetic Survey of Smith Creek Valley, Nevada; A. F. Cambridge Research Labs. Final Scient. Rpt., Part VII, AFCRL-66-848.
- Soske, J. L., Unpublished notes on seismic refraction.

PART VII.

AEROMAGNETIC SURVEY OF SMITH CREEK VALLEY, NEVADA

by

Iraj A. Salehi

ABSTRACT

An airborne magnetometer survey was conducted in Smith Creek Valley, Nevada, in the summer of 1965. The survey strongly indicated a rock body--perhaps a volcanic plug covered by the valley fill--with reverse remanent magnetization. It also indicated the existence of several blocks, in the basement, with normal magnetization.

The maximum depth to the basement was found to be approximately 3700 ft.

No definite proof of major faulting could be obtained but indications of a major geological boundary, lithological if not structural, were observed along the central part of the valley and parallel to the general structural trend.

ACKNOWLEDGEMENTS

The writer wishes to express his gratitude to the late Professor J. L. Soske and Professor G. A. Thompson for their assistance, counsel, and advice during the completion of the present work. The writer is also indebted to Mr. Sheldon Breiner for providing the observatory record of the geomagnetic field during the survey and for his assistance in acquiring an extra magnetometer and numerous spare parts.

TABLE OF CONTENTS

	<u>Page</u>
ABSTRACT	ii
ACKNOWLEDGEMENTS	iii
TABLE OF CONTENTS	iv
LIST OF ILLUSTRATIONS	v
<u>Chapter</u>	
I. INTRODUCTION	1
II. GENERAL INFORMATION	2
III. COLLECTION OF DATA	4
IV. DATA CORRECTIONS AND PREPARATION OF THE TOTAL INTENSITY MAP	6
V. RESIDUAL AND SECOND VERTICAL DERIVATIVE MAPS	8
VI. INTERPRETATIONS	11
VII. DEPTH ESTIMATIONS	13
VIII. ANALYTICAL STUDIES AND MODEL COMPUTATIONS	14
IX. CONCLUSIONS AND RECOMMENDATIONS	19
BIBLIOGRAPHY	20

LIST OF ILLUSTRATIONS

FIGURE	TITLE	PAGE
1.	Smith Creek Valley location map with flight line grid.	3
2.	Total magnetic intensity map of Smith Creek Valley, Nevada.	7
3.	Residual map of Figure 2.	9
4.	Second derivative map of Figure 2.	10
5.	Total magnetic intensity profile with interpretation along line AA' in Figure 2.	15
6.	Total magnetic intensity profile with interpretation along line BB' in Figure 2.	15
7.	Total magnetic intensity profile with interpretation along line CC' in Figure 2.	16
8.	Total magnetic intensity profile with interpretation along line DD' in Figure 2.	16
9.	Total magnetic intensity profile with interpretation along line EE' in Figure 2.	17
10.	Total magnetic intensity profile with interpretation along line FF' in Figure 2.	17
11.	Total magnetic intensity profile with interpretation along line HH' in Figure 2.	18

I. INTRODUCTION

For the purpose of study of the Basin and Range structures the Department of Geophysics at Stanford University started a series of magnetic, gravity and seismic surveys in Dixie Valley, Nevada, in the summer of 1964. Later it was found necessary to extend these investigations to some of the other localities in this general area. As the first part of the latter phase an airborne magnetometer survey was conducted in Smith Creek Valley in the summer of 1965.

The main objective of this survey was to obtain a first estimate of the basement depth in the valley and to investigate the existence and attitude of possible faults below the valley fill.

A ground survey of the area was also made to investigate the existence of some reversely magnetized rock units as indicated from the interpretation and analysis of the data. A few oriented samples were collected and the direction of polarization was examined.

II. GENERAL INFORMATION

Smith Creek Valley is located between $39^{\circ} 00'$ and $39^{\circ} 00'$ North latitude and $117^{\circ} 25'$ and $117^{\circ} 26'$ West longitude in the Basin and Range province of Nevada. It is separated from Dixie Valley by Desatoya Mountain, Edwards Creek Valley and Clan Alpine Mountain. The area is accessible by U. S. Highway 50 (Fig. 1).

Smith Creek Valley is a rather narrow, almost north-south trending valley bounded by the Shoshone Mountains on the east and Desatoya Mountain on the west. Similar to many other valleys in this physiographic province, the boundaries between the valley and the confining ranges are steeply dipping normal faults.

The north and south extremes of the valley terminate gradually into elevated hills of much lower altitude than the ranges.

To the knowledge of the writer, no information on the geology of Smith Creek Valley has been published and no maps are available. On the basis of a very short field trip to the area and some personal discussions* it appears that, except for the south central parts of the Shoshone which are composed of some Mesozoic rocks, the ranges are mainly Tertiary volcanic material such as tuffaceous rhyolitic and felsic rocks and occasional mafic flows. The valley fill is assumed to be composed mostly of lake and stream deposits.

*Dr. Bonham, University of Nevada

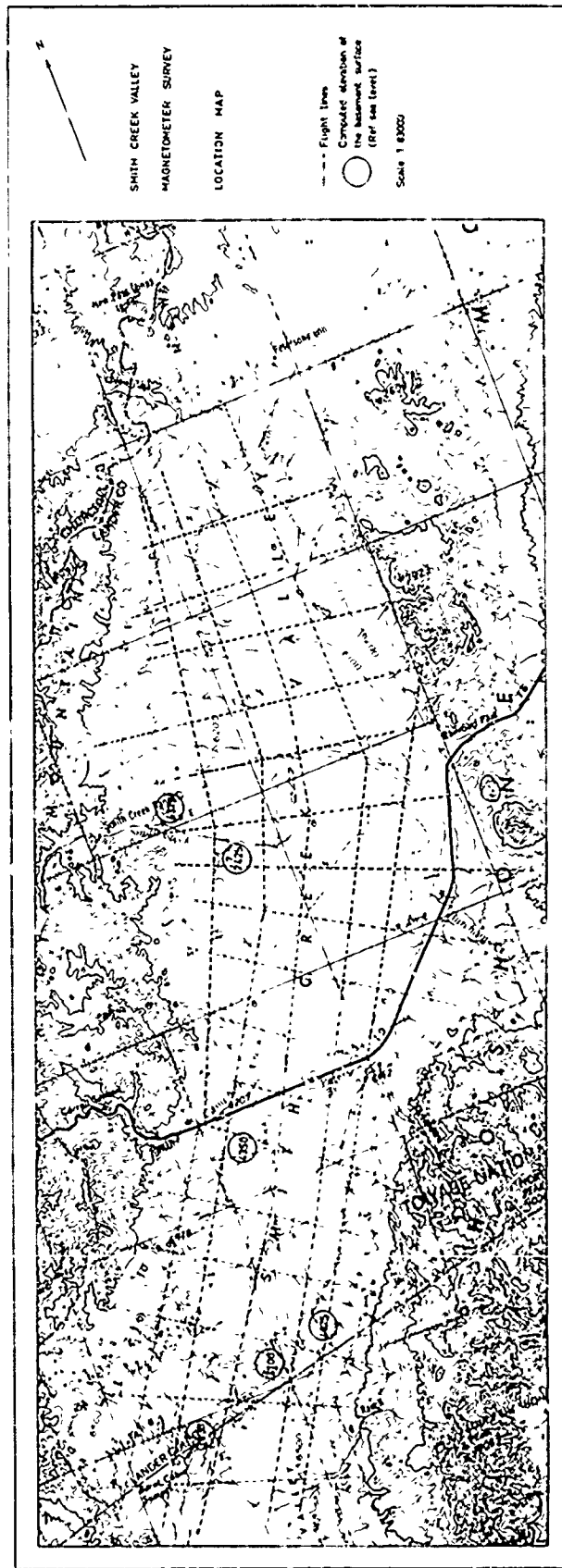


Figure 1. Smith Creek Valley location map with flight line grid. Computed basement depths from sea level are circled.

III. COLLECTION OF DATA

Flight elevation was maintained at 7500 ft above sea level throughout the survey. It was necessary to reset the altimeter every hour or so in order to maintain a constant flight elevation. Flight speed varied slightly from one line to another due to the wind speed and direction. Nevertheless, an air speed of approximately 75 miles per hour was maintained.

A Varian M 49 proton precession magnetometer was used. The sensing head was towed at the end of a 120 ft long nylon tow cord to eliminate the magnetic effect of the plane; and to prevent roll and spin of the head a stabilizer tail was attached to it. Considering the inclination of the towing cord during the flight, the effective flight elevation was approximately 75 ft below the plane altitude, i.e., 7425 ft with respect to sea level.

The addition of 120 ft of transmission cable to the original cable between the sensing head and the main instrument caused a voltage drop. In order to have a strong polarizing voltage an external battery was put in series between the instrument's internal battery and the sensing head through the polarizing circuit.

Although the M 49 magnetometer is equipped with an automatic polarizing device, this device was not used, because the noise of the plane made it difficult to hear the precession signal. In the event that some background noise was present on the reading dial, as was the case most of the time, the precession signal could not be distinguished from the instrument noise and consequently some readings would have been missed. Therefore the instrument was polarized manually every ten seconds.

The survey was carried out in the following manner: the projected flight lines were marked on the program map and the points where the lines would cross road intersections or other landmarks were numbered as checkpoints. Using the aerial photographs and the topographic sheets, the flight lines were so arranged that each line would pass through as many landmarks as possible. The pilot and the recorder each had a copy of the program map during the flights.

When the flight elevation and orientation were achieved the pilot would signal the operator to start and he would immediately start a stopwatch and make the first reading. From then on he would make a reading every ten seconds. When the plane reached a checkpoint the pilot would read out the checkpoint number and the operator would give the time. The recorder took note of the time and checkpoint number. Since the spacing between the checkpoints was reasonably short this arrangement removed the effect of the air speed variations considerably.

IV. DATA CORRECTIONS AND PREPARATION OF THE TOTAL INTENSITY MAP

The values of the diurnal variations of the earth's magnetic field during the survey hours were obtained from the continuous record made by Varian Associates at Menlo Park, California. It was assumed that the difference of these variations between Menlo Park and Smith Creek Valley was small enough to be neglected. The magnitude of the diurnal variations during the survey hours was 30 Gammas at the most and the average anomaly encountered in the survey was of the order of 400 Gammas.

After correction for the diurnals the data were plotted on a map in the following order: since the time interval for flying from one checkpoint to the next and the number of readings recorded between these two points were known, the data points were linearly distributed between the checkpoints assuming a constant air speed over the interval. This scheme removed the effect of the speed variations. Nevertheless, the absolute position of the data points is perhaps accurate within 250 ft, this inaccuracy being due to probable navigational uncertainties. However, the maximum mistie at the intersection of the flight lines did not exceed 15 Gammas and the mistie, where it existed, was removed by giving more weight to the line over which the checkpoints were closer together as compared to the intersecting line.

The direction and magnitude of the regional gradient of the normal geomagnetic field were computed from the Total Intensity Chart of the United States (1955). This gradient was found to be 2 1/2 Gammas per mile in N 25 E direction.

The regional gradient was removed from the map by taking a N 65 W reference line at the left edge of the map and subtracting the regionals computed by the mentioned 2 1/2 Gamma gradient from the original data.

The total intensity map (Fig. 2) was then prepared by contouring the corrected data at 50 Gamma intervals, taking the reference level as 53000 Gammas. This reference level is the value for the normal geomagnetic field at the survey location as given by the Total Intensity Chart.

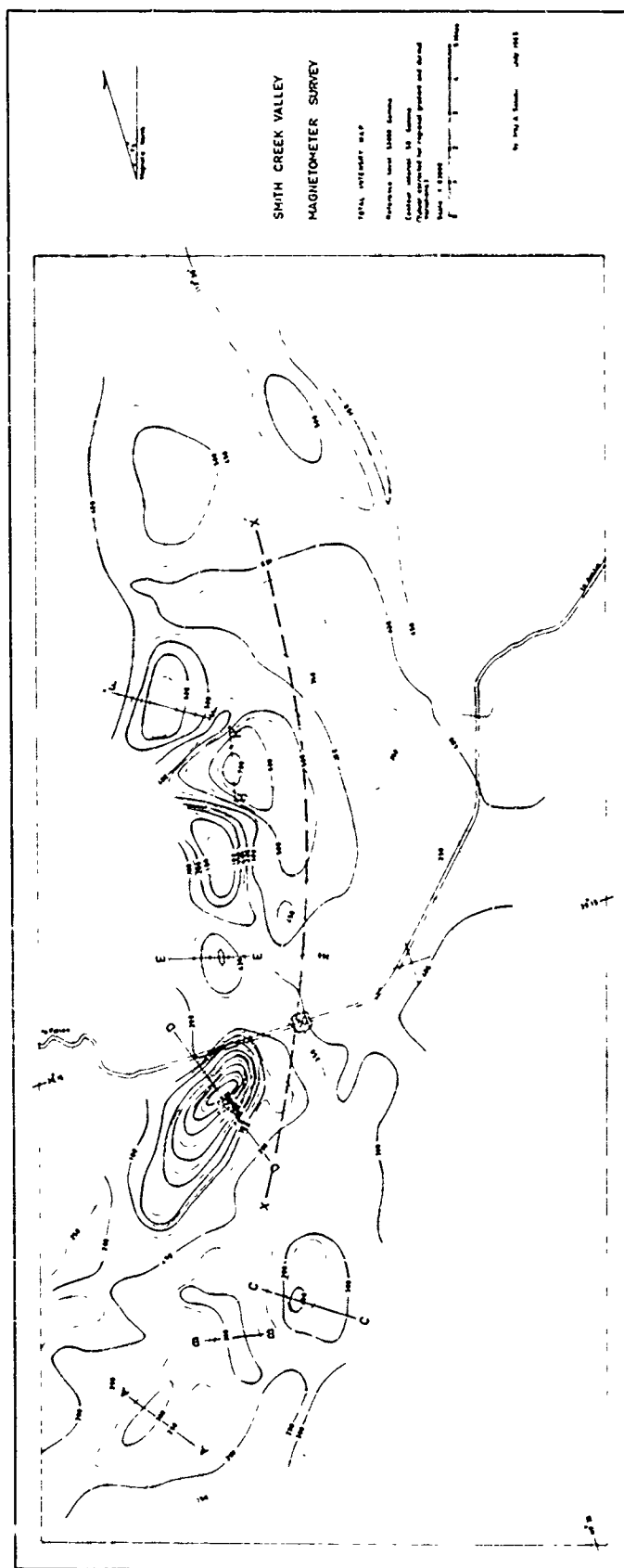


Figure 2. Total magnetic intensity map of Smith Creek Valley, Nevada.

V. RESIDUAL AND SECOND VERTICAL DERIVATIVE MAPS

An Algol computer program was written for computing the residual and second vertical derivative values using the nine-point scheme explained by Henderson and Zeitz (1949).

Since the main interest in the survey was study of the larger magnetic features presumably related to the basement, a grid interval of one mile was chosen so that the effect of the smaller near-surface sources would be attenuated.

Figures 3 and 4 are the residual and second derivative maps.

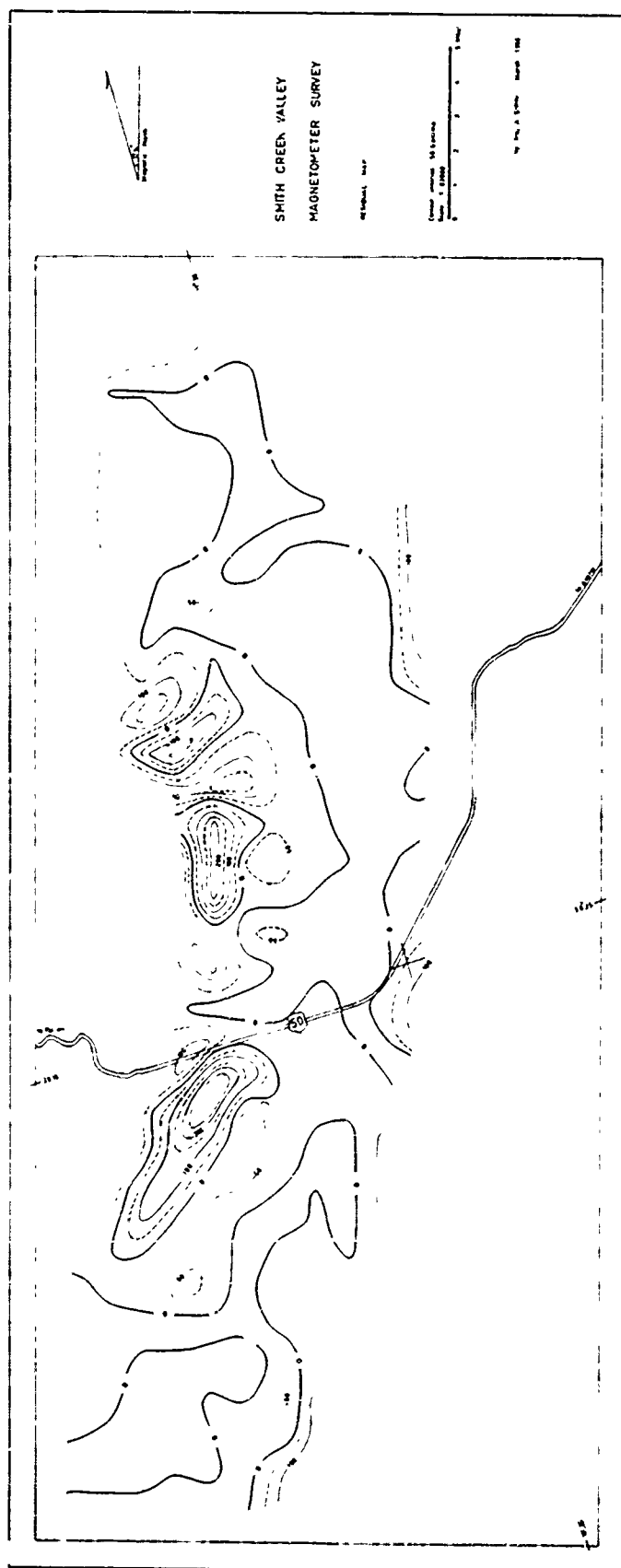


Figure 3. Residual map of Figure 2.

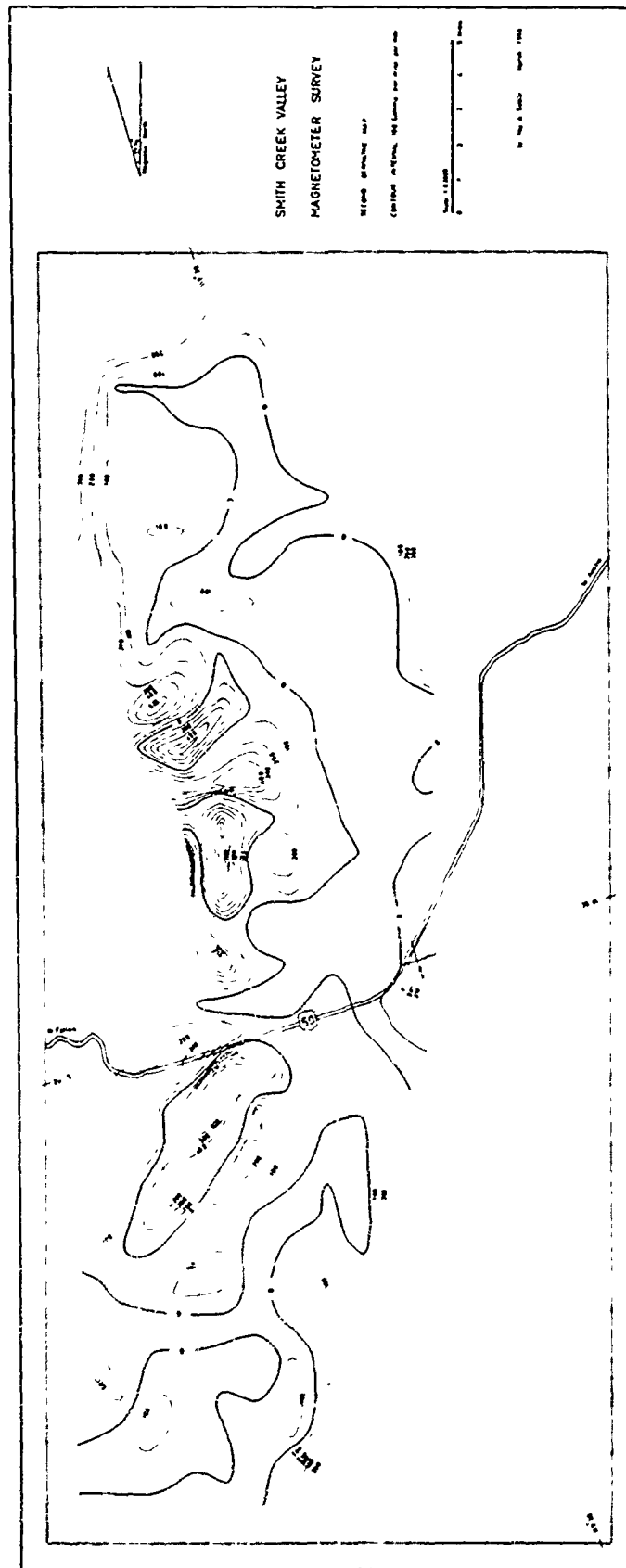


Figure 4. Second derivative map of Figure 2.

VI. INTERPRETATIONS

The most pronounced feature observed on the total intensity, residual, and the second derivative maps, is a closed negative anomaly south of Highway 50. The lowest observed field value is 53,000 Gammas; the observed field even over the non-magnetic rock bodies is not expected to be lower than 53,000 Gammas. One possibility for having this kind of closed low is the existence of a rock body with reverse remanent magnetization. Of course, should there exist a very strong positive anomaly associated with the low, it would be interpreted as part of the anomaly due to a rather low-dipping magnetic body. Since no such feature exists, it can be interpreted as due to a block with reverse remanent magnetization. Unfortunately, there are no exposures corresponding to this negative anomaly. The samples of volcanic rocks collected from the neighboring areas did not show reverse remanent magnetization. This implies that the suggested reversal is restricted to a confined body, perhaps a volcanic plug.

On examination of the central parts of the maps a clear character difference between the western and eastern halves of the contoured area can readily be seen. Actually, a hypothetical line, XX', (Fig. 2) can be drawn to separate these two zones. On the west side of XX' several isolated anomalies and rather high magnetic gradients characterize the zone while to the east of this line the field variations are very gentle. Based on this observation one could consider XX' as marking a lithological boundary across which the gross magnetic properties of the adjacent rock units change, i.e., the block west of the line consists of an assortment of different blocks with sufficient magnetization contrasts to produce the isolated anomalies while the block east of the line is magnetically homogeneous.

A second interpretation would be to assume that the line represents the approximate position of a fault with the downthrown block to the east. The throw of this fault should be large enough that the anomalies from

the downthrown block are not distinguished due to their great depth. This interpretation, however, faces the difficulty that one would expect to observe a high gradient parallel to the line if it represents a fault. Alternatively, one can speculate that the anomalies west of the line are perhaps related to several volcanic plugs aligned along a fracture zone parallel to the main boundary faults in the valley and that the line represents the boundary of this fracture zone.

A third and more conservative interpretation is to ignore the line altogether and assume that the anomalies in the western part of the mapped area are due to some confined rock bodies with marked magnetization contrasts--and it happens that no such bodies are present in the eastern part. A somewhat subjective view of the writer is that this third possibility is improbable.

The total intensity map also displays three small closed highs in the southern portion of the map and two very gentle highs in the northern parts. These features are almost completely absent on the residual and second derivative maps. Now, considering the fact that the grid spacing for making the residual and second derivative maps was one mile, this would result in the attenuation of anomalies from sources somewhat smaller than the grid size. It can be concluded that these anomalies are related to smaller near-surface rock bodies.

VII. DEPTH ESTIMATIONS

Estimation of depth of burial for the anomalies was made where possible. The estimated values are given on the location map (Fig. 1) and are with respect to sea level.

The depth estimates were made either by the so-called half-width formula or by the scheme suggested by Peters (1949). In this scheme a profile is plotted across the anomaly and a tangent is drawn to the anomaly curve at the point of inflection. A second line with slope half the slope of the tangent is then constructed. Two tangents are drawn to the anomaly curve parallel to the second line. The horizontal distance between these two points of tangencies is related to depth by a constant multiplying factor C . The value of C ranges between 1.2 and 2.0 depending on the width-to-depth ratio. An intermediate value of 1.6 was selected for depth estimations. Depth estimates were all modified by model computations.

VIII. ANALYTICAL STUDIES AND MODEL COMPUTATIONS

The values for "effective magnetic susceptibility contrast," K , were computed from the total intensity map using the method described by Green (1960) and Reford (1964). The formula for susceptibility contrast given by Green and modified by Reford is:

$$\Delta K = \frac{\Delta T}{2\eta \cdot T \cdot \sin^2 I}$$

where ΔK is the effective susceptibility contrast. ΔT is the maximum anomaly, I is the inclination, and T is the effective inducing field. This formula is applicable when the remanent and induced magnetizations are in the same direction.

After evaluation of the effective magnetic susceptibility contrast model computations were carried out for assumed two-dimensional bodies. The formulas used for these computations were either the standard Z 2 KZ or the formula given by Hays and Scharon (1963). A computer program in Algol was written for this latter formula.

Figures 5 to 11 represent the computed models. The solid lines are the plot of the observed values and the small crosses represent the computed points. The ΔK is the effective magnetic susceptibility contrast and in the case of profile DD' it is a fictitious negative value.

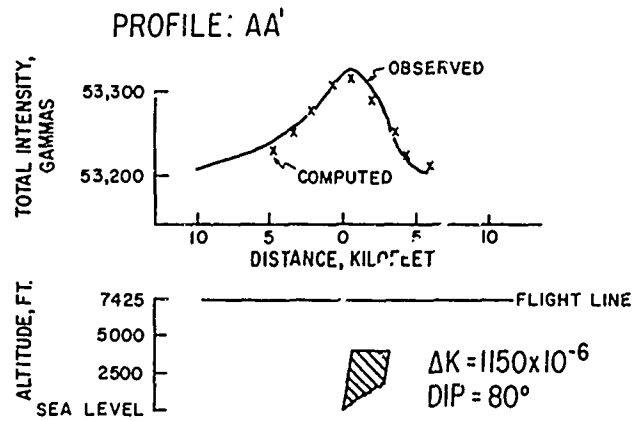


Figure 5. Total magnetic intensity profile with interpretation along line AA' in Figure 2.

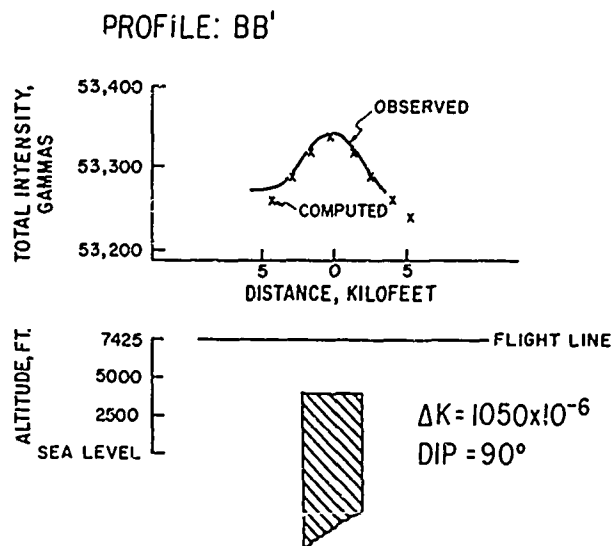


Figure 6. Total magnetic intensity profile with interpretation along line BB' in Figure 2.

PROFILE: CC'

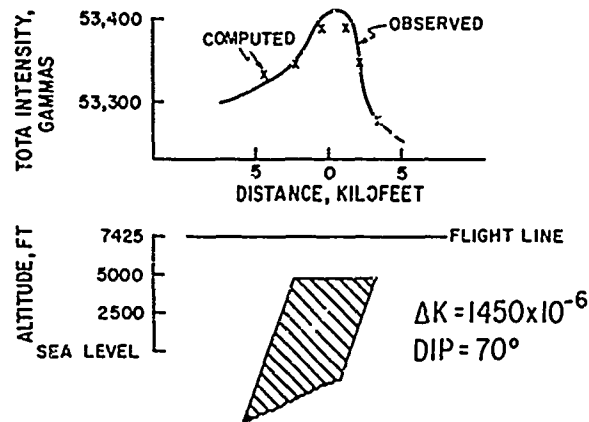


Figure 7. Total magnetic intensity profile with interpretation along line CC' in Figure 2.

PROFILE: DD'

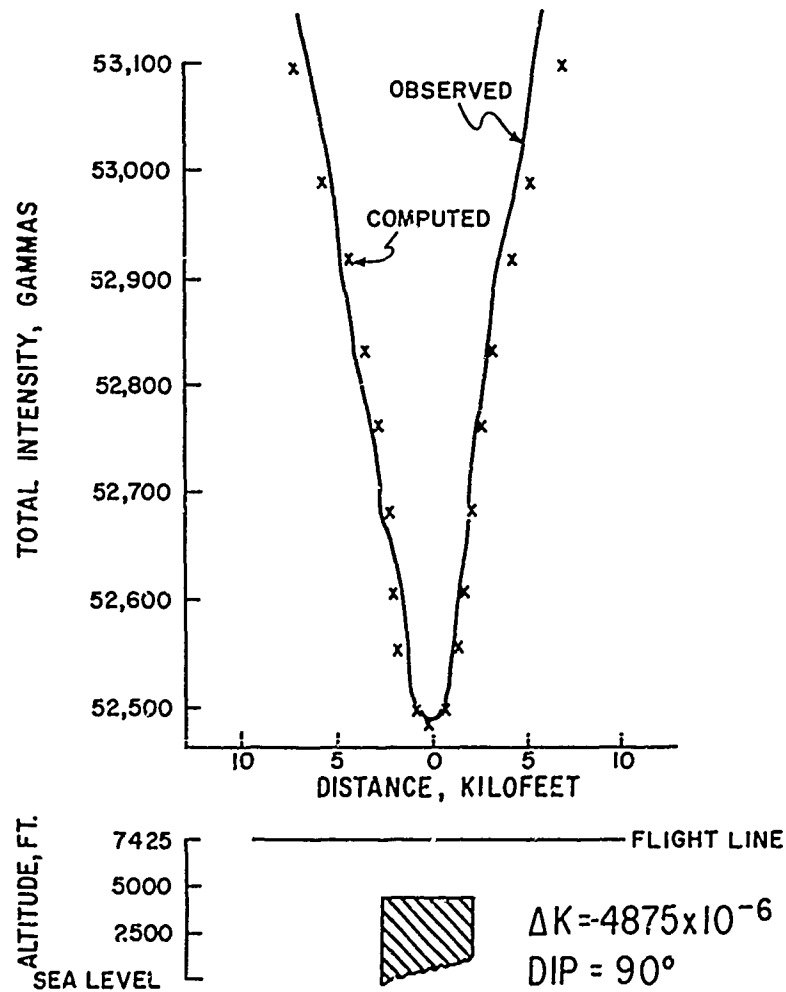


Figure 8. Total magnetic intensity profile with interpretation along line DD' in Figure 2.

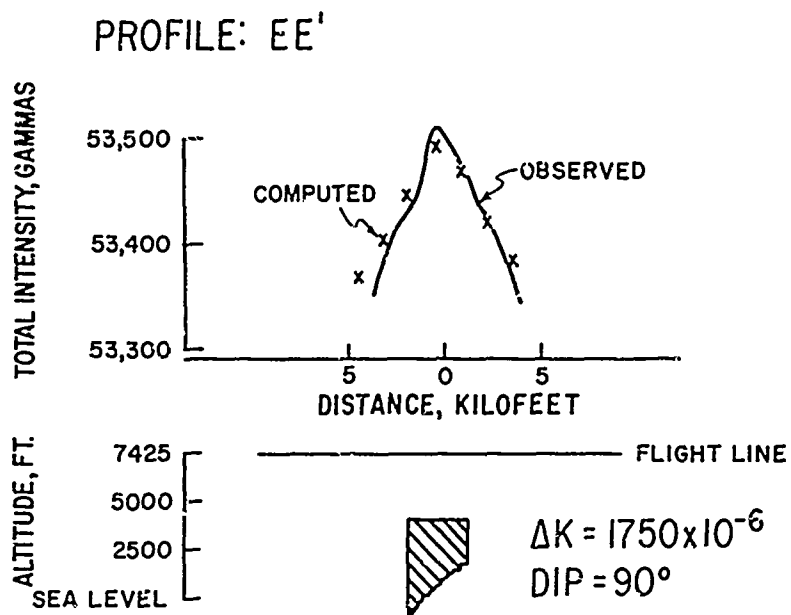


Figure 9. Total magnetic intensity profile with interpretation along line EE' in Figure 2.

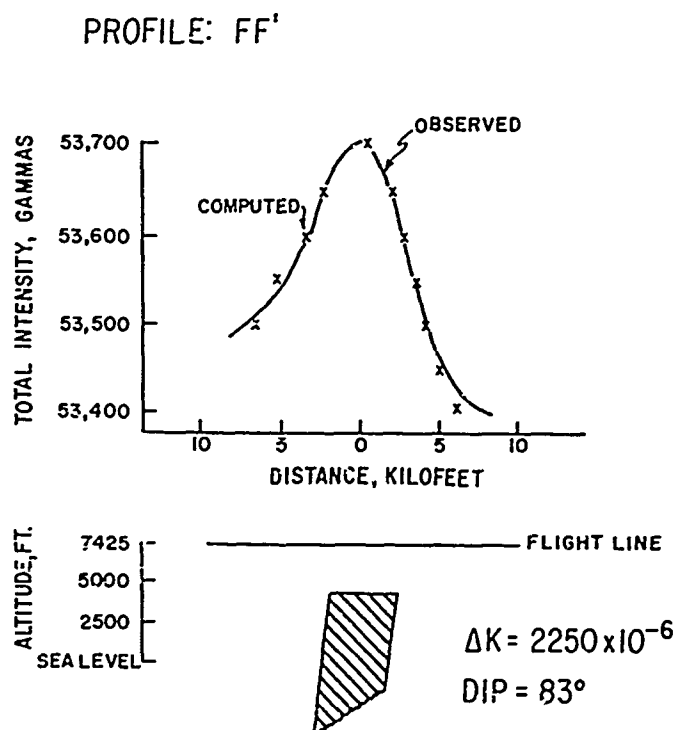


Figure 10. Total magnetic intensity profile with interpretation along line FF' in Figure 2.

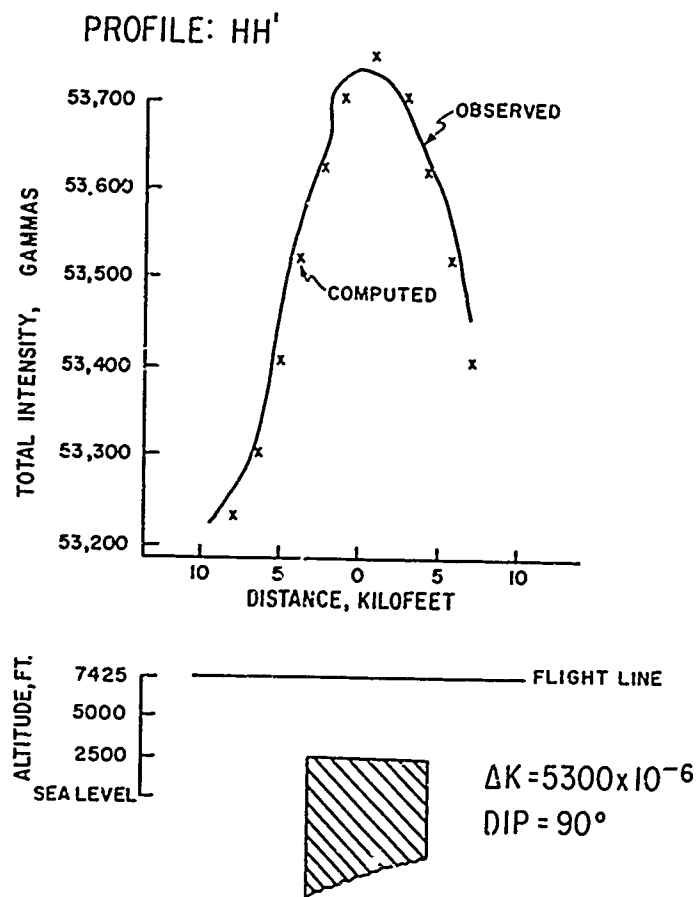


Figure 11. Total magnetic intensity profile with interpretation along line HH' in Figure 2.

IX. CONCLUSIONS AND RECOMMENDATIONS

From the interpretations of the magnetic data the following conclusions may be drawn:

- a. The existence of a rock body with reverse remanent magnetization, perhaps a volcanic plug, is strongly indicated.
- b. The maximum depth of the basement is about 3700 ft below the fill and the average depth to the basement is roughly 2500 ft.
- c. It is probable that a normal fault parallel to the general trend of the valley extends along the central parts of the surveyed area.

The following are recommended for future studies:

- a. A reconnaissance geological survey for at least the western parts of the Shoshone Mountains and the eastern parts of Desatoya Mountain for correlation purposes across the valley.
- b. A refraction seismograph survey along at least three longitudinal profiles along the valley and five or six transverse profiles across the valley for obtaining some definite information about the possible faults.

BIBLIOGRAPHY

- Green, R., 1960, Remanent Magnetization and the Interpretation of Magnetic Anomalies; Geophysical Prospecting, Vol. 8, pp. 83-110.
- Hays, W. W., and Scharon, L., 1963, An Example of the Influences of Remanent Magnetization on Magnetic Intensity Measurements; Geophysics, Vol. 28, pp. 1037-1048.
- Henderson, R. G., and Zeitz, I., 1949, Computation of Second Vertical Derivatives of Magnetic Field; Geophysics, Vol. 14, pp. 508-516.
- Peters, L. J., 1949, The Direct Approach to Magnetic Interpretation and its Practical Application; Geophysics, Vol. 14, pp. 290-340.
- Reford, M. S., and Sumner, J. S., 1964, Aeromagnetism: A Review Article; Geophysics, Vol. 29, pp. 482-516.
- United States Coast and Geodetic Survey, 1955, Total Intensity Chart of the United States.

PART VIII.

SEISMIC REFRACTION STUDY OF FOURMILE FLAT, NEVADA

by

M. Darroll Wood

ABSTRACT

Four reversed seismic refraction profiles were shot west of the Sand Springs Range in the Fourmile Flat area of west central Nevada. The Cenozoic rocks in this area, compared to their counterparts northeast of the Sand Springs Range in southern Dixie Valley, are shallower and structurally simpler. Velocities ranging from 18,300 to 15,500 ft/sec are assumed to represent basement, which lies at a maximum depth of 3500 ft. The basement deepens to the southwest. In places, the slope is nearly 13° but flattens toward the south to a maximum depth of 3000 ft with no detectable tendency to shallow near the Cocoon mountain front. Volcanics are possibly indicated by a wedge of 10,600 ft/sec material in the southeast thinning out in the north where the basement is shallow and its slope minimal. A 9300 ft/sec layer with a thickness of 1000 ft overlies the 10,600 ft/sec volcanic wedge and basement; this layer is also probably volcanic but may include consolidated Cenozoic sediments. A thin 6700 ft/sec section covers the low velocity volcanics near the playa and is interpreted as clay and silty material. The total thickness of the 6700 ft/sec material (assuming no volcanic interbeds) ranges from a maximum of 1000 ft nearest the playa to less than 500 ft under more distant profiles.

TABLE OF CONTENTS

	<u>Page</u>
ABSTRACT	i
TABLE OF CONTENTS	iii
LIST OF ILLUSTRATIONS	iv

Chapter

I. INTRODUCTION	1
II. ANALYSIS OF SEISMIC PROFILES	3
A. Profile F1	3
B. Profile F2	4
C. Profile F3	6
D. Profile F4	8
III. CONCLUSIONS	11
BIBLIOGRAPHY	13

LIST OF ILLUSTRATIONS

FIGURE	TITLE	PAGE
1.	Location Map.	2
2.	Time-distance curves and cross-section of Profile F1.	4
3.	Time-distance curves and cross-section of Profile F2.	5
4.	Time-distance curves and cross-section of Profile F3.	7
5.	Time-distance curves and cross-section of Profile F4.	9

I. INTRODUCTION

During the summer and winter of 1965, four reversed seismic refraction profiles were shot in the Fourmile Flat area (Fig. 1) of west central Nevada. This work was undertaken to extend the detailed picture of basement structure and basin fill found in Dixie Valley.

Previous geological and geophysical work in this and surrounding areas is discussed by Meister (Part I.) In addition, Part I contains the field procedure also applicable to this study.

Refraction line F3 was located in an E-W direction transverse to the probable structural trend; the remaining three profiles were set in a N-S direction. The length of the 24-geophone spread was 4600 ft for profiles F1 and F4 and 4800 ft for profiles F2 and F3. All shots except N3 of profile F2 were within 2 degrees of being on line.

True velocities were determined from the reversed apparent velocities. If the same velocity was recorded at more than one shot point a normal depth was computed from the delay time associated with that velocity recorded nearest the spread. This mitigates the risk associated with the imperative assumption that the refractor is continuous in attitude between the shot point and the spread. Depths to the same refractor from more distant shot points were calculated as a deviation from this normal depth associated with a corresponding change in delay time.

The assumption of refractor continuity was obviated in a case where the shot point involved was the most distant from the spread and near another shot point which was closer to its respective spread. In this case the interpretation associated with the latter shot point was carried over to the former shot point. This effected a continuity of structure among proximate sections of three profiles.

A computer program corrected the arrival times for a weathering zone above the datum specified for each profile. A weathering velocity of 2500 ft/sec was assumed on profiles F2 and F3 and 5700 ft/sec was measured for profiles F1 and F4 since the latter two profiles were shot during the winter and gave the understandably higher velocity.

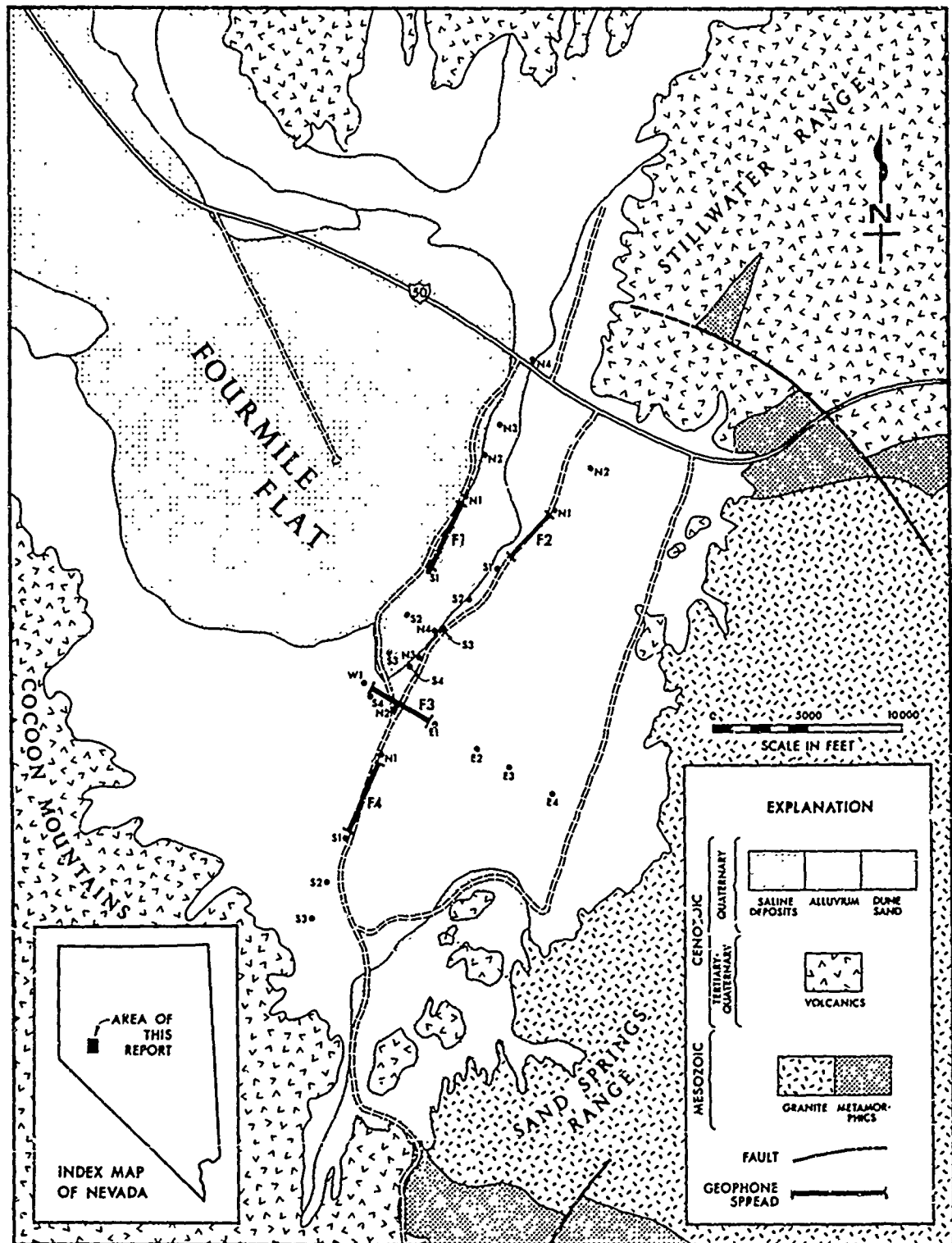


Figure 1. Location Map. Generalized geology from Vela Uniform Project Shoal Report VUF-1001 by Nevada Bureau of Mines, 1965.

II. ANALYSIS OF SEISMIC PROFILES

A. Profile F1

A four-velocity model was chosen for this profile with arrival times corrected to a 3970-ft datum. The 250-ft thickness of unconsolidated sediments associated with a 5700 ft/sec velocity was determined from shot points S1 and N1 and assumed to remain uniform under the entire profile. The normal depth was computed from the intercept time of the 6800 ft/sec velocity segment at S1. In addition, this velocity (± 200 ft/sec) was recorded at shot points S2 and N1 with the same intercept time. The zero intercept time at shot point N2 is arbitrary, since no time break could be established.

A normal depth to the lower surface of the 6800 ft/sec material was established under shot point S2 in addition to that depth associated with shot point delay times at shot points S3 and S4. Assuming that there is no unusual difference in intercept time at shot point N2 as compared to shot points S2, S3, and N3, then the lower surface of the 6800 ft/sec material is also essentially horizontal.

Basement was reversed on shot points N4, N3, and S3, and an even higher velocity was recorded on S4. A real velocity of 16,600 ft/sec was determined from N4 and S3; the higher 18,800 ft/sec velocity may have come from an intrabasement refractor. A normal depth of 3300 ft was determined under shot point S3 and a corresponding dip of 4.5° between shot points N4 and S3. The small intercept time recorded at N3 suggests local relief in the basement.

B. Profile F2

Profile F2 strikes N 40° E and is 3500 ft east of profile F1. A four velocity model was chosen that differed little from F1 except the weathering velocity for correction to a 4000 ft datum was dropped to 2500 ft/sec.

Figure 2. Time-distance curves and cross-section of profile Fl.

An unreversed 6700 ft/sec velocity from the N1 curve was assumed to be real and to correspond to horizontal material under the entire profile with a calculated thickness of 250 ft. The normal depth to this layer was determined from the intercept time at S1 since no reliable time break could be established at shot point N1.

A 9800 ft/sec apparent velocity derived from N1 was assumed to be from the same refractor associated with the 8200 ft/sec apparent velocity recorded from shot point S1. This would indicate a local dip down to the north with the thickness of the layer varying similar to profile F1.

Basement velocities of 13,900 and 14,900 ft/sec recorded at shot points S1, S2, and S3, indicate a sloping basement down to the south. A zero time break could not be established for shot points N1 and N2. The normal depth to basement was calculated at shot point S1. The rate at which the basement deepens to the south conforms with the same trend found for profile F1; however, the maximum depth is shallower by 1500 ft.

C. Profile F3

The four velocity model chosen for this transverse profile differs markedly from profiles F1 and F2 by the presence of a 10,700 ft/sec velocity also found on profile F4. This unreversed velocity was derived from shot point E2 and was assumed to be a true velocity because a 10,500 ft/sec velocity was recorded from reversed shot points N3 and S3 of profile F4. A normal depth of 1000 ft was determined from the intercept time at shot point E2.

The two high apparent velocities of 13,100 and 13,900 ft/sec recorded from shot points E3 and E4 respectively were assumed to be down dip velocities of the basement. A basement velocity of 16,000 ft/sec was derived by averaging the reversed basement velocities from profiles F1 and F2. A normal depth of 350 ft under E3 with a 13° dip to the west was then determined. The general magnitude and direction of the basement slope is corroborated from previous work (Gimlett, 1965). The basement depth corresponds to the same depth (± 50 ft) of the 10,700 ft material

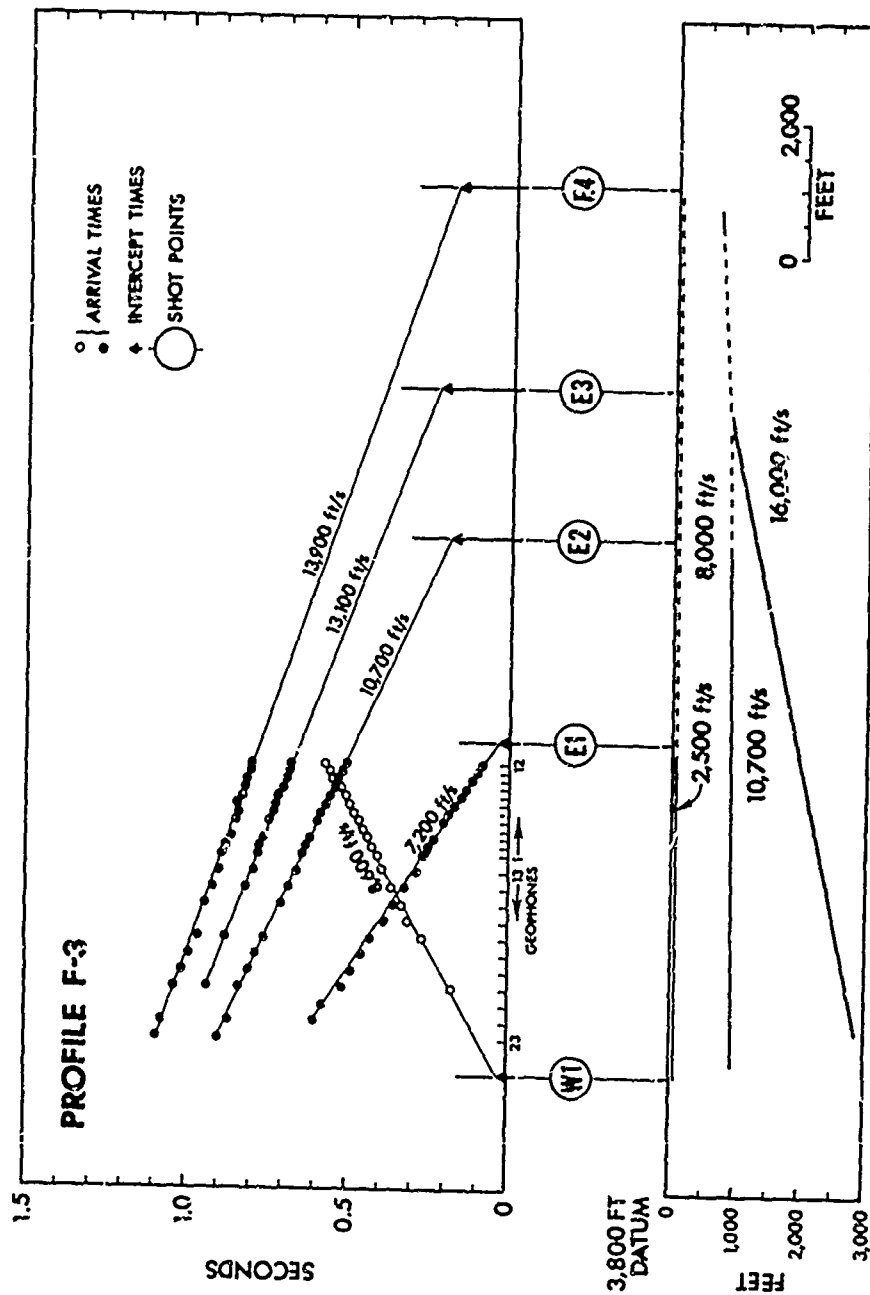


Figure 4. Time-distance curves and cross-section of Profile F3.

determined from shot point E1. A shallower depth to basement under shot point E4 was computed from the shot point delay time associated with shot points E3 and E4. The interpretation is simply that the 10,700 ft/sec material represents a wedge of volcanics whose lower surface rests on sloping basement.

The 8600 and 7200 ft/sec velocities determined from shot points W1 and E1 respectively were considered as the apparent velocities associated with a westerly dipping 8000 ft/sec velocity refractor. This 900-ft thick layer was assumed to cap the entire profile. This material was interpreted to be a heterogeneous layer correlating with the combination of the 6700 and 9000 ft/sec material on profile F2 and the 6800 and 9300 ft/sec material under profile F1. If this correlation is valid, then possibly a wedge of volcanics might also be present starting under S3 of profile F1 and thickening as the basement deepens to the south. This supposition is supported by information from profile F4.

D. Profile F4

A five-velocity model was used to describe the material beneath a 4100-ft datum of profile F4. This is the only profile containing all velocities encountered in the survey. All velocities were reversed except the basement on the south side of the spread.

The small difference in reversed apparent velocities indicated insignificant southerly dips of all layers. Even the 14,900 ft/sec unreversed velocity, if considered to be basement, must, from similar and reversed velocities found on profiles F1 and F2, also dip less than 3° to the south. An average of the true basement velocities under profiles F1 and F2 was assumed to apply as a true basement velocity of 16,000 ft/sec under profile F4.

Shot points N3 and N4 are flanked by the southern shot points of profiles F1 and F2, both of which indicate a south-sloping basement. Since shot points N3 and N4 of this profile lie close to shot points S4

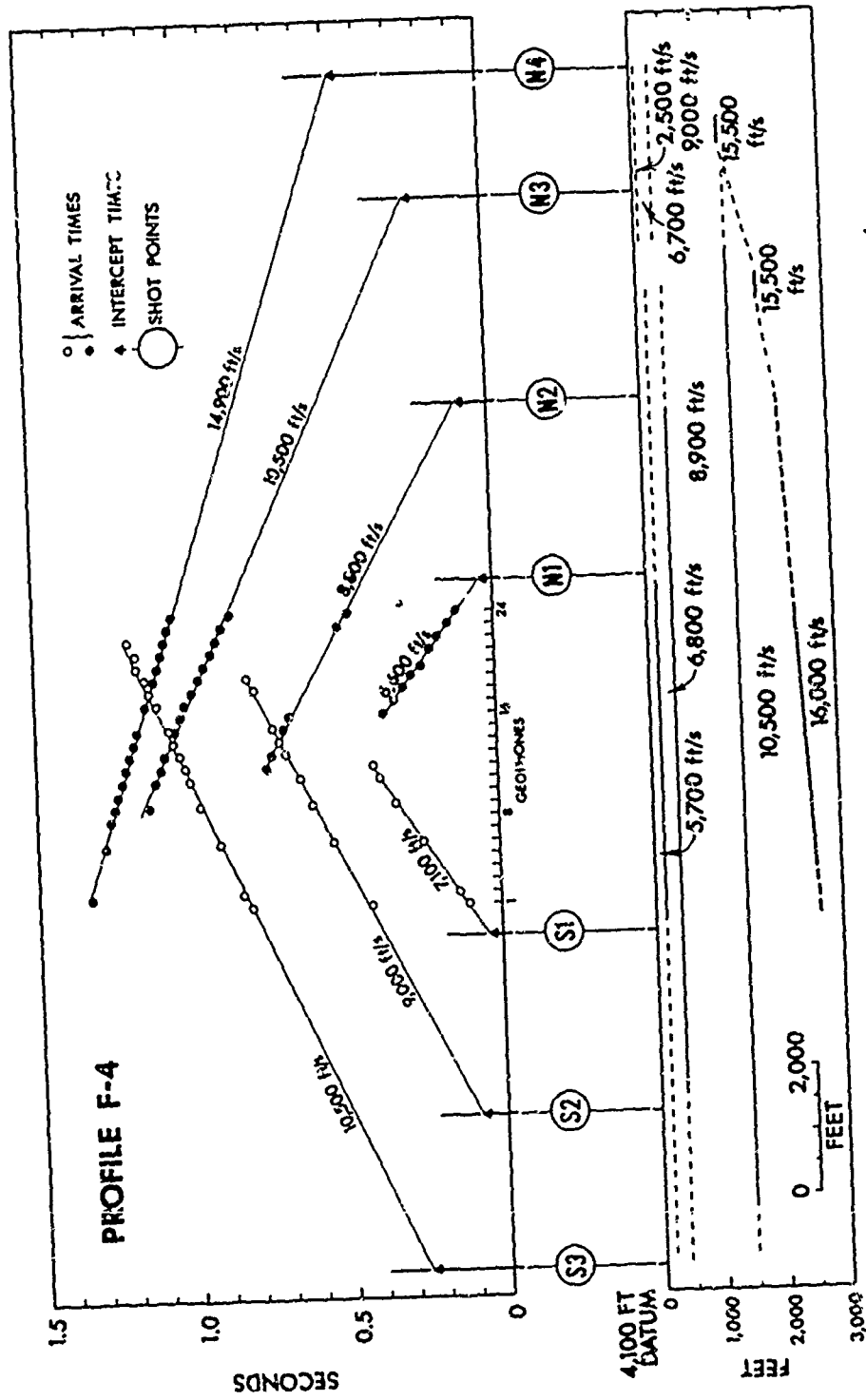


Figure 5. Time-distance curves and cross-section of Profile F4.

and S3 respectively of profile F2, there must be reasonable continuity of information between them. Therefore, the apparent horizontality of all refractors beneath the entire length of profile F4 could not hold. The assumption of continuity of the refractor surface between the spread and the two most distant shot points was obviated. The normal depth that would have been calculated under shot point N3 was assumed to apply only under the center of the spread. In addition, the interpretation of horizons beneath shot points S4 and S3 was carried over to N3 and N4. The horizontality, depth and thickness of the 8900 ft/sec layer calculated under profile F4 persists if the 9000 ft/sec material carried over from S3 is indeed the same.

Thus, there is no significant change in depth, thickness, or attitude of the sediments and lower velocity volcanics capping this profile due to this transfer. However, the basement shallows to the same depth as the higher velocity volcanics under the spread. The wedge shape of the volcanics lying on the basement determined under profile F3 now appears under profile F4 which strikes 80° to profile F3.

III. CONCLUSIONS

A synthesis of the various two-dimensional models into a three-dimensional interpretation appears cogent within the constraints imposed by each model.

Depths to refractors at points of intersection and adjacent portions of different profiles are in reasonable agreement. The errors in common depth points to basement associated with profiles F1 and F3 as well as F4 and F3 are in the same direction and could be reduced if the extrapolated slope calculated at shot point E2 for profile F3 were to steepen in the last few hundred feet under the spread. This cannot and would not be detected on the arrival time curve. It should also be recalled that the high velocity found on shot point S4 was considered to come from an intrabasement refractor. Consequently, the depth must be shallower than indicated. There are other possible ways to reduce the depth at F1S4 by 500 ft, but the major uncertainty is the real trend of the basement slope under the western one-third of the spread of profile F3. This is a consequence of not having reversed the basement on that side and consequently being forced to extrapolate a slope.

Within this mis-tie range of common depth to basement, it appears that the 16,000 ft/sec basement under the north to eastern parts of the survey is shallow and deepens gradually to the southwest. The most westerly surveyed area shows no tendency for the basement to become shallower than the 3500-ft depth indicated there.

A wedge of 10,500 ft/sec volcanics resting on the steeper and deeper parts of the basement under the south and east profiles appears to be the northern extension of the surface exposures prevalent in the Cocoon mountains and as isolated small areal exposures to the southeast. Meister (Part I) correlates a seismic velocity boundary below which the velocity increases to an average of 10,000 ft/sec to similar velocities measured in rhyolitic tuffs and flows at White Rock Canyon and at Mud Springs in Dixie Valley. He reports that this boundary is characteristic of the entire Dixie Valley region and represents a distinct stratigraphic

horizon within the valley fill. If this characteristic is applicable in Fourmile Flat area then the 9000 ft/sec layer capping the entire survey may also be volcanic. Volcanics (Fig. 1) in the Fourmile Flat area have been mapped collectively as olivine basalt, andesite, rhyolite, dacite and tuff.

The 6700 ft/sec layer absent only on the east-west profile may correspond to the clays and silty material common in the lower parts of closed basins.

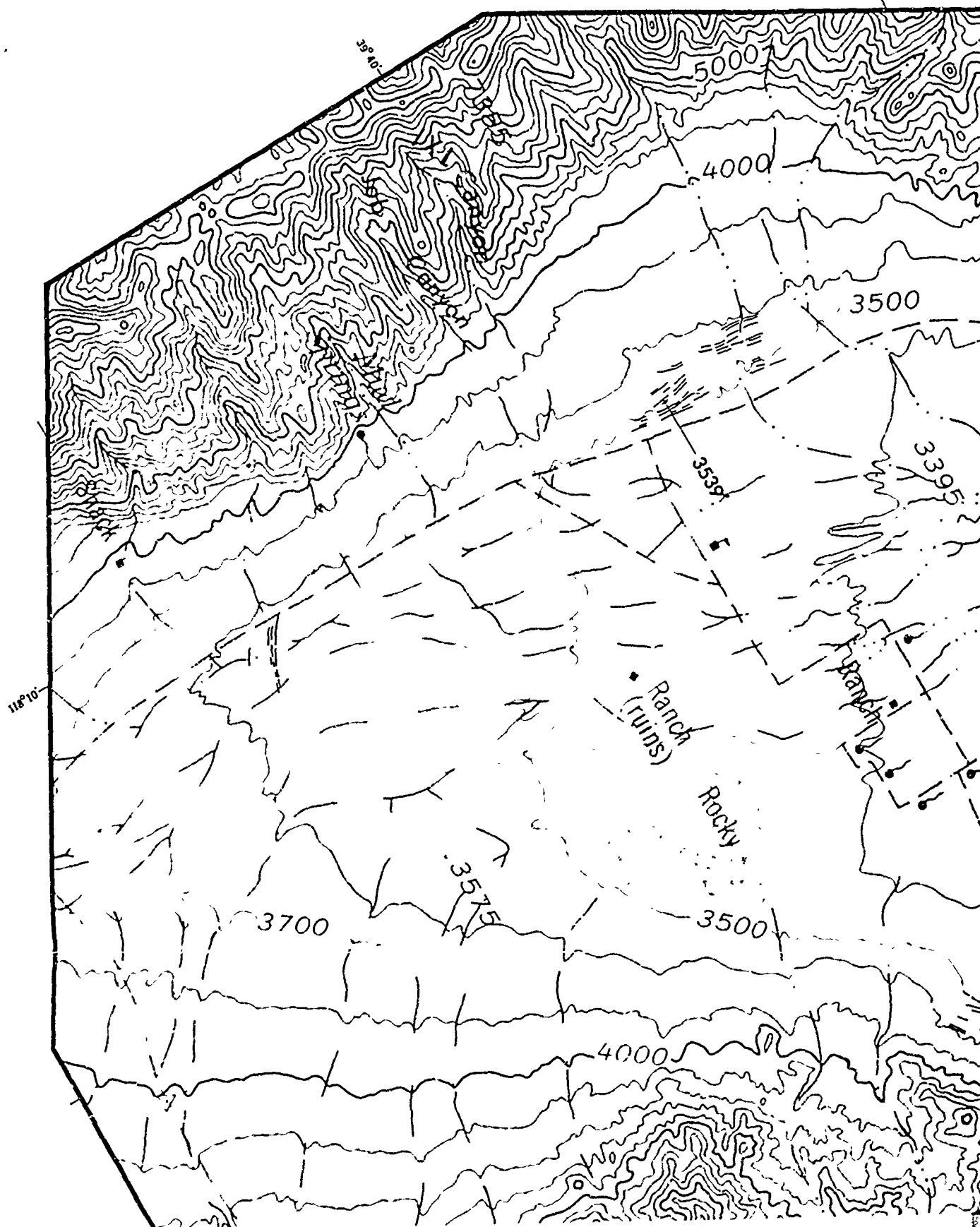
The total thickness of low velocity sediments (assuming that no volcanics are interbedded with material 6800 ft/sec and less) ranges from a maximum thickness of 1000 ft nearest the playa to less than 500 ft on more distant profiles.

BIBLIOGRAPHY

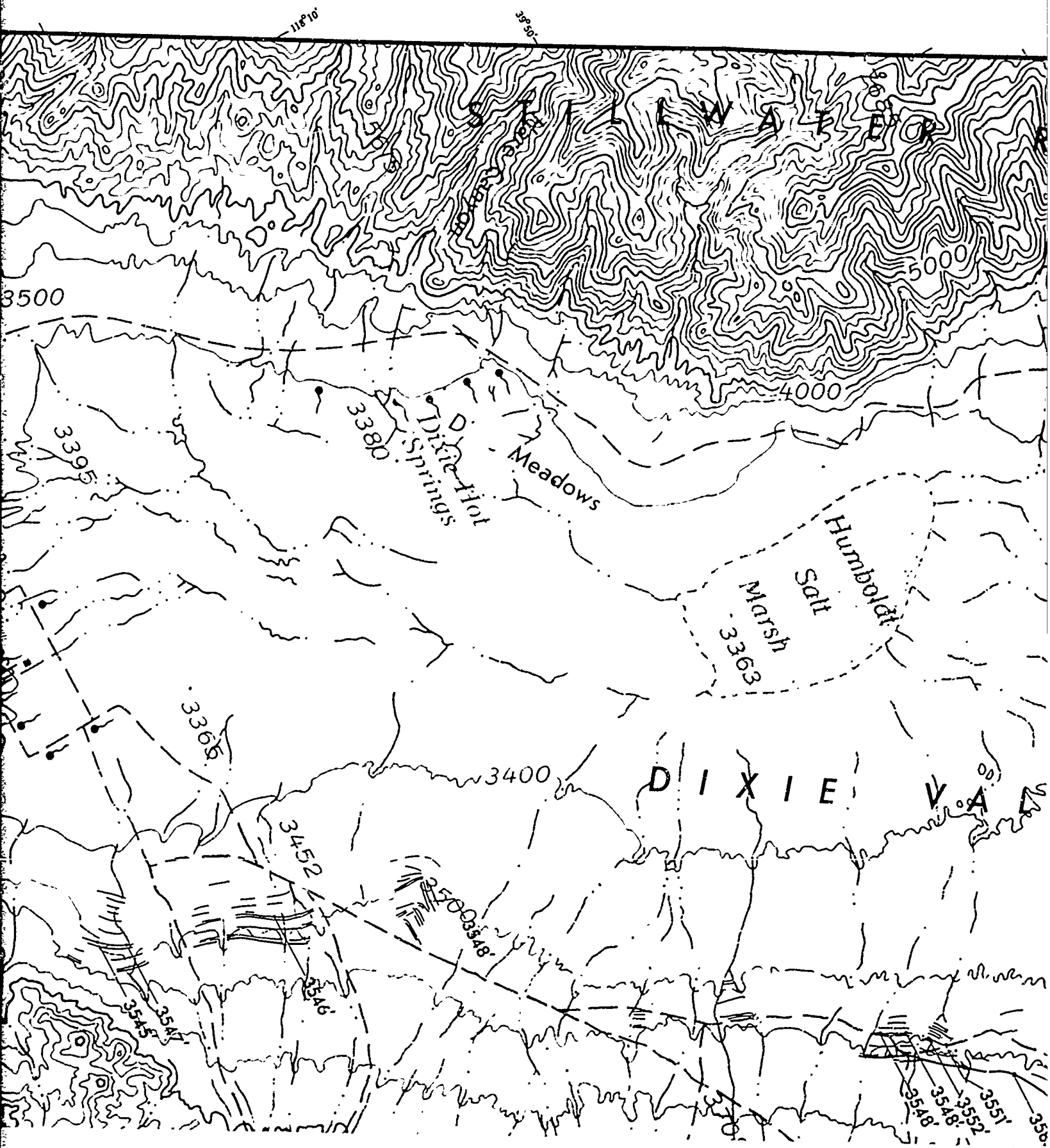
- Gimlett, James I., 1965, Refraction Survey; Final Report--Geological, Geophysical, Chemical, and Hydrological Investigations of the Sand Springs Range, Fairview Valley, and Fourmile Flat, Churchill County, Nevada, Report to Atomic Energy Commission for Shoal Project, Vela Uniform Program, pp. 49-53.
- Hawkins, L.V., 1961, The Reciprocal Method of Routine Shallow Seismic Refraction Investigations; Geophysics, Vol. 26, pp. 806-819.
- Meister, L.J., 1967, Seismic Refraction Study of Dixie Valley, Nevada; A. F. Cambridge Research Labs. Final Scient. Rpt. Part I, AFCRL-66-848.
- Nettleton, L.L., 1940, Geophysical Prospecting for Oil; New York, McGraw-Hill, 444 pp.
- Page, B.M., 1965, Preliminary Geologic Map of a Part of the Stillwater Range, Churchill County, Nevada; Nevada Bureau of Mines Map 28.

A

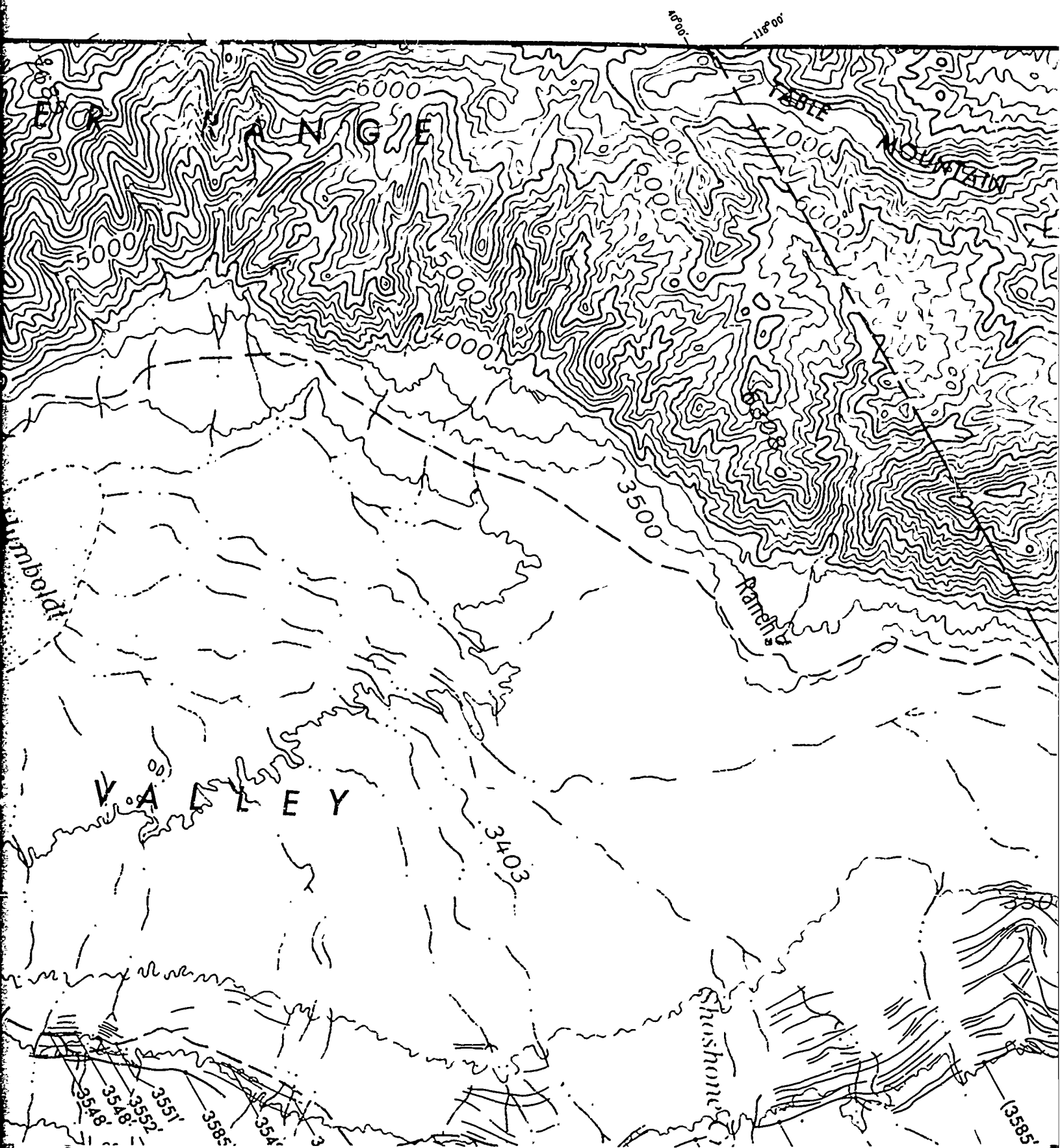
PLATE 2

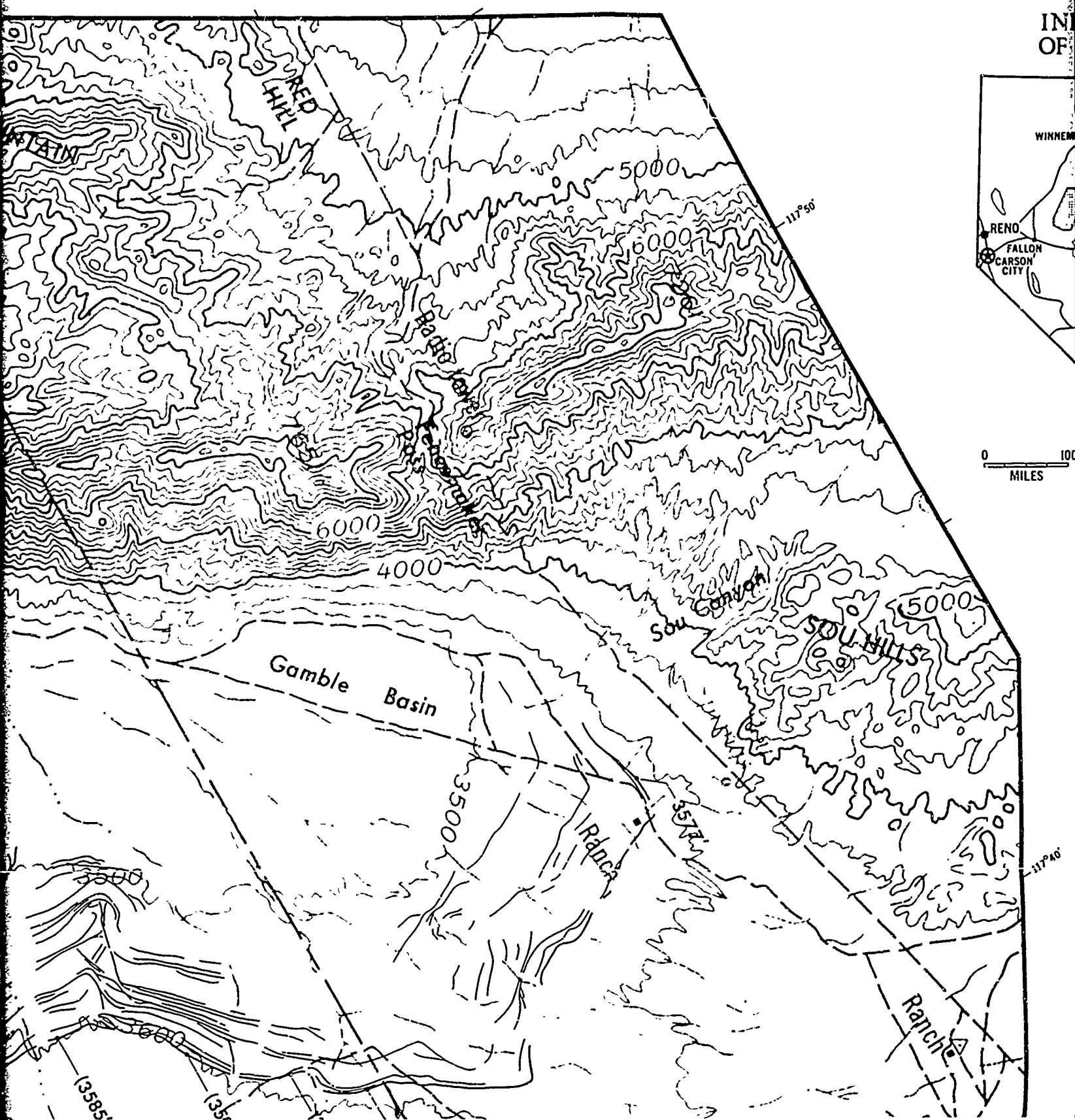


E

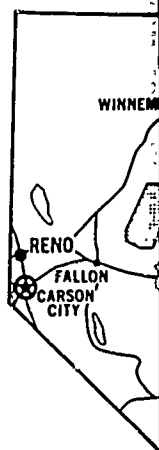


C







IN
OF

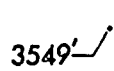


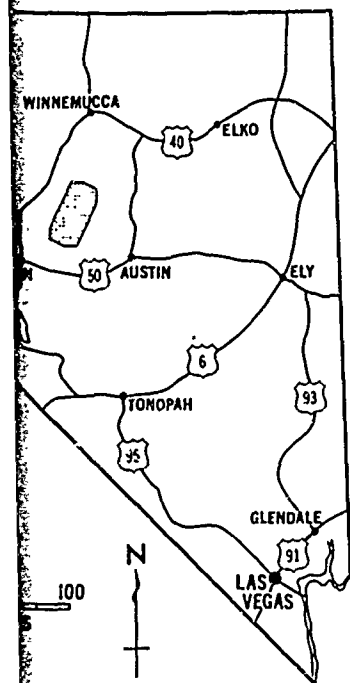
0 100
MILES

INDEX MAP OF NEVADA

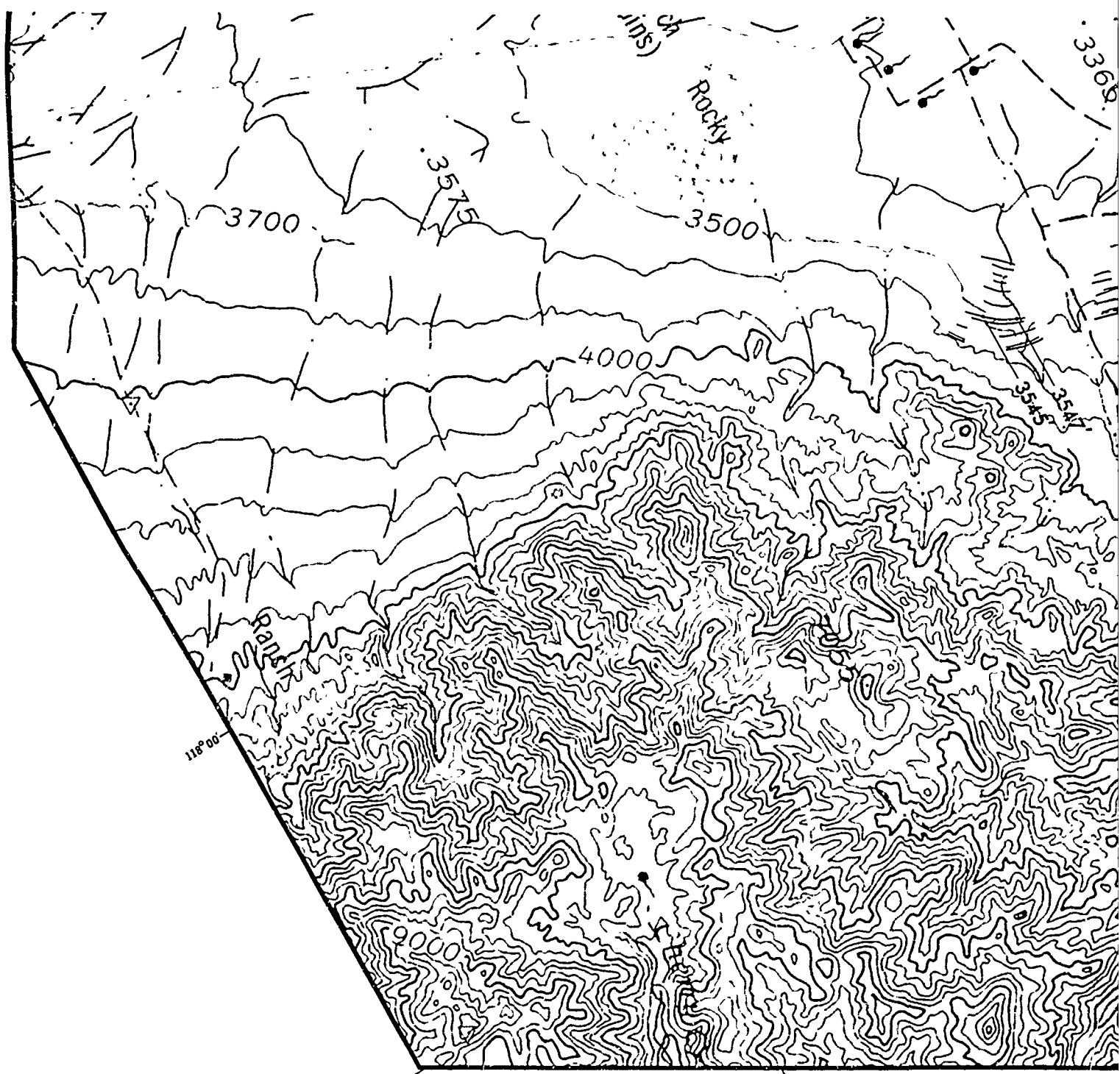
EXPLANATION

-  Crest of pluvial lake beach ridge
-  Crest of highest pluvial lake beach ridge

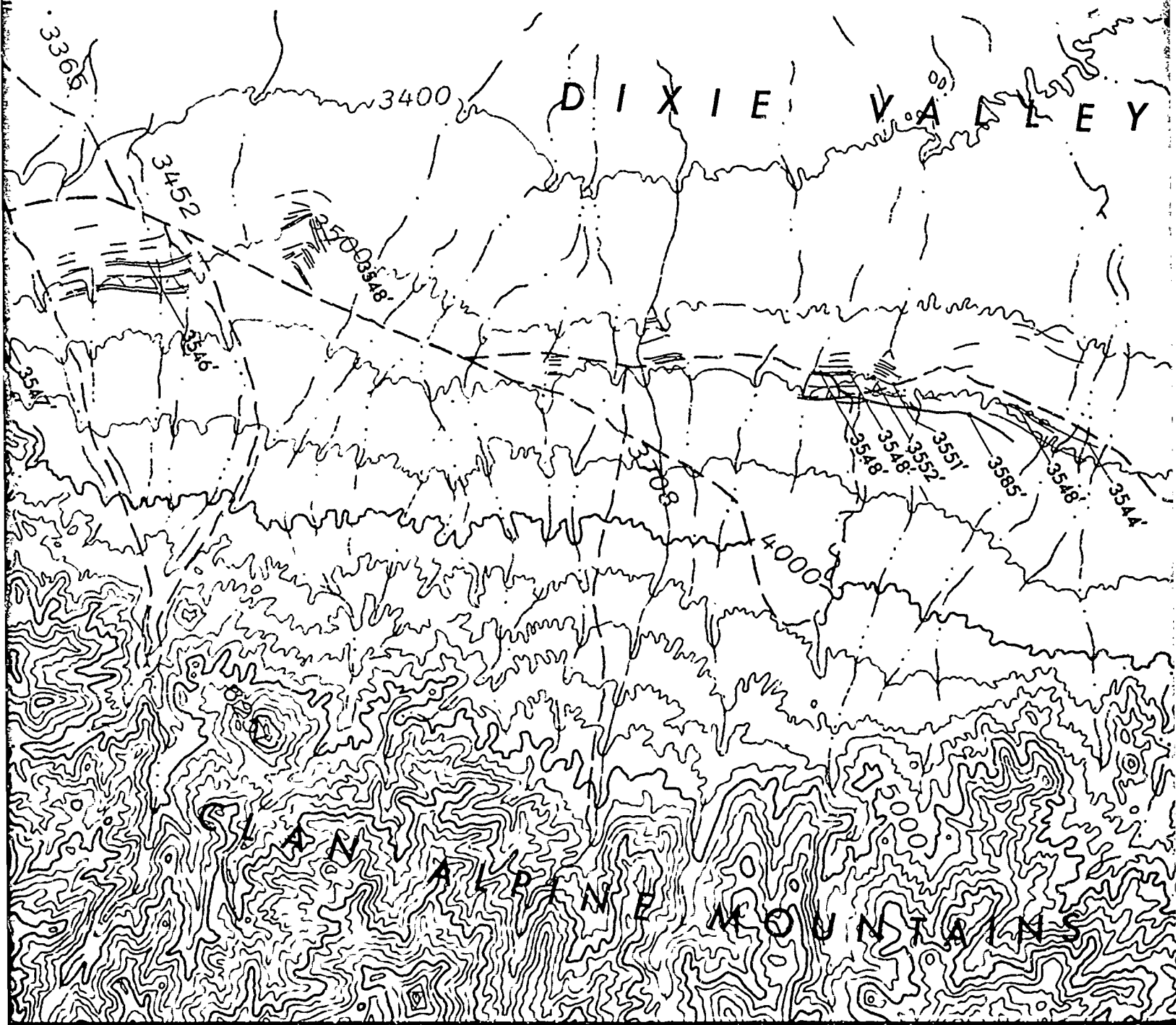
 Beach ridge elevation. Elevations in parentheses taken from U.S.G.S. 7½ quads. with possible error of ±3 ft.



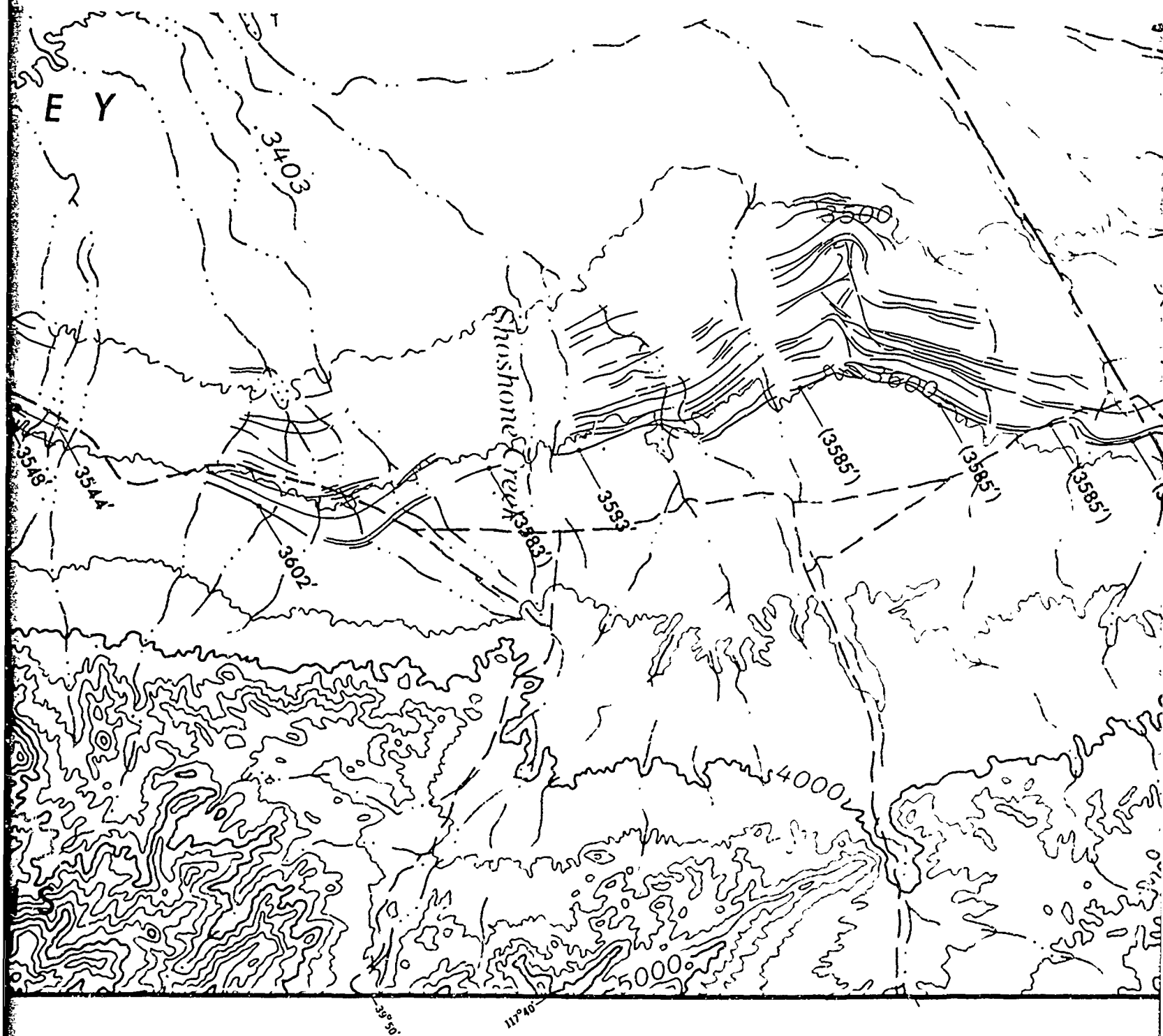
BLANK PAGE



Base enlarged and modified from A.M.S.
Lovelock, Millet, Reno and Winnemucca
1:250 000 topographic quadrangles



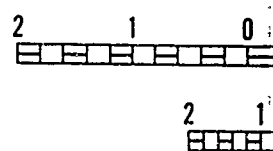
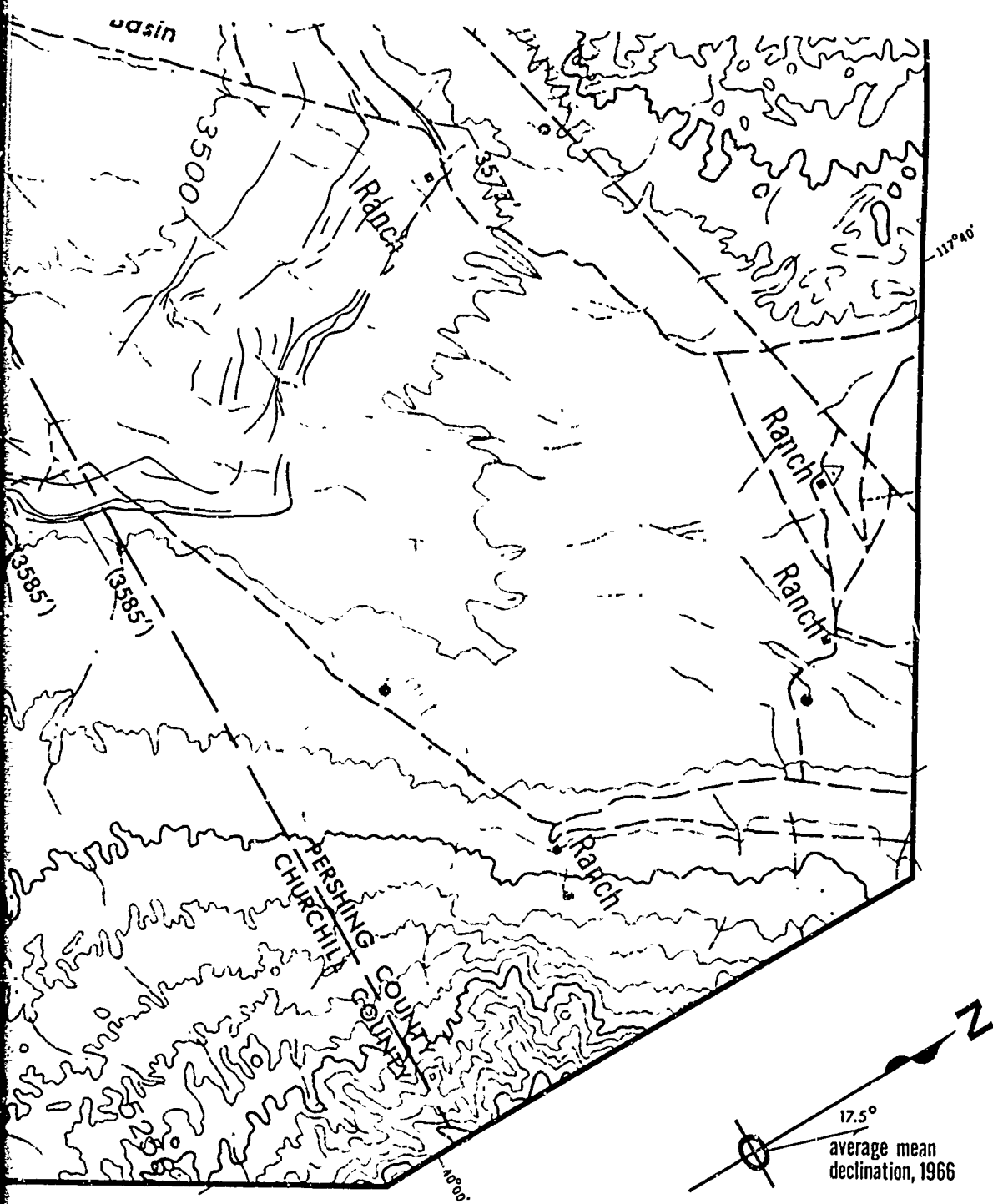
PHOTOGEOLOGIC MAP OF DIXIE VALLEY CHURCHILL AND PERSHING COUNTIES



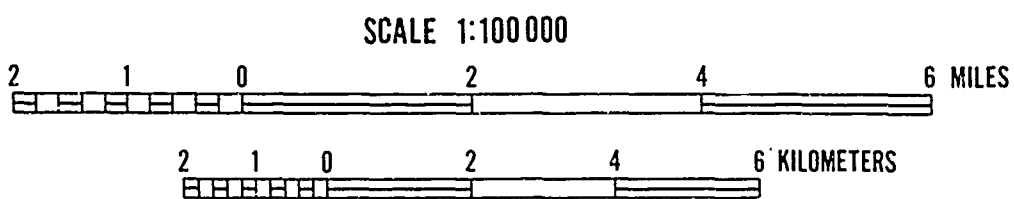
Photogeology by

OF DIXIE VALLEY

COUNTIES, NEVADA



Geology by Dennis B. Burke 1965-66

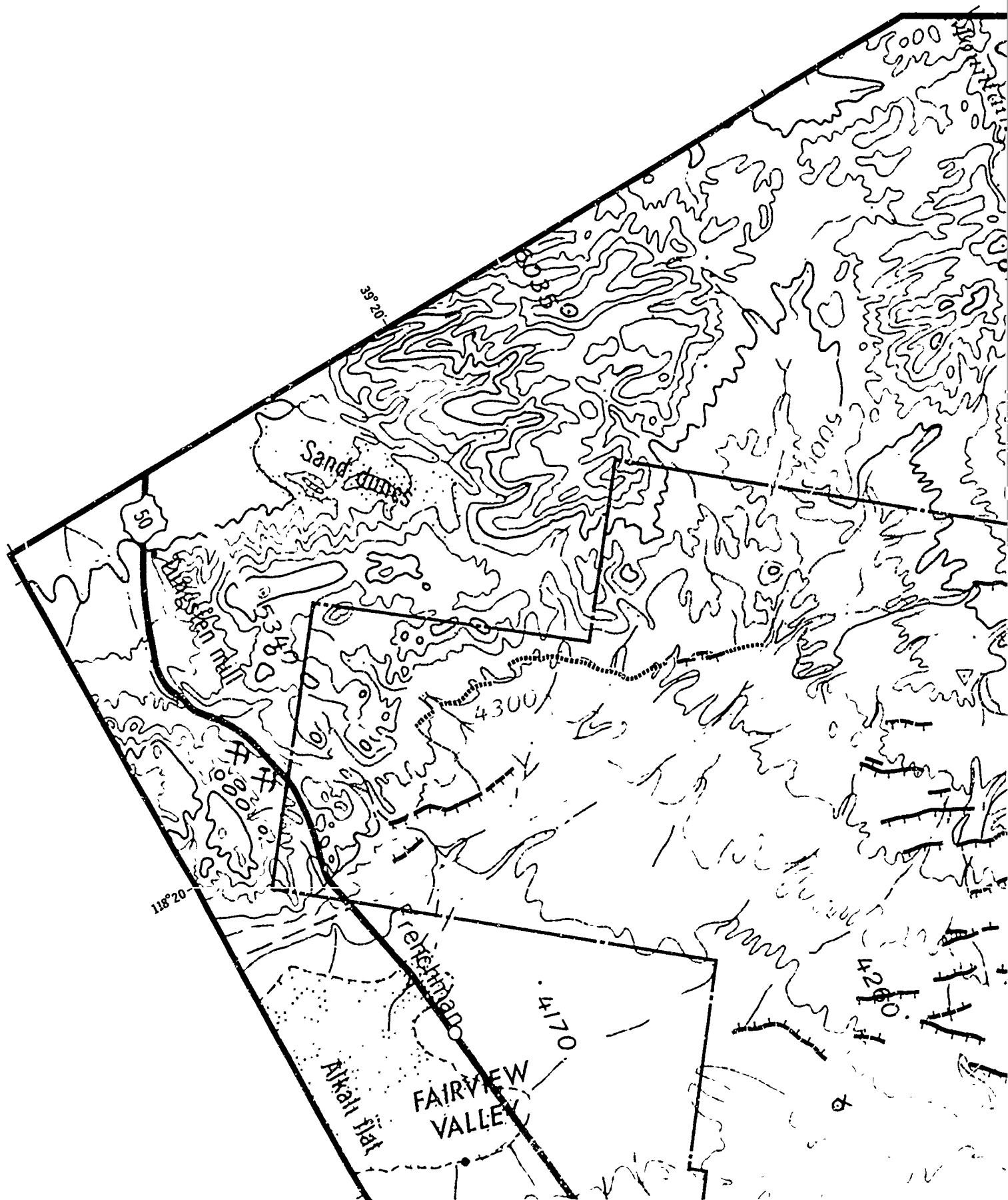


CONTOUR INTERVAL 200 FEET

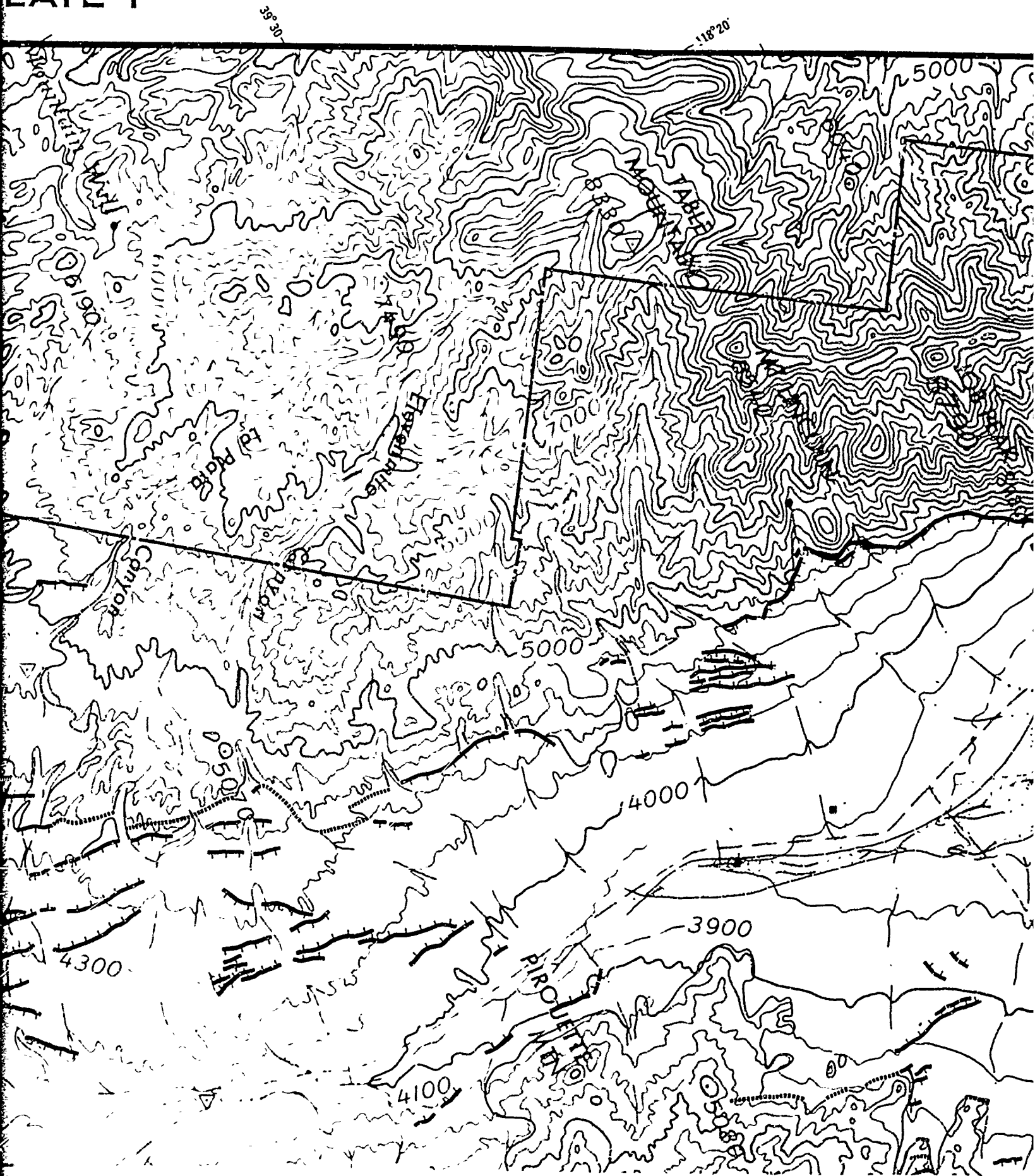
J

BLANK PAGE

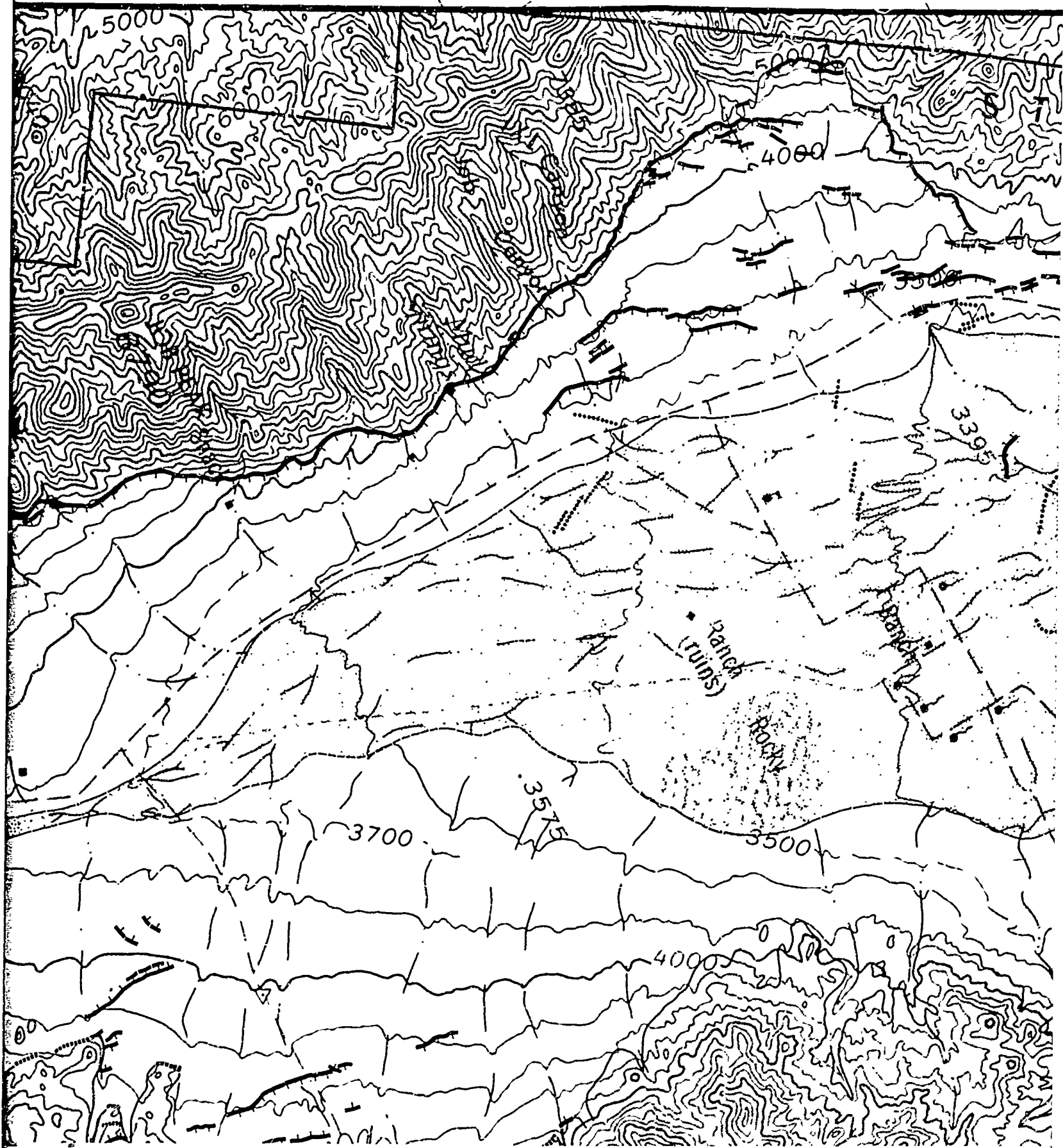
PLAT



LATE 1

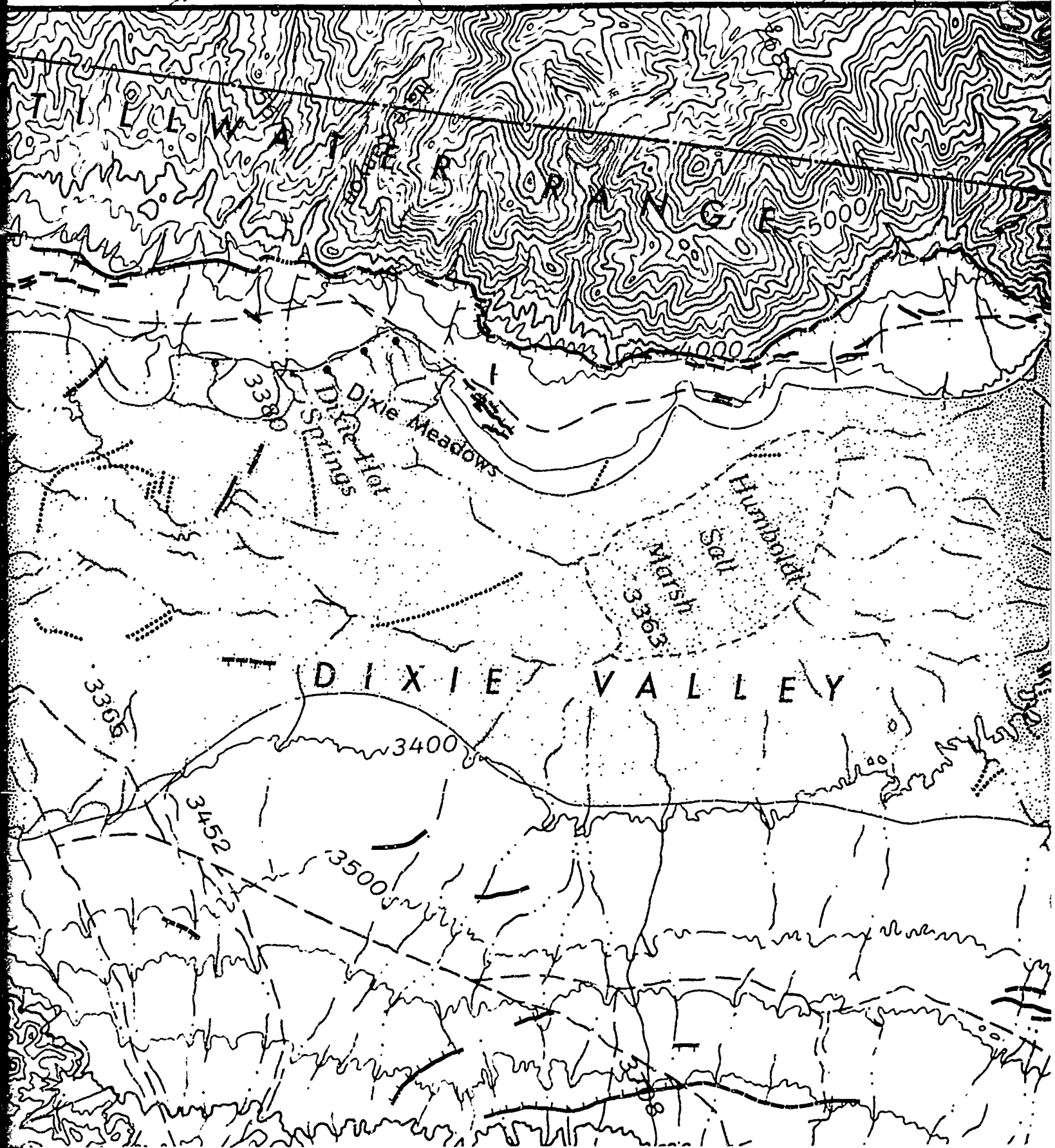


59° 40'



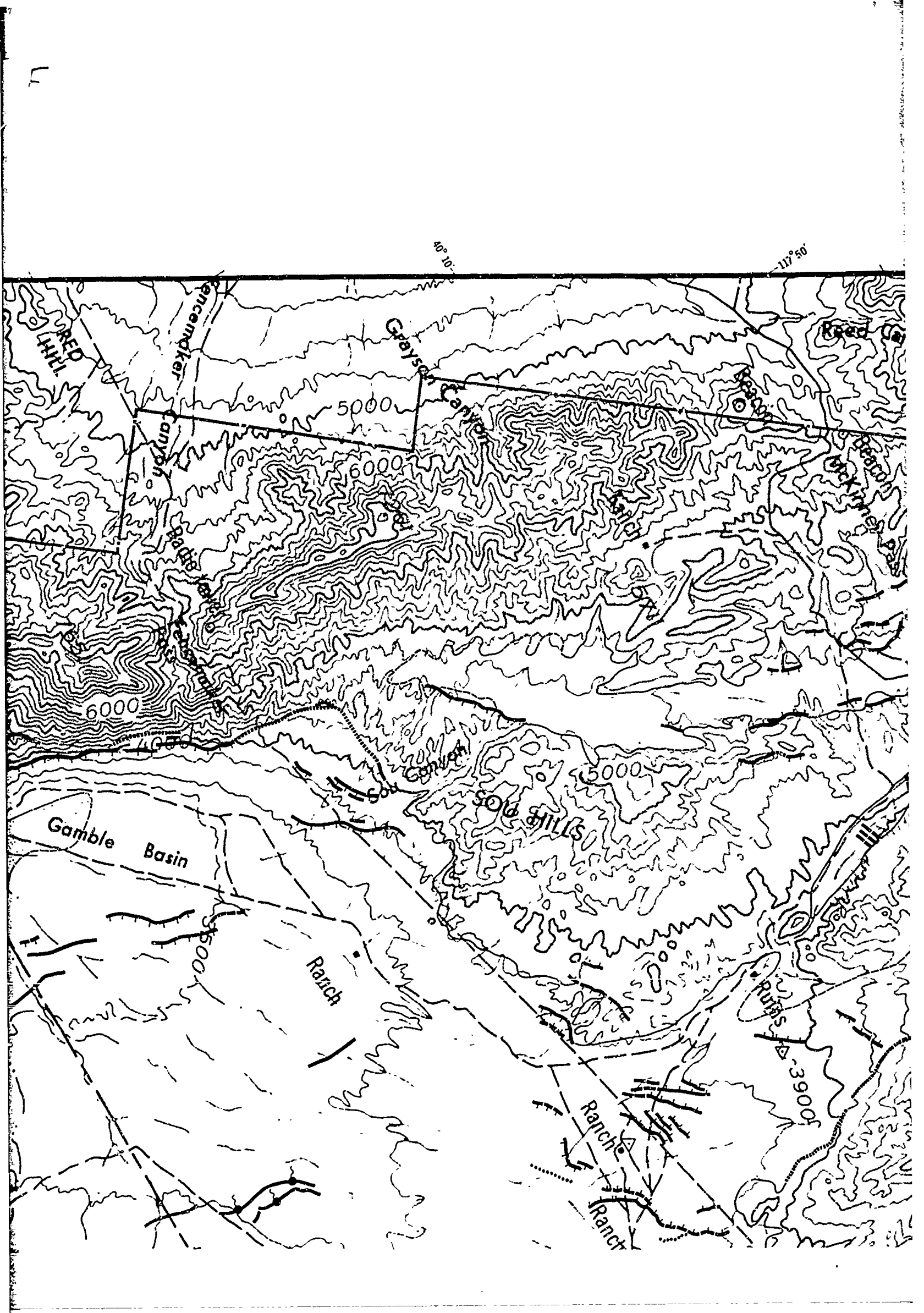
118° 10'

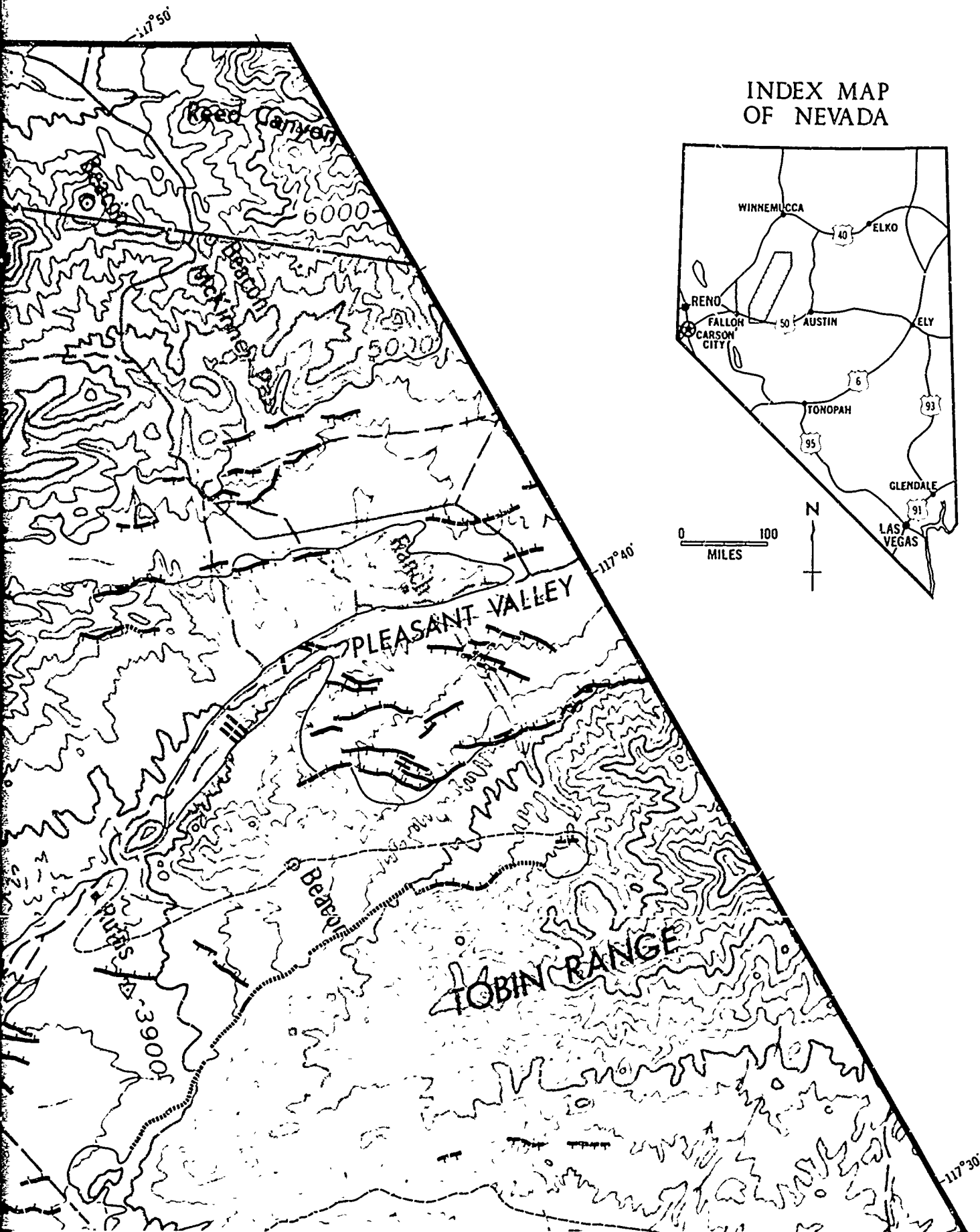
39° 50'





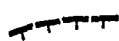



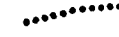
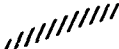



E

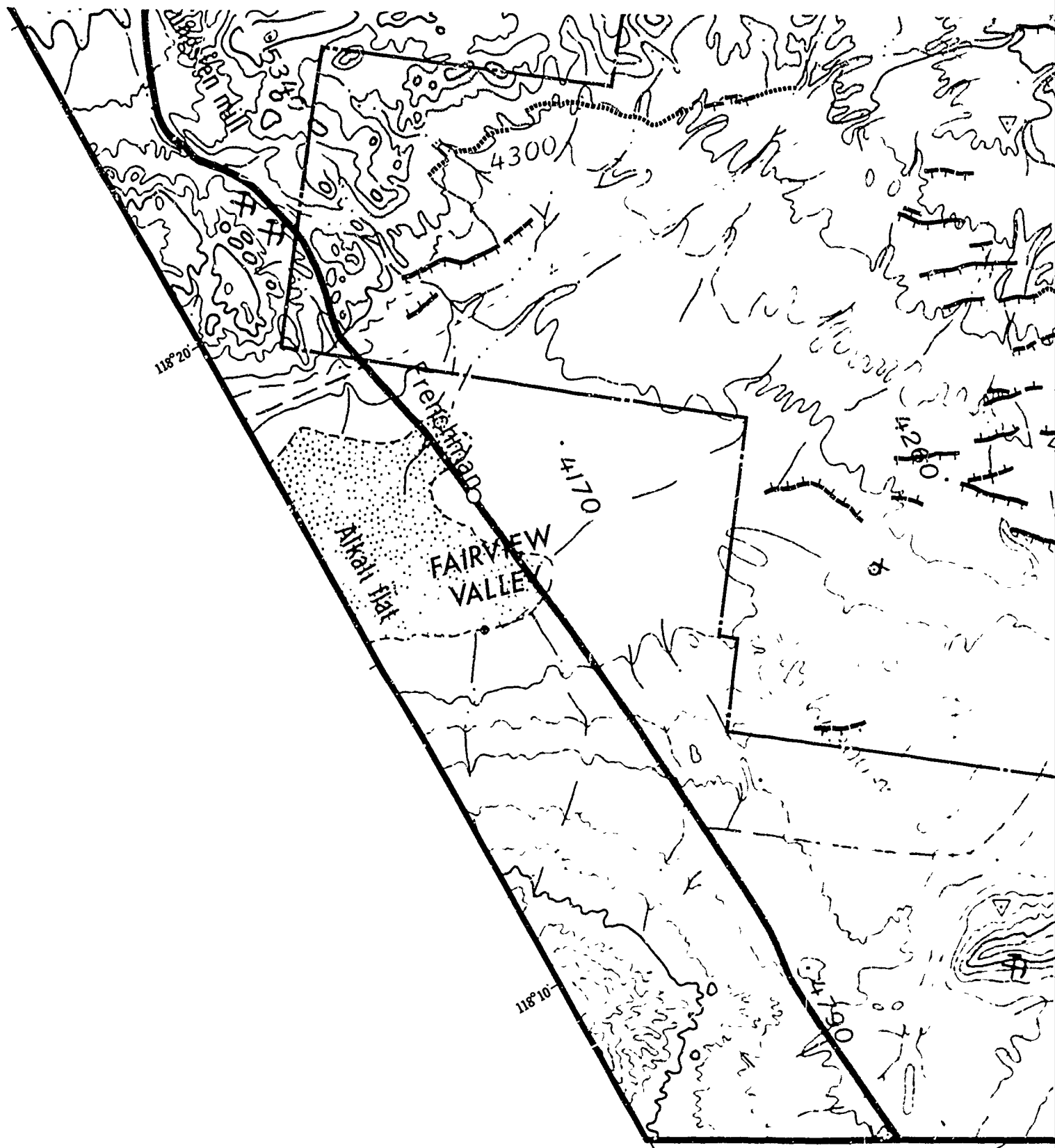






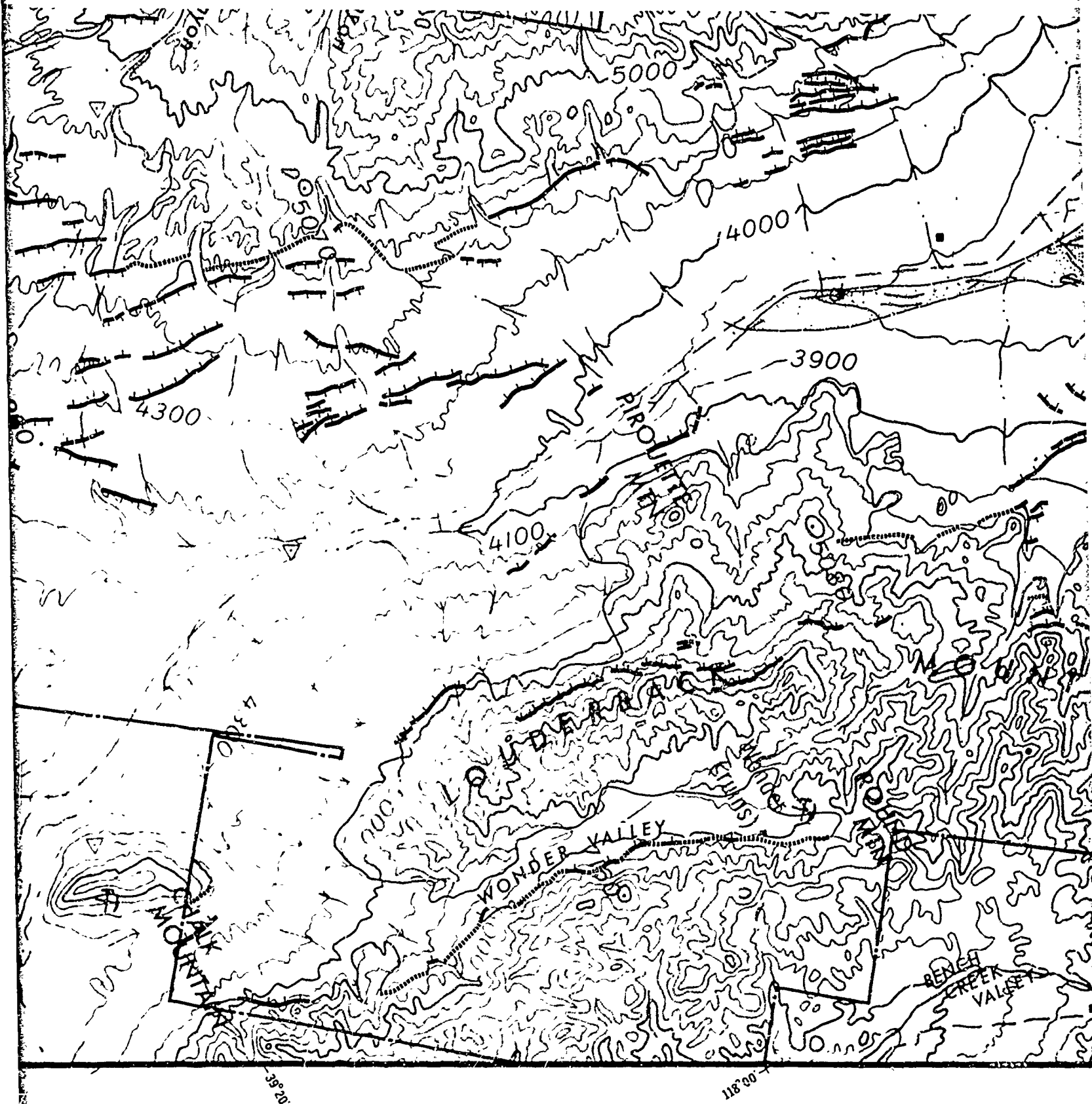
EXPLANATION

- 
 Fault scarplet within alluvium or at the bedrock-alluvium contact. Hachures on the downthrown side
- 
 Fault scarplet within alluvium; scarplet removed from original position by spring sapping and slumping. Springs (diagrammatic) on the downthrown side
- 
 Scarplet of probable fault origin within alluvium or at the bedrock-alluvium contact. Hachures on the downthrown side
- 
 Fault within alluvium with no topographic expression at the limits of stereoscopic resolution. Determined by tonal, textural and vegetation lineaments
- 
 Probable fault within alluvium with no topographic expression at the limits of stereographic resolution. Determined by tonal, textural and vegetation lineaments
- 
 Probable fault at the bedrock-alluvium contact. No scarplet present
- 
 Narrow lineament of unknown origin
- 
 Broad lineament of unknown origin
- 
 Generalized bedrock-alluvium contact. Dashed where alluvium becomes thin and discontinuous
- 
 Generalized outer limits of fans. Short dashed where gradational
- 
 Limits of stereo coverage



Base enlarged and modified from A.M.S.
Lovelock, Millet, Reno and Winnemucca
1:250 000 topographic quadrangles

I



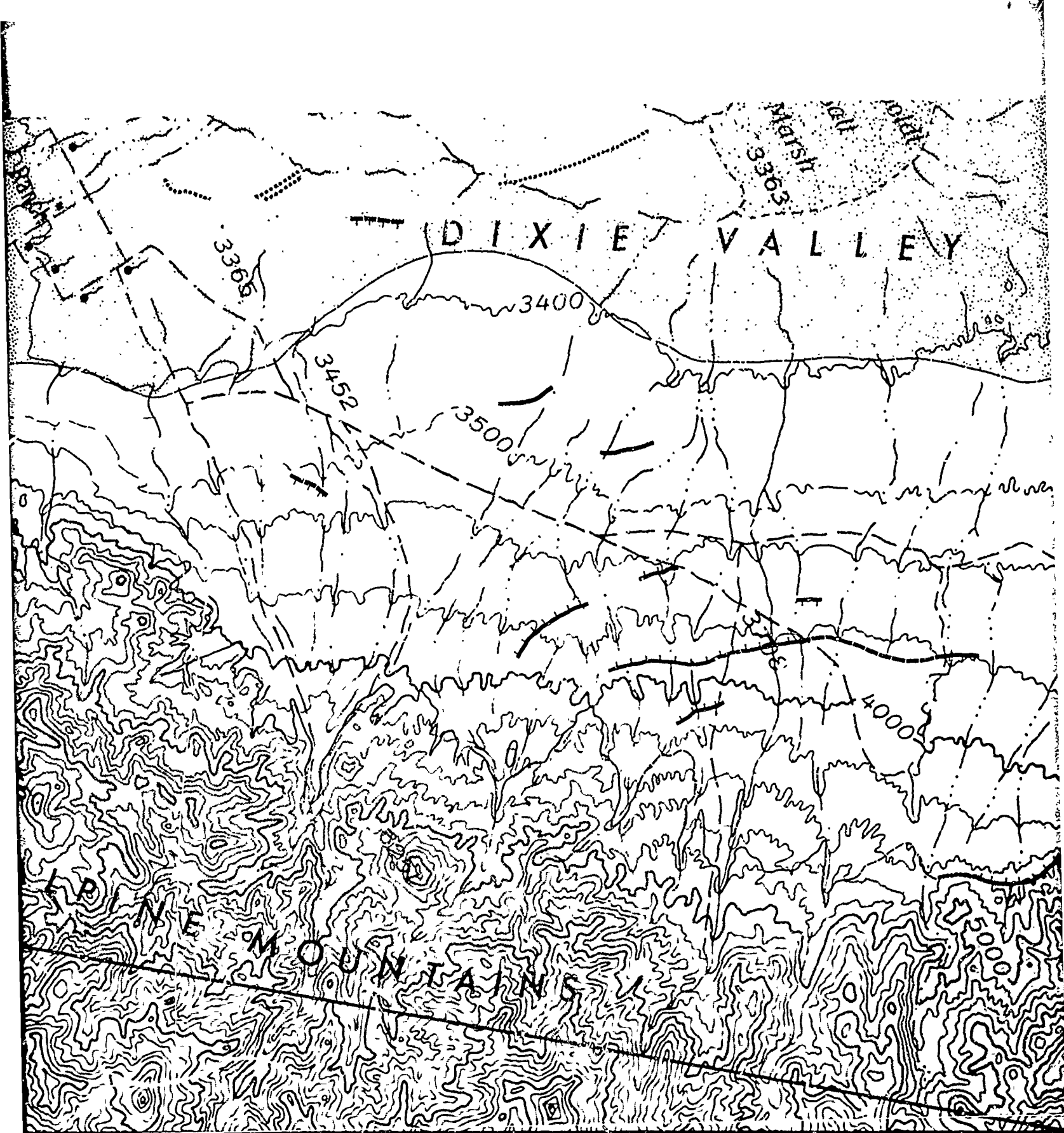
L.M.S.
cca

J



PHOT
C

K



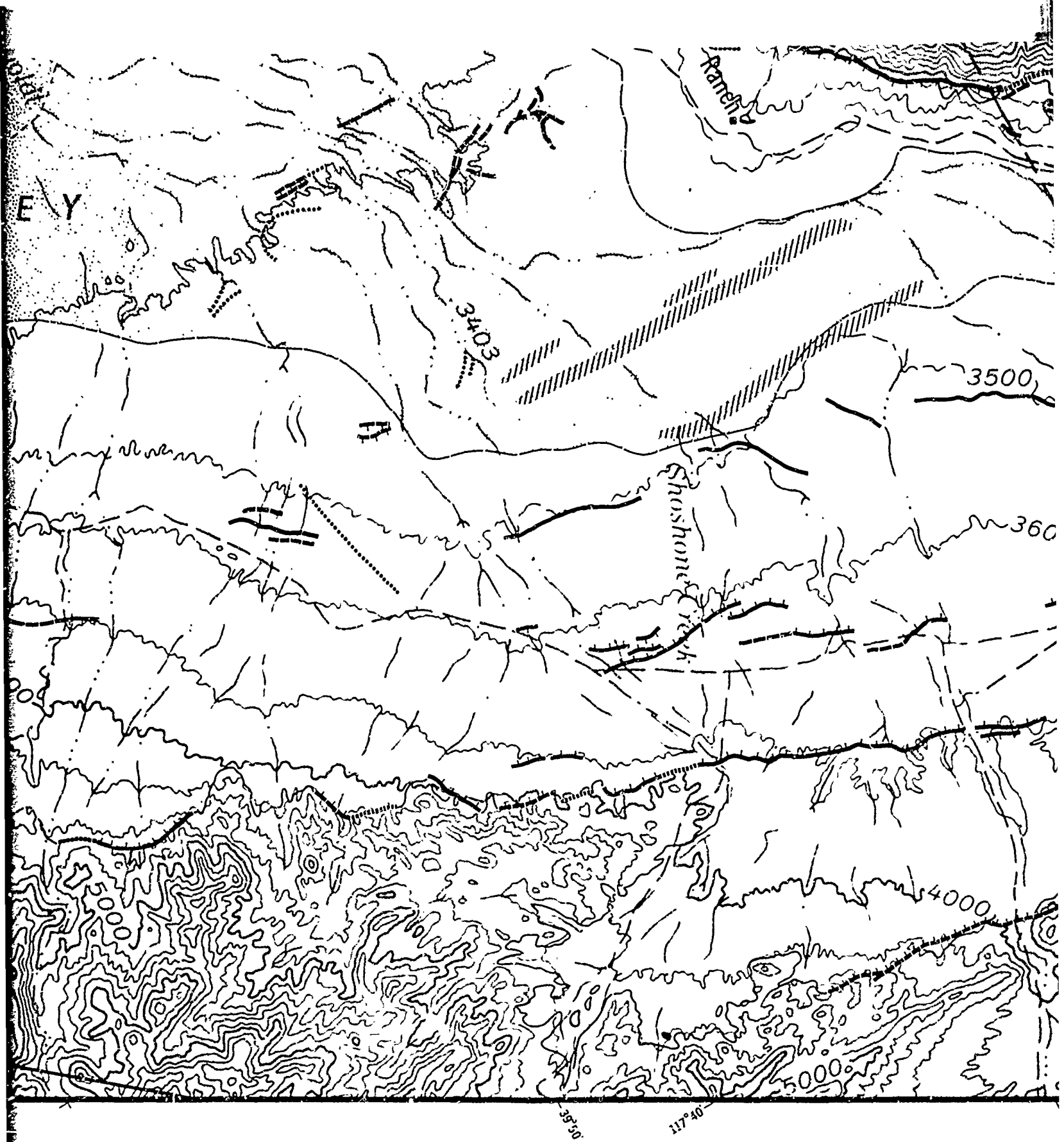
117°50'

39°40'

PHOTOGEOLOGIC MAP OF DIXIE VALLEY

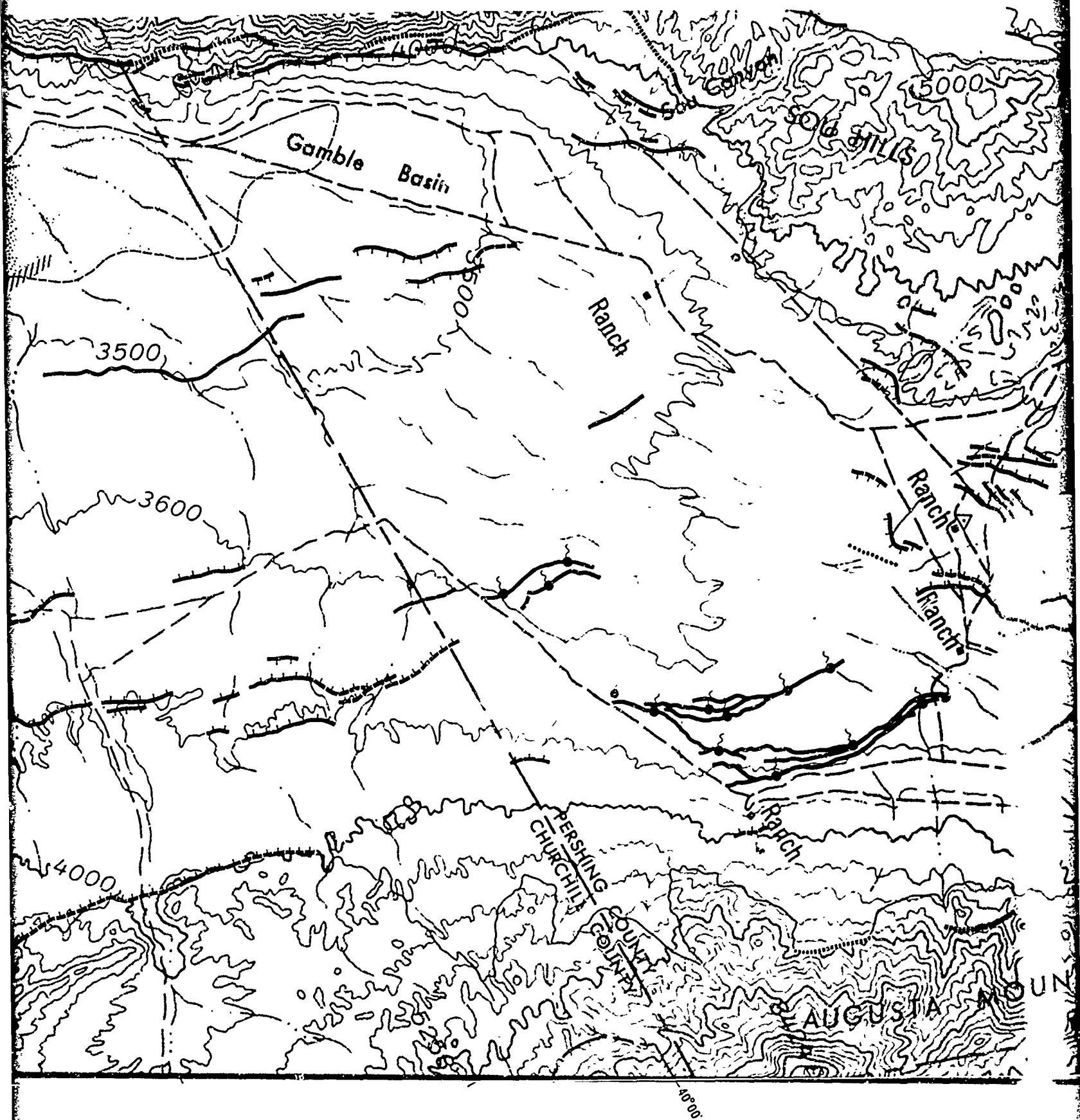
CHURCHILL AND PERSHING COUNTIES, NEVADA

L



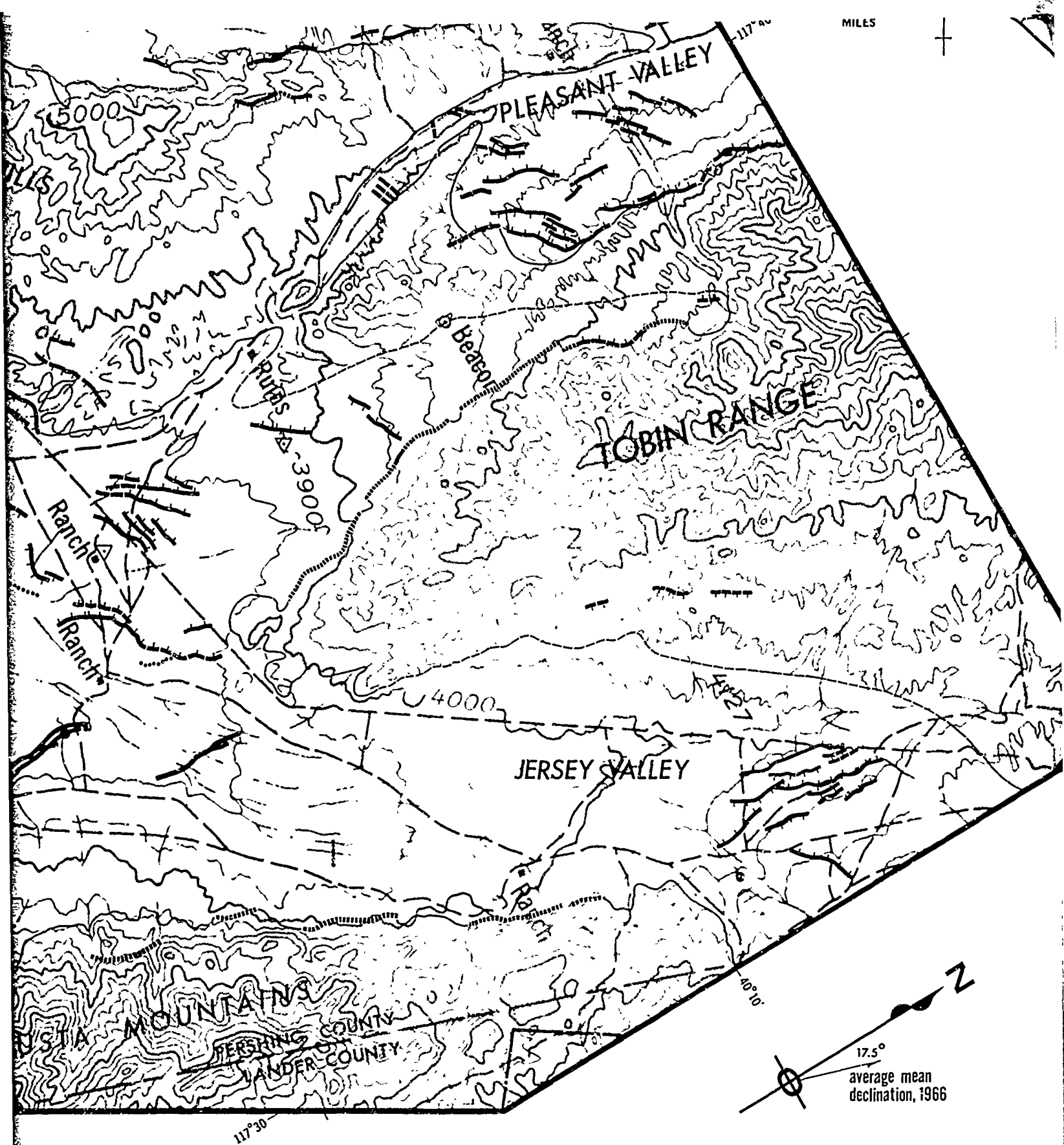
VALLEY

NEVADA

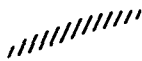


Pho ed

N



Photogeology by Dennis B. Burke 1965-66



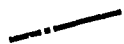
Broad lineament of unknown origin



Generalized bedrock-alluvium contact. Dashed where alluvium becomes thin and discontinuous



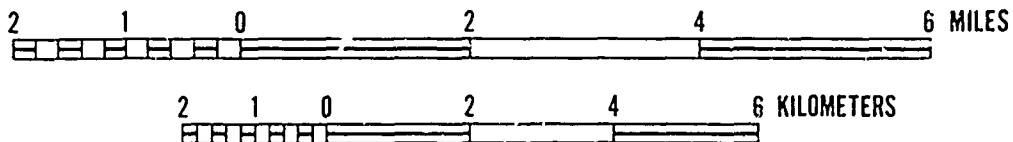
Generalized outer limits of fans. Short dashed where gradational



Limits of stereo coverage



SCALE 1:100 000



CONTOUR INTERVAL 200 FEET

P

Unclassified

Security Classification

DOCUMENT CONTROL DATA - R&D		
<i>(Security classification of title, body of abstract and indexing annotation must be entered when the overall report is classified)</i>		
1. ORIGINATING ACTIVITY <i>(Corporate author)</i> Department of Geophysics Stanford University Stanford, California, 94305		2a. REPORT SECURITY CLASSIFICATION Unclassified
		2b. GROUP
3. REPORT TITLE GEOPHYSICAL STUDY OF BASIN-RANGE STRUCTURE, DIXIE VALLEY REGION, NEVADA		
4. DESCRIPTIVE NOTES <i>(Type of report and inclusive dates)</i> Final Scientific Report. Period covered: Jan.1964-Dec.1966.		Approved Aug.3,1967
5. AUTHOR(S) <i>(Last name, first name, initial)</i> George A. Thompson, Laurent J. Meister, Alan T. Herring, Thomas E. Smith, Dennis B. Burke, Robert L. Kovach, Robert O. Burford, Iraj A. Salehi, and M. Darroll Wood		
6. REPORT DATE July, 1967	7a. TOTAL NO. OF PAGES 286	7b. NO. OF REFS 95
8a. CONTRACT OR GRANT NO. DASA Project 5710 AF19(628)-3867	9a. ORIGINATOR'S REPORT NUMBER(S) Final Report (Parts I - VIII)	
b. PROJECT NO., Task No., Work Unit No. 8623-03 01		
c. TASK DOD Element: 61445014, 7600801D	9b. OTHER REPORT NO(S) <i>(Any other numbers that may be assigned this report)</i>	
d. DOD Subelement: 681309, 68920G5207	AFCRL-66-848	
10. AVAILABILITY/LIMITATION NOTICES		
11. SUPPLEMENTARY NOTES This research was supported in part by Defense Atomic Support Agency through Air Force Weapons Laboratory		12. SPONSORING MILITARY ACTIVITY Air Force Cambridge Research Laboratories (CRJ), L.G. Hanscom Field Bedford, Massachusetts 01730
13. ABSTRACT The study aims to determine the subsurface structure and origin of a tectonically active part of the Basin and Range province, which has structural similarities to the ocean ridge and rift system and to continental block-fault structures such as the Rift Valleys of East Africa. A variety of techniques was utilized, including seismic refraction, gravity measurements, magnetic measurements, photogeologic mapping, strain analysis of existing geodetic data, and elevation measurements on shorelines of ancient lakes. Dixie Valley contains more than 10,000 feet of Cenozoic deposits and is underlain by a complex fault trough concealed within the main graben. The bounding faults, studied by side refraction, are markedly crooked in strike and comparatively constant in dip. Dip-slip motion predominates. The computed strain energy is comparable to the energy derived from the magnitudes of the 1954 earthquakes. Ancient beach ridges record a maximum 14 feet of westward tilting in approximately the last 10,000 years; the valley has been subsiding with little net tilting.		

DD FORM 1473
1 JAN 64

Unclassified

Security Classification

Unclassified

Security Classification

14. KEY WORDS	LINK A		LINK B		LINK C	
	ROLE	WT	ROLE	WT	ROLE	WT
Earth sciences Geophysical surveys Structural geology Faults (geology) Basin and Range province Nevada Dixie Valley Smith Creek Valley Fourmile Flat Aeromagnetic surveys Seismic refraction surveys Aerial photographic surveys Strain analysis Maps						

INSTRUCTIONS

1. **ORIGINATING ACTIVITY:** Enter the name and address of the contractor, subcontractor, grantee, Department of Defense activity or other organization (*corporate author*) issuing the report.

2a. **REPORT SECURITY CLASSIFICATION:** Enter the overall security classification of the report. Indicate whether "Restricted Data" is included. Marking is to be in accordance with appropriate security regulations.

2b. **GROUP:** Automatic downgrading is specified in DoD Directive 5200.10 and Armed Forces Industrial Manual. Enter the group number. Also, when applicable, show that optional markings have been used for Group 3 and Group 4 as authorized.

3. **REPORT TITLE:** Enter the complete report title in all capital letters. Titles in all cases should be unclassified. If a meaningful title cannot be selected without classification, show title classification in all capitals in parenthesis immediately following the title.

4. **DESCRIPTIVE NOTES:** If appropriate, enter the type of report, e.g., interim, progress, summary, annual, or final. Give the inclusive dates when a specific reporting period is covered.

5. **AUTHOR(S):** Enter the name(s) of author(s) as shown on or in the report. Enter last name, first name, middle initial. If military, show rank and branch of service. The name of the principal author is an absolute minimum requirement.

6. **REPORT DATE:** Enter the date of the report as day, month, year, or month, year. If more than one date appears on the report, use date of publication.

7a. **TOTAL NUMBER OF PAGES:** The total page count should follow normal pagination procedures, i.e., enter the number of pages containing information.

7b. **NUMBER OF REFERENCES:** Enter the total number of references cited in the report.

8a. **CONTRACT OR GRANT NUMBER:** If appropriate, enter the applicable number of the contract or grant under which the report was written.

8b, 8c, & 8d. **PROJECT NUMBER:** Enter the appropriate military department identification, such as project number, subproject number, system numbers, task number, etc.

9a. **ORIGINATOR'S REPORT NUMBER(S):** Enter the official report number by which the document will be identified and controlled by the originating activity. This number must be unique to this report.

9b. **OTHER REPORT NUMBER(S):** If the report has been assigned any other report numbers (*either by the originator or by the sponsor*), also enter this number(s).

10. **AVAILABILITY LIMITATION NOTICES:** Enter any limitations on further dissemination of the report, other than those imposed by security classification, using standard statements such as:

- (1) "Qualified requesters may obtain copies of this report from DDC."
- (2) "Foreign announcement and dissemination of this report by DDC is not authorized."
- (3) "U. S. Government agencies may obtain copies of this report directly from DDC. Other qualified DDC users shall request through _____."
- (4) "U. S. military agencies may obtain copies of this report directly from DDC. Other qualified users shall request through _____."
- (5) "All distribution of this report is controlled. Qualified DDC users shall request through _____."

If the report has been furnished to the Office of Technical Services, Department of Commerce, for sale to the public, indicate this fact and enter the price, if known.

11. **SUPPLEMENTARY NOTES:** Use for additional explanatory notes.

12. **SPONSORING MILITARY ACTIVITY:** Enter the name of the departmental project office or laboratory sponsoring (*paying for*) the research and development. Include address.

13. **ABSTRACT:** Enter an abstract giving a brief and factual summary of the document indicative of the report, even though it may also appear elsewhere in the body of the technical report. If additional space is required, a continuation sheet shall be attached.

It is highly desirable that the abstract of classified reports be unclassified. Each paragraph of the abstract shall end with an indication of the military security classification of the information in the paragraph, represented as (TS), (S), (C), or (U).

There is no limitation on the length of the abstract. However, the suggested length is from 150 to 225 words.

14. **KEY WORDS:** Key words are technically meaningful terms or short phrases that characterize a report and may be used as index entries for cataloging the report. Key words must be selected so that no security classification is required. Identifiers, such as equipment model designation, trade name, military project code name, geographic location, may be used as key words but will be followed by an indication of technical context. The assignment of links, rules, and weights is optional.

Unclassified

Security Classification